



Syntheses of N-Heterocyclic carbenes-stabilized metallic nanoclusters and nanoparticles

Victoire Asila

► To cite this version:

Victoire Asila. Syntheses of N-Heterocyclic carbenes-stabilized metallic nanoclusters and nanoparticles. Material chemistry. Sorbonne Université, 2022. English. NNT : 2022SORUS087 . tel-04536004

HAL Id: tel-04536004

<https://theses.hal.science/tel-04536004>

Submitted on 7 Apr 2024

HAL is a multi-disciplinary open access archive for the deposit and dissemination of scientific research documents, whether they are published or not. The documents may come from teaching and research institutions in France or abroad, or from public or private research centers.

L'archive ouverte pluridisciplinaire **HAL**, est destinée au dépôt et à la diffusion de documents scientifiques de niveau recherche, publiés ou non, émanant des établissements d'enseignement et de recherche français ou étrangers, des laboratoires publics ou privés.

Sorbonne Université

ÉCOLE DOCTORALE PHYSIQUE ET CHIMIE DES MATERIAUX (ED 397)

Laboratoire de Chimie de la Matière Condensée de Paris (UMR 7574, Sorbonne Université)

Syntheses of N-heterocyclic carbenes-stabilized metallic nanoclusters and nanoparticles

Présentée par Victoire ASILA

THÈSE DE DOCTORAT DE PHYSIQUE ET CHIMIE DES MATERIAUX

Dirigée par Corinne Chanéac et François Ribot

Soutenance prévue le 6 avril 2022

Devant le jury compose de :

| | | |
|--------------------|------------------------|-----------------------|
| Aude Demessence | Chercheuse CNRS | Rapporteur |
| Stéphane Mornet | Directeur de recherche | Rapporteur |
| Luke Mac Aleese | Chercheur CNRS | Examineur |
| Louis Fernsterbank | Professeur | Examineur |
| Corinne Chanéac | Professeure | Directrice de thèse |
| François Ribot | Directeur de recherche | Co-Directeur de thèse |

Acknowledgments

First, I would like to sincerely thank Professor. Louis Fernsterbank, D.R. Stéphane Mornet, Dr. Luke Mac Aleese, Dr. Aude Demessence for accepting to review my thesis and be part of my Jury.

I would like to express my sincere and warm gratitude to Professor. Corinne Chanéac and D.R. François Ribot for allowing me to work within the Laboratoire de Chimie de la Matière Condensée de Paris. They have been supporting and encouraging me during these years from the beginning, through the 2020 lock down, during difficult times of illness, and to this very moment.

I would also like to thank Denis Lesage from IPCM laboratory for the many mass spectrometry experiments, for his patience and scientific guidance. He was of great help for the development of an efficient nanoclusters mass spectrometry analysis. In this process, he also spend hours finding on spectra analysis and I am grateful for that.

I would like to extend my gratitude to several people who collaborated with me on this project: Dr. Sandra Casale on HRTEM-EDX analyses, Dr. Dimitri Mercier for XPS analyses, Dr. Lise Abiven on photoluminescence measurements. I would also like to thank Thomas Naillon, for his help in the Ag₂S syntheses during his Master's internship.

I would like to thank all the members of the LCMCP laboratory. Indeed, the overall working environment was great. I will not forget all the time shared together and the laughter. I think especially of the great PhD students I met during these years. There are too many of them to cite them all but they made my years in LCMCP very pleasant.

I would like to finish by thanking my family and my friends who have been a great support system for me, especially my dad Patrick (he deserved his name being cited for always pushing me to do better and believing in me).

Last but not least, I thank my dear husband who has been nothing but the best to me during these PhD years.

Table of Contents

| | |
|--|-----------|
| CHAPTER I: STATE OF THE ART ON GOLD NANOCCLUSERS | 9 |
| I.A. Chemistry and reactivity of gold nanoclusters | 9 |
| I.B. Synthesis of usual gold nanoclusters | 12 |
| I.B.1. Phosphine protected gold nanoclusters | 12 |
| I.B.2. Thiolate protected gold nanoclusters | 14 |
| I.C. NHC protected gold nanoclusters | 20 |
| I.C.1. N-heterocyclic carbenes structure | 20 |
| I.C.2. NHC-Metals complexes | 23 |
| I.C.3. NHC stabilized gold nanoclusters synthesis | 28 |
| I.D. Conclusion | 31 |
| References | 32 |
| CHAPTER II: GOLD NANOCCLUSERS CHARACTERIZATION DEVELOPMENTS | 41 |
| II.A. UV-Vis spectroscopy and X-Ray diffraction crystallography contribution for gold nanoclusters characterization | 41 |
| II.A.1. Theoretical and experimental UV-Vis spectroscopy studies of gold nanoclusters | 41 |
| II.A.2. X-Ray crystallography studies on gold nanoclusters | 44 |
| II.B. Mass spectrometry purpose and development for the analysis of gold nanoclusters | 45 |
| II.B.1. ESI-QTOF mass spectrometry | 46 |
| II.B.2. ESI-FTICR mass spectrometry | 51 |
| II.B.3. Analysis of MS spectral data for identification of unknown gold nanoclusters | 54 |
| II.C. Conclusion | 56 |
| References | 57 |
| CHAPTER III: SYNTHESSES OF N-HETEROCYCLIC CARBENE STABILIZED GOLD NANOCCLUSERS FROM IMIDAZOLIUM SALTS AND AUCLPPH₃ | 61 |
| III.A. Imidazolium salts | 62 |
| III.A.1. Synthesis | 62 |
| III.A.2. Characterization by liquid state NMR | 63 |
| III.B. Nanoclusters synthesis | 64 |
| III.B.1. Synthesis and morphology | 64 |
| III.B.2. Mass spectrometry (MS) analysis | 71 |

Table of contents

| | |
|--|------------|
| III.C. Conclusion | 86 |
| References | 87 |
| CHAPTER IV: SYNTHESIS OF N-HETEROCYCLIC CARBENE STABILIZED GOLD NANOCLUSTERS FROM IMIDAZOLIUM SALTS AND HAuCl₄.3H₂O | 89 |
| IV.A. Non water dispersible nanoclusters using HAuCl₄.3H₂O | 90 |
| IV.A.1. Imidazolium salts synthesis | 87 |
| IV.A.2. Non water dispersible nanoclusters synthesis | 88 |
| IV.B. NHC stabilized water dispersible nanoclusters using HAuCl₄.3H₂O | 110 |
| IV.B.1. Water soluble imidazolium salt synthesis | 107 |
| IV.B.2. Water soluble nanoclusters synthesis | 108 |
| IV.C. Conclusion | 119 |
| CHAPTER V: SYNTHESIS OF N-HETEROCYCLIC CARBENE STABILIZED SILVER SULFIDE NANOPARTICLES | 123 |
| V.A. Introduction on silver sulfide nanoparticles | 123 |
| V.A.1. Ag ₂ S nanoparticles for applications | 124 |
| V.A.2. Ag ₂ S crystalline structure | 125 |
| V.A.3. Ag ₂ S synthesis pathway. State of the art. | 126 |
| V.B. Synthesis of Ag₂S NPs by conventional heating | 129 |
| V.C. Synthesis of Ag₂S NPs by using imidazolium salt: imid-PEG₄ | 132 |
| V.C.1. Choice of the heating method and of the ligand. | 132 |
| V.C.2. Microwave assisted synthesis pathway | 133 |
| V.C.3. Photoluminescence properties of Ag ₂ S nanoparticles | 147 |
| V.D. Synthesis using Ag-NHC complex: Ag-NHC-PEG₄ | 151 |
| V.D.1. Synthesis of complex Ag-NHC-PEG ₄ | 151 |
| V.D.2. Microwave assisted NPs synthesis | 152 |
| V.D.3. Further characterization of Ag ₂ S NPs | 156 |
| V.D.4. Low temperature synthesis | 159 |
| V.E. CONCLUSION | 161 |
| REFERENCES | 162 |
| CONCLUSION | 165 |
| References | 170 |

Table of contents

APPENDIX 171

ABSTRACT 185

Table of contents

Introduction

By definition, one nanometer is one billionth of a meter. One nanometer is about as long as our fingernail grows in one second. It's a size scale that we can't see with naked eyes but has drawn tremendous attention to researchers (and also worries to many people). The scientific interest comes from the fact that reducing the size of a material to the nanometer scale, changes its physical and chemical intrinsic properties. Also, at the nanometric size, controlling the surface chemistry is mandatory to ensure stability of the nanostructures in various environment. At the nano scale, materials are in a metastable state because of the very high surface energy compared to an object at the micron scale. To obtain such objects, it is necessary to limit the growth of the nanoobjects and to stabilize them with regards to an evolution in suspension. According to La Mer's model regarding the particles formation, after the nucleation step, phenomena of growth happen, first by the diffusion of the monomers in the solution, and then by aging process due to the high solubility and surface energy of small particles in solution. In this final step, the size of particles increases by Oswald ripening (dissolution of the smallest particles and redeposition of the dissolved species on the surface of larger crystals), by aggregation, by coalescence/oriented attachments of the nanoobjects (particles rotate in the range of 0.5–1 nm to make contact with an alignment of atomic lattices and grow together into a single crystal) or by diffusion of monomers along the surface of a nanomaterial to change the shape of the nanoobject (intraparticle growth). For particular nanoobjects such as nanoclusters, the formation mechanism is not yet well described. Nanoclusters could be considered as “super nuclei” since their evolution can lead to the formation of bigger nanoparticles during the ripening stage or to their redissolution in molecular complexes of low nuclearity.¹ Nanoclusters correspond to well-defined molecular structure.²

The choice of ligands is critical for the synthesis of nanoobjects since they play a role in the shape, stability and dispersion of the nanomaterials. Indeed, ligands have a role in the nanoparticles colloidal stability as they contribute to minimize the surface energy, in the regulation of the nanoparticles solubility and in their functionality (e.g. active components complexation ability). Thus, the choice of the ligand involves several important parameters. One of them is the chemical composition of the nanoobject surface that must be taken into account, since the nature and strength of bonding between the ligand and the surface is strongly correlated to the type of nanomaterials (oxide, sulfide, metal). The strength of the ligand binding drives the colloidal stability of the nanomaterials during the growth step. The ligand must be sufficiently complexing to lower the surface energy and prevent the formation of larger particles but not too complexing to preserve the metal core at the detriment of redissolution into monometallic molecular species.³ It is in this context that N-heterocyclic carbenes (NHCs)⁴, carbon-based organic molecules, are being increasingly used as ligand. In molecular chemistry, they have been widely employed as ligands for various transition metal complexes over the last two decades. Indeed, they form stable metal-ligand bonds which resist harsh conditions. For anti-cancer therapy, Au-NHC complexes have been explored aiming at better chemotherapeutic index in terms of increased bioavailability and fewer side effects than their platinum counterparts. A report by Bertrand *et al.* showed the antiproliferative effects of caffeine based NHC Au(I) complex, $[\text{Au}(\text{caffein-2-ylidene})_2][\text{BF}_4]$.⁵ The complex appeared to be poorly toxic on non-cancerous human embryonic kidney cells *in vitro*. NHCs are thus promising ligands for the stabilization of stable gold and silver sulfide nanomaterials of interest. Regarding materials

Introduction

science,^{6,7} Weidner *et al.* reported the synthesis of NHC-based Self-Assembled Monolayers (SAMs) on solid gold substrates using 1,3-diethylbenzimidazol-2-ylidene.⁸ Later, Crudden *et al.* reported the synthesis of ultra-stable self-assembled monolayers of N-heterocyclic carbenes on gold.⁹ These SAMs demonstrated considerably greater resistance to heat and chemical reagents than their thiol-based counterparts. Also, several teams developed NHC stabilized AuNCs syntheses.^{10,11,12} In our laboratory, Hippolyte *et al.* reported new syntheses of N-heterocyclic carbene-stabilized gold nanoparticles in different ways. The team was able to obtain stable nanoparticles synthesized from a separate gold source, an imidazolium salt and sodium borohydride or from an NHC-borane and a gold source.^{13,14}

This thesis describes the use of NHCs as ligands to stabilize gold nanoclusters and silver sulfide nanostructures. In 2018, when I started this thesis, the main goal was the synthesis of NHC stabilized gold nanoclusters under the supervision of Pr. Corinne Chanéac and Dr. François Ribot at LCMCP (Laboratoire de Chimie de la Matière Condensée de Paris) and nothing had been reported yet on this topic. During the course of the thesis, first NHC capped gold nanoclusters syntheses were reported by Narouz *et al.*^{15,16} and by Shen *et al.*^{17,18}. These teams were able to obtain nanoclusters through ligand exchange¹⁵ or by the reduction of gold-NHC complexes. The commonly used separation method of the nanocluster was through crystallization followed by Single-crystal X-ray Diffraction analysis done by Pr. Hannu Häkkinen. Then, the properties of the nanoclusters that crystallized were further studied. In this case, we did not have an insight of the suspensions complete composition after synthesis since only species that crystallize are clearly identified. In this context, we decided to conduct a study on the kinetics of the nanocluster formation and their stability over time. We aim at having a better understanding of the formation of all species according to the synthesis parameters (choice of precursor, solvent, time, etc.). For this purpose, we developed an analysis method mainly based on mass spectrometry, and a homemade data software to be able to characterize the suspension with its diversity of molecular clusters including high mass species. This part of the thesis was developed in collaboration with Denis Lesage from IPCM (Institut Parisien de Chimie Moléculaire) laboratory. With this approach, we were able to analyze the composition of complex mixtures of nanoclusters, and demonstrate the very large diversity of species with different nuclearities and chemical compositions. The effect of the ligands on the formation of gold nanoclusters was studied by varying both NHC ligands and gold precursors, highlighting the competition between phosphine and NHC ligands in nanoclusters structure regarding nuclearity and chemical composition. We also extended the study to another type of particles of interest, silver sulfide nanoparticles using NHCs ligands. In this part of the work, we focused on the synthesis of silver sulfide nanoparticles, dispersible in water, and emitting in a precise window of the infrared for future applications in *in vivo* imaging and nanothermometry.

The manuscript consists in an introductive first chapter, then four experimental chapters, a conclusion and appendix.

The first chapter is a general introduction on gold nanoclusters. We described the chemistry and reactivity particular to gold nanoclusters. Then, usual phosphine and thiolate protected gold nanoclusters synthesis were outlined. Finally, we made a state of the art on NHCs and the NHC stabilized gold nanoclusters syntheses, which were reported during the course of this thesis.

The second chapter focus on the characterization and optical properties of gold nanoclusters. We discussed the most relevant technics for nanocluster characterization such as UV-Vis

Introduction

spectroscopy, X-Ray Diffraction spectroscopy and finally the technic that we had retained, the Mass Spectrometry (MS). The various mass spectrometry devices that we used were presented. More specifically, we presented the methodology that we developed for mass spectrometry analysis of complex gold nanoclusters mixtures.

The third chapter is related to the development of gold nanoclusters synthesis stabilized by phosphine and NHCs. This synthesis uses AuClPPh_3 as gold source, different imidazolium salt as NHC precursors and sodium borohydride, as both base and reducing agent. The aim of this study was to understand the behavior of NHC ligands when it is in competition with phosphine ligands. Also, the composition of the nanoclusters and their stability toward aging was studied thanks to mass spectrometry analysis among other techniques.

The fourth chapter present the synthesis of NHC capped gold nanoclusters. $\text{HAuCl}_4 \cdot 3\text{H}_2\text{O}$ was used with various imidazolium salt, NaH as a base and sodium borohydride as a reducing agent. We studied the composition of the nanoclusters in the mixture, their stability is correlated to the type of ligands and the reaction conditions that favors the formation of gold nanoclusters over gold complexes, such as $[\text{Au}(\text{NHC})_2]^+$, or gold nanoparticles are identified.

The fifth and last chapter describe the synthesis and characterization of silver sulfide nanoparticles stabilized by NHCs. A water soluble PEGylated imidazolium salt was synthesized and used to crystallize Ag_2S NPs through conventional and microwave heating. The morphology and composition of the particles were studied. We also got interested in the photoluminescence properties of some of NHC- Ag_2S particles. The goal being to synthesize NPs emitting in the NIR-II window.

Finally, we concluded this work by summarizing the results obtained in this work and by presenting the future prospects for these projects.

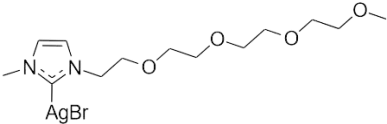
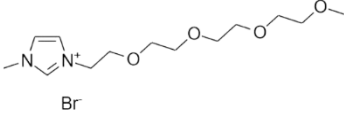
References

- (1) Thanh, N. T. K.; Maclean, N.; Mahiddine, S. Mechanisms of Nucleation and Growth of Nanoparticles in Solution. *Chem. Rev.* **2014**, *114* (15), 7610–7630. <https://doi.org/10.1021/cr400544s>.
- (2) Jin, R.; Zeng, C.; Zhou, M.; Chen, Y. Atomically Precise Colloidal Metal Nanoclusters and Nanoparticles: Fundamentals and Opportunities. *Chem. Rev.* **2016**, *116* (18), 10346–10413. <https://doi.org/10.1021/acs.chemrev.5b00703>.
- (3) Heuer-Jungemann, A.; Feliu, N.; Bakaimi, I.; Hamaly, M.; Alkilany, A.; Chakraborty, I.; Masood, A.; Casula, M. F.; Kostopoulou, A.; Oh, E.; Susumu, K.; Stewart, M. H.; Medintz, I. L.; Stratakis, E.; Parak, W. J.; Kanaras, A. G. The Role of Ligands in the Chemical Synthesis and Applications of Inorganic Nanoparticles. *Chem. Rev.* **2019**, *119* (8), 4819–4880. <https://doi.org/10.1021/acs.chemrev.8b00733>.
- (4) Herrmann, W. A. N-Heterocyclic Carbenes: A New Concept in Organometallic Catalysis. *Angew. Chem. Int. Ed.* **2002**, *41* (8), 1290–1309. [https://doi.org/10.1002/1521-3773\(20020415\)41:8<1290::AID-ANIE1290>3.0.CO;2-Y](https://doi.org/10.1002/1521-3773(20020415)41:8<1290::AID-ANIE1290>3.0.CO;2-Y).
- (5) Bertrand, B.; Stefan, L.; Pirrotta, M.; Monchaud, D.; Bodio, E.; Richard, P.; Le Gendre, P.; Warmerdam, E.; de Jager, M. H.; Groothuis, G. M. M.; Picquet, M.; Casini, A. Caffeine-Based Gold(I) N-Heterocyclic Carbenes as Possible Anticancer Agents: Synthesis and Biological Properties. *Inorg. Chem.* **2014**, *53* (4), 2296–2303. <https://doi.org/10.1021/ic403011h>.
- (6) Smith, C. A.; Narouz, M. R.; Lummis, P. A.; Singh, I.; Nazemi, A.; Li, C.-H.; Crudden, C. M. N-Heterocyclic Carbenes in Materials Chemistry. *Chem. Rev.* **2019**, *119* (8), 4986–5056. <https://doi.org/10.1021/acs.chemrev.8b00514>.
- (7) Zhukhovitskiy, A. V.; MacLeod, M. J.; Johnson, J. A. Carbene Ligands in Surface Chemistry: From Stabilization of Discrete Elemental Allotropes to Modification of Nanoscale and Bulk Substrates. *Chem. Rev.* **2015**, *115* (20), 11503–11532. <https://doi.org/10.1021/acs.chemrev.5b00220>.
- (8) Weidner, T.; Baio, J. E.; Mundstock, A.; Große, C.; Karthäuser, S.; Bruhn, C.; Siemeling, U. NHC-Based Self-Assembled Monolayers on Solid Gold Substrates. *Aust. J. Chem.* **2011**, *64* (8), 1177–1179. <https://doi.org/10.1071/CH11173>.
- (9) Crudden, C. M.; Horton, J. H.; Ebraliidze, I. I.; Zenkina, O. V.; McLean, A. B.; Drevniok, B.; She, Z.; Kraatz, H.-B.; Mosey, N. J.; Seki, T.; Keske, E. C.; Leake, J. D.; Rousina-Webb, A.; Wu, G. Ultra Stable Self-Assembled Monolayers of N-Heterocyclic Carbenes on Gold. *Nat. Chem.* **2014**, *6* (5), 409–414. <https://doi.org/10.1038/nchem.1891>.
- (10) Man, R. W. Y.; Li, C.-H.; MacLean, M. W. A.; Zenkina, O. V.; Zamora, M. T.; Saunders, L. N.; Rousina-Webb, A.; Nambo, M.; Crudden, C. M. Ultrastable Gold Nanoparticles Modified by Bidentate N-Heterocyclic Carbene Ligands. *J. Am. Chem. Soc.* **2018**, *140* (5), 1576–1579. <https://doi.org/10.1021/jacs.7b08516>.
- (11) Salorinne, K.; Man, R. W.; Li, C.-H.; Taki, M.; Nambo, M.; Crudden, C. M. Water-Soluble N-Heterocyclic Carbene-Protected Gold Nanoparticles: Size-Controlled Synthesis, Stability, and Optical Properties. *Angew. Chem. Int. Ed.* **2017**, *56* (22), 6198–6202.
- (12) Vignolle, J.; Tilley, T. D. N-Heterocyclic Carbene-Stabilized Gold Nanoparticles and Their Assembly into 3D Superlattices. *Chem. Commun.* **2009**, No. 46, 7230–7232.
- (13) Hippolyte, L. New Syntheses of N-Heterocyclic Carbene-Stabilized Gold Nanoparticles, Sorbonne université, 2018.

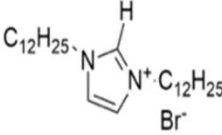
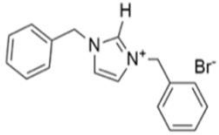
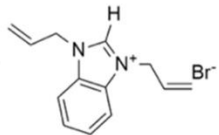
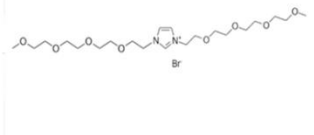
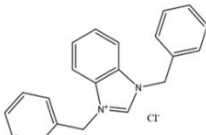
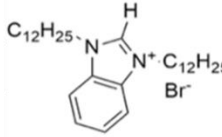
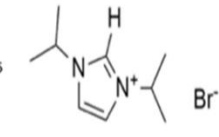
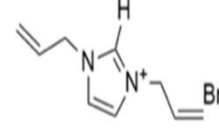
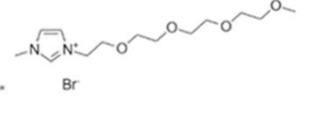
Introduction

- (14) Bridonneau, N.; Hippolyte, L.; Mercier, D.; Portehault, D.; Murr, M.; Marcus, P.; Fensterbank, L.; Chanéac, C.; Ribot, F. N-Heterocyclic Carbene-Stabilized Gold Nanoparticles with Tunable Sizes. *Dalton Trans.* **2018**, 47. <https://doi.org/10.1039/C8DT00416A>.
- (15) Narouz, M. R.; Osten, K. M.; Unsworth, P. J.; Man, R. W. Y.; Salorinne, K.; Takano, S.; Tomihara, R.; Kaappa, S.; Malola, S.; Dinh, C.-T.; Padmos, J. D.; Ayoo, K.; Garrett, P. J.; Nambo, M.; Horton, J. H.; Sargent, E. H.; Häkkinen, H.; Tsukuda, T.; Crudden, C. M. N-Heterocyclic Carbene-Functionalized Magic-Number Gold Nanoclusters. *Nat. Chem.* **2019**, 11 (5), 419–425. <https://doi.org/10.1038/s41557-019-0246-5>.
- (16) Narouz, M. R.; Takano, S.; Lummis, P. A.; Levchenko, T. I.; Nazemi, A.; Kaappa, S.; Malola, S.; Yousefalizadeh, G.; Calhoun, L. A.; Stamplecoskie, K. G.; Häkkinen, H.; Tsukuda, T.; Crudden, C. M. Robust, Highly Luminescent Au₁₃ Superatoms Protected by N-Heterocyclic Carbenes. *J. Am. Chem. Soc.* **2019**, 141 (38), 14997–15002. <https://doi.org/10.1021/jacs.9b07854>.
- (17) Shen, H.; Deng, G.; Kaappa, S.; Tan, T.; Han, Y.-Z.; Malola, S.; Lin, S.-C.; Teo, B. K.; Häkkinen, H.; Zheng, N. Highly Robust but Surface-Active: An N-Heterocyclic Carbene-Stabilized Au₂₅ Nanocluster. *Angew. Chem. Int. Ed.* **2019**, 58 (49), 17731–17735. <https://doi.org/10.1002/anie.201908983>.
- (18) Shen, H.; Xu, Z.; Hazer, M. S. A.; Wu, Q.; Peng, J.; Qin, R.; Malola, S.; Teo, B. K.; Häkkinen, H.; Zheng, N. Surface Coordination of Multiple Ligands Endows N-Heterocyclic Carbene-Stabilized Gold Nanoclusters with High Robustness and Surface Reactivity. *Angew. Chem. Int. Ed.* **2021**, 60 (7), 3752–3758. <https://doi.org/10.1002/anie.202013718>.

Annotations

| | |
|-------------------------|---|
| ACT | Acetonitrile |
| Ag-NHC-PEG ₄ |  |
| Au | Gold |
| AuNP | Gold nanoparticle |
| DCM | Dichloromethane |
| DDTC | Diethyldithiocarbamate |
| DMSO | Dimethyl sulfoxide |
| DPA | D-penicillamine |
| equiv. | Equivalent |
| ESI | Electrospray ionization |
| EtOH | Ethanol |
| Imid | imidazol-2-ylidene |
| Imid-PEG ₄ |  |
| IR | Infrared |
| LSPR | Localized surface plasmon resonance |
| MeOH | Methanol |
| MS | Mass spectrometry |
| NCs | Nanoclusters |
| NHC | N-heterocyclic carbenes |
| NIR | Near infrared |
| NMR | Nuclear magnetic resonance |
| NP | Nanoparticle |
| NPs | Nanoparticles |
| ODE | 1-octadecene |
| PEG | Polyethylene glycol |
| PL | Photoluminescence |
| RSH | Thiol ligand |
| SG | Glutathione |
| TEM | Transmission electron microscopy |
| TEM | Transmission electronic microscopy |
| THF | Tetrahydrofuran |
| TOAB | Tetraoctylammonium bromide |
| UV | Ultra-violet |
| UV-vis | UV-visible |
| XPS | X-ray Photoelectron spectroscopy |

Annotations

| C12-Br (1,3-didodecylimidazolium bromide) | Benzyl-Br (1,3-dibenzylimidazolium bromide) | bAllyl-Br (1,3-diallylbenzimidazolium bromide) | imidBisPEG ₄ (1,3-ditetraethyleneglycolimidazolium bromide) | bBenzyl-Cl (1,3-dibenzylbenzimidazolium chloride) |
|---|---|---|--|---|
|  |  |  |  |  |
| bC12-Br (1,3-didodecylbenzimidazolium bromide) | iPr-Br (1,3-diisopropylimidazolium bromide) | Allyl-Br (1,3-diallylimidazolium bromide) | imidPEG ₄ (1-methyl, 3-tetraethyleneglycolimidazolium bromide) | |
|  |  |  |  | |

Annotations

PART I - NHC STABILIZED GOLD NANOCLUSTERS: A STUDY ON SYNTHESIS AND CHARACTERIZATION

Chapter I: State of the art on gold nanoclusters

I.A. Chemistry and reactivity of gold nanoclusters

Gold metal was chosen in this study for its very interesting photo-physical properties. Although bulk gold metal is considered to be chemically inert, researches have shown that this statement is not true for gold in its nanometric form.

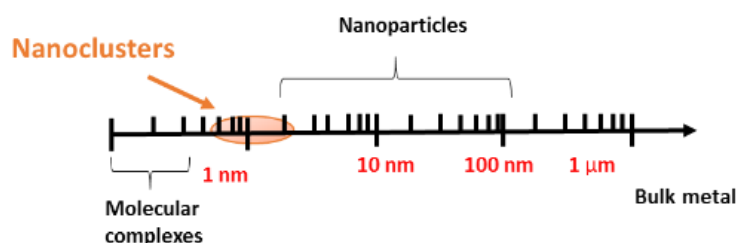


Figure I-1: Size relationship between individual molecules, nanoclusters, nanoparticles and bulk material

At a nanometric size, gold exhibits various characteristic properties depending on the particle size (among other parameters). Two types of nanometric objects can be distinguished:

- Small particles referred to as gold nanoparticles which size varies between two to hundreds of nanometers.
- Ultrasmall particles referred to as gold nanoclusters which size varies between 1 to about 2 nm.¹

However, the size is not the only parameter taken into account to completely differentiate gold nanoclusters and gold nanoparticles (Figure I-1). As it is well known, gold nanoparticles exhibit a localized surface plasmon resonance (LSPR) due to collective oscillation of the free electrons upon excitation (it causes a characteristic enhancement of the local field around the nanoparticle). The resonance frequency of the oscillations depends on the dielectric properties of the metal, the surrounding media (Figure I-2) and also the shape and size of the nanoparticles. For example, spherical gold nanoparticles usually exhibit a characteristic plasmon absorption band in UV-Visible spectroscopy in the range of 500-600 nm.^{2,3} The suspensions are also usually characterized by their red color.

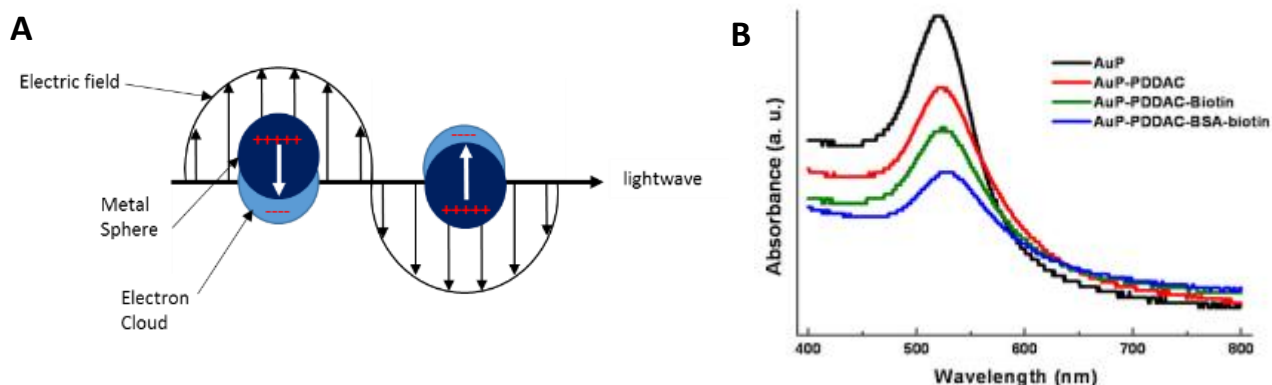


Figure I-2: [A] Schematic diagram of electron charge displacement in metallic nanoparticles. [B] UV-visible absorbance spectra of polyelectrolyte functionalized AuNPs conjugated with different biomolecules.³

When it comes to gold nanoclusters, plasmonic behaviors are not observed. However discrete energy level transitions do occur. It is said that gold nanoclusters have a “molecular like” behavior. They are the link between atoms and nanoparticles. These precise gold nanoclusters properties will be developed in chapter II. Although gold nanoclusters and gold nanoparticles are made of the same metal and both at the nanometric scale, their structural organization are different. While the structural organization for all gold nanoparticles is similar to the one in gold metal with a periodical organization of the atoms, gold nanoclusters that are composed of smaller number of atoms in the metallic core, present a molecular organization which depends on the nuclearity. For example, Au₁₃ and Au₂₅ nanoclusters have a different structural organization (Figure I-3 and Figure I-4). Indeed, Au₂₅ nanoclusters core is usually composed of icosahedral Au₁₃ core and an exterior shell composed of Au₂- Ligands motifs (Figure I-3).⁴

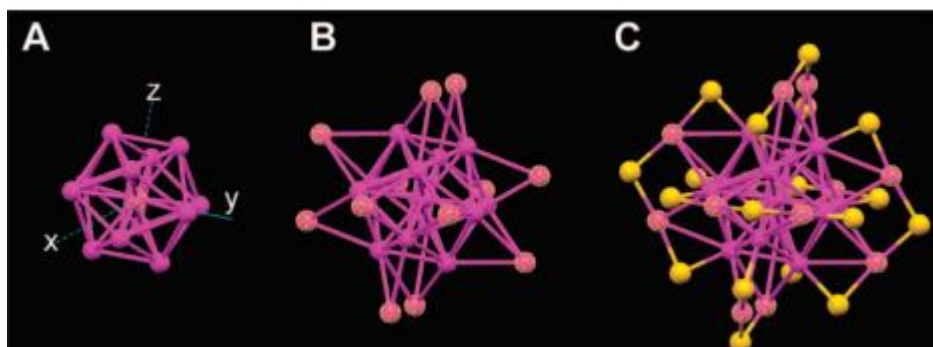


Figure I-3 Crystal structure of a Au₂₅(SR)₁₈ (R = phenylethyl group): [A] the icosahedral Au₁₃ core; [B]) the Au₁₃ core plus the exterior 12 Au atoms; [C] the whole Au₂₅ nanocluster protected by 18 thiolate ligands (Au = magenta; S = yellow).⁴

Regarding gold nanoclusters, there is a number of atoms that can be exactly counted and their properties are sensitive to their precise atomic composition. In the ≤ 2 nm size range, the nanoclusters are composed of countable number of atoms (consisting of five to hundreds of gold atoms) and their properties are extremely sensitive to their exact atomic composition: adding or removing gold atoms significantly changes the structure and then the electronic and optical properties of the nanoclusters.⁵ Gold nanoclusters exhibit many unique properties such

as luminescence,^{6,7,8} catalytic activity,⁹ chirality¹⁰ and magnetism¹¹. These properties make them attractive for a wide range of applications such as chemical sensing,¹² photocatalysis,¹³ biological labelling,¹⁴ etc.

For example, in 2009 Muhammed *et al.*, reported the synthesis of Au₂₂, Au₂₃ and Au₃₃ glutathione capped gold nanoclusters.¹⁴ The nanoclusters were obtained by etching of Au₂₅ glutathione protected nanoclusters. Different properties were observed with Au₂₂ and Au₂₃ being highly water soluble and fluorescent with quantum yields of 2.5 and 1.3%, respectively. By contrast, Au₃₃ nanocluster was only soluble in organic solvents and less fluorescent, with a quantum yield of 0.1%. Among the synthesized nanoclusters, Au₂₃ exhibited interesting biological components detection properties. Indeed, quenching of Au₂₃ fluorescence in the presence of Cu²⁺ ions in biological media happened and thus it showed potential use as Cu²⁺ sensor.

Another interesting example for the use of gold nanoclusters is the reversible switching of magnetism in thiolate protected Au₂₅ nanoclusters reported by Zhu *et al.*¹¹ The team showed that the paramagnetism is reversibly switchable by controlling the charge state of the nanoclusters.¹¹ The magnetic properties of the nanoclusters were evaluated with electron paramagnetic resonance (EPR) spectroscopy. The EPR signal disappeared after the [Au₂₅(SR)₁₈]⁰ nanoclusters were treated with NaBH₄ to produce the anionic form [Au₂₅(SR)₁₈]⁻. When [Au₂₅(SR)₁₈]⁻ nanoclusters were treated again with H₂O₂, the EPR signal was recovered. Therefore, the paramagnetism in the Au₂₅ nanocluster can be switched on or off simply by controlling the charge state. The obtained results showed the interest of gold nanoclusters as paramagnetic probes.

Also, regarding their catalytic properties, the most active nano-gold catalysts have been shown to be around 1 to 3 nm in size.¹⁵ Indeed, the high catalytic activity of these smaller nanoclusters is generally attributed to two main effects: scalable effects and quantum confinement effects.¹¹ The decrease of the particle size in nanoclusters leads to an increased surface-to-volume ratio which results into a higher ratio of low-coordinated surface atoms. These surface atoms arrangements allow for better breakage and making of bonds in catalytic cycles. Lavenn *et al.*,¹⁶ reported in 2015, the deposition of Au₂₅(SPh-*p*NH₂)₁₇ nanoclusters (gold particles average diameter of 0.9 ± 0.2 nm and gold loading of 1.07 wt%) on mesoporous silica SBA-15. This catalyst has been used in the oxidation of benzyl alcohol. Comparison for the oxidative dehydrogenation of benzyl alcohol with other standard catalysts such as Au@TiO₂-WGC (gold particles average diameter of 3.5 ± 1.5 nm and gold loading of 1.5 wt%) was performed. A value of 50% conversion of the alcohol after 20 h for catalyst Au@TiO₂ was obtained when for Au₂₅(SPh-*p*NH₂)₁₇@SBA-15 catalyst (calcinated at 400 °C), 50% conversion of the alcohol after only 45 min was obtained.¹⁶ Also, Au₂₅(SPh-*p*NH₂)₁₇@SBA-15 has a good selectivity for benzaldehyde at half conversion. Although, it was reported that the presence of ligands prevented oxygen dissociation and was an obstacle to aerobic dehydrogenation of benzyl alcohol, calcination of the catalyst did increase the catalytic activity. The size of the particle went from 0.9 to 1.8 nm (limited size growth) and a maximum of activity was observed at a calcination temperature of 400 °C corresponding to complete loss of the ligands. This example shows how the use of gold nanoclusters in catalysis can be very promising because of high activity but also for better understanding of the cluster size influence on the catalytic activity. There are various examples of the use of gold nanoclusters for different applications and other examples will be developed later in this chapter. Indeed, studies of gold nanoclusters properties stabilized with diverse ligands have been reported.

The synthesis of metal nanoclusters usually relies on the reduction of a metal salt in the presence of protecting ligands. Several experimental parameters affect the type of nanoclusters obtained: the nature and concentration of the reducing agent, the solvent, the reaction temperature, the reaction time, the nature and concentration of the ligand. Indeed, some ligands have received

particular attention in the aim of obtaining stable gold nanoclusters. First studies on gold nanoclusters in the 70s were about phosphine protected gold nanoclusters,^{17,18} followed by thiolate, selenolate or acetylene protected gold nanoclusters.^{19,20,21} More recently a new type of ligands for gold nanoclusters synthesis drew particular attention: N-heterocyclic carbenes (NHCs). Our focus will be in the next part on the synthesis of gold nanoclusters obtained using the main ligands used in literature, phosphines and thiolates then we will describe the synthesis of NHC capped gold nanoclusters.

I.B. Synthesis of usual gold nanoclusters

I.B.1. Phosphine protected gold nanoclusters

Phosphine ligands exhibit two characters, they are both σ donors and π back-donors. The single electron pair of the phosphorus is responsible of the σ donation towards empty orbitals of the metals. The π -back-donation occurs from filled metal orbitals to empty orbitals of the phosphorus ligands. According to literature, π back-donation occurs from the d orbitals of the metals into the σ^* orbitals of the phosphorus ligand.²² The electronic parameters of phosphines ligands have been investigated by various methods. One of the known procedure determines the electronic changes at the metal center of phosphorus and non-phosphorus mixed ligand complexes, depending on the nature of the phosphine ligands, by IR and NMR spectroscopies.^{23,24} For mixed carbonyl phosphine complexes, the carbonyl stretching IR frequencies are useful when we want to compare the electronic parameters of various phosphines ligands toward a given metal. For example, the electronic properties of the ligands can be determined by comparison of the IR stretching frequency of the carbonyl ligands in trans $\text{RhCl}(\text{CO})\text{L}_2$ with L being a diphenyl-substituted phosphinite ligand and a monodentate phosphorus amidite ligand.²⁵ Based on these considerations, Tolman has described an electronic parameter to determine electron donor-acceptor properties for various phosphine ligands in coordinated metallic complex $\text{NiL}(\text{CO})_3$ (L = ligand) using $\text{P}(\text{t-Bu})_3$ as phosphine reference ligand. The electronic parameter is obtained through differences in the IR frequencies of the symmetric CO stretching (ν_{CO}). From these ν_{CO} values, it was concluded that the more a phosphine ligand is electron donor, the more the ν_{CO} frequency decreases. In contrary, the more a phosphine ligand is electron withdrawing, the more the ν_{CO} frequency increases. Phosphines being two electron donors that engage a lone pair for binding to metals and thus considered as good σ -donors, the phosphines with the lower ν_{CO} should be better ligands according to Tolman's parameter. As an example, the value for PPh_3 is 2068.9 cm^{-1} when for PF_3 it is 2110.8 cm^{-1} . It means that according to Tolman's parameter PPh_3 are better ligands than PF_3 . When comparing the values for 70 monodentate phosphorus ligands, it was shown that PPh_3 is a very good ligand for metal binding.²⁶

The bulkiness of the ligand must also be taken into account. The most often used parameter to measure the steric bulk of a phosphine ligand in a metal complex, is the Tolman's θ parameter. This parameter was introduced to reveal the ability of phosphorus ligands to compete the coordination positions on $\text{Ni}(0)$ that could not be explained in terms of their electronic character. The steric parameter θ for symmetric ligands (all three substituents are the same) is the apex angle of a cylindrical cone, from the center of the P atom, which includes the van der Waals radii of the outermost atoms of the ligand at the perimeter of the cone. If there are internal degrees of freedom, the substituents are folded back to give a minimum cone. For unsymmetrical ligands, the parameter can be calculated by using a model to minimize the sum

of half-angles given by: $\theta = (2/3) \sum \theta_i/2$. However, studies showed that ligands rarely form a perfect cone. An analysis of crystal structures has shown that the angles realized in the structure are smaller than the θ predicted values using this model.²⁷ Determining the electron donor properties and the bulkiness of the phosphine ligands towards metals could help at a better understanding of the variation of stability and structure of gold nanoclusters depending on the type of phosphine ligand.

Nowadays, there are high performances computer models that simultaneously evaluate steric hindrance and electronics parameters. They provide ligands tables that allow predictive replacement of phosphines by others type of phosphines. It is useful for applications such as the optimization of catalytic activity for example.²⁸

As we have just seen, phosphines ligands can be considered as morphology and properties directing agents for metal complexes, thus there is an interest in using them to synthesize AuNCs. Moreover, the strong gold-P interactions compared to previously used ligands such as citrates increase the attractivity for this ligand. PPh₃ is one of the most used phosphine due to its strong sigma donor ability (see previous paragraph) and due to its easy synthesis. An example of PPh₃ capped AuNCs of interest are PPh₃protected Au₁₁ NCs. It's one of the smallest gold nanocluster having at least one gold atom surrounded by a neighboring metal atom.²⁹ Furthermore, the phosphine to ligand ratio on the surface of the AuNCs can be controlled to understand the effect of different bonding types between ligands and the gold surface defined in Green's covalent bond classification.³⁰

The first examples of phosphines protected gold nanoclusters can be attributed to Naldini *et al.* in 1966.³¹ This team reported that they obtained 1,2-bisdiphenylphosphine-ethan (DPE) protected Au₆ nanoclusters (Au₆(DPE)₂Cl₂). It was characterized by infrared spectroscopy. Anion exchange with low nucleophilic character such as perchlorate, hexafluorophosphate, and tetraphenylborate indicated that the two chlorine atoms are not equivalent in the structure. They compared the obtained band at 288 cm⁻¹ for [Au₆(DPE)₂Cl]PF₆ with the chlorine to metal band of ClAu(DPE)AuCl, the precursor metallic complex, at 325 cm⁻¹, and concluded that the band shift to lower wavelength, was due to a bridging chloride in the Au₆ cluster. Few years later, Au₁₁(PPh₃)₇(SCN)₃ was synthesized and reported by the same team.³² The structure was resolved by X-ray diffraction studies. A large number of phosphine protected gold nanoclusters with different gold atom number, were later isolated and characterized. Also computationally modelling using DFT (Density functional theory) were done to predict energetically stable structures.

Concerning their structures, many phosphine protected gold nanoclusters are based on a centered icosahedral Au₁₃ metal core (Figure I-4) which is capped by the ligands. For the nanoclusters containing more than 13 gold atoms, most of them follow this growth pattern: the Au₁₃ icosahedron serves as a primary building block, which undergoes further growth by sharing a common Au vertex with other Au₁₃ units to form polyicosahedral supraclusters.^{33,34,35}

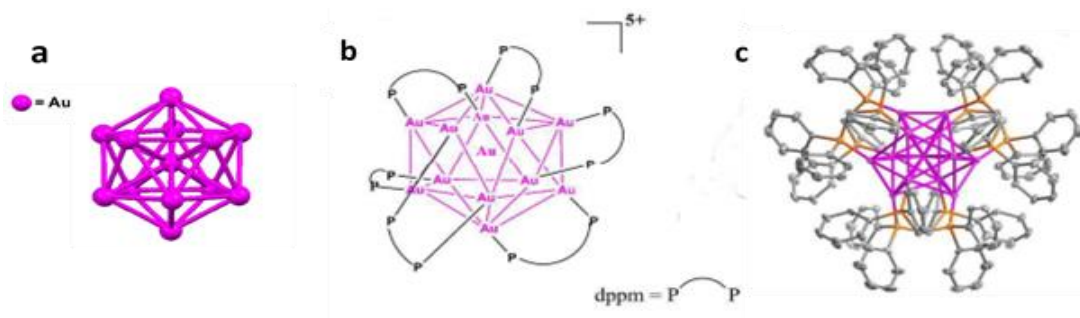


Figure I-4: Icosahedral Au_{13} of PPh_3 ($\text{dppm} = \text{Ph}_2\text{PCH}_2\text{PPh}_2$) capped gold nanoclusters (view without ligands (a), schematic view with ligands (b), X-ray crystal structure (c))^{33,34,35}

However, phosphine protected gold nanoclusters present a low stability. For example, study of their suspensions over time unveils their tendency to undergo photodegradation under ambient conditions. This problem limits their use in regards to industrial applications. To overcome these issues, researchers decided to use thiolates as protecting ligands, since a strong gold-thiolate interactions had been discovered in self-assembled monolayers (SAMs) of thiolates on bulk gold surfaces during the late 1980s by Nuzzo and Allara.³⁶

Thus, two strategies have been developed to increase the gold nanoclusters stability:

- Having a mix of thiolates and phosphines in the gold nanoclusters structure,
- Using 100% of thiolates ligands.

I.B.2. Thiolate protected gold nanoclusters

First of all, thiolates and phosphine ligands do not only have different bonding energy to gold. Indeed, phosphines ligands prefer to bind to the top sites of gold atoms while thiolates typically tend to bridge two gold atoms in nanocluster structures. Thiolate capped AuNCs

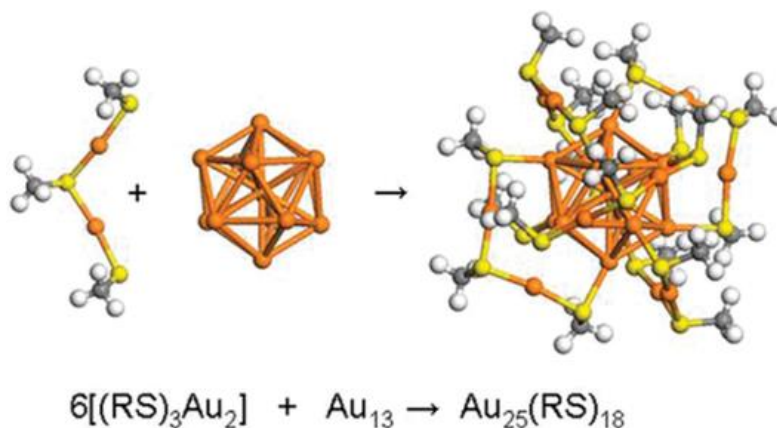


Figure I-5 “Staple” motif: structure of $\text{Au}_{25}(\text{RS})_{18}$ nanocluster consisting of an icosahedral Au_{13} core protected by 6 RS-Au-SR-Au-SR unit.³⁷

form linear RS-Au-SR and RS-Au-SR-Au-SR bonding motif called « staple motifs » (Figure I-5).³⁷ Indeed, Jadzinsky *et al.* succeeded in crystallizing $\text{Au}_{102}(\text{SR})_{44}$ clusters and found that all 44 thiolate groups formed linear RS-Au-SR motifs on the nanocluster surface, which they termed the “staple” motif.³⁸

This statement can be observed in several nanocluster structures such as in a mixed phosphine and thiolate-protected $[\text{Au}_{25}(\text{PPh}_3)_{10}(\text{SC}_2\text{H}_5)_5\text{Cl}_2]^{2+}$ (Figure I-6) nanocluster synthesized by Shichibu *et al.* in 2007, obtained by reacting phosphine-capped Au_{11} clusters with an excess of ethanethiol.³⁹

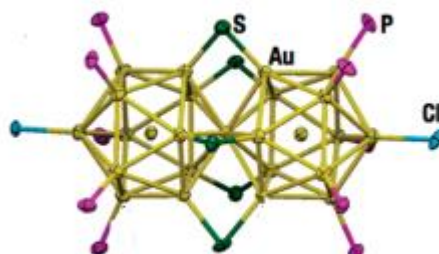


Figure I-6 . Schematic illustrations of the molecular structures of $[\text{Au}_{25}(\text{PPh}_3)_{10}(\text{SC}_2\text{H}_5)_5\text{Cl}_2]^{2+}$ nanocluster³⁹

The gold core of this cluster can be seen as being composed of two icosahedral Au_{13} cores joined by sharing a common vertex gold atom.³⁹ Gold-thiolate chemistry interest started in the 1980's thanks to the researches on SAMs as stated previously. Then, in the 1990's, researchers like Brust *et al.*⁴⁰ developed synthesis of only thiolates capped nanoparticles and in 2005 the first study determining gold nanoclusters structure.⁴¹

In general, the synthesis of AuNCs is done by bottom-up or top-down approaches (Figure I-7). The top-down approach is based on getting the AuNCs from larger materials (nanoparticles) by reducing the size of the fragments by etching (Figure I-7, left). Some of the etching process are ligand induced etching,⁴² others are temperature induced etching for example.⁴³ In the bottom-up way, AuNCs are built by chemical reactions in solution starting from molecular species (Figure I-7, right).⁴⁴ These two paths have both distinct advantages and disadvantages.⁴⁵ In the top down synthesis path, the addition of ligand or heating make it quite simple to pursue, however tuning of the reaction conditions to stop the degradation process of gold nanoparticles to form only gold nanoclusters (and not molecular specie) is difficult. Bottom-up procedure by chemical reduction method, for example, is one of the simplest methods used for "one step" preparation of nanoclusters. However various limitations are associated with reducing agents such as toxicity, high reactivity or poor reducing ability, high cost and impurities.

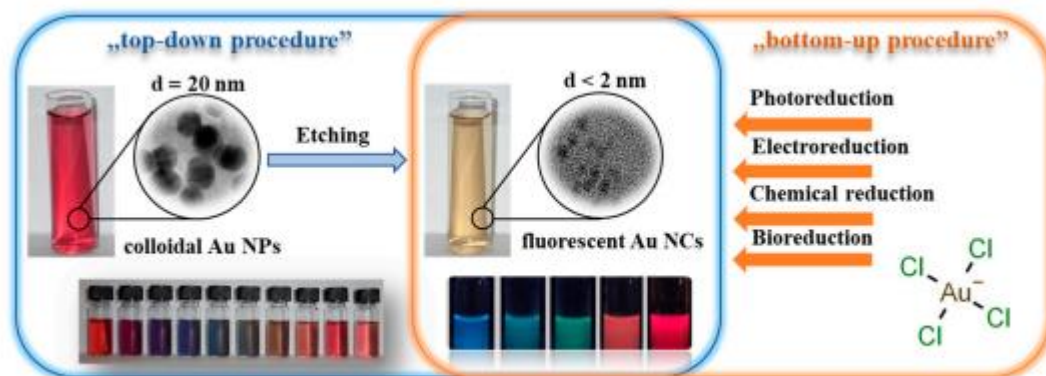


Figure I-7: Synthesis of AuNCs by "top down" and "bottom up" approaches.⁴⁴

In 1994, Brust *et al.* reported the synthesis of very small gold particles that he referred to as gold protected nanoclusters thanks to a two phase's method using a phase transfer catalyst.⁴⁰ They were not able to determine the nanocluster formula or structure at that time since only UV-Vis spectroscopy, TEM, IR and XPS were performed thus the team could not determine if gold nanoclusters or very small gold nanoparticles were synthesized. It is only in 2005 that the first mass spectrometry study giving gold nanocluster formula was reported (from Au_{10} to Au_{39} thiolate protected nanoclusters).⁴¹

Later, Zhu *et al.* highlighted three main steps for thiolates protected AuNCs synthesis:⁴⁶

- Phase transfer of gold precursor (AuCl_4^-) from aqueous solution to toluene using tetraoctylammonium bromide (TOAB) as the phase-transfer reagent
- Au(III) reduction to Au(I) using thiolate ligand (dodecanethiol named HSR in the following)
- Au(I) reduction to Au(0) using an aqueous sodium borohydride solution in the presence of dodecanethiol. The surface reaction with thiolate ligands takes place during metal nucleation and growth.

The team developed a kinetically controlled one-step method for synthesizing $\text{Au}_{25}(\text{SR})_{18}$ isolated nanoclusters with high purity (Figure I-8).⁴⁶ To synthesize $[\text{Au}_{25}(\text{SR})_{18}]$, they decreased the temperature to 0°C during the first step of $[\text{Au}(\text{I}): \text{SR}]$ formation and allowed the reaction to run for 1h after slowing down the stirring. After this time, the stirring was increased to 1000 rpm and then the reducing agent (aqueous solution of NaBH_4 , 10 eq.) was added all at once and left for 24 hours under stirring. In UV spectroscopy the crude mixture showed optical behavior related to $\text{Au}_{25}(\text{SR})_{18}$ NCs without further purification.

The type of AuNCs synthesized depends on the synthetic conditions. As an example, we can consider the synthesis of $\text{Au}_{25}(\text{SR})_{18}$ and $\text{Au}_{144}(\text{SR})_{60}$, reported by Jin *et al.* The differences between these two syntheses are really not significant. Indeed, the stirring speed during the reduction of Au(III) into Au(I) is different and there is an additional thermal treatment at 80°C applied to obtain pure $\text{Au}_{144}(\text{SR})_{60}$.^{46,47} Thus, we can see that they were able to carry out the reactions by controlling the reaction temperature and the aggregation conditions for the $[\text{Au}(\text{I})-\text{SR}]_x$ intermediates.

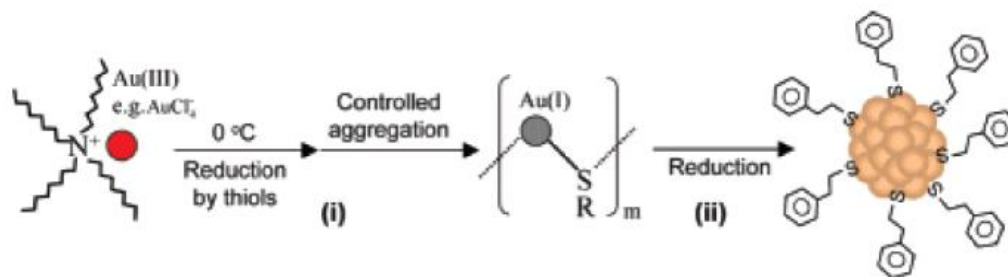


Figure I-8: Synthesis of $\text{Au}_{25}(\text{SR})_{18}$ nanoclusters reported by Zhu *et al.*⁴⁶

In 2009, Wu *et al.* optimized the synthesis of $\text{Au}_{25}(\text{SR})_{18}$ nanoclusters. Their approach was based on one phase size focusing method in THF, improving the purity of the crude mixture, and the yield of Au_{25} NCs.⁴⁸ The reactions conditions are similar to the synthesis performed by Zhu *et al.*,⁴⁶ however the reaction was allowed to further proceed for over 60 hours (aging process) and not only 24 hours.

The use of ESI mass spectrometry (Figure I-9), led to the discovery of numerous Au-thiolate nanoclusters including $\text{Au}_{19}(\text{SR})_{13}$,⁴⁹ $\text{Au}_{38}(\text{SR})_{24}$,⁵⁰ $\text{Au}_{55}(\text{SR})_{31}$,⁵¹ $\text{Au}_{102}(\text{SR})_{44}$ ⁵² or $\text{Au}_{144}(\text{SR})_{60}$.⁴⁷

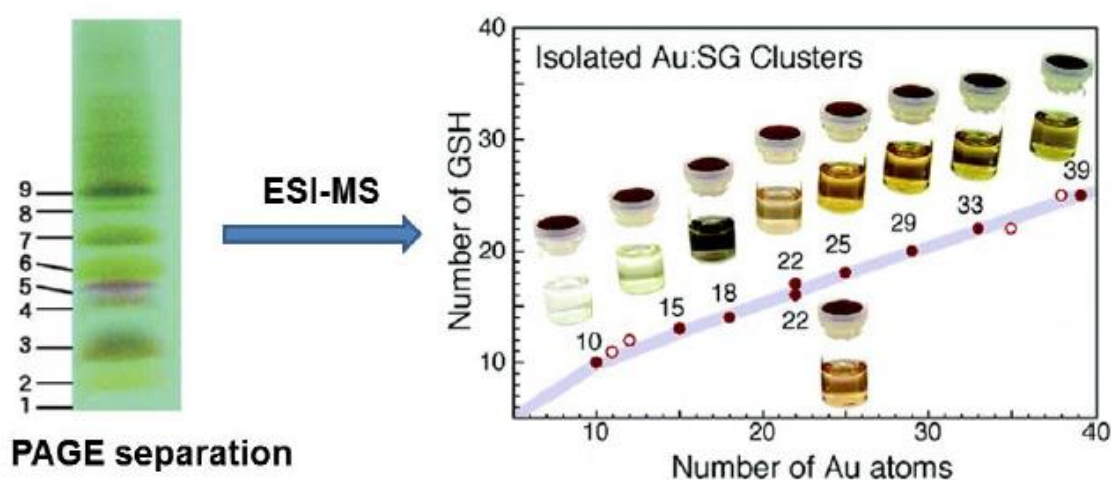


Figure I-9: Isolation and identification of atom-precise glutathionate protected gold nanoclusters through PAGE separation of $\text{Au}_n(\text{SG})_m$ nanoclusters mixture followed by ESI-MS analyses⁴¹

The nanoclusters were separated through PAGE (polyacrylamide gel electrophoresis) which is an electrophoresis separation technique usually used for proteins that allows separation by mass. The medium is a polyacrylamide-based discontinuous gel and SDS (sodium dodecyl sulfate) is used to mask the analytes intrinsic charges. Upon application of a constant electric field, the proteins migrate towards the anode, each with a different speed, depending on its mass. Usually for nanoclusters the gels are made in higher concentration (~40%) than the gels used in protein separations.⁵³ Moreover, single crystal X-ray crystallography allowed to find out the atom packing structures of some of these nanoclusters has been used in several examples.⁵⁴ The first X-ray crystal structure of a thiolate protected nanocluster was of a

$\text{Au}_{102}(\text{p-MBA})_{44}$ (p-MBA = p-mercaptopbenzoic acid) which was reported in 2007 (Figure I-10).³⁸

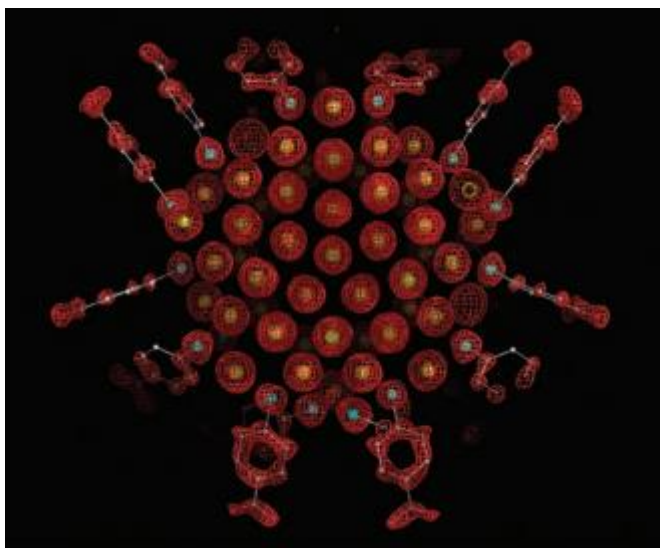


Figure I-10: First X-ray crystal structure of the $\text{Au}_{102}(\text{p-MBA})_{44}$ nanoclusters. Electron density map (red mesh) and atomic structure (gold atoms depicted as yellow spheres, and p-MBA shown as framework and with small spheres [sulfur in cyan, carbon in gray, and oxygen in red]).³⁸

Thiolates capped AuNCs synthesis methods have been successfully developed and researchers started to use their interesting properties for application such as catalysis and imaging.

Different factors affect the catalytic behavior of thiolate protected AuNCs. One of the factors can be the type of ligands due to electronic and steric effects. For example, shorter aliphatic chains allow easier penetration of substrates and so facilitate their interaction with gold atoms enhancing a desired reaction. Also, for aromatic ligands $\pi - \pi$ stacking between the ligand and the reagent can improve the catalytic process.⁵⁵ An example of catalytic reaction using AuNCs is CO oxidation tested with $\text{Au}_{25}(\text{SR})_{18}$ (SR = phenylethanethiol) in 2012 by Jin *et al.*⁴⁹ $\text{Au}_{25}(\text{SR})_{18}$ was deposited on different oxides supports (TiO_2 , CeO_2 , Fe_2O_3) to study the support effect. Supported $\text{Au}_{25}(\text{SR})_{18}$ catalytic activity was tested in a fixed bed reactor after a pretreatment step in O_2 atmosphere. The reaction was performed at different temperatures, starting from room temperature up to 160°C . $\text{Au}_{25}(\text{SR})_{18}$ on TiO_2 support exhibited no activity and $\text{Au}_{25}(\text{SR})_{18}$ on Fe_2O_3 support showed low activity whatever the temperature. In contrast, $\text{Au}_{25}(\text{SR})_{18}$ on CeO_2 support showed 94 % conversion at 80°C and 100% conversion at 100°C . CeO_2 has been known to be one of the best supports in CO oxidation. In the second part of this study, $\text{Au}_{25}(\text{SR})_{18}/\text{CeO}_2$ is calcined at different temperatures to study the ligand effect. The CO oxidation on intact $\text{Au}_{25}(\text{SR})_{18}/\text{CeO}_2$ does not work (Figure I-11.a). The increase in temperature allows partial or complete dethiolation of the supported NCs depending on temperature value (Figure I.8b and c). Indeed, with the increase of the partial removal of the thiolate ligands, active oxygen species on the support interacts with CO near Au accessible sites and then forms CO_2 (Figure I-11.b). This suggests that $\text{Au}_{25}(\text{SR})_{18}/\text{CeO}_2$ interface should be the catalytically active centers for CO oxidation. When total calcination occurs, other Au sites become accessible, and

State of the art on gold nanoclusters

CO and atmospheric O₂ bound at the gold/ceria interface and at the NCs surface to form CO₂ (Figure I-11.c).^{56,57} It appears that the Au nanoclusters do not increase significantly in size even after the complete removal of thiolate ligands and high-temperature treatment. It probably means that there is a strong interaction between the gold nanoclusters and CeO₂ rods to prevent their agglomeration at high temperatures.

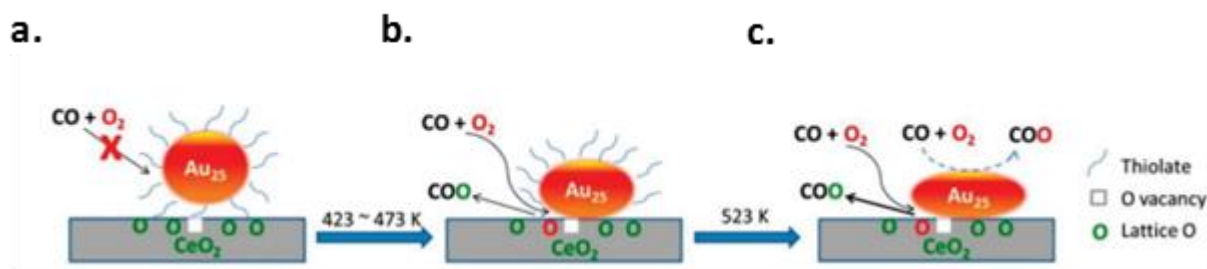


Figure I-11 Oxidation mechanism on Au₂₅(SR)₁₈/CeO₂ depending on ligand density.⁵⁷

In 2018, Li *et al.* also studied the catalytic behavior of supported thiolate-protected NCs on CeO₂ for CO oxidation by investigating three series of catalysts, including Au₃₈(SR)₂₄ with three types of ligands, Au₃₆(SR')₂₄ with four types of ligands, and Au₂₅(SR'')₁₈ with three types of ligands.⁵⁸ Doing comparison of the catalytic activity within each series (Au₃₈, Au₃₆, or Au₂₅), it was identified that the steric hindrance of the ligand at the interface between the thiolate, Au, and CeO₂, can be a limiting factor. Indeed, the ligand blocks the CO adsorption onto Au sites like illustrated in figure I-11.a before heat treatment and thus negatively affects the activation of CO at the Au₂₅(SR'')₁₈/CeO₂ interface. Other important factor is the AuNCs structure. Indeed, comparison between Au₃₈ and Au₃₆ NCs revealed that Au₃₈(SR)₂₄/CeO₂ has an optimum activity in CO oxidation when pretreated at 150 °C, whereas the Au₃₆(SR')₂₄/CeO₂ performance does not change much with pretreatment temperatures.⁵⁸

Other non-catalytic applications were found for SR protected AuNCs. Shang *et al.* reported DPA-capped AuNCs studied for cell internalization.⁵⁹ The AuNCs had good stability over the physiologically pH range of 5 to 9. Cell viability upon exposure to DPA capped AuNCs was examined by a trypan blue exclusion assay and no reduction in viability was apparent after incubation even at a high concentration. It shows that they have good biocompatibility potential. The capability of imaging of DPA capped AuNCs internalized by human cancer (HeLa) cells was tested. Luminescence from the NCs ingested by the HeLa cells could easily be seen inside the cells after incubation of 2 h using confocal microscopy with two-photon excitation.⁵⁹

Various others interesting applications have been demonstrated for SR protected AuNCs. This highlights the interest of finding new ligands that can increase the stability of gold nanoclusters, increase the diversity of cluster nuclearity, and improve their promising properties for extending the possible applications field. In this way, our group interest focused on the use of NHCs as privileged stabilizing ligands for AuNCs synthesis. NHCs have been known for many years but their interest grew in the last decade in material chemistry. They are characterized by their ability to strongly bind metals and high structure variability. Density functional theory (DFT) calculations predicted differences in the Au-NHC bond and the Au-S bond interaction energies: 40 to 45 kcal.mol⁻¹ for Au-S^{60,61} and 46 to 122 kcal.mol⁻¹ for NHC-Au-L complexes depending

on the nature of L (*e.g.* NHC-Au-H = 46 kcal.mol⁻¹ / NHC-Au-Br = 67 kcal.mol⁻¹).⁶² Moreover, their use as efficient stabilizing ligand for nanoparticles^{63,64} has been reported and the interest for gold nanoclusters involving NHC has been growing. Indeed, during the thesis, other researcher's team also developed NHC protected nanoclusters synthesis pathways. In the next part of this chapter, we first report the state of the art on NHCs ligands and after the state of the art on NHC stabilized gold nanoclusters of the three latest years (no synthesis of NHC capped nanoclusters had been published before).

I.C. NHC protected gold nanoclusters

NHCs have been known for many years in molecular chemistry but their interest grew in the last decade for material chemistry and more precisely in nanochemistry. Indeed carbenes, were considered to be very reactive with short living species that could not be isolated. Their isolation and stabilization were a big turning point in their use in chemistry.

I.C.1. N-heterocyclic carbenes structure

N-heterocyclic carbenes (NHCs) are carbon-based organic molecules that have been extensively employed for their interesting properties in the past years. Indeed, their ability to bind any transition metal (in low or high oxidation states) and also other elements (beryllium, sulfur ...) make them great ligands in organometallic and inorganic coordination chemistry. Also, they can stabilize and activate metal centers in different catalytic steps of organic syntheses (C-H activation, C-O bond formation ...).⁶⁵ NHCs are the most stable aminocarbenes (in comparison to the more fragile acyclic aminocarbenes).⁶⁶ For this carbene, the divalent carbon atom (carbenic carbon) is part of a five atoms ring and linked to at least one nitrogen atom. NHCs with six- and seven-membered rings have also been reported.⁶⁷ The sp²-hybrid orbital on the "carbenic" carbon is typically described as σ orbital and thus NHCs behave like a σ-donor ligands with two available electrons (Figure I-12).⁶⁸ They can substitute classical two electrons donor ligands such as amines or phosphines in metal coordination chemistry. They are thus highly nucleophilic molecules.

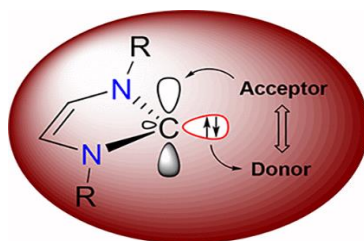
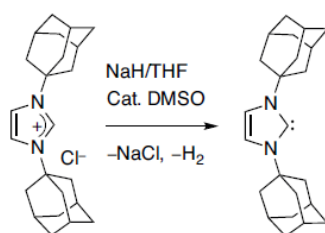


Figure I-12: Schematic representation of NHC imidazole-2-ylidene and orbitals of the "carbenic" carbon

The NHC stability is in part ensured by the bulkiness of the N substituents (-R) on the ring preventing dimerization, and also by the electronic effects induced by the nitrogen atoms.^{69,70} Indeed, there is an overall electronic stabilization by mesomeric interaction between the nitrogen atoms lone pairs and the empty p orbital of the sp² hybridized carbenic carbon. The stabilization energy is approximately 70 kcal.mol⁻¹.⁷¹ The cyclic nature of the NHC also influence the electrons arrangement of the carbenic carbon because it can contribute to an additional stabilization of 25 kcal.mol⁻¹.^{65,71} This explains why NHCs are electron-rich nucleophilic species, whereas other carbenes, like Fisher carbenes, are generally more electrophilic being strong π -acceptors.⁷²

In the early 90's, Arduengo *et al.* isolated the first stable N-heterocyclic carbenes, 1,3-di-1-adamantylimidazol-2-ylidene, thanks to bulky adamantyl substituents on both nitrogen atoms of the imidazole ring (Scheme I-1).⁷³ The team was also able to carry an analysis of its crystal structure showing that the adamantyl N substituents added steric hindrance, which contributes to the kinetic stability. Also, it showed there is sufficient room at the carbene center for chemical reaction to take place. It was the real beginning of a special interest for this type of ligands, particularly in the organometallic chemistry field.



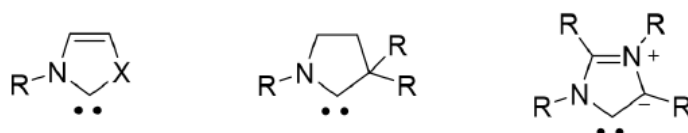
*Scheme I-1 Synthesis of the first isolated 1,3-di-1-adamantylimidazol-2-ylidene by Arduengo et al.*⁷³

NHCs are usually prepared from the corresponding "azolium" salts, more stable, by deprotonation. The most common NHCs, that are quite easy to prepare, are derived from imidazoline, imidazole, 1,2,4-triazole, and benzimidazole salts, giving respectively imidazolin-2-ylidene, imidazole-2-ylidene, triazole-2-ylidene, and benzimidazole-2-ylidene (Scheme I-2.A). NHC precursors can be prepared using several methods. One of the most used synthesis pathway is carried out by the quaternization of the nitrogen atoms of the imidazole ring by reaction with primary alkyl-/aryl- halides in presence of a strong base (Scheme I-2.B). With this procedure, it is possible to introduce two different substituents on the N atoms by reacting an imidazole with different primary alkyl- /aryl- halides leading to unsymmetrically substituted NHCs. The disadvantage is that this method is mainly limited to primary alkyl halides because secondary and tertiary alkyl halides are subject to unwanted elimination reactions.



Scheme I-2: [A] Scheme of common NHC structures imidazolin-2-ylidene, imidazole-2-ylidene, triazole-2-ylidene, and benzimidazole-2-ylidene. [B] Synthesis pathway of an imidazolium salt by quaternization of the nitrogen atoms of the imidazole ring with primary alkyl-/aryl- halides in presence of a strong base.

The presence of the two N atoms is not requisite to the stability of NHCs. Thus, “abnormal” NHCs are NHCs with an imidazole ring deprotonated in the C5 position (Scheme I-3). For example, NHCs where one of the nitrogen atoms is replaced by other atoms (oxygen giving oxazol-2-ylidene, sulfur giving thiazol-2-ylidene, carbon giving pyrrolidin-2-ylidene) have been reported.^{74,75} These change in the structure usually give different electronic properties to the carbenes and, as potential ligands, it allows to tune the reactivity of the complexes. Indeed, the N substituents can be more or less bulky, more or less electron donors or acceptors etc.

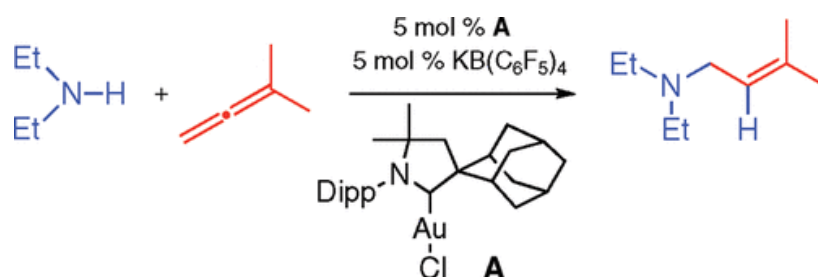


Scheme I-3 Three examples of "Abnormal" NHC structures where one N atom is replaced by other atoms.

I.C.2. NHC-Metals complexes

I.C.2.a. NHC-Metals complexes synthesis

NHCs have been employed as ligands for the formation of transition metal complexes. Indeed, they form complexes that stay stable under reactions conditions where other would break down. For example, Bertrand and coworkers reported studies of intermolecular hydroamination reactions of allenes and alkynes. They showed that a gold catalysts based on abnormal NHC ligands have amazing thermal stability.^{76,77} Indeed, the reactions of allene's aminations are carried out at temperatures up to 200 °C (165°C in the following example) (Scheme I-4).



Scheme I-4: Cationic NHC-gold(I) complex promoting the addition of non-tertiary amines to a variety of allenes at (130–165°C) forming allylic amines^{76,77}

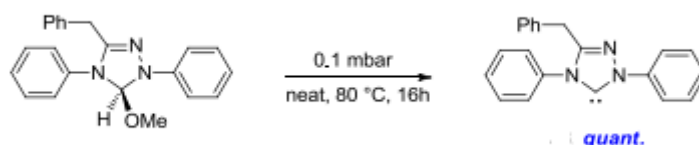
NHCs are able to bind a wide range of metallic and non-metallic species. In fact, examples of NHC complexes have been reported for all transition metals⁷⁸ as well as for a large range of main group elements.⁷⁹ In most metallic complexes, both N sites of the heterocycle can be linked to different type of R substituents that bring variability in terms of steric and electronic properties of the NHC ligands. Vaddamanu *et al.* reported how n-alkyl group can influence the luminescence properties in the crystalline state of gold(I)-N-heterocyclic carbene (NHC) complexes.⁸⁰ Density Functional Theory calculations were carried out for three Au(I)-NHC complexes using NHC ligands precursors, N-(9-acridinyl)-N'-(n-butyl)-imidazolium chloride [1], N-(9-acridinyl)-N'-(n-pentyl)-imidazolium chloride [2], and [N-(9-acridinyl)-N'-(n-hexyl)-imidazolium chloride [3]. The fluorescence decay pattern and fluorescence lifetimes of gold(I) complexes were largely different from each other's. In the solid-state, the emission properties are different (yellow emission for [1], greenish-yellow emission for [2], and blue emission for [3]).

Transition metal complexes of NHCs are mainly formed using four main synthesis methods:

- The first one consists on the reaction of a transition metal complex with a free carbene that is generated *in situ* by imidazolium deprotonation due to instability of free carbenes. An example of *in situ* NHC generation is the use of masked carbenes, which was first introduced by Enders and co-workers.⁸¹ They found that the thermal decomposition of a methoxy adduct under reduced pressure induced the formation of the NHC by elimination of methanol (Scheme I-5).⁸¹ Accordingly, masked carbenes have been thermally decomposed in the presence of a metal source to generate the corresponding NHC metal complexes. This relevant method permits a

State of the art on gold nanoclusters

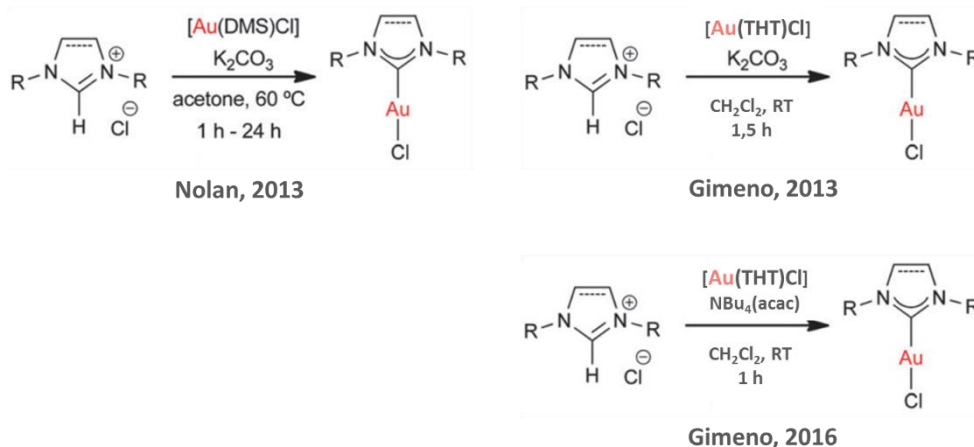
large choice of transition metal complexes as starting material. However, the isolation of the desired NHC is not always easy and the use of strong bases can sometimes be incompatible with the carbene's functional groups or with the desired final complex.



Scheme I-5 Thermal decomposition of methoxy NHC precursor its analogous NHC.⁸¹

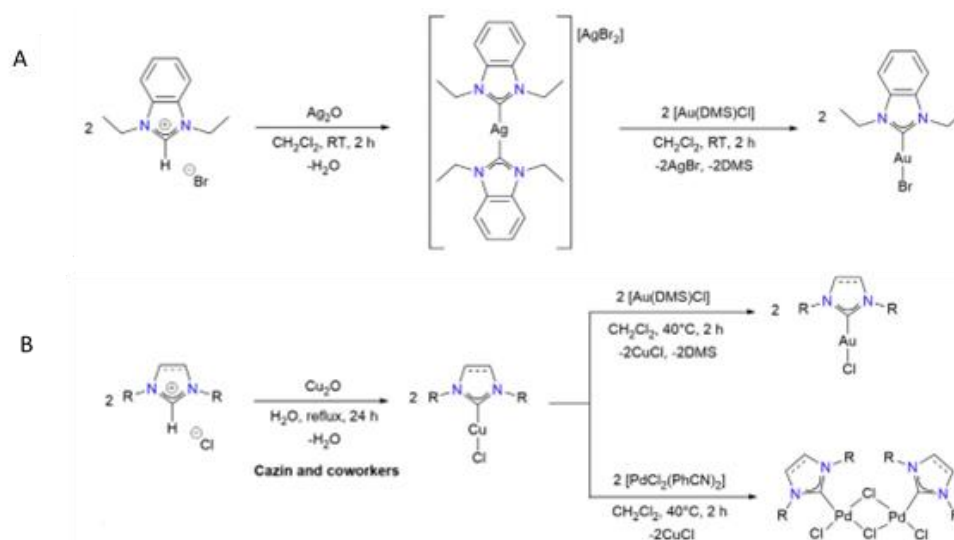
- The second one is the reaction of a transition metal complex, which has a basic anion, with an imidazolium salt. This procedure works best if the imidazolium salt contains an anion, such as chloride or bromide. This is a gentle method to prepare metal complexes but limited to the imidazolium salt with anions such as chloride or bromide, because if not, this anion has to be provided by additional inorganic salts in the reaction medium.

- The third one is the reaction of a transition metal salt with an imidazolium salt in the presence of a weak base. An equilibrium between the imidazolium salt form and the carbene (deprotonated form) is established if the reaction is performed with a gentle base (such as K_2CO_3 , NEt_3 , or NaOAc). The equilibrium is shifted towards the carbene by strong coordination of the NHC ligand to the transition metal. Examples have been reported such as for the synthesis of $[\text{Au}(\text{NHC})\text{Cl}]$ in Scheme I-6.^{82,83,84}



Scheme I-6 Synthesis of $[\text{Au}(\text{NHC})\text{Cl}]$ complex using the weak base route reported by Nolan in 2013⁸² and Gimeno in 2013⁸³ and 2016⁸⁴

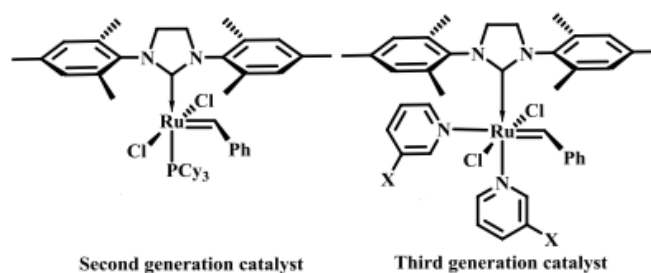
- The last one is a transmetalation reaction using protected Ag-NHC complexes as NHC transfer agent to once again avoid the synthesis of free carbenes. Usually, silver complexes are synthesized by reaction of the corresponding imidazolium salts with silver oxide in the first reaction step. Then another metallic complex with labile ligands is added to transfer the NHC.^{85,86,87} Two examples are given on the scheme I-7. They illustrate this synthesis way reported by Lin *et al.* and Cazin *et al.* This latter does not use an Ag-NHC complex but a Cu-NHC complex.^{88,89}



Scheme I-7: [A] Synthesis of $[\text{Ag}(\text{NHC})_2][\text{AgBr}_2]$ and transmetalation on gold center.⁸⁷
 [B] Preparation of $[\text{Cu}(\text{NHC})\text{Cl}]$ complex and transmetalation on gold and palladium centers.⁸⁶

I.C.2.b. Applications of NHC-Metals complexes

Metal complexes with N-heterocyclic carbene ligands are mostly investigated for their catalytic properties. For example, the second and third generation of Grubbs catalysts are used for the olefin metathesis in organic and polymer chemistry.⁹⁰ The initiation rate is increased more than a million times from the second to the third generation catalyst by replacing the phosphine ligand with more labile pyridine ligands (Scheme I-8). The main application of fast-initiating catalysts is as initiators for ring opening metathesis polymerization.



Scheme I-8 Example of second and third generation Grubbs' catalyst

Regarding other applications, NHCs gave promising results concerning photophysical and photochemical properties when coordinated to luminescent metal. It was reported that NHC acts as high field strength ligand, which gives rise to high energy emissions and, consequently, to a blue shift, which is needed to obtain the desired blue color for organic light emitting diode (OLED) applications.⁹¹ For example, a series of NHC-Iridium complexes were used as a dopant for the fabrication of a Yellow OLED (Figure I-13).⁹²

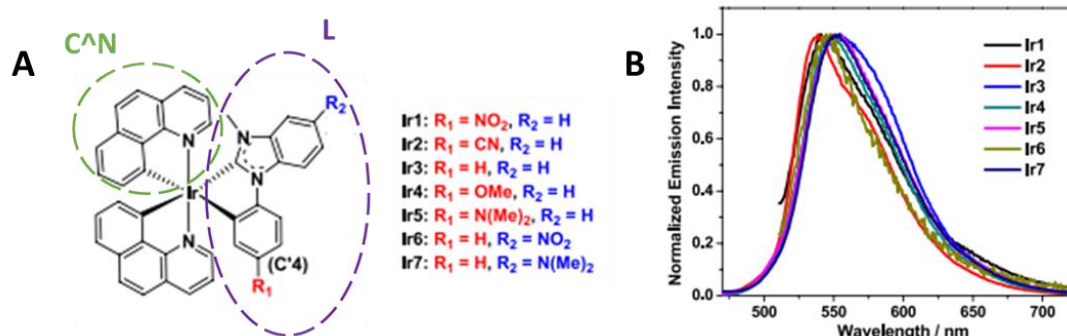


Figure I-13 [A] NHC iridium complexes used for the fabrication of yellow OLEDs ($(C^{\wedge}N)_2Ir(NHC)-Ir(III)$: 3-methyl-1-(4-nitrophenyl)benzimidazol-3-ium iodide (**L1**), 1-(4-cyanophenyl)-3-methylbenzimidazol-3-ium iodide (**L2**), 3-methyl-1-phenylbenzimidazol-3-ium iodide (**L3**), 1-(4-methoxyphenyl)-3-methylbenzimidazol-3-ium iodide (**L4**), 1-(4-dimethylaminophenyl)-3-methylbenzimidazol-3-ium iodide (**L5**), 5-nitro-3-methyl-1-phenylbenzimidazol-3-ium iodide (**L6**), and 5-dimethylamino-3-methyl-1-phenylbenzimidazol-3-ium iodide (**L7**)) and benzo[h]-quinoline as the $C^{\wedge}N$ ligand. [B] Experimental emission spectra of NHC-iridium complexes Ir1 ($\lambda_{ex} = 434$ nm), Ir2 ($\lambda_{ex} = 437$ nm), Ir3 ($\lambda_{ex} = 442$ nm), Ir4 ($\lambda_{ex} = 444$ nm), Ir5 ($\lambda_{ex} = 445$ nm), Ir6 ($\lambda_{ex} = 433$ nm), and Ir7 ($\lambda_{ex} = 444$ nm) in deoxygenated toluene at room temperature.⁹²

The cyclometalated iridium(III) complexes (named $[(C^{\wedge}N)_2Ir(R-NHC)]$) were bearing NHC ligands (derived from 1-phenylbenzimidazole) and benzo[h]quinoline ligands (named $C^{\wedge}N$). All complexes exhibited π, π^* charge transfer (d,d transitions at ca. 440 nm) that originated from the $C^{\wedge}N$ ligand (Figure I-13.A) and very weak metal-to-ligand charge transfer and ligand-to-ligand charge transfer (beyond 500 nm). Also, yellow π, π^* metal-to-ligand charge transfer emission at room temperature in fluid solutions is observed. Moreover, all complexes exhibited long-lived (except Ir1 and Ir6) and oxygen-sensitive bright yellow luminescence. Generally, electron-withdrawing substituents caused minor blue shifts of the low-energy absorption band and the emission band, while the electron-donating substituents induced red shifts (Figure I-13.B). The results were obtained through spectroscopic methods and time-dependent density functional theory.⁹²

NHC-Au complexes also received a great interest for their photophysical properties. In 2014, Gimeno *et al.* reported the synthesis of luminescent NHC-gold(I) complexes.⁹¹ Their lifetimes and high quantum yields make them good candidates for future application as OLEDs. However, for OLEDs applications iridium or platinum complexes are generally preferred to gold complexes, as they possess the best luminescent characteristics so far.⁹¹

Metal NHC species have also shown to be good candidates as potential drugs for treating various biological afflictions and diseases. Some of the first reports on biological activity of metal NHC complexes were published in the very late 90's by Durmaz *et al.*, who reported the

antibacterial properties of ruthenium(II) and rhodium(I) NHC complexes.⁹³ The growing interest in these bioactive NHC drugs is mostly focused on antimicrobial and anticancer activity. For example, platinum-based organometallic complexes are studied as anticancer agents especially due to the discovery of the antitumor properties of cisplatin.⁹⁴ In this context platinum NHC complexes were also investigated. Wai-Yin Sun *et al.* reported that platinum NHC complexes (Figure I-14.A) exhibits *in vivo* significant inhibition of tumor growth in the nude mice model.⁹⁵ The NHC ligands allow great biological stability of the complexes while the platinum induces an anti-cancerous effect. X-ray crystal structures revealed that the orientation of the NHC ligand disfavors the approach of two [(C[^]N[^]N)Pt^{II}]⁺ (where HC[^]N[^]N = 6-phenyl-2,2'-bipyridine) planes in close proximity. These mononuclear complexes have thus a low tendency to aggregate in solutions, maximizing the probability for such NHC-platinum complexes to enter inside cancerous cells.

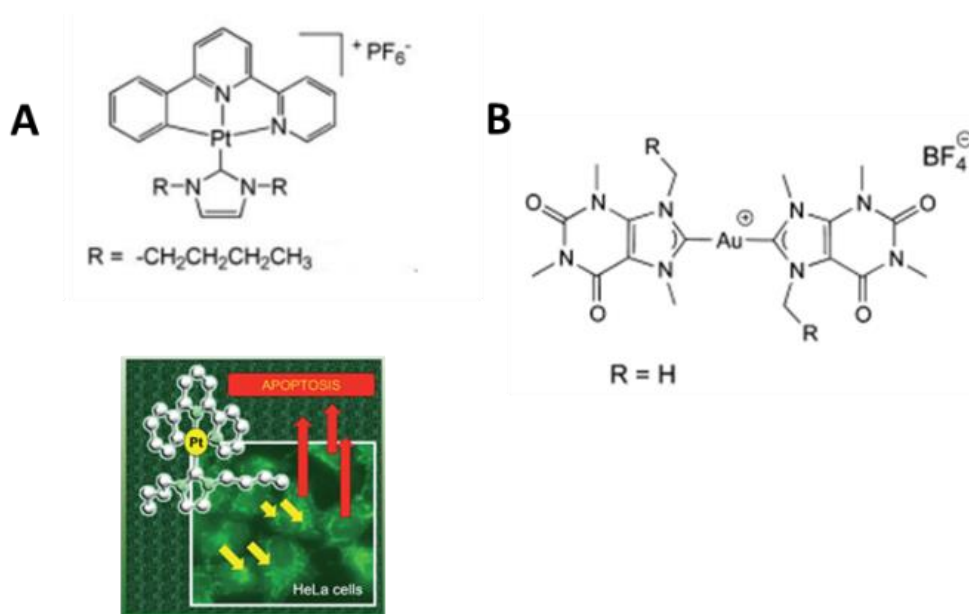


Figure I-14: [A] Representation of NHC platinum complex [(C[^]N[^]N)Pt^{II}(NHC)]⁺ reported by Che *et al.* with high anticancer potential.⁹⁵ [B] Cytotoxic compound based on a benzimidazol-2-ylidene core for anticancer properties against human ovarian cancer cells.⁹⁶

For anti-cancer therapy, Au-NHC complexes have also been explored aiming at possible better chemotherapeutic index in terms of increased bioavailability and fewer side effects than their platinum counterparts. A report by Bertrand *et al.* showed the antiproliferative effects of caffeine based NHC Au(I) complex, [Au(caffeine-2-ylidene)₂][BF₄]. Indeed, caffeine and its analogues have drawn attention for their possible therapeutic applications as anticancer agents. Various complexes were tested *in vitro* on the human ovarian cancer A2780 cell line, its cisplatin resistant variant (A2780/R), on human ovarian cancer SKOV3 cells and on the human lung cancer A549 cell line. Moreover, they also studied the selectivity of the Au-NHC complexes for cancerous cells compared to healthy cells. Indeed, the gold complexes were tested on human embryonic kidney HEK-293T cells. One of the complex (Figure I-14.B), showed interesting anticancer properties *in vitro* against the human ovarian cancer cell line A2780 and its cisplatin resistant variant A2780/R. Furthermore, it appeared to be poorly toxic

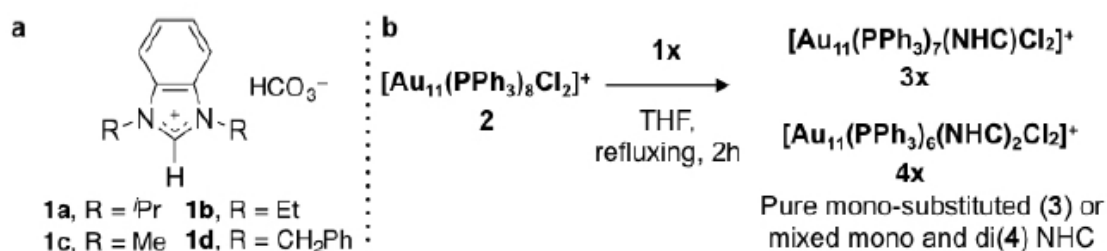
on non-cancerous human embryonic kidney cells *in vitro*. It also showed low toxicity in healthy tissues *ex vivo* in liver and in kidney slices.⁹⁶

As we have seen, NHCs can be used for many applications in association with transition metals due to their interesting binding ability and their structure versatility. However, even though metallic NHC complexes have showed promising results in the biomedical field for example, gold nanoclusters have intrinsic great properties that make them better candidates for some of these applications. To name just two of them, their highly fluorescence ability or their possible magnetic properties (see previous part I.B).⁵⁴ In the following part, NHCs will be presented for their use as stabilizing ligands for the synthesis gold nanoclusters. Very few examples, have yet been reported but so far the synthesis gave promising results.

I.C.3. NHC stabilized gold nanoclusters synthesis

In the beginning of this thesis in 2018, there was no reported examples of NHC capped gold nanoclusters in the literature. However, the stabilization of gold nanoparticles by NHC had been studied by our team with the development of a synthesis method of stable NHC capped gold nanoparticles with tunable size.⁶³ The aim at obtaining monodispersity and displaying different properties led to growing interest on the synthesis of NHC stabilized gold nanoclusters.

The first synthesis of mixed PPh₃ and NHC capped gold nanoclusters was reported in 2019, at the end of my PhD first year, by Narouz *et al.* who performed ligand exchange on a phosphine protected gold nanocluster. They used [Au₁₁(PPh₃)₈Cl₂]Cl in the presence of benzimidazolium hydrogenocarbonate salts in THF and under reflux (Scheme I-9). Benzimidazolium hydrogenocarbonate salts are in equilibrium with NHC•CO₂ adducts, which correspond to masked NHC. This process resulted in the formation of new NHC containing nanoclusters.⁹⁷ The number of PPh₃ exchanged on Au₁₁ nanoclusters depends on the NHC structure (Scheme I-9 (a)), the number of NHC equivalents relative to gold (1.2, 5 or 9 equiv.) introduced and the reaction conditions (addition of water or not).



Scheme I-9: (a) Structure of NHC precursors (benzimidazolium bearing different R organic groups, 1x = 1a, 1b, 1c and 1d) employed in the study for ligand exchange. (b) Reaction of [Au₁₁(PPh₃)₈Cl₂]Cl (2) with corresponding NHC precursors (1x) giving rise to monosubstituted NHC (3x) and disubstituted NHC (4x) Au₁₁ nanoclusters.⁹⁷

Narouz *et al.* were able to observe great stability for mixed PPh₃ and NHC protected gold nanoclusters, greater than for pure phosphine capped gold nanoclusters. They observed a better stability of the nanoclusters when only one NHC substitutes one PPh₃ inside the gold nanocluster structure. Also, the performance of various clusters in electrocatalytic CO₂ reduction was found to correlate with nanoclusters stability. The most stable cluster (corresponding to nanocluster 3c with R= Me) was also the most active in electrocatalysis. DFT

studies associated with single crystal X-ray diffraction revealed the structure for mono-exchanged NHC 3a ($R = i\text{Pr}$) nanocluster. It confirmed that the most favorable position for the NHC is P2 (Figure I-15), in agreement with the as-obtained monosubstituted NHC clusters ($[\text{Au}_{11}(\text{PPh}_3)_7(\text{NHC})\text{Cl}_2]\text{Cl}$). However, according to DFT, introduction of NHC onto the phosphine protected nanocluster was found to be thermodynamically favorable at most sites, with the exception of phosphine P8. This later position gives an unfavorable reaction energy change, probably due to steric constraints (Figure I-15).⁹⁷

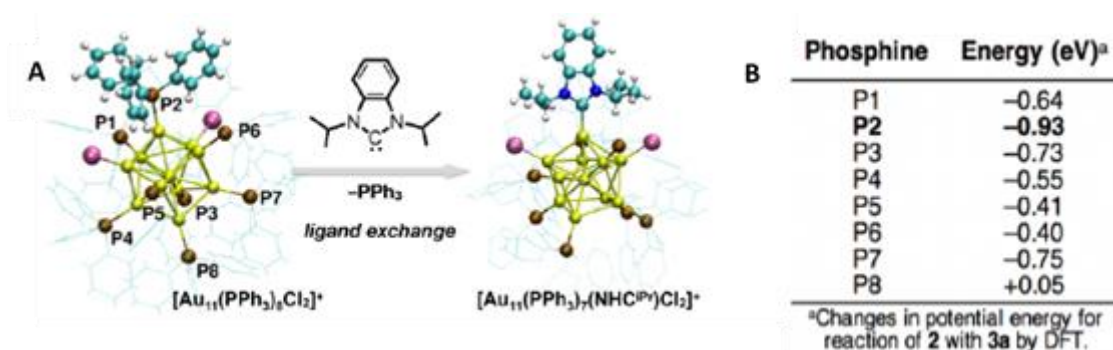


Figure I-15[A] Labelling of phosphines in $[\text{Au}_{11}(\text{PPh}_3)_8\text{Cl}_2]\text{Cl}$ and position of NHC ligand exchanged on structure. [B] DFT-predicted changes in potential energy for reaction shown for each phosphine.⁹⁷

This ligand exchange method allowed the first reported synthesis of mixed PPh_3 and NHC capped gold nanoclusters. Shortly after in 2019, the same team reported the synthesis of highly luminescent NHC protected Au_{13} nanoclusters. They obtained a full NHC capped nanocluster, namely $[\text{Au}_{13}(\text{NHC})_9\text{Cl}_3]^{2+}$, from NHC–Au–Cl complexes, as monomeric precursors, in the presence of NaBH_4 acting as reducing agent (yield: 6.6% based on Au). These clusters were shown to have higher stability than the corresponding phosphine clusters toward heating treatment (Figure I-16). Moreover, naphthyl-containing nanoclusters were found to emit at 730 nm when excited at 485 nm in fluorescence studies. A quantum yield of 16.0% was obtained, which is more than twice the best QY previously reported for Au_{13} nanoclusters (Figure I-16).^{98,99}

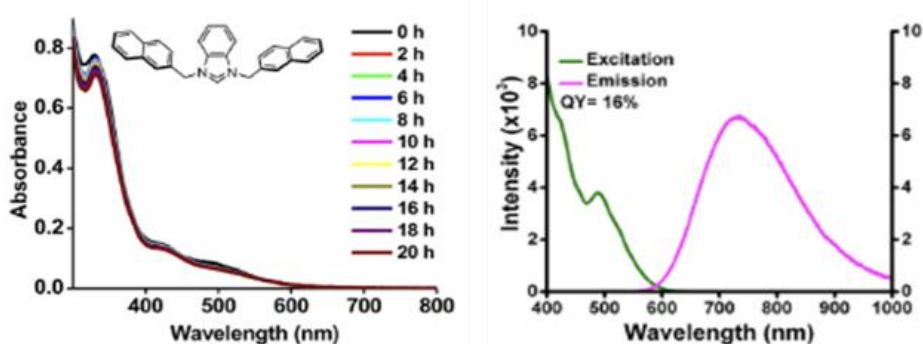


Figure I-16: UV-vis spectra of naphthyl-containing Au nanoclusters before and after 20h of heating in acetonitrile at 70 °C (left) followed by fluorescence characterization of compound (right): in pink, emission spectrum (with 485nm excitation) and in green, excitation spectrum (monitoring 730nm emission).⁹⁹

The same year, Shen *et al.* published the synthesis of $[\text{Au}_{25}(\text{}^i\text{Pr}_2\text{-bimy})_{10}\text{Br}_7]^{2+}$ ($\text{}^i\text{Pr}_2\text{-bimy}$ = 1,3-diisopropylbenzimidazolin-2-ylidene). In this case, the team used as gold precursor a mixture of AuSMe_2Cl and $\text{}^i\text{Pr}_2\text{-bimyAuBr}$, dissolved in ethanol, on which they added a fresh solution of NaBH_4 in ethanol. The reaction proceeded for 20h to give a brown AuNCs suspension. According to this team, these NCs displayed ultra-high thermal and air stability in solution, above all other reported Au_{25} NCs.¹⁰⁰

Inspired by this synthesis, the same team reported in 2021 the synthesis of $\text{Au}_{44}(\text{}^i\text{Pr}_2\text{-bimy})_9(\text{PA})_6\text{Br}_8$, which features carbenes (1,3-diisopropylbenzimidazolin-2-ylidene, $\text{}^i\text{Pr}_2\text{-bimy}$), alkynyls (phenylacetylide, PA), and halides (Br).¹⁰¹ They observed that when used as catalyst, this AuNC displays different reactivity toward different substrates. For example, it is highly efficient in hydration of aromatic alkynes, especially those bearing electron-donating groups, while it is practically inactive towards aliphatic alkynes. Failure of the hydration activity for aliphatic alkynes can be explained by the fact that they cannot be exchanged onto the surface of $\text{Au}_{44}(\text{}^i\text{Pr}_2\text{-bimy})_9(\text{PA})_6\text{Br}_8$.

For all these reported AuNCs involving carbenes as ligand, there are few similarities in the reaction conditions. Indeed, the syntheses are performed using gold-NHC complexes and sodium borohydride as a strong reducing agent.

As we can see the interest on NHC protected AuNCs is growing with interesting very recent publications on their stability and properties. The literature on NHC protected gold nanoclusters shows that their synthesis is based on the reduction of NHC-gold complexes. Mixtures of gold nanoclusters are usually obtained with both nuclearity and number of ligands varying among the species. Accordingly, characterizations are mostly done on crystallized gold nanoclusters (mass spectrometry or XDR). Indeed, there are several nanoclusters structures synthesized at the same time and crystallization, using empirical process, is the only purification process which has been reported so far for NHC protected AuNCs. In addition, the reaction yields are usually low (around 20%)¹⁰⁰ and no strategy to improve them was reported.

Our team did adopt another strategy based on the use of imidazolium salt, gold complexes and a reducing agent. Mass spectrometry of the nanoclusters mixtures was performed to follow aging of the suspension in order to study the kinetic of formation and the stability of the various obtained species. In the following study, NHCs are used as stabilizing ligands for the synthesis gold nanoclusters in Chapter III and IV and we will mainly focus our attention exclusively on imidazole-2-ylidenes and benzimidazole-2-ylidenes that are the most widely used NHC ligands.

I.D. Conclusion

To conclude, in this first chapter we reviewed the chemistry and reactivity of gold nanoclusters and the different gold nanoclusters synthesis that have been reported in the literature stabilized by various types of ligands, such as phosphines and thiolate. Also, various potential applications were presented. Moreover, we reviewed N-heterocyclic carbene (NHC) ligands synthesis methods and structures, which will be used throughout this thesis to stabilize our nanostructures. As we previously explained, their ability to act as electron donors and the resulting stable bonds to most transition metals make them excellent ligands for all kind of metallic structures, such as metallic complexes, gold nanoparticles and eventually gold nanoclusters.

One of the major challenges in gold nanoclusters characterization is finding techniques that give us precise atomic composition (nuclearity and number of ligands). The next chapter presents the various characterizations methods that were developed to obtain information on gold nanoclusters composition, structures and properties.

References

- (1) Schmid, G.; Fenske, D. Metal Clusters and Nanoparticles. *Philosophical Transactions of the Royal Society A: Mathematical, Physical and Engineering Sciences*, 2010, 368, 1207–1210.
- (2) Samsuri, N.; Mukhtar, W. M.; Abd Rashid, A. R.; Dasuki, K.; Yussuf, A. Synthesis Methods of Gold Nanoparticles for Localized Surface Plasmon Resonance (LSPR) Sensor Applications. *EPJ Web Conf.* **2017**, 162, 01002. <https://doi.org/10.1051/epjconf/201716201002>.
- (3) Li, X.; Jiang, L.; Zhan, Q.; Qian, J.; He, S. Localized Surface Plasmon Resonance (LSPR) of Polyelectrolyte-Functionalized Gold-Nanoparticles for Bio-Sensing. *Colloids Surf. Physicochem. Eng. Asp.* **2009**, 332 (2), 172–179. <https://doi.org/10.1016/j.colsurfa.2008.09.009>.
- (4) Zhu, M.; Aikens, C. M.; Hollander, F. J.; Schatz, G. C.; Jin, R. Correlating the Crystal Structure of A Thiol-Protected Au₂₅ Cluster and Optical Properties. *J. Am. Chem. Soc.* **2008**, 130 (18), 5883–5885. <https://doi.org/10.1021/ja801173r>.
- (5) Qian, H.; Zhu, M.; Wu, Z.; Jin, R. Quantum Sized Gold Nanoclusters with Atomic Precision. *Acc. Chem. Res.* **2012**, 45 (9), 1470–1479. <https://doi.org/10.1021/ar200331z>.
- (6) Yong, Y.; Li, C.; Li, X.; Li, T.; Cui, H.; Lv, S. Ag₇Au₆ Cluster as a Potential Gas Sensor for CO, HCN, and NO Detection. *J. Phys. Chem. C* **2015**, 119 (13), 7534–7540. <https://doi.org/10.1021/acs.jpcc.5b02151>.
- (7) Tian, R.; Zhang, S.; Li, M.; Zhou, Y.; Lu, B.; Yan, D.; Wei, M.; Evans, D. G.; Duan, X. Localization of Au Nanoclusters on Layered Double Hydroxides Nanosheets: Confinement-Induced Emission Enhancement and Temperature-Responsive Luminescence. *Adv. Funct. Mater.* **2015**, 25 (31), 5006–5015. <https://doi.org/10.1002/adfm.201501433>.
- (8) Zheng, J.; Zhou, C.; Yu, M.; Liu, J. Different Sized Luminescent Gold Nanoparticles. *Nanoscale* **2012**, 4 (14), 4073–4083. <https://doi.org/10.1039/C2NR31192E>.
- (9) Li, G.; Jin, R. Atomically Precise Gold Nanoclusters as New Model Catalysts. *Acc. Chem. Res.* **2013**, 46 (8), 1749–1758. <https://doi.org/10.1021/ar300213z>.
- (10) Knoppe, S.; Bürgi, T. Chirality in Thiolate-Protected Gold Clusters. *Acc. Chem. Res.* **2014**, 47 (4), 1318–1326. <https://doi.org/10.1021/ar400295d>.
- (11) Zhu, M.; Aikens, C. M.; Hendrich, M. P.; Gupta, R.; Qian, H.; Schatz, G. C.; Jin, R. Reversible Switching of Magnetism in Thiolate-Protected Au₂₅ Superatoms. *J. Am. Chem. Soc.* **2009**, 131 (7), 2490–2492. <https://doi.org/10.1021/ja809157f>.
- (12) Guan, G.; Cai, Y.; Liu, S.; Yu, H.; Bai, S.; Cheng, Y.; Tang, T.; Bharathi, M. S.; Zhang, Y.-W.; Han, M.-Y. High-Level Incorporation of Silver in Gold Nanoclusters: Fluorescence Redshift upon Interaction with Hydrogen Peroxide and Fluorescence Enhancement with Herbicide. *Chem. – Eur. J.* **2016**, 22 (5), 1675–1681. <https://doi.org/10.1002/chem.201504064>.
- (13) Kogo, A.; Sakai, N.; Tatsuma, T. Photocatalysis of Au₂₅-Modified TiO₂ under Visible and near Infrared Light. *Electrochem. Commun.* **2010**, 12 (7), 996–999. <https://doi.org/10.1016/j.elecom.2010.05.021>.
- (14) Muhammed, M. A. H.; Verma, P. K.; Pal, S. K.; Kumar, R. C. A.; Paul, S.; Omkumar, R. V.; Pradeep, T. Bright, NIR-Emitting Au₂₃ from Au₂₅: Characterization and Applications Including Biolabeling. *Chem. – Eur. J.* **2009**, 15 (39), 10110–10120. <https://doi.org/10.1002/chem.200901425>.

- (15) Qian, H.; Eckenhoff, W. T.; Bier, M. E.; Pintauer, T.; Jin, R. Crystal Structures of Au₂ Complex and Au₂₅ Nanocluster and Mechanistic Insight into the Conversion of Polydisperse Nanoparticles into Monodisperse Au₂₅ Nanoclusters. *Inorg. Chem.* **2011**, *50* (21), 10735–10739. <https://doi.org/10.1021/ic2012292>.
- (16) Lavenn, C.; Demessence, A.; Tuel, A. Au₂₅(SPh-PNH₂)₁₇ Nanoclusters Deposited on SBA-15 as Catalysts for Aerobic Benzyl Alcohol Oxidation. *J. Catal.* **2015**, *322*, 130–138. <https://doi.org/10.1016/j.jcat.2014.12.002>.
- (17) Bellon, P. L.; Cariati, F.; Manassero, M.; Naldini, L.; Sansoni, M. Novel Gold Clusters. Preparation, Properties, and X-Ray Structure Determination of Salts of Octakis(Triarylphosphine)Enneagold, [Au₉L₈]X₃. *J. Chem. Soc. Chem. Commun.* **1971**, No. 22, 1423–1424. <https://doi.org/10.1039/C29710001423>.
- (18) van der Velden, J. W. A.; Bour, J. J.; Bosman, W. P.; Noordik, J. H. Synthesis and X-Ray Crystal Structure Determination of the Cationic Gold Cluster Compound [Au₈(PPh₃)₇](NO₃)₂. *J. Chem. Soc. Chem. Commun.* **1981**, No. 23, 1218–1219. <https://doi.org/10.1039/C39810001218>.
- (19) Jin, R.; Zhu, Y.; Qian, H. Quantum-Sized Gold Nanoclusters: Bridging the Gap between Organometallics and Nanocrystals. *Chem. – Eur. J.* **2011**, *17* (24), 6584–6593. <https://doi.org/10.1002/chem.201002390>.
- (20) Kurashige, W.; Yamazoe, S.; Kanehira, K.; Tsukuda, T.; Negishi, Y. Selenolate-Protected Au₃₈ Nanoclusters: Isolation and Structural Characterization. *J. Phys. Chem. Lett.* **2013**, *4* (18), 3181–3185. <https://doi.org/10.1021/jz401770y>.
- (21) Maity, P.; Tsunoyama, H.; Yamauchi, M.; Xie, S.; Tsukuda, T. Organogold Clusters Protected by Phenylacetylene. *J. Am. Chem. Soc.* **2011**, *133* (50), 20123–20125. <https://doi.org/10.1021/ja209236n>.
- (22) Marynick, D. S. ..Pi-Accepting Abilities of Phosphines in Transition-Metal Complexes. *J. Am. Chem. Soc.* **1984**, *106* (14), 4064–4065. <https://doi.org/10.1021/ja00326a048>.
- (23) Heutz, F. J. L.; Kamer, P. C. J. Modular Solid-Phase Synthesis, Catalytic Application and Efficient Recycling of Supported Phosphine–Phosphite Ligand Libraries. *Dalton Trans.* **2016**, *45* (5), 2116–2123. <https://doi.org/10.1039/C5DT03226A>.
- (24) Musina, E. I.; Balueva, A. S.; Karasik, A. A. Phosphines: Preparation, Reactivity and Applications. In *Organophosphorus Chemistry: Volume 48*; The Royal Society of Chemistry, 2019; Vol. 48, pp 1–63. <https://doi.org/10.1039/9781788016988-00001>.
- (25) van der Slot, S. C.; Duran, J.; Luten, J.; Kamer, P. C. J.; van Leeuwen, P. W. N. M. Rhodium-Catalyzed Hydroformylation and Deuterioformylation with Pyrrolyl-Based Phosphorus Amidite Ligands: Influence of Electronic Ligand Properties. *Organometallics* **2002**, *21* (19), 3873–3883. <https://doi.org/10.1021/om010760y>.
- (26) Tolman, C. A. Electron Donor-Acceptor Properties of Phosphorus Ligands. Substituent Additivity. *J. Am. Chem. Soc.* **1970**, *92* (10), 2953–2956. <https://doi.org/10.1021/ja00713a006>.
- (27) Bilbrey, J. A.; Kazez, A. H.; Locklin, J.; Allen, W. D. Exact Ligand Cone Angles. *J. Comput. Chem.* **2013**, *34* (14), 1189–1197. <https://doi.org/10.1002/jcc.23217>.
- (28) Fey, N.; Garland, M.; Hopewell, J. P.; McMullin, C. L.; Mastroianni, S.; Orpen, A. G.; Pringle, P. G. Stable Fluorophosphines: Predicted and Realized Ligands for Catalysis. *Angew. Chem. Int. Ed Engl.* **2012**, *51* (1), 118–122. <https://doi.org/10.1002/anie.201105954>.

- (29) Konishi, K. Phosphine-Coordinated Pure-Gold Clusters: Diverse Geometrical Structures and Unique Optical Properties/Responses. *Struct. Bond.* **2014**, *161*, 49–86.
- (30) Green, M. L. H.; Parkin, G. Application of the Covalent Bond Classification Method for the Teaching of Inorganic Chemistry. *J. Chem. Educ.* **2014**, *91* (6), 807–816. <https://doi.org/10.1021/ed400504f>.
- (31) Naldini, L.; Cariati, F.; Simonetta, G.; Malatesta, L. Gold–Tertiary Phosphine Derivatives with Intermetallic Bonds. *Chem. Commun. Lond.* **1966**, No. 18, 647–648. <https://doi.org/10.1039/C19660000647>.
- (32) McPartlin, M.; Mason, R.; Malatesta, L. Novel Cluster Complexes of Gold(0)–Gold(I). *J. Chem. Soc. Chem. Commun.* **1969**, No. 7, 334–334. <https://doi.org/10.1039/C29690000334>.
- (33) Teo, B. K.; Zhang, H. Polyicosahedricity: Icosahedron to Icosahedron of Icosahedra Growth Pathway for Bimetallic (Au–Ag) and Trimetallic (Au–Ag–M; M : Pt, Pd, Ni) Supraclusters; Synthetic Strategies, Site Preference, and Stereochemical Principles. *Coord. Chem. Rev.* **1995**, *143*, 611–636. [https://doi.org/10.1016/0010-8545\(95\)01136-D](https://doi.org/10.1016/0010-8545(95)01136-D).
- (34) Teo, B. K.; Zhang, H.; Shi, X. Site Preference in Vertex-Sharing Polyicosahedral Supraclusters Containing Groups 10 and 11 Metals and Their Bonding Implications: Syntheses and Structures of the First Au–Ag–M (M = Pt, Ni) Biicosahedral Clusters [(Ph₃P)₁₀Au₁₂Ag₁₂PtCl₇]Cl and [(Ph₃P)₁₀Au₁₂Ag₁₂NiCl₇](SbF₆). *Inorg. Chem.* **1994**, *33* (18), 4086–4097. <https://doi.org/10.1021/ic00096a038>.
- (35) Zhang, S.-S.; Feng, L.; Senanayake, R. D.; Aikens, C. M.; Wang, X.-P.; Zhao, Q.-Q.; Tung, C.-H.; Sun, D. Diphosphine-Protected Ultrasmall Gold Nanoclusters: Opened Icosahedral Au₁₃ and Heart-Shaped Au₈ Clusters. *Chem. Sci.* **2018**, *9* (5), 1251–1258. <https://doi.org/10.1039/C7SC03566G>.
- (36) Nuzzo, R. G.; Fusco, F. A.; Allara, D. L. Spontaneously Organized Molecular Assemblies. 3. Preparation and Properties of Solution Adsorbed Monolayers of Organic Disulfides on Gold Surfaces. *J. Am. Chem. Soc.* **1987**, *109* (8), 2358–2368.
- (37) Akola, J.; Walter, M.; Whetten, R. L.; Häkkinen, H.; Grönbeck, H. On the Structure of Thiolate-Protected Au₂₅. *J. Am. Chem. Soc.* **2008**, *130* (12), 3756–3757. <https://doi.org/10.1021/ja800594p>.
- (38) Jadzinsky Pablo D.; Calero Guillermo; Ackerson Christopher J.; Bushnell David A.; Kornberg Roger D. Structure of a Thiol Monolayer-Protected Gold Nanoparticle at 1.1 Å Resolution. *Science* **2007**, *318* (5849), 430–433. <https://doi.org/10.1126/science.1148624>.
- (39) Shichibu, Y.; Negishi, Y.; Watanabe, T.; Chaki, N. K.; Kawaguchi, H.; Tsukuda, T. Biicosahedral Gold Clusters [Au₂₅(PPh₃)₁₀(SCnH_{2n+1})₅Cl₂]₂⁺ (n = 2–18): A Stepping Stone to Cluster-Assembled Materials. *J. Phys. Chem. C* **2007**, *111* (22), 7845–7847. <https://doi.org/10.1021/jp073101t>.
- (40) Brust, M.; Walker, M.; Bethell, D.; Schiffrin, D. J.; Whyman, R. Synthesis of Thiol-Derivatised Gold Nanoparticles in a Two-Phase Liquid–Liquid System. *J. Chem. Soc. Chem. Commun.* **1994**, No. 7, 801–802. <https://doi.org/10.1039/C39940000801>.
- (41) Negishi, Y.; Nobusada, K.; Tsukuda, T. Glutathione-Protected Gold Clusters Revisited: Bridging the Gap between Gold(I)-Thiolate Complexes and Thiolate-Protected Gold Nanocrystals. *J. Am. Chem. Soc.* **2005**, *127* (14), 5261–5270. <https://doi.org/10.1021/ja042218h>.

- (42) Duan, H.; Nie, S. Etching Colloidal Gold Nanocrystals with Hyperbranched and Multivalent Polymers: A New Route to Fluorescent and Water-Soluble Atomic Clusters. *J. Am. Chem. Soc.* **2007**, *129* (9), 2412–2413.
- (43) Schaaff, T. G.; Whetten, R. L. Controlled Etching of Au:SR Cluster Compounds. *J. Phys. Chem. B* **1999**, *103* (44), 9394–9396. <https://doi.org/10.1021/jp993229d>.
- (44) Ungor, D.; Dekany, I.; Csapó, E. Reduction of Tetrachloroaurate(III) Ions With Bioligands: Role of the Thiol and Amine Functional Groups on the Structure and Optical Features of Gold Nanohybrid Systems. *Nanomaterials* **2019**, *9*, 1229. <https://doi.org/10.3390/nano9091229>.
- (45) Lin, C.-A. J.; Yang, T.-Y.; Lee, C.-H.; Huang, S. H.; Sperling, R. A.; Zanella, M.; Li, J. K.; Shen, J.-L.; Wang, H.-H.; Yeh, H.-I. Synthesis, Characterization, and Bioconjugation of Fluorescent Gold Nanoclusters toward Biological Labeling Applications. *ACS Nano* **2009**, *3* (2), 395–401.
- (46) Zhu, M.; Lanni, E.; Garg, N.; Bier, M. E.; Jin, R. Kinetically Controlled, High-Yield Synthesis of Au₂₅ Clusters. *J. Am. Chem. Soc.* **2008**, *130* (4), 1138–1139. <https://doi.org/10.1021/ja0782448>.
- (47) Qian, H.; Jin, R. Controlling Nanoparticles with Atomic Precision: The Case of Au₁₄₄(SCH₂CH₂Ph)₆₀. *Nano Lett.* **2009**, *9* (12), 4083–4087. <https://doi.org/10.1021/nl902300y>.
- (48) Wu, Z.; Suhan, J.; Jin, R. One-Pot Synthesis of Atomically Monodisperse, Thiol-Functionalized Au₂₅ Nanoclusters. *J. Mater. Chem.* **2009**, *19* (5), 622–626. <https://doi.org/10.1039/B815983A>.
- (49) Wu, Z.; MacDonald, M. A.; Chen, J.; Zhang, P.; Jin, R. Kinetic Control and Thermodynamic Selection in the Synthesis of Atomically Precise Gold Nanoclusters. *J. Am. Chem. Soc.* **2011**, *133* (25), 9670–9673. <https://doi.org/10.1021/ja2028102>.
- (50) Qian, H.; Eckenhoff, W. T.; Zhu, Y.; Pintauer, T.; Jin, R. Total Structure Determination of Thiolate-Protected Au₃₈ Nanoparticles. *J. Am. Chem. Soc.* **2010**, *132* (24), 8280–8281. <https://doi.org/10.1021/ja103592z>.
- (51) Qian, H.; Jin, R. Synthesis and Electrospray Mass Spectrometry Determination of Thiolate-Protected Au₅₅(SR)₃₁ Nanoclusters. *Chem. Commun.* **2011**, *47* (41), 11462–11464. <https://doi.org/10.1039/C1CC15099E>.
- (52) Levi-Kalishman, Y.; Jadzinsky, P. D.; Kalishman, N.; Tsunoyama, H.; Tsukuda, T.; Bushnell, D. A.; Kornberg, R. D. Synthesis and Characterization of Au₁₀₂(p-MBA)₄₄ Nanoparticles. *J. Am. Chem. Soc.* **2011**, *133* (9), 2976–2982. <https://doi.org/10.1021/ja109131w>.
- (53) Negishi, Y.; Hashimoto, S.; Ebina, A.; Hamada, K.; Hossain, S.; Kawawaki, T. Atomic-Level Separation of Thiolate-Protected Metal Clusters. *Nanoscale* **2020**, *12* (15), 8017–8039. <https://doi.org/10.1039/D0NR00824A>.
- (54) Jin, R.; Zeng, C.; Zhou, M.; Chen, Y. Atomically Precise Colloidal Metal Nanoclusters and Nanoparticles: Fundamentals and Opportunities. *Chem. Rev.* **2016**, *116* (18), 10346–10413. <https://doi.org/10.1021/acs.chemrev.5b00703>.
- (55) Li, J.; Nasaruddin, R. R.; Feng, Y.; Yang, J.; Yan, N.; Xie, J. Tuning the Accessibility and Activity of Au₂₅(SR)₁₈ Nanocluster Catalysts through Ligand Engineering. *Chem. – Eur. J.* **2016**, *22* (42), 14816–14820. <https://doi.org/10.1002/chem.201603247>.
- (56) Nie, X.; Qian, H.; Ge, Q.; Xu, H.; Jin, R. CO Oxidation Catalyzed by Oxide-Supported Au₂₅(SR)₁₈ Nanoclusters and Identification of Perimeter Sites as Active Centers. *ACS Nano* **2012**, *6* (7), 6014–6022. <https://doi.org/10.1021/nn301019f>.

- (57) Wu, Z.; Jiang, D.; Mann, A. K. P.; Mullins, D. R.; Qiao, Z.-A.; Allard, L. F.; Zeng, C.; Jin, R.; Overbury, S. H. Thiolate Ligands as a Double-Edged Sword for CO Oxidation on CeO₂ Supported Au₂₅(SCH₂CH₂Ph)₁₈ Nanoclusters. *J. Am. Chem. Soc.* **2014**, *136* (16), 6111–6122. <https://doi.org/10.1021/ja5018706>.
- (58) Li, Y.; Chen, Y.; House, S. D.; Zhao, S.; Wahab, Z.; Yang, J. C.; Jin, R. Interface Engineering of Gold Nanoclusters for CO Oxidation Catalysis. *ACS Appl. Mater. Interfaces* **2018**, *10* (35), 29425–29434. <https://doi.org/10.1021/acsami.8b07552>.
- (59) Shang, L.; Dörlich, R. M.; Brandholt, S.; Schneider, R.; Trouillet, V.; Bruns, M.; Gerthsen, D.; Nienhaus, G. U. Facile Preparation of Water-Soluble Fluorescent Gold Nanoclusters for Cellular Imaging Applications. *Nanoscale* **2011**, *3* (5), 2009–2014. <https://doi.org/10.1039/C0NR00947D>.
- (60) Nuzzo, R. G.; Zegarski, B. R.; Dubois, L. H. Fundamental Studies of the Chemisorption of Organosulfur Compounds on Gold (111). Implications for Molecular Self-Assembly on Gold Surfaces. *J. Am. Chem. Soc.* **1987**, *109* (3), 733–740.
- (61) Rao, C. N. R. *Trends in Chemistry of Materials: Selected Research Papers of CNR Rao*; World Scientific, 2008; Vol. 1.
- (62) Marchione, D.; Belpassi, L.; Bistoni, G.; Macchioni, A.; Tarantelli, F.; Zuccaccia, D. The Chemical Bond in Gold(I) Complexes with N-Heterocyclic Carbenes. *Organometallics* **2014**, *33* (16), 4200–4208. <https://doi.org/10.1021/om5003667>.
- (63) Bridonneau, N.; Hippolyte, L.; Mercier, D.; Portehault, D.; Murr, M.; Marcus, P.; Fensterbank, L.; Chanéac, C.; Ribot, F. N-Heterocyclic Carbene-Stabilized Gold Nanoparticles with Tunable Sizes. *Dalton Trans.* **2018**, *47*. <https://doi.org/10.1039/C8DT00416A>.
- (64) Man, R. W. Y.; Li, C.-H.; MacLean, M. W. A.; Zenkina, O. V.; Zamora, M. T.; Saunders, L. N.; Rousina-Webb, A.; Nambo, M.; Crudden, C. M. Ultrastable Gold Nanoparticles Modified by Bidentate N-Heterocyclic Carbene Ligands. *J. Am. Chem. Soc.* **2018**, *140* (5), 1576–1579. <https://doi.org/10.1021/jacs.7b08516>.
- (65) Herrmann, W. A. N-Heterocyclic Carbenes: A New Concept in Organometallic Catalysis. *Angew. Chem. Int. Ed.* **2002**, *41* (8), 1290–1309. [https://doi.org/10.1002/1521-3773\(20020415\)41:8<1290::AID-ANIE1290>3.0.CO;2-Y](https://doi.org/10.1002/1521-3773(20020415)41:8<1290::AID-ANIE1290>3.0.CO;2-Y).
- (66) Slaughter, L. M. Acyclic Aminocarbenes in Catalysis. *ACS Catal.* **2012**, *2* (8), 1802–1816. <https://doi.org/10.1021/cs300300y>.
- (67) Kirmse, W. The Beginnings of N-Heterocyclic Carbenes. *Angew. Chem. Int. Ed.* **2010**, *49* (47), 8798–8801. <https://doi.org/10.1002/anie.201001658>.
- (68) Huynh, H. V. Electronic Properties of N-Heterocyclic Carbenes and Their Experimental Determination. *Chem. Rev.* **2018**, *118* (19), 9457–9492. <https://doi.org/10.1021/acs.chemrev.8b00067>.
- (69) Denk, M. K.; Hatano, K.; Ma, M. E. Nucleophilic Carbenes and the Wanzlick Equilibrium: A Reinvestigation. *Tetrahedron Lett.* **1999**, *40*, 2057–2060.
- (70) Hopkinson, M. N.; Richter, C.; Schedler, M.; Glorius, F. An Overview of N-Heterocyclic Carbenes. *Nature* **2014**, *510* (7506), 485–496. <https://doi.org/10.1038/nature13384>.
- (71) Morales-Morales, D.; Jensen, C. G. *The Chemistry of Pincer Compounds*; Elsevier, 2011.
- (72) Dröge, T.; Glorius, F. The Measure of All Rings—N-Heterocyclic Carbenes. *Angew. Chem. Int. Ed.* **2010**, *49* (39), 6940–6952. <https://doi.org/10.1002/anie.201001865>.

- (73) Arduengo, A. J.; Harlow, R. L.; Kline, M. A Stable Crystalline Carbene. *J. Am. Chem. Soc.* **1991**, *113* (1), 361–363. <https://doi.org/10.1021/ja00001a054>.
- (74) Lavallo, V.; Canac, Y.; Präsang, C.; Donnadieu, B.; Bertrand, G. Stable Cyclic (Alkyl)(Amino)Carbenes as Rigid or Flexible, Bulky, Electron-Rich Ligands for Transition-Metal Catalysts: A Quaternary Carbon Atom Makes the Difference. *Angew. Chem. Int. Ed Engl.* **2005**, *44* (35), 5705–5709. <https://doi.org/10.1002/anie.200501841>.
- (75) Kelemen, Z.; Hollóczki, O.; Oláh, J.; Nyulászi, L. Oxazol-2-Ylidenes. A New Class of Stable Carbenes? *RSC Adv.* **2013**, *3* (21), 7970–7978. <https://doi.org/10.1039/C3RA41177J>.
- (76) Kinjo, R.; Donnadieu, B.; Bertrand, G. Gold-Catalyzed Hydroamination of Alkynes and Allenes with Parent Hydrazine. *Angew. Chem.* **2011**, *123* (24), 5674–5677.
- (77) Kinjo, R.; Donnadieu, B.; Bertrand, G. Gold-Catalyzed Hydroamination of Alkynes and Allenes with Parent Hydrazine. *Angew. Chem.* **2011**, *123* (24), 5674–5677.
- (78) Hahn, F. E.; Jahnke, M. C. Heterocyclic Carbenes: Synthesis and Coordination Chemistry. *Angew. Chem. Int. Ed Engl.* **2008**, *47* (17), 3122–3172. <https://doi.org/10.1002/anie.200703883>.
- (79) Nesterov, V.; Reiter, D.; Bag, P.; Frisch, P.; Holzner, R.; Porzelt, A.; Inoue, S. NHCs in Main Group Chemistry. *Chem. Rev.* **2018**, *118* (19), 9678–9842. <https://doi.org/10.1021/acs.chemrev.8b00079>.
- (80) Vaddamanu, M.; Sathyanarayana, A.; Masaya, Y.; Sugiyama, S.; Kazuhisa, O.; Velappan, K.; Nandeshwar, M.; Hisano, K.; Tsutsumi, O.; Prabusankar, G. Acridine N-Heterocyclic Carbene Gold(I) Compounds: Tuning from Yellow to Blue Luminescence. *Chem. Asian J.* **2021**, *16* (5), 521–529. <https://doi.org/10.1002/asia.202001380>.
- (81) Enders, D.; Breuer, K.; Raabe, G.; Runsink, J.; Teles, J. H.; Melder, J.-P.; Ebel, K.; Brode, S. Preparation, Structure, and Reactivity of 1, 3, 4-Triphenyl-4, 5-dihydro-1H-1, 2, 4-triazol-5-ylidene, a New Stable Carbene. *Angew. Chem. Int. Ed. Engl.* **1995**, *34* (9), 1021–1023.
- (82) Collado, A.; Gómez-Suárez, A.; Martin, A. R.; Slawin, A. M. Z.; Nolan, S. P. Straightforward Synthesis of [Au(NHC)X] (NHC = N-Heterocyclic Carbene, X = Cl, Br, I) Complexes. *Chem. Commun.* **2013**, *49* (49), 5541–5543. <https://doi.org/10.1039/C3CC43076F>.
- (83) Visbal, R.; Laguna, A.; Gimeno, M. C. Simple and Efficient Synthesis of [MCl(NHC)] (M = Au, Ag) Complexes. *Chem. Commun.* **2013**, *49* (50), 5642–5644. <https://doi.org/10.1039/C3CC42919A>.
- (84) Gimeno, M.; Johnson, A. An Efficient and Sustainable Synthesis of NHC Gold Complexes. *Chem Commun* **2016**, *52*. <https://doi.org/10.1039/C6CC05190A>.
- (85) Hameury, S.; de Frémont, P.; R. Breuil, P.-A.; Olivier-Bourbigou, H.; Braunstein, P. Synthesis and Characterization of Oxygen-Functionalised-NHC Silver(i) Complexes and NHC Transmetalation to Nickel(II). *Dalton Trans.* **2014**, *43* (12), 4700–4710. <https://doi.org/10.1039/C3DT52773E>.
- (86) Lin, I. J. B.; Vasam, C. S. Preparation and Application of N-Heterocyclic Carbene Complexes of Ag(I). *Coord. Chem. Rev.* **2007**, *251* (5), 642–670. <https://doi.org/10.1016/j.ccr.2006.09.004>.
- (87) Cure, J.; Poteau, R.; Gerber, I.; Gornitzka, H.; Hemmert, C. Dimeric Gold Bis(Carbene) Complexes by Transmetalation in Water. *Organometallics* **2012**, *31*. <https://doi.org/10.1021/om2009183>.
- (88) Furst, M. R. L.; Cazin, C. S. J. Copper N-Heterocyclic Carbene (NHC) Complexes as Carbene Transfer Reagents. *Chem. Commun.* **2010**, *46* (37), 6924–6925. <https://doi.org/10.1039/C0CC02308F>.

- (89) Wang, H. M.; Lin, I. J. Facile Synthesis of Silver (I)–Carbene Complexes. Useful Carbene Transfer Agents. *Organometallics* **1998**, *17* (5), 972–975.
- (90) Love, J. A.; Morgan, J. P.; Trnka, T. M.; Grubbs, R. H. A Practical and Highly Active Ruthenium-Based Catalyst That Effects the Cross Metathesis of Acrylonitrile. *Angew. Chem. Int. Ed Engl.* **2002**, *41* (21), 4035–4037. [https://doi.org/10.1002/1521-3773\(20021104\)41:21<4035::AID-ANIE4035>3.0.CO;2-I](https://doi.org/10.1002/1521-3773(20021104)41:21<4035::AID-ANIE4035>3.0.CO;2-I).
- (91) Visbal, R.; Gimeno, M. C. N-Heterocyclic Carbene Metal Complexes: Photoluminescence and Applications. *Chem. Soc. Rev.* **2014**, *43* (10), 3551–3574. <https://doi.org/10.1039/C3CS60466G>.
- (92) Liu, B.; Javed, M. A.; Guo, J.; Xu, W.; Brown, S. L.; Ugrinov, A.; Hobbie, E. K.; Kilina, S.; Qin, A.; Sun, W. Neutral Cyclometalated Iridium(III) Complexes Bearing Substituted N-Heterocyclic Carbene (NHC) Ligands for High-Performance Yellow OLED Application. *Inorg. Chem.* **2019**, *58* (21), 14377–14388. <https://doi.org/10.1021/acs.inorgchem.9b01678>.
- (93) Durmaz, R.; Kucukbay, H.; Cetinkaya, E.; Çetinkaya, B. Antimicrobial Activity of Rhodium (I) and Ruthenium (II) Carbene Complexes Derived from Benzimidazole against Staphylococcus Aureus Isolates. *Turk. J. Med. Sci.* **1997**, *27*, 59–61.
- (94) Hartinger, C. G.; Dyson, P. J. Bioorganometallic Chemistry—from Teaching Paradigms to Medicinal Applications. *Chem. Soc. Rev.* **2009**, *38* (2), 391–401. <https://doi.org/10.1039/B707077M>.
- (95) Wai-Yin Sun, R.; Lok-Fung Chow, A.; Li, X.-H.; Yan, J. J.; Sin-Yin Chui, S.; Che, C.-M. Luminescent Cyclometalated Platinum(II) Complexes Containing N-Heterocyclic Carbene Ligands with Potent in Vitro and in Vivo Anti-Cancer Properties Accumulate in Cytoplasmic Structures of Cancer Cells. *Chem. Sci.* **2011**, *2* (4), 728–736. <https://doi.org/10.1039/C0SC00593B>.
- (96) Bertrand, B.; Stefan, L.; Pirrotta, M.; Monchaud, D.; Bodio, E.; Richard, P.; Le Gendre, P.; Warmerdam, E.; de Jager, M. H.; Groothuis, G. M. M.; Picquet, M.; Casini, A. Caffeine-Based Gold(I) N-Heterocyclic Carbenes as Possible Anticancer Agents: Synthesis and Biological Properties. *Inorg. Chem.* **2014**, *53* (4), 2296–2303. <https://doi.org/10.1021/ic403011h>.
- (97) Narouz, M. R.; Osten, K. M.; Unsworth, P. J.; Man, R. W. Y.; Salorinne, K.; Takano, S.; Tomihara, R.; Kaappa, S.; Malola, S.; Dinh, C.-T.; Padmos, J. D.; Ayoo, K.; Garrett, P. J.; Nambo, M.; Horton, J. H.; Sargent, E. H.; Häkkinen, H.; Tsukuda, T.; Crudden, C. M. N-Heterocyclic Carbene-Functionalized Magic-Number Gold Nanoclusters. *Nat. Chem.* **2019**, *11* (5), 419–425. <https://doi.org/10.1038/s41557-019-0246-5>.
- (98) Shichibu, Y.; Konishi, K. HCl-Induced Nuclearity Convergence in Diphosphine-Protected Ultrasmall Gold Clusters: A Novel Synthetic Route to “Magic-Number” Au₁₃ Clusters. *Small* **2010**, *6* (11), 1216–1220. <https://doi.org/10.1002/sml.200902398>.
- (99) Narouz, M. R.; Takano, S.; Lummis, P. A.; Levchenko, T. I.; Nazemi, A.; Kaappa, S.; Malola, S.; Yousefalizadeh, G.; Calhoun, L. A.; Stampelcoskie, K. G.; Häkkinen, H.; Tsukuda, T.; Crudden, C. M. Robust, Highly Luminescent Au₁₃ Superatoms Protected by N-Heterocyclic Carbenes. *J. Am. Chem. Soc.* **2019**, *141* (38), 14997–15002. <https://doi.org/10.1021/jacs.9b07854>.
- (100) Shen, H.; Deng, G.; Kaappa, S.; Tan, T.; Han, Y.-Z.; Malola, S.; Lin, S.-C.; Teo, B. K.; Häkkinen, H.; Zheng, N. Highly Robust but Surface-Active: An N-Heterocyclic Carbene-Stabilized Au₂₅ Nanocluster. *Angew. Chem. Int. Ed.* **2019**, *58* (49), 17731–17735. <https://doi.org/10.1002/anie.201908983>.
- (101) Shen, H.; Xu, Z.; Hazer, M. S. A.; Wu, Q.; Peng, J.; Qin, R.; Malola, S.; Teo, B. K.; Häkkinen, H.; Zheng, N. Surface Coordination of Multiple Ligands Endows N-Heterocyclic Carbene-

State of the art on gold nanoclusters

Stabilized Gold Nanoclusters with High Robustness and Surface Reactivity. *Angew. Chem. Int. Ed.* **2021**, *60* (7), 3752–3758. <https://doi.org/10.1002/anie.202013718>.

CHAPTER II: Gold nanoclusters characterization developments

Gold nanoclusters are quite difficult to characterize due to their specificity, an intermediate state between molecules and nanoparticles. There are well-established analytical techniques used to obtain information on the composition of AuNCs and information on their structure (*such as*: transmission electron microscopy (TEM), X-Ray diffraction (XRD), *but also*: X-Ray photoelectron spectrometry (XPS) ...). However, they are not always accurate enough to address all information such as size, chemical composition and structure or they are not easy to execute. Hence, there is an interest to develop further characterization techniques. Two particular techniques have been used: (i) UV-Vis spectroscopy which is fast and allows us to know if we have clusters (absence of plasmon absorption peak) or nanoparticles (presence of plasmon absorption peak) and (ii) mass spectrometry which allows us to obtain the chemical composition of the mixture without discriminating the species (as opposed to other techniques such as diffraction on monocrystals where we only saw the specie in a mixture of metallic clusters that crystallizes) and to obtain the chemical formula of the clusters.

II.A. UV-Vis spectroscopy and X-Ray diffraction crystallography contribution for gold nanoclusters characterization

II.A.1. Theoretical and experimental UV-Vis spectroscopy studies of gold nanoclusters

Nanoclusters stand out to gold nanoparticles. Indeed, gold nanoparticles have a metallic state characterized by plasmonic excitations, while nanoclusters exhibit a molecular state with discrete energy levels and particular single electron transitions. Nanoclusters are therefore, situated in between gold nanoparticles and molecular complexes. This size domain is interesting to study the size effects on catalytic activities, for example. Indeed, obtaining monodispersed nanoclusters is one of the objectives for catalysis, to have a better fundamental understanding of the mechanisms involved.

The ultra-small size of nanoclusters generates quantum confinement effects which result in discrete energy levels transitions visible on UV-Vis spectroscopy (Figure II-1). These single electron transitions of HOMO-LUMO type are different from the collective mode of electron excitation encountered in the localized surface plasmon resonance (LSPR) characteristic of gold nanoparticles. In terms of applications, the discrete energy level structure of these nanoclusters conduct the availability of electrons for redox processes and the interactions with the adsorbate reactant molecules in catalytic processes, for example. The free-electron model can be referred for describing gold nanoclusters, even though it is an approximation since it doesn't take into account the surface effects and the influence of the ligands on the electronic structure.¹

2 nm is approximatively the particle size, at and below which, quantum confinement effects dominate over surface plasmon resonance (Figure II-1). The optical properties in absorption are characteristic of the HOMO-LUMO transitions of nanoclusters molecular orbitals diagram (Figure II-2).¹

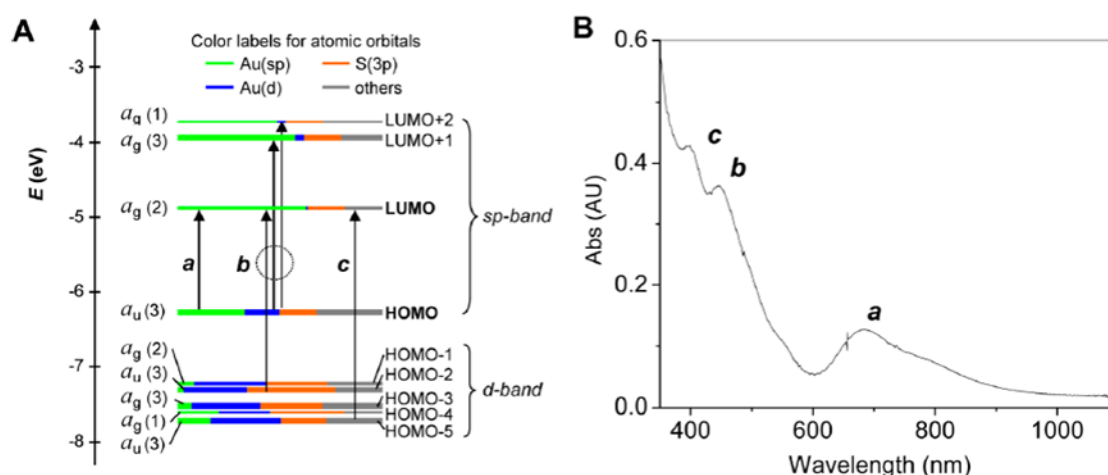


Figure II-1 (A) Kohn-Sham orbital level diagram and (B) peak assignment for the UV-Vis absorption spectrum of $[Au_{25}(SR)_{18}]^-$ nanoclusters.¹

Jin *et al.* revealed three bands located at 688, 450 and 400 nm on the optical absorption spectrum of the well known $Au_{25}(SCH_2CH_2Ph)_{18}^-$ gold nanocluster.² TD-DFT (Time-dependent density-functional theory) experiments showed that the optical bands were due to particular excitations. For example, the band at 688 nm was due to HOMO-LUMO excitation (Figure II-1). Also, adding 13 gold atoms in the gold nanocluster completely modify the metal core structure thus the optical properties. Indeed, Tsunoyama *et al.* reported the UV-Vis spectrum of gold nanocluster $Au_{38}(SR)_{24}$.³ For this nanocluster the lowest energy transition was at 1370 nm and corresponded to HOMO-LUMO excitation. It means that depending on their stoichiometry gold nanoclusters show a specific profile of the absorption spectra. The optical absorption spectra cannot be understood as a simple linear combination of the core and ligands spectra. It was proven that gold nanoclusters UV-Vis spectra are strongly influenced by the Au-Au length in their inner metal cores. However, the electronic interactions of the ligands with the core also influence the orbital energies and hence the optical absorption spectra.^{2,4} Other studies, reported by Lugo *et al.*, unveiled that the charge redistribution between the gold core and the ligand shell can be controlled by the electron donor or acceptor character of the protecting ligands.^{5,6} This has a direct effect on the UV-Vis spectra because the more negative the partial charge of the metal core is, the more the spectrum will be red shifted. To conduct this study on the effect of the global charge states, the team used thiolate protected Au_{25} nanoclusters as models.

They discussed three cluster models: cluster $Au_{25}(SCH_3)_{18}^{-1}$, cluster $Au_{25}(SCH_3)_{18}^{+1}$ and cluster $Au_{25}(SPh)_{18}^{-1}$. They calculated the Au_{13} icosahedral core partial charges for all of them (Figure II-2).

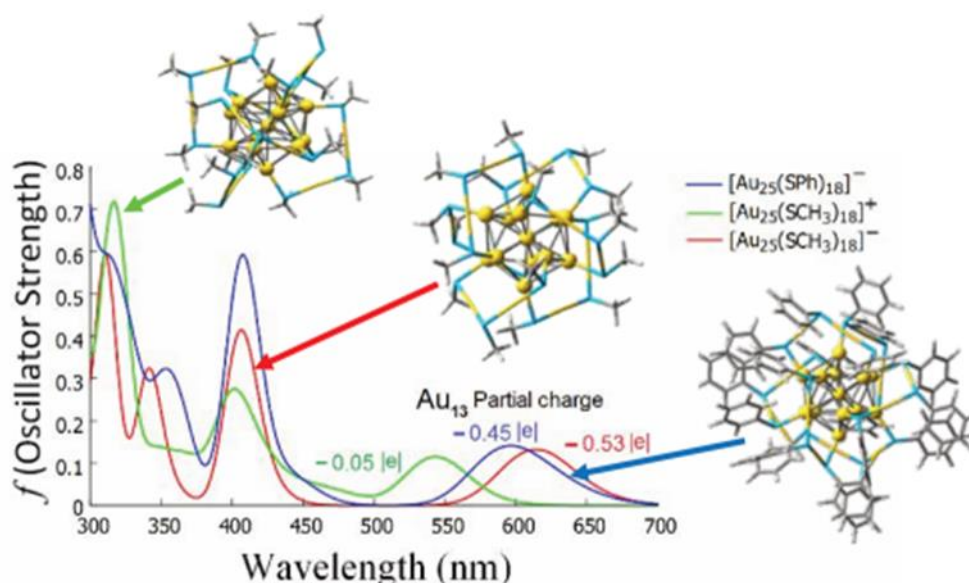


Figure II-2 DT-DFT computed optical absorption spectra of the anions $\text{Au}_{25}(\text{SCH}_3)_{18}^-$, $\text{Au}_{25}(\text{SPh})_{18}^-$ and the cation $\text{Au}_{25}(\text{SCH}_3)_{18}^+$.⁶

Thus, it seems possible by UV-Vis spectroscopy analysis to gain major information on the nanoclusters optical properties and on the effect of the different protecting ligands. In our case, this characterization technique could help identifying very rapidly the formation of gold nanoclusters (opposed to formation of nanoparticles) or assess the electron donating or withdrawing ability of the ligands for example.

This technique has also limitations since, the details regarding interfacial electronic interactions, electronic structure of the nanoclusters, and environmental perturbations are difficult to extract from experimental spectra. Indeed, broadening effects common to electronic spectroscopy, environmental heterogeneity, ligand dissociation equilibria, and sample impurities contribute to the breadth of the line shapes on the experimental spectra. Without well-defined features in these spectra, comparison to theoretically predicted electronic spectra is very difficult and no conclusions on potential electronic properties trends can be made.⁷ Several options have been tested to solve this problem such as the cooling of gold nanoclusters to cryogenic temperatures reported by Ramakrishna *et al.* They demonstrated that cooling considerably sharpens the UV-Vis absorption spectra, implying that thermal vibrational broadening greatly reduces the spectral details observed in room temperature measurements.⁸ Also, Negishi *et al.* showed that chromatographic separation of mixtures improves the resolution of the UV-Vis spectra.⁹ When direct experimental determination is not possible, much of the knowledge of features of gold nanoclusters electronic structure comes from the use of DFT.¹⁰ Other characterization techniques have been developed to increase knowledge on gold nanoclusters structural properties such as X-Ray crystallography.

II.A.2. X-Ray crystallography studies on gold nanoclusters

X-ray crystallography has long been used in molecular chemistry for the structure determination of organic molecules, proteins and organometallic compounds. The use of X-Ray crystallography on gold nanoclusters has been a major breakthrough as it allowed to obtain precise gold nanocluster structure and gold atoms/ligand positions relative to each other. The X-Ray crystals determination confirmed the predicted hypothesis obtained through theoretical methods (DFT) most of the time. For example, X-Ray crystallography performed on $[\text{Au}_{25}(\text{L})_{18}]^-$ (L =ligand) nanoclusters with various ligands showed that each nanoclusters organize into different patterns due to different inter-ligand interactions, albeit the Au_{25} core is the same (Figure II-3).¹¹ For thiols protected Au_{25} NCs, $[\text{Au}_{25}(\text{L})_{18}]^-$ is composed of 25 gold atoms and has 13 atoms icosahedron inner core that remains the same in various $[\text{Au}_{25}(\text{L})_{18}]^-$ formulation with different types of ligands.^{2,12} The remaining 12 atoms of gold go to the surface and form 6 dimeric staple-like motifs: $-\text{L}-\text{Au}-\text{L}-\text{Au}-\text{L}-$ (Figure II-3). In the structure of $[\text{Au}_{25}(\text{SC}_2\text{H}_4\text{Ph})_{18}]^-$ (Figure II-3), the ligands are less crowdedly arranged on the surface along the C_3 axis, exposing two “pockets” cavities.² These “pockets” were identified to be the active sites for electrochemical reduction of CO_2 .¹³ In comparison, for $[\text{Au}_{25}(\text{SC}_{10}\text{H}_7)_{18}]^-$ (SC_7H_{10} = 1-naphthalenethiolate), which has the same stoichiometry (both $\text{Au}_{25}\text{SR}_{18}$) as $[\text{Au}_{25}(\text{SC}_2\text{H}_4\text{Ph})_{18}]^-$, the ligand shell displays non-covalent interactions between the 1-naphthalene groups involving π - π stacking (Figure II-3).¹⁴ In the structure of Au_{25} , there are 6 pairs of $-\text{L}-\text{Au}-\text{L}-\text{Au}-\text{L}-$ dimeric staples, which makes 18 ligands. There are 6 pairs of ligands in π - π interaction, and 6 other ligands localized in the equator of the core (Figure II-3). The 6 pairs of π - π stacked ligands are found by X-Ray crystallography to be around the quasi- C_3 axis of the Au_{25} core and covers the two “pockets” at the top and bottom. This structural difference would probably affect its catalytic activity. Moreover, in addition to the different patterns caused by the different interactions between thiolate ligands, a structural rearrangement of the six $-\text{L}-\text{Au}-\text{L}-\text{Au}-\text{L}-$ motifs can happen on the icosahedral Au_{13} inner core. It was reported for the nanocluster $[\text{Au}_{25}(\text{C}\equiv\text{CPh}(\text{CF}_3)_2)_{18}]^-$, where $-\text{C}\equiv\text{C}-\text{Au}$ motifs are almost linear. Indeed, alkynyl ligands adopt a more stretched conformation along the surface, compared to thiolate ligands.¹¹ If the alkynyl protected Au_{25} would adopt the same ligand pattern as of thiolate protected Au_{25} nanoclusters, unreasonable contacts between phenyl groups would occur. The steric hindrance of alkynyl ligands is responsible here for the D_3 arrangement of this Au_{25} nanocluster.

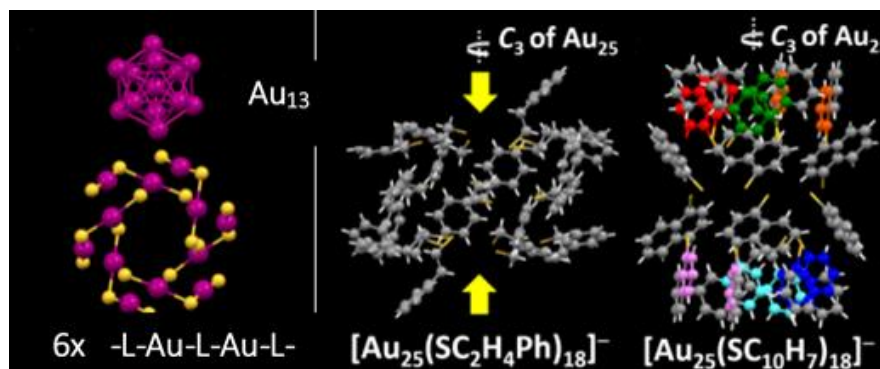


Figure II-3 The structure of $\text{Au}_{25}\text{L}_{18}$ core (L = ligand). Different patterns formed by ligands on the surface of $[\text{Au}_{25}(\text{L})_{18}]^-$ for $[\text{Au}_{25}(\text{SC}_2\text{H}_4\text{Ph})_{18}]^-$ and $[\text{Au}_{25}(\text{SC}_{10}\text{H}_7)_{18}]^-$.¹¹

Gold nanoclusters characterization developments

Single crystal X-Ray diffraction study is a good characterization method to obtain gold nanoclusters structure and accordingly their formula. It also allows association of the gold nanoclusters structure to their properties. It shows the influence of interaction with ligands on the structure (ligand conformation and also general structure rearrangements). Thanks to X-Ray crystallography even bigger gold nanocluster structures were revealed such as Au₁₄₄(SR)₆₀ nanocluster.¹⁵

The highest challenge relies on how to obtain single crystals of high quality, especially with very bulky or long chained ligands. Also, with crystallization we only look at what crystallizes and it is not necessarily characteristic of every species in solution, especially in the case of clusters mixture. To be able to precisely study the type of gold nanoclusters that are synthesized in our protocols, we chose another characterization method that does not require crystals and can directly be used on suspensions: mass spectrometry.

Whetten *et al.* did work to determine the chemical composition of gold nanoclusters in the 1-3 nm size range, using mass spectrometry in the 10–300 kDa mass range.¹⁶ Since then, MS has been growingly used for the characterization of various types of metallic nanoclusters. Most MS analyses conducted on gold nanoclusters were done using either ESI or MALDI ionization sources in both positive and negative modes.^{17,18}

II.B. Mass spectrometry purpose and development for the analysis of gold nanoclusters

Mass spectrometry is based on the analysis of ions in gas phase formed, for instance, by protonation or deprotonation of the species of interest. As a result, it gives [M-H]⁺ cations or [M-H]⁻ anions (M = specie of interest) in positive and negative mode respectively. Charging may also be induced by intake of small ions such as of Na⁺ or K⁺. It can also give fragmented parts of the species due to the strong ionization. The mass measurement relies on the ability of electric and magnetic fields to separate charged particles based on their mass to charge ratio (m/z).¹⁹ The ions are then detected and the information processed to display the mass spectrum. The mass spectra show the relative abundance (it is relative abundance of the ions in the gas phase one to another and not the amount of the species in the starting material) on the Y axis and the mass to charge ratio on the X axis. As one can imagine the product is not preserved during the analysis by mass spectrometry. However, it is not critical since this technique consumes very minute quantities of product (µg and less).

Globally, a typical mass analyzer is composed of (Figure II-4):

- a device that volatilize and ionize the species into a cloud of charged particles (under high vacuum or at atmospheric pressure)
- a mass analyzer that separates ions according to their mass-to-charge ratio (under high vacuum)
- a detector that records the ions relative intensity (under high vacuum) with a data analyzer and computer to display the mass spectrum

In some mass spectrometers the analyzer and the detector form one element (analyzer-detector).

Gold nanoclusters characterization developments

There are different types of each devices that compose a mass spectrometers. Each combination has advantages and disadvantages, depending on the type of compounds that must be analyzed.²⁰ For example, there are quadrupole, time of flight–or ion trapping based mass analyzers. The mass spectrum that is obtained is optimized to determine the specie composition. It can also give information on the structure (through fragmentation of the species, for example). Moreover, when the analyzed compound has been databased (into repertories) it is easier to find its structure.

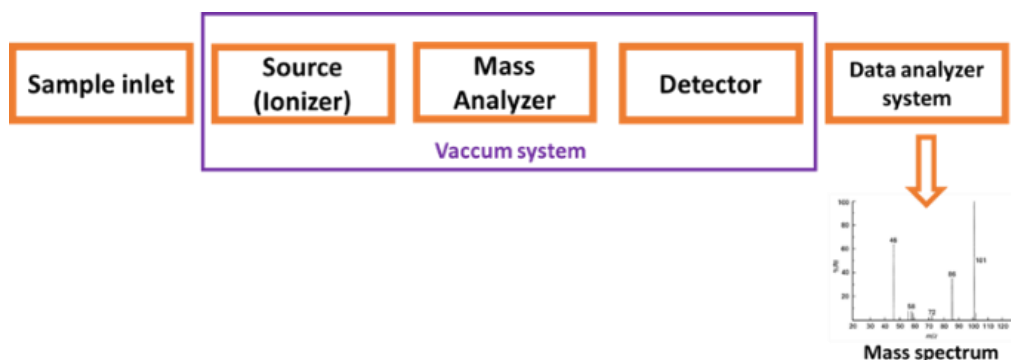


Figure II-4 Set-up of a Mass Spectrometer with the different components.

In this thesis, the samples ionization was done by electrospray ionization (ESI). Several mass analyzers have been tested with a focus on Time of Flight (TOF) and Fourier-transform ion cyclotron resonance (FT-ICR).

II.B.1. ESI-QTOF mass spectrometry

II.B.1.a. ESI ionization source

The electrospray ionization source was created by Fenn *et al.* in 1984 to analyze high mass compounds that cannot be accessed by conventional ion sources.²¹ The interest of this source relies on the fact that it is quite simple in use, requires a low quantity of product and allows to limit the fragmentation of molecules in the source. Also, this source is a soft ionization source allowing easy observation of the precursor ions, which is not the case for conventional source like electronic impact ionization.²² Therefore, weak bonds such as non-covalent bonds are preserved in the gas phase. Moreover, it allows to observe compounds of high mass and charge. ESI ionization allows the transformation of the liquid phase sample to a gaseous phase sample while charging the molecules (positively or negatively depending on the mode of use of the spectrometer). A volatile solvent (methanol, etc.) facilitates desolvation during ionization.

Basically, ESI works as followed: a dilute solution of the compound of interest is introduced at a low rate (a few $\mu\text{L}/\text{min}$) into a metal capillary using for instance a syringe pump. A high electrical voltage is applied between the metal capillary and the inlet of the mass spectrometer, usually from 2 to 5 kV. This leads the liquid to form a Taylor cone at the tip of the capillary from which small droplets containing an excessive amount of charges are emitted. To ease the spraying process, nebulizing gas are usually introduced with the sample solution. Moreover, a heated gas ($200\text{--}300^\circ\text{C}$) is also used to help the desolvation of charged droplets. These charges will be distributed on the surface of the droplets (Gauss law).²³ The produced droplets move towards the entrance of the mass spectrometer and, along the way, produce the ions (Figure II-5).²⁴ Indeed, the droplets migrate towards the entrance of the mass spectrometer under the effect

Gold nanoclusters characterization developments

of the electric field and of the nebulization gas. Their diameter depends on the value of the electric potential, the flow rate of the solution, the nature of the solvent and gas temperature. The size of the droplets gradually decreases by evaporation of the solvent, using gas and heating. When the electrostatic repulsions between surface charges exceed the surface tension of the droplet, the so-called Rayleigh limit, the fission of the droplet into several smaller droplets occurs.²⁵ This fission will take place several times before the entrance of the spectrometer to produce increasingly small and charged droplets, which can reach nanometric sizes. At the Rayleigh limit the average charge on each droplet is given by Q_{Rayleigh} :

$$Q_{\text{Rayleigh}} = 8\pi R^{3/2} \sqrt{\gamma \epsilon_0}$$

where R is the radius of the droplet, γ the surface tension and ϵ_0 the vacuum permittivity.

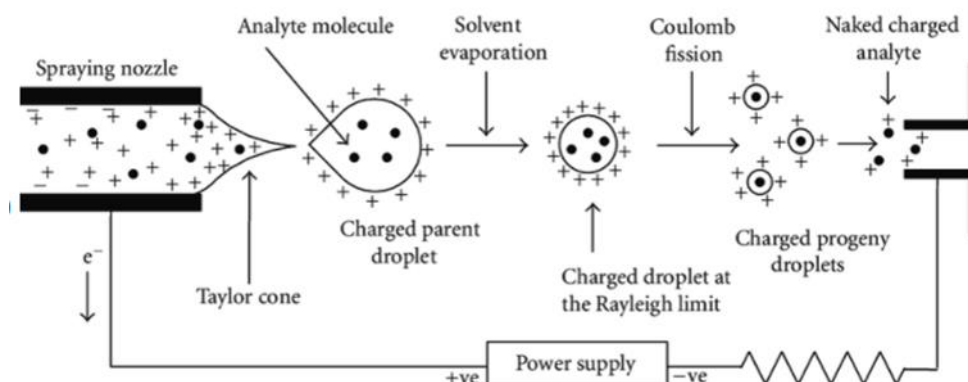


Figure II-5 Pictorial representation of the electrospray ionization (ESI) operating in positive ion mode²³

Three different mechanisms have been proposed for the production of ions from charged droplets: the ion evaporation model (IEM), the charge residue model (CRM) and Chain Ejection Model (CEM).

IEM is based on the idea that during the process of evaporation/fission of solvents when the radii of the droplets becomes smaller than 10 nm, instead of Coulomb fission, the droplets start emitting the analyte ions.²⁶ In fact, due to the high electric field produced by charged droplets whose radii are close to the Rayleigh radius, the solvated ions are ejected from the droplet surface to form a small cluster composed of a few molecules of solvent. It will then evaporate during the journey in the mass spectrometer thanks to the gas (Figure II-6). It is assumed that the mechanism of electrospraying of low molecular weight ions is achieved through IEM.

For CRM, the repetition of the evaporation/fission process leads to the formation of a few droplets containing solvent, ionic charges and a single macro-molecule.²⁷ Then further evaporation of the solvent from these droplets leads to the generation of ions analytes (Figure II-6). Studies have shown that ions are formed through CRM in ESI source for proteins with compact globular structure in which the hydrophobic parts are folded inside the molecule and where the polar parts are located on the outside (mostly in neutral aqueous solutions).²⁸

CEM is used to describe the formation of ions in ESI source for unfolded proteins or nonpolar polymer chains that are disordered, partially hydrophobic and have the ability to bind a large number of ionic charges.^{23,29} After repeated solvent evaporation/fission processes, when fine

Gold nanoclusters characterization developments

droplets are formed, the unfolded and disordered chains move to the surface of the droplet. Then, the protein chain is gradually ejected from the droplet (Figure II-6).^{29,30}

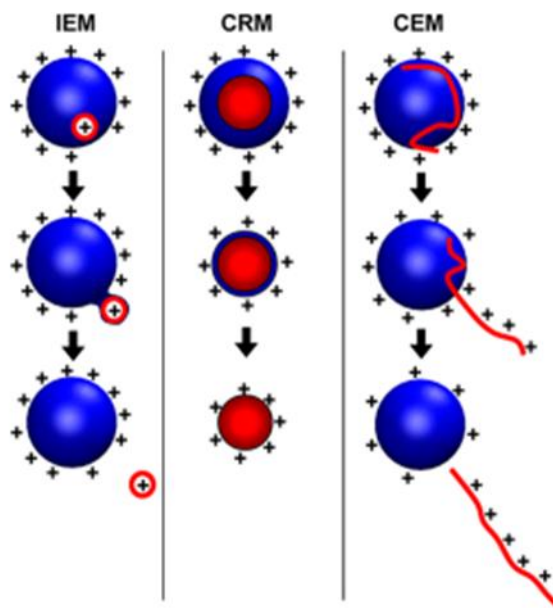


Figure II-6 Different proposed mechanisms for electrospray ionization: ion evaporation model (IEM), charged residue model (CRM), and chain ejection model (CEM).²²

These three ionization models are not really separated as they depend on the starting compound nature. Thanks to the development of molecular dynamics (MD) simulations, researchers were able to conclude on which ionization model did happen for a precise analyte.³¹

The use of electrospray ionization source is a great way to ionize gold nanoclusters, our species of interest, in a soft way and avoid over-fragmentation. Actually, the first unfragmented mass spectra were obtained using ESI (glutathione capped Au₂₅ NC).^{16,32} However, some compounds are traditionally difficult to ionize (such as alkanethiolates for example) but pre-oxidation or pre-reduction of gold nanoclusters using Ce(SO₄)₂ or NaBH₄ can allow the observation of relatively large, intact gold nanoclusters.³³ Another solution to enhance ionization that can allow the observation of highly charged gold nanoclusters is ligand exchange.³⁴ ESI can be associated with various mass analyzer but in this thesis two of them were chosen: Quadrupole-Time-of-Flight (Q-TOF) and Fourier Transform-Ion Cyclotron Resonance (FT-ICR) mass analyzers. Soft ionization sources have proven to be extremely versatile to ionize and transfer intact gold nanoclusters in the gas phase of the mass spectrometer.

II.B.1.b. Quadrupole-time-of-flight mass analyzer

The quadrupole-time-of-flight (Q-TOF) is a mass analyzer based partially on the ion's time-of-flight (TOF). During the time-of-flight (TOF) process, the ions are accelerated at the inlet of the flight tube by using an intense and uniform electrostatic field over the same distance. All these ions acquire the same kinetic energy. Subsequently, the ions are simultaneously ejected from the source and start their journey keeping a constant speed. All the ions are then separated, according to the speed they acquired in the acceleration zone, before reaching the detector placed at the other end of the flight tube. A high vacuum is maintained in order to avoid possible collisions of the ions with residual species present in the flight tube. The time taken by the ions to reach the detector is correlated to their m/z ratio. Indeed, the speed is inversely proportional to the square root of the m/z ratio of the ion considered ($E_c = 1/2 mv^2$), the lightest ions arrive first at the level of the detector due to their flight speed. This type of analyzer has no limit in m/z ratio but has a limitation coming from the sensitivity of the detectors for high m/z ratios. This system allows determination of the m/z ratio of various ions as a function of their time of flight. The TOF mass analyzer is mainly combined with pulsed ionization sources such as MALDI (Matrix Assisted Laser Dissociation Ionization) because it is not adapted with a constant arrival flow of ions. For ESI, pulsed injection of ions into the TOF is necessary to allow their analysis (injection is done along the z axis called injection 'pusher').^{35,36} Also, TOF analyzers incorporate a reflectron device for kinetic energy dispersion correction and spatial spread of ions having the same m/z but varying velocities. The reflectron correction allows ions of the same m/z to arrive at the detector at the same time. The reflectron device also increases the flight path length, allowing mass resolution improvement.³⁷

The Q-TOF mass analyzer is composed of the association of ³⁸:

- a hexapole to transfer and focus ions
- a quadrupole capable of operating as a mass filter for the selection of particular ions based on their m/z or in radio frequency (RF) only mode where all ions are transmitted through the quadrupole without selection.
- a collision cell where ions collide with neutral gas molecules such as N_2 or Ar, resulting in fragmentation of the ions by a process known as collision-induced dissociation (CID). It can also be used in RF only mode without fragmentation of ions
- a TOF analyzer in an orthogonal position where ions are accelerated orthogonally to their original direction (pulsed) then enter the flight tube where mass separation occurs (as explained previously).

After passing through, the ions are detected and a mass spectrum is obtained. Detection of ions is achieved by a detector system known as a time-to-digital converter which converts the time-of-flight of the ion into a mass signal.^{39,40}

Q-TOF mass spectrometry is an analytical technique that combines the benefits of two different mass analyzers. With Q-TOF, samples can be measured faster (fast data acquisition) and with an increased sensitivity in comparison to quadrupoles. ESI Q-TOF can provide high-accuracy and high resolution data for the analytes. Although Q-TOF uses time as a key metric, other techniques use frequency as measurement reference, such as FT-ICR (Fourier Transform-Ion Cyclotron Resonance) mass spectrometry. This technique uses accurate measurements of frequency, and then Fourier transform provides ions m/z . Mass resolution generally increases from Q-TOF to FT-ICR mass spectrometry and for the highest level of performances, scientists

Gold nanoclusters characterization developments

typically choose FT-ICR, even though it also comes with its own limitations as we will see later.

II.B.2. ESI-FTICR mass spectrometry

We previously saw that Q-TOF uses time as a key metric, but other techniques use frequency as measurement reference. It is the case of FT-ICR (Fourier Transform-Ion Cyclotron Resonance) mass spectrometry. This technique uses accurate measurements of frequency, and then Fourier transform provides ions m/z . Mass resolution generally increases from Q-TOF to FT-ICR mass spectrometry and for the highest level of performances, scientists typically choose FT-ICR, even though it also comes with its own limitations as we will see later.

The concept of mass spectrometry using the ionic cyclotronic resonance was invented in 1974 by Comisarow and Marshall.⁴¹ It is based on works that demonstrated that a charged particle subjected to a magnetic field, B , perpendicular to its motion is constrained to a circular motion whose angular frequency is independent of the radius of the particle's orbit. This frequency is expressed by the following cyclotronic equation:

$\omega = qB/m$ where ω is the angular frequency, q the particle charge, m the particle mass and B the magnetic field. The angular frequency of an ion is inversely proportional to its m/z .

It is therefore possible to separate ions of different m/z by making them rotate in a cell and detecting a periodical signal. By applying the Fourier transform to this periodical signal, its different frequencies can be separated and, accordingly, the different m/z . These works also show that it is possible to excite a charged particle to very large kinetic energies by simply using a magnetic field. FT-ICR analyzers are thus composed of a superconducting magnet in the middle of which is located a cell in which the ions will be able to be excited, separated and detected.

FT-ICR mass spectrometry involves a series of steps. After production of the ions in the source, they are transferred to the analyzer through electrostatic devices (quadrupole). First, ions are cooled, focused, and accumulated. Next, the ions go in a Penning trap (ICR cell), which stores the ions and excites them to their cyclotron frequencies. These frequencies are related to the ions m/z (1 MHz for a 7 Tesla magnet, for m/z 100 ions). The processing, followed by the Fourier transform of the data, gives the mass spectrum of a sample. FT-ICR analyzer is composed of a cylindrical ICR cell under high vacuum inside a superconductor magnet. It is composed of 6 trapping plates: two trapping plates perpendicular to B , two excitation plates and two detection plates. The electric field generated by the trapping plates combined to the magnetic field of the magnet generate a well of potential which keep the ions in the middle of the cell and hinders their movement along the z axis (principle of Penning trap).^{42,43} The trapping frequency (ν_T) of an ion can be described by the following formula where d is the distance between the plates, V_T the trapping tension that is applied, q the charge of the ion and α , a geometrical coefficient:

$$\nu_T = \frac{1}{2\pi} \sqrt{\frac{2qV_T\alpha}{md^2}}$$

The ions describe a movement of magnetron and cyclotron type rotation around the magnetic field vector B and pursue a helical trajectory. These movement are due to the fact that Penning's trap is not perfect (no perfect homogeneity of electric and magnetic field), thus the radial

Gold nanoclusters characterization developments

component of the electric field generates the magnetron movement. This movement disturbs the cyclotron frequency of the ions and therefore induces a frequency dispersion.⁴⁴ The reduced cyclotron frequency (ν_{cr}) and the magnetron frequency (ν_m) can be expressed by the equations:

$$\nu_{cr} = \frac{\nu_c}{2} + \sqrt{\left(\frac{\nu_c}{2}\right)^2 - \frac{\nu_T^2}{2}}$$

$$\nu_m = \frac{\nu_c}{2} - \sqrt{\left(\frac{\nu_c}{2}\right)^2 - \frac{\nu_T^2}{2}}$$

where ν_c is the cyclotron frequency of the ion.

This frequency being inversely proportional to the m/z , the lower the ion's m/z , the more negligible is the influence of the magnetron. In order to limit the impact of the trapping frequency on the generation of magnetron motion and therefore on the cyclotron frequency, low trapping potentials are used.

In general, the detection experiments within an FT-ICR takes place in four main steps (Figure II-7).⁴⁵ The first step corresponds to the accumulation of ions in the ICR cell. However, it is impossible to directly measure the cyclotron frequency since the packets of ions describe inconsistent movements of low amplitude. Indeed, their movements are not in phase because of the differences in kinetic energies and orbits radii between the ions. It is therefore essential to go through an excitation phase. This second step induces a coherent overall movement and gives the same orbit to the ions. Excitation plates generate an electric sinusoidal field and when the excitation frequency coincides with the cyclotron frequency of the compound, the latter then enters into resonance by absorbing the energy applied. Then, these pulses induce an increase of the ions orbit radii. The ions are only excited at a frequency corresponding to their cyclotronic frequency, meaning that each population of ions is excited separately and in packet. Each package then describes a circular trajectory perpendicular to the magnetic field, the cyclotron motion, with an angular frequency inversely proportional to their m/z ratio. In other words, ions with low m/z spin faster than high m/z ions. Unlike the cyclotron frequency, the radius of this orbit is not proportional to m/z . Finally, detector plates record the current induced by the coherent rotary movement in packets of ions, making it possible to obtain a decreasing sinusoidal signal, the FID (Free Induction Decay).⁴⁶ This periodic signal is transformed into a frequency signal by application of the Fourier transformation, then converted into a mass spectrum.

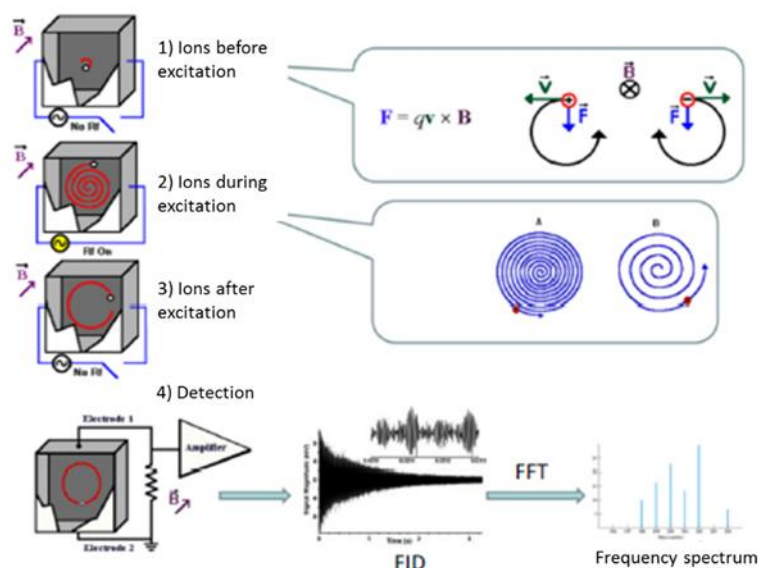


Figure II-7 Four main steps of an analysis within an FT-ICR instrument. ⁴⁴

Ghaste *et al.* reported that the FT-ICR mass spectrometry platforms can be considered as the most advanced mass analyzers in terms of high accuracy and resolving power with sub-parts-per-million mass accuracy.⁴⁷ Mass resolution is great with this technique but there are cons to each technique. First of all this method uses large superconducting magnets, which are expensive. Also speed is not one of FT-ICR's strong points, since the trapped ions lead to a longer data accumulation. We were able to conduct experiment with great results even though the analysis of high mass compounds such as gold nanoclusters by Q-TOF analyzer seem to be easier. With FT-ICR, when the samples contain a high number of species (meaning high number of ions), a lot of adjustments are needed to separate the isotopes, while for smaller mass species separation occurred easier. In fact, the resolution is constant with the m/z for the Q-TOF ($m/\Delta m$ 40,000 for our Q-TOF, acquisition speed 20Hz) while the resolution decreases with m/z for the FT-ICR ($m/\Delta m$ 120,000 for m/z 200 and 20,000 for m/z 2000 for a 7 Tesla magnet and 1 Hz detection. A frequency of 0.1 Hz provides a resolution greater than 1,000,000).

Q-TOF MS and FT-ICR MS combined to ESI sources allows for accurate characterization of charge state of the metal core and of the number of ligands for gold nanoclusters. MS also enables monitoring the evolution of these characteristics during synthesis and during ageing of the samples. As it is often the case in gold nanoclusters synthesis, dispersity is observed. The number of protecting ligands and also the number of core gold atoms can vary between the different species. In these cases, ESI mass spectrometry associated with a correlation algorithm can help in spectra interpretation.

II.B.3. Analysis of MS spectral data for identification of unknown gold nanoclusters

The analysis of spectral data from mass spectra is getting easier and easier with the years due to the availability of large spectral libraries for compounds identification. However, libraries do not include much references on gold nanoclusters.

Gold nanoclusters contain a definite number of metal atoms, protected by a defined number of ligands. Therefore, the mass spectra obtained show similarities with mass spectra of large molecules. Generally, they display patterns from which we can get the exact formula of gold nanoclusters. Depending on the ionization source, species with different charges are observed, yielding to a series of peaks. When simple spectra are acquired with good mass resolution and accuracy, it is often possible to resolve an isotopic pattern and determine the monoisotopic mass of the nanoclusters. For a given compound the monoisotopic mass is the mass of the isotopic peak whose elemental composition is composed of the most abundant isotopes of its elements. Then, the precise atomic composition can be found, based on a match between the measured value of the monoisotopic mass (on mass spectrum) and the one computed for potential candidate raw formulas. The found atomic composition can also be consolidated by the comparison of the experimental isotopic pattern (relative intensity of the different peaks) to simulated isotopic distributions often available on the mass spectrometry data processing softwares. Consequently, even if there are a lot of peaks in the mass spectra, it may be possible to find the precise atomic composition corresponding to each peak using expensive high resolution and high precision instruments. However, when carrying out the experiments on very complex gold nanocluster suspensions, our team faced the difficulty to associate each peak to an atomic composition. First of all, the synthesis of various different gold nanoclusters led to charge and mass dispersion.⁴⁸ Then, the assignment process was extremely time consuming with spectra where we could not associate all the peaks to a formula. However, determining the atomic formula in a sample containing a mixture of various clusters is very interesting to follow the relative species stability, for example. A few softwares have been developed to help in identifying unknown compounds on mass spectra such as Smile MS. It helps to get small molecule analysis faster thanks to the incredibly robust X-rank algorithm developed by GeneBio.⁴⁹ It allows to screen a sample containing unknown small molecules against spectral libraries. However, no such software has been developed for compounds such as gold nanoclusters yet.

In our case, thanks to the collaboration with Denis Lesage and François Simon (IPCM, SU), an algorithm was developed to facilitate the attribution of atomic composition to each pattern and obtain gold nanoclusters formula. This software was developed using Labview. It allows to sort out possible raw formula which the commercial tool on the included spectrometer software does not allow. The operator needs however to enter some information and put some constraints.

There are different steps in the identification of species on a mass spectrum:

- First, thanks to a data analysis software (in our case Compass data analysis Bruker MS software) the mass spectrum is displayed.
- Then, a pattern associated to an analyte is chosen (for us gold nanoclusters).
- Next, the monoisotopic peak of the motif of interest is located.

Gold nanoclusters characterization developments

- Subsequently, the software on Labview is opened and the monoisotopic mass value, the charge, an uncertainty, the number of different elements (elements: groups that can be atoms but also ligands) are recorded. Then, the elements must be entered (enumeration of the metal, ligands, potential atoms present in the samples) followed by their respective exact mass. For each element, one must enter a minimum and maximum quantity of the element in the final nanocluster composition (to focus on a size range and speed the software processing). Also, relative uncertainty in mass and an X factor (not always necessary, used to shift monoisotopic peak when it is hard to find due to a low intensity) is added (Figure II-8).
- The software will suggest one or several potential propositions for the compound formula.
- Then, to discriminate and choose the right formula among the propositions, the experimental spectrum is displayed on the data analysis software from the mass spectrometer, and is compared to a simulated spectrum. To do so, a simulation of the pattern is carried out by entering the proposed formulas (from the Labview algorithm), the charge and the monoisotopic mass. Then, the experimental pattern and the simulated pattern are superimposed to compare the isotopic pattern and choose the correct formula.

This Labview software helped in finding formula that fitted to the right mass with the right elements and helped save a high number of working hours for spectra analysis. An example, on a specific pattern is for $\text{Au}_{10}(\text{PPh}_3)_8\text{Br}^+$ nanocluster identification in a mixture of gold nanoclusters. The monoisotopic pic was at m/z 4147.34 for a monocharged specie. The synthesis was carried out from a gold source with phosphine and NHC ligands and reduction was done with sodium borohydride (Figure II-8). Based on the monoisotopic mass, two compositions can be proposed: $\text{Au}_{10}(\text{PPh}_3)_8\text{Br}^+$ and $\text{Au}_8(\text{NHC})_3(\text{PPh}_3)_5\text{Na}_2^+$. $\text{Au}_{10}(\text{PPh}_3)_8\text{Br}^+$ nanocluster formula was chosen after comparison of experimental and simulated theoretical isotopic patterns for both formula suggestions (another example for $\text{Au}_{129}(\text{PPh}_3)_{24}^{3+}$ nanocluster identification is given in appendix).

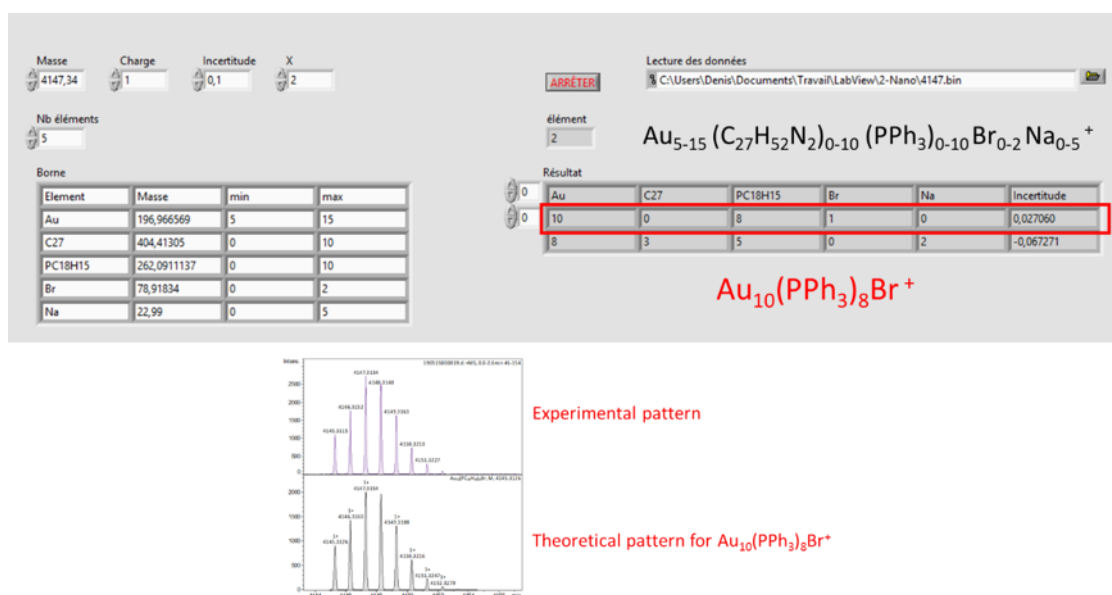


Figure II-8 Labview developed software for identification of gold nanoclusters for very complex mixtures: example of $\text{Au}_{10}(\text{PPh}_3)_8\text{Br}^+$ nanocluster identification.

Mass spectrometry makes it possible to obtain both information related to the chemical formulas of gold nanoclusters. It is crucial to develop mass spectrometry analyzes independent of the complexity of the sample in order to respond to increasingly complex issues. The development of analysis software is the first answer to these issues. Mass spectrometry opens a wide range of possibilities when associated with other analysis techniques, even though in this thesis we will focus only on classical mass spectrometry.

II.C. Conclusion

As seen in this chapter, characterization of gold nanoclusters is far from trivial. Due to their ultrasmall size and properties, some characterization methods have been developed to fit their specificity. UV-Vis spectroscopy can highlight their optical properties with the ability to observe transitions of discrete energy levels. Also, some effect of the protecting ligands on the nanoclusters can be assessed thanks to UV-Vis spectroscopy. However, it does not give any information on the nanoclusters composition. On the contrary, single-crystal X-Ray diffraction gives precise structural information on nanoclusters crystal with positioning of the gold atoms and the ligand chains, as well as being a great purification method to separate gold nanoclusters. But, the limiting step of this method relies on its nature which is crystal analysis when not all gold nanoclusters do crystallize. Also it does not allow study of the overall species in suspensions and stability of nanoclusters structure over time. A lot of methods are used for gold nanoclusters characterization such a XPS (sensitive to sample purity and need to analyze each nanocluster separately), TEM (gold nanoclusters observation and possibility to have mean size but no atomic composition information) etc.

Mass spectrometry has been a method of choice for nanoclusters characterization (single nanocluster or mixture) and for study of stability. There is a great variety in the MS ionizer and analyzer but our interest focused on soft ionization method ESI and two type of analyzers: Q-TOF and FT-ICR. Working with two analyzers is a great way to confirm the reliability of the mass spectra results when analyzing very complex samples. Also, these two analyzers allow obtaining mass spectra with high resolution and accuracy for very small molecules to bigger gold nanoclusters. The development of an algorithm for data analysis has been a turning point of this thesis for the following of nanoclusters synthesis and stability over time and in different reaction conditions. The first use of this developed characterization method will be presented in the next chapter for the characterization of complex gold nanoclusters mixtures. The synthesis have been carried out from gold source AuClPPh_3 , imidazolium salts as NHC precursors and sodium borohydride as base and reducing agent. The analysis of suspensions with dozens and dozens of gold nanoclusters of various nuclearity stabilized by two different ligands was very challenging.

References

- (1) Qian, H.; Zhu, M.; Wu, Z.; Jin, R. Quantum Sized Gold Nanoclusters with Atomic Precision. *Acc Chem Res* **2012**, *45* (9), 1470–1479. <https://doi.org/10.1021/ar200331z>.
- (2) Zhu, M.; Aikens, C. M.; Hollander, F. J.; Schatz, G. C.; Jin, R. Correlating the Crystal Structure of A Thiol-Protected Au₂₅ Cluster and Optical Properties. *J. Am. Chem. Soc.* **2008**, *130* (18), 5883–5885. <https://doi.org/10.1021/ja801173r>.
- (3) Tsunoyama, H.; Nickut, P.; Negishi, Y.; Al-Shamery, K.; Matsumoto, Y.; Tsukuda, T. Formation of Alkanethiolate-Protected Gold Clusters with Unprecedented Core Sizes in the Thiolation of Polymer-Stabilized Gold Clusters. *J. Phys. Chem. C* **2007**, *111* (11), 4153–4158. <https://doi.org/10.1021/jp067025q>.
- (4) Aikens, C. M. Origin of Discrete Optical Absorption Spectra of M₂₅(SH)₁₈– Nanoparticles (M = Au, Ag). *J. Phys. Chem. C* **2008**, *112* (50), 19797–19800. <https://doi.org/10.1021/jp8090914>.
- (5) Lugo, G. J.; Schwanen, V.; Fresch, B.; Remacle, F. Charge Redistribution Effects on the UV_Vis Spectra of Small Ligated Gold Clusters: A Computational Study. *Journal of Physical Chemistry C* **2015**, *119*, 10969–10980.
- (6) Preciado, L.; Gustavo, J. Dynamics of Ligands on Gold Surfaces to Obtain Janus Nanoclusters : A Theoretical and Experimental Investigation; 2016.
- (7) Zhang, S.-S.; Feng, L.; Senanayake, R. D.; Aikens, C. M.; Wang, X.-P.; Zhao, Q.-Q.; Tung, C.-H.; Sun, D. Diphosphine-Protected Ultrasmall Gold Nanoclusters: Opened Icosahedral Au₁₃ and Heart-Shaped Au₈ Clusters. *Chem. Sci.* **2018**, *9* (5), 1251–1258. <https://doi.org/10.1039/C7SC03566G>.
- (8) Devadas, M. S.; Bairu, S.; Qian, H.; Sinn, E.; Jin, R.; Ramakrishna, G. Temperature-Dependent Optical Absorption Properties of Monolayer-Protected Au₂₅ and Au₃₈ Clusters. *J. Phys. Chem. Lett.* **2011**, *2* (21), 2752–2758. <https://doi.org/10.1021/jz2012897>.
- (9) Niihori, Y.; Koyama, Y.; Watanabe, S.; Hashimoto, S.; Hossain, S.; Nair, L. V.; Kumar, B.; Kurashige, W.; Negishi, Y. Atomic and Isomeric Separation of Thiolate-Protected Alloy Clusters. *J. Phys. Chem. Lett.* **2018**, *9* (17), 4930–4934. <https://doi.org/10.1021/acs.jpcclett.8b02211>.
- (10) MacLeod Carey, D.; Muñoz-Castro, A. Evaluation of N-Heterocyclic Carbene Counterparts of Classical Gold Clusters; Bonding Properties of Octahedral CAu₆, Icosahedral Au₁₃Cl₂, and Bi-Icosahedral Au₂₅Cl₂ Cores from Relativistic DFT Calculations. *J. Phys. Chem. C* **2019**, *123* (19), 12466–12473. <https://doi.org/10.1021/acs.jpcc.9b01254>.
- (11) Li, Y.; Jin, R. Seeing Ligands on Nanoclusters and in Their Assemblies by X-Ray Crystallography: Atomically Precise Nanochemistry and Beyond. *J. Am. Chem. Soc.* **2020**, *142* (32), 13627–13644. <https://doi.org/10.1021/jacs.0c05866>.
- (12) Gunawardene, P. N.; Corrigan, J. F.; Workentin, M. S. Golden Opportunity: A Clickable Azide-Functionalized [Au₂₅(SR)₁₈]– Nanocluster Platform for Interfacial Surface Modifications. *J. Am. Chem. Soc.* **2019**, *141* (30), 11781–11785. <https://doi.org/10.1021/jacs.9b05182>.
- (13) Kauffman, D. R.; Alfonso, D.; Matranga, C.; Qian, H.; Jin, R. Experimental and Computational Investigation of Au₂₅ Clusters and CO₂: A Unique Interaction and Enhanced Electrocatalytic Activity. *J. Am. Chem. Soc.* **2012**, *134* (24), 10237–10243. <https://doi.org/10.1021/ja303259q>.
- (14) Li, G.; Abroshan, H.; Liu, C.; Zhuo, S.; Li, Z.; Xie, Y.; Kim, H. J.; Rosi, N. L.; Jin, R. Tailoring the Electronic and Catalytic Properties of Au₂₅ Nanoclusters via Ligand Engineering. *ACS Nano* **2016**, *10* (8), 7998–8005. <https://doi.org/10.1021/acsnano.6b03964>.
- (15) Yan, N.; Xia, N.; Liao, L.; Zhu, M.; Jin, F.; Jin, R.; Wu, Z. Unraveling the Long-Pursued Au₁₄₄ Structure by x-Ray Crystallography. *Science Advances*, 2018, *4*, eaat7259.
- (16) Schaaff, T. G.; Knight, G.; Shafigullin, M. N.; Borkman, R. F.; Whetten, R. L. Isolation and Selected Properties of a 10.4 KDa Gold: Glutathione Cluster Compound. *The Journal of Physical Chemistry B* **1998**, *102* (52), 10643–10646.
- (17) Chen, T.; Yao, Q.; Nasaruddin, R. R.; Xie, J. Electrospray Ionization Mass Spectrometry: A Powerful Platform for Noble-metal Nanocluster Analysis. *Angewandte Chemie International Edition* **2019**, *58* (35), 11967–11977.

- (18) Lu, Yizhong., Chen, Wei., Mingos, D. M. P., Broda, Janine., *Gold Clusters, Colloids and Nanoparticles I*; Mingos, Springer, 2014; pp 117-153.
- (19) Kaltashov, I. A.; Eyles, S. J. *Mass Spectrometry in Biophysics: Conformation and Dynamics of Biomolecules*; John Wiley & Sons, 2005; Vol. 12.
- (20) Gross, J. H. Fragmentation of Organic Ions and Interpretation of EI Mass Spectra. In *Mass Spectrometry*; Springer, 2004; pp 223–330.
- (21) Yamashita, M.; Fenn, J. B. Application of Electrospray Mass Spectrometry in Medicine and Biochemistry. *Iyo Masu Kenkyukai Koenshu* **1984**, 9, 203–206.
- (22) De Hoffmann, E.; Stroobant, V. *Mass Spectrometry: Principles and Applications*; John Wiley & Sons, 2007.
- (23) Konermann, L.; Ahadi, E.; Rodriguez, A. D.; Vahidi, S. *Unraveling the Mechanism of Electrospray Ionization*; ACS Publications, 2013.
- (24) Banerjee, S.; Mazumdar, S. Electrospray Ionization Mass Spectrometry: A Technique to Access the Information beyond the Molecular Weight of the Analyte. *International journal of analytical chemistry* **2012**, 2012, 282574. <https://doi.org/10.1155/2012/282574>.
- (25) Rayleigh, Lord. XX. On the Equilibrium of Liquid Conducting Masses Charged with Electricity. *The London, Edinburgh, and Dublin Philosophical Magazine and Journal of Science* **1882**, 14 (87), 184–186.
- (26) Iribarne, J. V.; Thomson, B. A. On the Evaporation of Small Ions from Charged Droplets. *The Journal of chemical physics* **1976**, 64 (6), 2287–2294.
- (27) Dole, M.; Mack, L. L.; Hines, R. L.; Mobley, R. C.; Ferguson, L. D.; Alice, M. B. Molecular Beams of Macroions. *The Journal of chemical physics* **1968**, 49 (5), 2240–2249.
- (28) De La Mora, J. F. Electrospray Ionization of Large Multiply Charged Species Proceeds via Dole’s Charged Residue Mechanism. *Analytica chimica acta* **2000**, 406 (1), 93–104.
- (29) Ahadi, E.; Konermann, L. Modeling the Behavior of Coarse-Grained Polymer Chains in Charged Water Droplets: Implications for the Mechanism of Electrospray Ionization. *The Journal of Physical Chemistry B* **2012**, 116 (1), 104–112.
- (30) Chung, J. K.; Consta, S. Release Mechanisms of Poly (Ethylene Glycol) Macroions from Aqueous Charged Nanodroplets. *The Journal of Physical Chemistry B* **2012**, 116 (19), 5777–5785.
- (31) Ahadi, E.; Konermann, L. Surface Charge of Electrosprayed Water Nanodroplets: A Molecular Dynamics Study. *Journal of the American Chemical Society* **2010**, 132 (32), 11270–11277.
- (32) Negishi, Y.; Nobusada, K.; Tsukuda, T. Glutathione-Protected Gold Clusters Revisited: Bridging the Gap between Gold(I)-Thiolate Complexes and Thiolate-Protected Gold Nanocrystals. *J Am Chem Soc* **2005**, 127 (14), 5261–5270. <https://doi.org/10.1021/ja042218h>.
- (33) Chaki, N. K.; Negishi, Y.; Tsunoyama, H.; Shichibu, Y.; Tsukuda, T. Ubiquitous 8 and 29 KDa Gold: Alkanethiolate Cluster Compounds: Mass-Spectrometric Determination of Molecular Formulas and Structural Implications. *Journal of the American Chemical Society* **2008**, 130 (27), 8608–8610.
- (34) Tracy, J. B.; Kalyuzhny, G.; Crowe, M. C.; Balasubramanian, R.; Choi, J.-P.; Murray, R. W. Poly (Ethylene Glycol) Ligands for High-Resolution Nanoparticle Mass Spectrometry. *Journal of the American Chemical Society* **2007**, 129 (21), 6706–6707.
- (35) Guilhaus, M.; Selby, D.; Mlynski, V. Orthogonal Acceleration Time-of-flight Mass Spectrometry. *Mass spectrometry reviews* **2000**, 19 (2), 65–107.
- (36) Chernushevich, I. V.; Ens, W.; Standing, K. G. Peer Reviewed: Orthogonal-Injection TOFMS for Analyzing Biomolecules. *Analytical Chemistry* **1999**, 71 (13), 452A-461A.
- (37) Mamyrin, B. A. Time-of-Flight Mass Spectrometry (Concepts, Achievements, and Prospects). *International Journal of Mass Spectrometry* **2001**, 206 (3), 251–266.
- (38) Zheng, F.; Zhang, Y.; Zhang, Y.; Han, Y.; Zhang, L.; Bouyssiére, B.; Shi, Q. Aggregation of Petroporphyrins and Fragmentation of Porphyrin Ions: Characterized by TIMS-TOF MS and FT-ICR MS. *Fuel* **2021**, 289, 119889. <https://doi.org/10.1016/j.fuel.2020.119889>.
- (39) Gross, J. H. *Mass Spectrometry: A Textbook*; Springer Science & Business Media, 2006.
- (40) Chernushevich, I. V.; Loboda, A. V.; Thomson, B. A. An Introduction to Quadrupole–Time-of-flight Mass Spectrometry. *Journal of mass spectrometry* **2001**, 36 (8), 849–865.

Gold nanoclusters characterization developments

- (41) Comisarow, M. B.; Marshall, A. G. Frequency-Sweep Fourier Transform Ion Cyclotron Resonance Spectroscopy. *Chemical Physics Letters* **1974**, 26 (4), 489–490.
- (42) Brown, L. S.; Gabrielse, G. Geonium Theory: Physics of a Single Electron or Ion in a Penning Trap. *Reviews of Modern Physics* **1986**, 58 (1), 233.
- (43) Marshall, A. G.; Hendrickson, C. L.; Jackson, G. S. Fourier Transform Ion Cyclotron Resonance Mass Spectrometry: A Primer. *Mass spectrometry reviews* **1998**, 17 (1), 1–35.
- (44) Dunbar, R. C.; Chen, J. H.; Hays, J. D. Magnetron Motion of Ions in the Cubical ICR Cell. *International journal of mass spectrometry and ion processes* **1984**, 57 (1), 39–56.
- (45) Ichou, F. Mise En Place d'une Méthode de Calibration Pour Construire Une Base de Données MS/MS et Développement d'un Outil Pour l'identification En ESI-HR-MS/MS de Composés Organophosphorés, Paris 6, 2013.
- (46) Hopf, F. A.; Shea, R. F.; Scully, M. O. Theory of Optical Free-Induction Decay and Two-Photon Superradiance. *Physical Review A* **1973**, 7 (6), 2105.
- (47) Ghaste, M.; Mistrik, R.; Shulaev, V. Applications of Fourier Transform Ion Cyclotron Resonance (FT-ICR) and Orbitrap Based High Resolution Mass Spectrometry in Metabolomics and Lipidomics. *International journal of molecular sciences* **2016**, 17 (6), 816.
- (48) Le Guevel, X.; Tagit, O.; Rodríguez, C. E.; Trouillet, V.; Leal, M. P.; Hildebrandt, N. Ligand Effect on the Size, Valence State and Red/near Infrared Photoluminescence of Bidentate Thiol Gold Nanoclusters. *Nanoscale* **2014**, 6 (14), 8091–8099.
- (49) Köhler, C.; Grobosch, T.; Binscheck, T.; Surmann, P. Development of a Systematic Toxicological Screening Method Using an Automated Online-SPE-LC-QqTOF System (XLC-QqTOF). *Toxichem Krimtech* **2011**, 78, 224–228.

CHAPTER III: SYNTHESSES OF N-HETEROCYCLIC CARBENE STABILIZED GOLD NANOCCLUSERS FROM IMIDAZOLIUM SALTS AND AuClPPh₃

This chapter describes our first synthesis of gold nanoclusters stabilized by NHC ligand and our study of nanoclusters synthesis pathways using various imidazolium salts as NHC precursors and AuClPPh₃ as a gold source.

Various strategies have been developed for the synthesis of stable gold nanoclusters (AuNCs). In the early time, the research was focused on gas state metal clusters.¹ Since these metal clusters in the gas phase were short-lived and hard to functionalize, solution-phase synthesis was developed in the late 90s. These synthetic strategies lead to gold nanoclusters with enhanced stability. The first approach relies on the reduction of gold ions into atoms, and then, AuNCs are formed from the nucleation of Au atoms. However, there is a possibility of forming gold nanoparticles instead of nanoclusters due to the possibility of AuNCs aggregation. Hence, the importance of using efficient protecting ligands to stabilize the AuNCs. The other approach for synthesizing AuNCs comes from nanoparticles or larger nanoclusters degradation. It relies on etching of larger particles into nanoclusters induced by heat, solvent or an etching molecule.² Generally, the stable gold nanoparticles are put in presence of an etchant in excess (molecule), then etching of the gold surface occurs via ligand exchange (small molecule vs NP stabilizing ligand) and finally, etchant-gold complexation forms gold nanoclusters. However, gold nanoparticles being quite stable, etching does not always occur and we need to find the precise molecule that can initiate the process. In our strategy, we will focus on the first approach by using strong reducing agents and strong capping agents to form and stabilize AuNCs in one step. Phosphine molecules have been widely used as a ligand for the preparation of AuNCs, especially PPh₃. The PPh₃-capped AuNCs are stable under ambient conditions and they are mostly synthesized through sodium borohydride reduction. Previous studies have shown that the reduction of gold complex such as AuClPPh₃ could give PPh₃-capped nanoclusters under certain conditions. Then, dodecanethiol is added and depending on the addition time, it gives either dodecanethiol-capped NCs or dodecanethiol-capped NPs.³ However, this publication did not give further indication on the exact structure of the synthesized NCs.

Also, theoretical studies showed that NHC-Au bound should be stronger than the phosphine-Au one, thus NHC should be better at stabilizing gold nanoclusters even though they have similar bonding patterns.⁴ Indeed, Muñoz-Castro *et al.* studied the interaction between PPh₃ and 1,3-bis-(diisopropyl)imidazol-2-ylidene, a NHC ligands and the CAu₆ core in C(Au₆L₆)²⁺ (L= ligand). The resulting cluster-ligand interaction exhibited interaction energy of -78.2 and -81.2 kcal·mol⁻¹, respectively per each PPh₃ and NHC ligands, corresponding to the more favorable bonding situation provided from NHC. The study was also conducted for Au₁₃ icosahedral core motifs interaction with ligands (between PPh₃ and 1,3-bis-(diisopropyl)imidazol-2-ylidene on Au₁₃Cl₂). The resulting cluster-ligand interaction exhibited interaction energy of -145.9 and -146.8 kcal·mol⁻¹, respectively. The results exposed a slight preference for the NHC ligands.

Based on these considerations, our goal, in this chapter, was to synthesize gold nanoclusters from AuClPPh₃ as gold precursor and NHC as complexing ligands in order to slow down the

Syntheses of n-heterocyclic carbene stabilized gold nanoclusters from imidazolium salts and AuClPPh₃

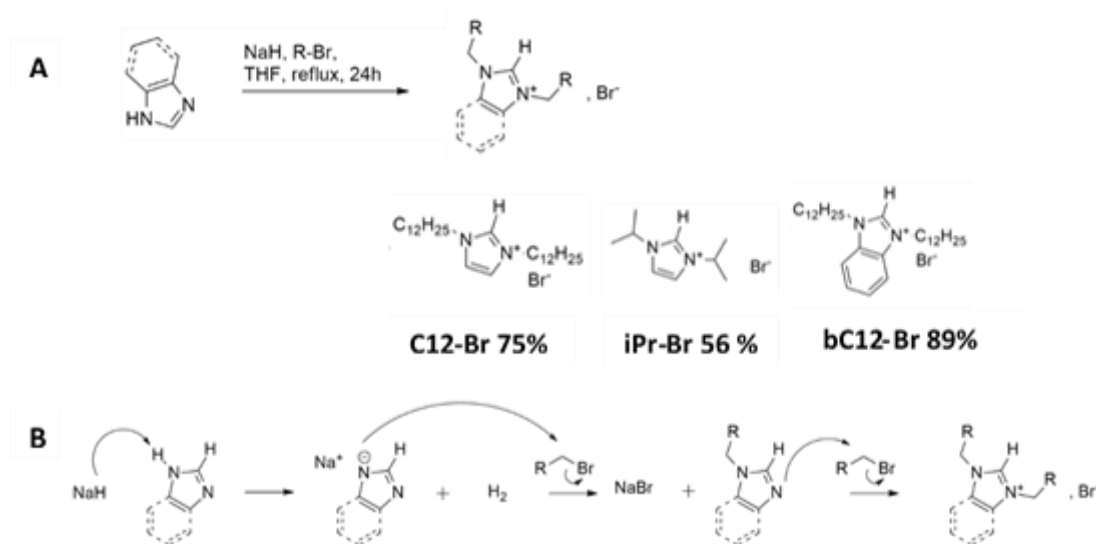
nucleation and to limit the growth of NCs. We studied the composition of the AuNCs when NHC and PPh₃ ligands are put in competition in a synthesis medium.

III.A. Imidazolium salts

III.A.1. Synthesis

Imidazolium ligands as NHC precursors were first synthesized. Variety in imidazolium structures would allow to see the influence of the steric hindrance of the NHC (benzimidazolium vs imidazolium, long side chains vs short side chains) on the AuNCs structure and stability. In this part, three (benz)imidazolium bromide salts were synthesized: 1,3-diisopropylimidazolium bromide (**iPr-Br**), 1,3-didodecylimidazolium bromide (**C12-Br**) and 1,3-didodecylbenzimidazolium bromide (**bC12-Br**). The same following general procedure was followed to synthesize them. In a round flask containing NaH (1.5 equiv.) under N₂, 40 mL of distilled THF was added. The flask was put in an ice bath and (benz)imidazole (≈35 mmol, 1 equiv.) was added slowly under stirring. Then, the corresponding alkyl bromide (2 equiv.) was added dropwise and the reaction medium was heated at 75°C for 24 h to 48 h while maintained under N₂) (Scheme III-1). For purification, dichloromethane was added in the suspensions to precipitate the salts, then the suspensions were filtered. Subsequently, ether was added to reprecipitate the product, and everything was filtered yielding white imidazolium and benzimidazolium powders.

The synthesis pathway relies on the deprotonation of the (benz)imidazole by NaH which is followed by nucleophile attack on the alkylbromide (Scheme III.1).



Scheme III-1 [A] Synthesis of imidazolium salts C12-Br, bC12-Br and iPr-Br in THF and [B] reaction pathway of imidazolium and benzimidazolium salts from imidazole and benzimidazole, NaH and alkyl bromide.

III.A.2. Characterization by liquid state NMR

For each ligand, NMR characterizations were conducted. It confirmed that the targeted imidazolium salts were synthesized.

The following reactions were carried out then the purified sample was dispersed in CDCl₃. An example of NMR characterization is iPr-Br imidazolium salt ¹H NMR experiment. The spectrum displayed signals corresponding to the imidazolium proton (label t, 1H, 11 ppm), the protons on the imidazolium cycle (d, 2H, 7.28 ppm) and the signals associated to the proton on the isopropyl chains (sept., 2H, 5 ppm / d, 12H, 1.63 ppm) (Figure III-1).

- iPr-Br imidazolium salt ¹H NMR

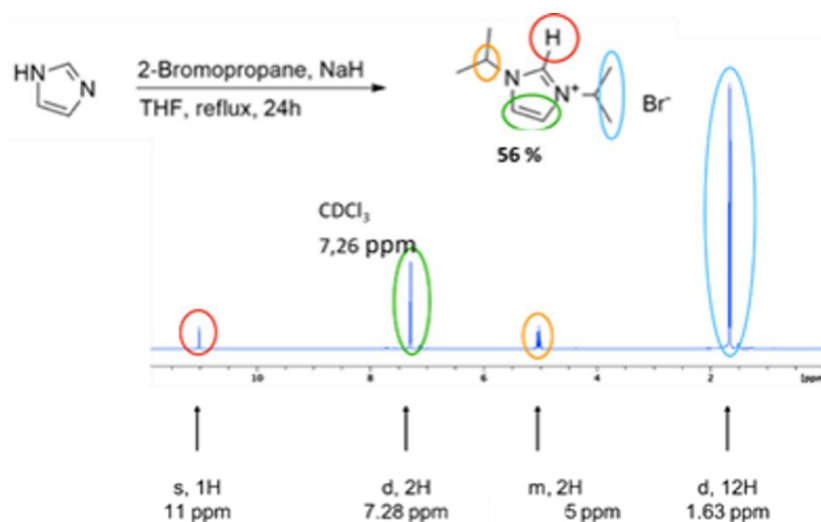
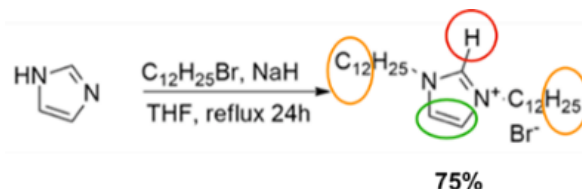


Figure III-1 Synthesis reaction conditions of ligand iPr-Br and ¹H NMR spectrum of iPr-Br in CDCl₃.

As the spectrum shows, the sample was well purified but also the corresponding signals to all the molecule's protons are clearly visible with the right multiplicity (Figure III-1).

- C12-Br imidazolium salt ¹H NMR



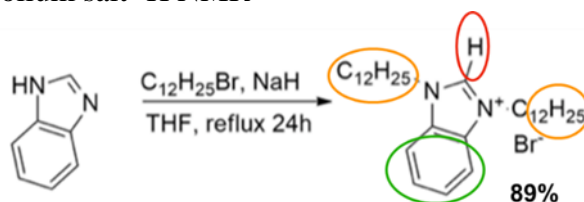
Scheme III-2 Synthesis reaction conditions of ligand C12-Br.

The same experiment was carried out for ligand C12-Br in CDCl₃. The synthesis of this ligand (Scheme III-2) was confirmed with the signals corresponding to the imidazolium proton (t, 1H, 10.68 ppm), the protons on the imidazolium cycle (d, 2H, 7.29 ppm) and the signals associated to the proton on the long C12 side chains (t, 4H, 4.39 ppm / m, 4H, 1.92 ppm / m, 18H, 1.27

Syntheses of n-heterocyclic carbene stabilized gold nanoclusters from imidazolium salts and AuClPPh₃

ppm / t, 6H, 0.91 ppm). Sometimes, the spectra showed that there are still traces of solvents used in the purification steps or coming from glassware. All the molecule's protons signals were clearly identified as well as their multiplicity.

- bC12 -Br imidazolium salt ¹H NMR



Scheme III-3 Synthesis reaction conditions of ligand bC12-Br.

Same experiment was also carried out for bC12-Br ligand synthesis (Scheme III-3) and we were able to identify the signals corresponding to the molecule protons. Indeed, the imidazolium proton signal was identified (s, 1H, 11.49 ppm), also the proton on the benzimidazolium cycle (m, 4H, 7.72 ppm) and the proton of the C12 side chains (t, 4H, 4.68 ppm / p, 4H, 2.12 ppm / m, 18H, 1.28 ppm / t, 6H, 0.9 ppm). All the remaining impurities were attributed to known solvents.

The imidazolium salts being synthesized and purified, the NPs synthesis part of the work is presented hereafter.

III.B. Nanoclusters synthesis

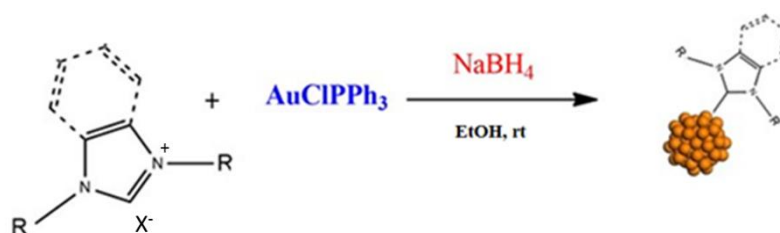
III.B.1. Synthesis and morphology

The synthesis was inspired from literature and nanoparticles synthesis methods that were previously developed in our laboratory. Hippolyte *et al.*,⁵ first developed a synthesis of gold nanoparticles in toluene at room temperature from NHC-borane (NHC-BH₃ as a ligand source and reducer) and AuClPPh₃. The team obtained a mixture of gold nanoparticles and ultra-small nanoparticles in these conditions. Then, they also developed a gold nanoparticles synthesis method in toluene at room temperature using imidazolium salts, various gold sources (not AuClPPh₃) and NaBH₄ as a reducing agent and a base. Indeed, the team confirmed that NaBH₄ could deprotonate the imidazolium/benzimidazolium salts thus no further addition of a base (such as NaH) was needed in these reaction conditions. Based on these results, we tried to merge both synthesis methods by using imidazolium salts, AuClPPh₃ in toluene and NaBH₄ as reducing agent and base. The idea was to shift the reaction toward the formation of the ultra-small particles (potentially gold nanoclusters). We kept the same concentrations and reactants proportions as Hippolyte *et al.* with 4 equiv. of imidazolium salt (iPr-Br or C12-Br or bC12-Br), 0.025 mmol of gold source in toluene and 10 equiv. of an aqueous solution of NaBH₄. The main difference from the synthesis of Hippolyte *et al.* was the use of AuClPPh₃ as a gold source with the imidazolium salt as a NHC precursor (instead of NHC-borane). Dark brown suspensions were obtained and TEM observation of the suspensions unveiled the formation of ultra-small particles. However, the biphasic system (water + toluene) produced emulsions that prevented phase separation thus efficient purification of the suspensions. To free ourselves from this problem, the syntheses were carried out in another organic solvent, dichloromethane. But

Syntheses of n-heterocyclic carbene stabilized gold nanoclusters from imidazolium salts and AuClPPh₃

the same emulsions as for the synthesis in toluene did form. After all these trials, carrying the synthesis in a monophasic medium was then chosen. A study of the literature highlighted ethanol as an interesting synthesis solvent. Li *et al.*³ reported a synthesis using AuClPPh₃ as a gold source in ethanol and upon addition of a reducing agent, the team obtained nanoclusters which then coalesced and grew into nanoparticles until their growth was halted by thiols addition. The synthesis was then performed in ethanol starting with AuClPPh₃, then adding imidazolium/benzimidazolium salts and then adding NaBH₄.

In a bottle, the imidazolium and benzimidazolium salts (0.1 mmol, 4 equiv.) presented in the previous part were dissolved in 2 mL ethanol. Then a solution of AuClPPh₃ (0.025 mmol, 1 equiv.) in 2 mL ethanol was added at room temperature under vigorous stirring (700 rpm). After 20 min, when the salts seem well dissolved in ethanol, a fresh solution of NaBH₄ in 3 mL EtOH was added. The suspensions color instantly changed from clear to brown and bubbling was observed. The reaction is stopped after 5 hours when there is no H₂ gassing anymore (Scheme III-4). Then, the solvent is evaporated and the black residue is sonicated in diethyl ether (1-2 ml). The solid is allowed to settle and the solvent is removed by pipet. Then, the solid is dissolved in dichloromethane (DCM) and loaded into a silica gel column packed with DCM/EtOH (10/1). The product is eluted with DCM/EtOH (9:1 v/v) to give a black solid that is redispersed in EtOH. This synthesis protocol is validated for the rest of the study.



Scheme III-4 Synthesis pathway of AuNCs in EtOH with imidazolium salts, AuClPPh₃ and NaBH₄.

III.B.1.a. Effect of nature of the ligand

The samples obtained from the as-described synthesis using AuClPPh₃ and imidazolium salts 1,3-diisopropylimidazolium bromide (**iPr-Br**), 1,3-didodecylimidazolium bromide (**C12-Br**) and 1,3-didodecylbenzimidazolium bromide (**bC12-Br**), were characterized. The goal of this part was to see a potential influence of the ligand on the particles nature (NCs or NPs) and to monitor their stability over time.

First test-synthesis was done without NHC ligands with only AuClPPh₃ and NaBH₄: a brown suspension is obtained and when observed by TEM it showed extra small particles, probably NCs sized 0.9 (\pm 0.16) nm (Figure III-2). However, the suspensions were only stable a couple hours when stored at room temperature or in the fridge (it started showing aggregates after a couple minutes).

Syntheses of n-heterocyclic carbene stabilized gold nanoclusters from imidazolium salts and AuClPPh₃

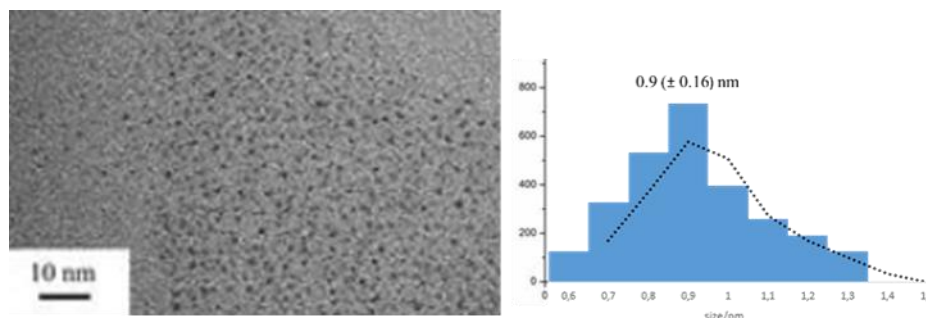


Figure III-2 TEM image of AuNCs synthesized from AuClPPh₃ and NaBH₄ in EtOH without NHC ligand.

When an imidazolium salt was added into the reaction medium, the brown suspensions stayed stable longer for all the ligands. TEM images showed very small sized particles with no particular effect of the ligand on the NCs morphology or size (Figure III-3). Indeed, for the synthesis with iPr-Br, C12-Br and bC12-Br, we obtained NCs with mean size 1.9 (± 0.3) nm, 1.4 (± 0.5) nm and 1.3 (± 0.4) nm respectively.

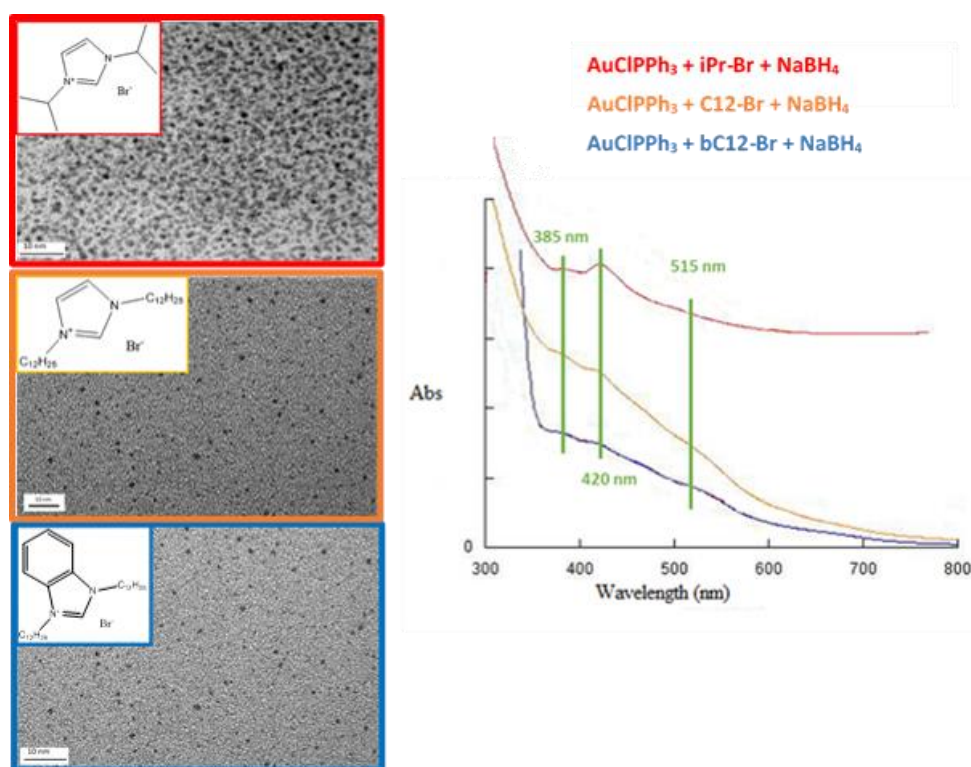


Figure III-317 TEM images and UV-Vis spectra of AuNCs synthesized from AuClPPh₃, imidazolium salt iPr-Br (red), C12-Br (orange), bC12-Br (blue) and NaBH₄ in EtOH.

It means that the nature of the ligand in our conditions do not change the nature of the NCs to NPs or bulk gold. UV-Vis spectroscopy was also done on the three samples (Figure III-3). No

Syntheses of n-heterocyclic carbene stabilized gold nanoclusters from imidazolium salts and AuClPPh₃

high intensity plasmon bands were noticed around 530 nm on the spectra as it is the case for spherical gold nanoparticles, whereas a few transitions can be seen (Figure III-3). For suspensions obtained when using imidazolium salt iPr-Br (red spectrum), there are one band around 385 nm, another one around 420 nm and a last one around 510 nm (very low intensity and broad band). For suspensions obtained when using imidazolium salt C12-Br (orange spectrum), the same bands are observed but with lower intensity (the absorption bands are much less defined). Finally, for suspensions obtained when using imidazolium salt bC12-Br (blue spectrum), there are also the same bands with lower intensity. One thing that can be noticed is that for the different samples, the transitions seem to be at the same location on the spectra: with this result alone no conclusion could be made on the effect of the ligand (Figure III-3). The interesting information relies on the positions of the transitions at 385, 420 and 510-515 nm. Indeed, a study of the literature shows that PPh₃ capped Au₁₁ nanoclusters have characteristic UV-Vis absorption peaks at ~312, 380, 416, and 500 nm, which is quite similar to the transitions that were experimentally observed in Figure III-3.⁶ It could indicate the formation of Au₁₁ nanoclusters in our reaction conditions.

This synthesis method produces gold nanoclusters with or without NHC ligands. However, the preliminary results show that there is a general stabilizing effect of the NHC ligands since the suspensions with imidazolium salts are more stable over time in comparison to the suspensions without imidazolium salts. Also, among the NHC ligands, there is no drastic difference with regards to NCs size and stability of the suspension over time. As the nature of the NHC ligand did not have noticeable effect on the particles size in TEM and on the general UV-Vis absorption spectra profiles, we were able to observe the obtention of ultra small particles by TEM exhibiting characteristics electronical transitions profiles in UV-Vis spectroscopy. Then, the effect of the quantity of ligand on the nanoclusters formation was studied. Synthesis using imidazolium salt C12-Br was chosen to conduct this study.

III.B.1.b. Effect of the ligand/Au ratio

Synthesis was done as previously described with AuClPPh₃ and 1, 4, 6 and 10 equiv. of C12-Br in EtOH. A fresh aqueous solution of reducing agent and base, NaBH₄, was added 20 minutes after. TEM observations and UV-Vis spectroscopy showed no change in the NPs average size and in the absorption spectra. However, visual observation of the suspensions showed that the stability of the suspensions with 1 equivalent of C12-Br lasted 2 weeks in comparison with the samples with 4, 6 and 10 equiv. of ligand which stayed stable for months. In the literature, the quantity of ligand in the formation of particles at the nanometric scale can be a determining parameter. Indeed, the ligand to gold ratio is known to have an influence on the size of gold nanoparticles and is used to control their size. Increasing the quantity of ligand can lead to the formation of smaller nanoparticles.⁷ Moreover, etching processes on gold nanoparticles to form gold nanoclusters by additional ligand addition also evidenced the effect of ligand to gold ratio in the gold nanoclusters synthesis.² However in our reaction's conditions, the effect of the quantity of the ligand between 4, 6 or 10 equiv. does not seem to bring any drastic change. As an example, the reaction using 4 equiv. of imidazolium salt and the one using 10 equiv. of imidazolium salt gave NCs sized 1.5 (± 0.3) nm and 1.5 (± 0.2) nm, respectively (Figure III-4). On UV-Vis spectroscopy graphs, no plasmon band were observed and the curves were similar to the one obtained on Figure III-3 for NCs synthesized with ligand C12-Br (see appendix).

Syntheses of n-heterocyclic carbene stabilized gold nanoclusters from imidazolium salts and AuClPPh₃

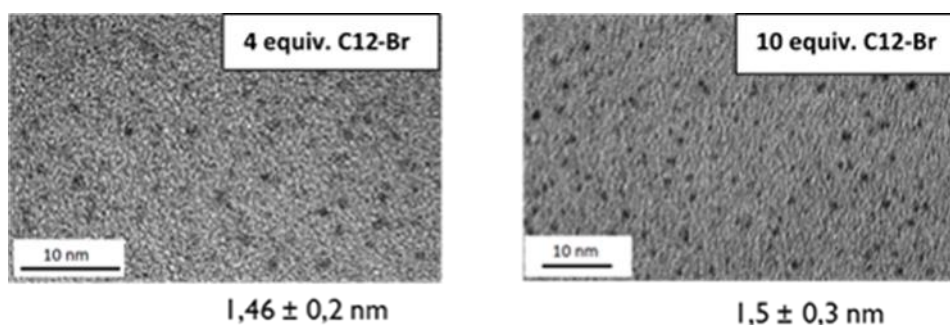


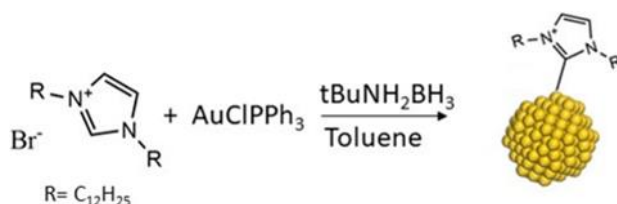
Figure III-4 TEM images of AuNCs synthesized from AuClPPh₃, C12-Br (4 and 10 equiv.) and NaBH₄ in EtOH.

The influence of other reaction parameters on the UV-Vis spectroscopy profiles and on the TEM average sizes were also studied. The reaction was reproduced using a milder reducing agent compare to NaBH₄ to study the effect of the strength of the reducing agent on the NCs formation.

III.B.1.c. Effect of nature of the reducing agent

Here, the synthesis was carried out as previously with ligand C12-Br but instead of NaBH₄, tBuNH₂BH₃ was used. The imidazolium and benzimidazolium salts (0.1 mmol, 4 equiv.) presented in the previous part were dissolved in 2 mL ethanol. Then a solution of AuClPPh₃ (0.025 mmol, 1 equiv.) in 2 mL ethanol was added at room temperature under vigorous stirring (700 rpm). After 20 min, when the salts seem well dissolved in ethanol, a fresh solution of tBuNH₂BH₃ in 3 mL EtOH was added. The suspensions color gradually changed from clear to brown after about five to ten minutes (which is way slower than with the synthesis with NaBH₄). Then, after about twenty minutes we observed complete aggregation of the suspension in these conditions.

To stabilize the formation of gold nanoclusters when using tBuNH₂BH₃, the reaction conditions were modified. Since this ligand is soluble in various organic solvents, we decided to change the reaction solvent to toluene and carried out the reaction at room temperature and at 70°C (Scheme III-5).



Scheme III-5 Synthesis pathway of AuNCs from C12-Br and tBuNH₂BH₃ in toluene.

When the synthesis was done at room temperature with 4 equiv. of C12-Br, a red wine suspension was obtained. TEM observation revealed extremely polydisperse nanoparticles with mean size being 43 (± 26) nm (Figure III-5.A). There were clearly 3 populations which sizes varies around 100 nm, 50 nm and 20 nm. A first explanation is that the reduction is too slow compared to the nucleation, which explains this strong growth of the nanoparticles. The three populations would be in agreement with several stages of nucleation and with a too slow reduction of gold. Since this reducing agent is milder compared to NaBH₄, we decided to heat

Syntheses of n-heterocyclic carbene stabilized gold nanoclusters from imidazolium salts and AuClPPh₃

up the suspensions to increase the rate of the reduction reaction. The synthesis was performed at 70°C with 4 equiv. C12-Br. A red wine suspension was obtained in less than 5 minutes after addition of the reducing agent. However, TEM showed 2 populations of particles, ultrasmall particles of size around 1 nm and bigger particles of size around 4 nm (Figure III-5.B). These TEM results are in favor of the synthesis of gold nanoparticles with a temperature effect. UV-Vis spectroscopy was carried out to gain further information.

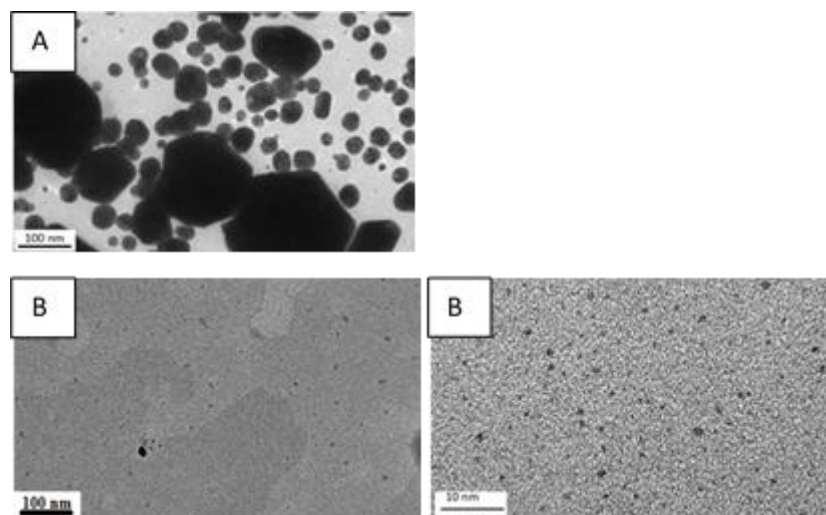


Figure III-5 TEM images of synthesis using AuClPPh₃, C12-Br and *t*BuNH₂BH₃ as reducing agent at (A) room temperature and at (B) 70°C.

UV-Vis spectroscopy was done on both samples (room temperature and 70°C). An absorption band around 520 nm was observed for both. The characteristic absorption plasmon band confirmed the presence of Au NPs in the samples (Figure III-6). The UV-Vis spectra are similar even though in the sample at 70°C, the main population are ultra-small particles. NPs population absorption profile overpowers the spectrum. There is not too much difference in position and width between the two spectra, we could have expected something else given the difference in size.

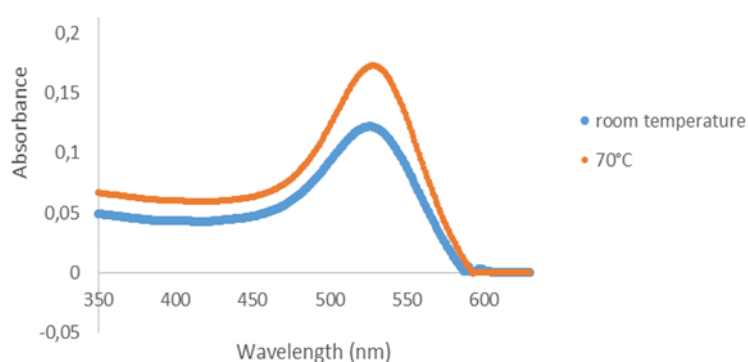


Figure III-6 UV-Vis spectra of gold nanoparticles synthesized using AuClPPh₃, C12-Br and *t*BuNH₂BH₃ as reducing agent, at room temperature (blue) and at 70°C (orange).

Controlling the kinetics of Au(I) reduction is essential for obtaining nanoclusters, indeed the use of a milder reducing agent produced gold nanoparticles instead of AuNCs in our reaction conditions. With the mild reducing agent, formation of gold NPs is favored. This result is not completely surprising because *t*BuNH₂BH₃ is a weaker base than NaBH₄ and thus has more difficulty deprotonating the imidazolium salts. As a consequence, less ligands would be

Syntheses of n-heterocyclic carbene stabilized gold nanoclusters from imidazolium salts and AuCIPPh₃

available to coordinate to the surface and the particles would be bigger and not stop at the NCs formation step. Also, tBuNH₂BH₃ is a weaker reducing agent compared to NaBH₄ favoring longer particles nucleation time compared to reduction. We were able to see that temperature can affect the reaction kinetic by favoring the formation of smaller particles in these conditions. Finally, we concluded that the conditions which were more favorable to the formation of stable NCs suspensions were the one with NaBH₄ as a reducing agent and at least 4 equiv. of imidazolium salt at room temperature.

Literature has shown that when it comes to ensure a precise size control, it is not only necessary to stop the growth of nanoclusters at an early stage but also that the complexation is strong enough to protect them from an Ostwald ripening step to prevent the nanocluster suspensions from turning into nanoparticles.⁸ Sodium Borohydride seem to be able to deprotonate the imidazolium and reduce gold at a good rate. There is a clear kinetic effect in the nanocluster formation mechanism that is highlighted here.

III.B.1.d. NMR Analysis

At this stage, we do not know if PPh₃ or NHC capped NCs only, or a mixture of both. We performed ³¹P NMR in deuterated derivative of toluene (toluene-d₈) and methanol (methanol-d₄) to see if there was signals of the phosphine bounded to gold NCs around 50 ppm as reported by Wang et al. for Au₁₁-PPh₃ clusters.⁹ It would give us a hint at the PPh₃ capped NCs formation. NMR analysis was done on the sample synthesized from C12-Br and NaBH₄ (Figure III-7).

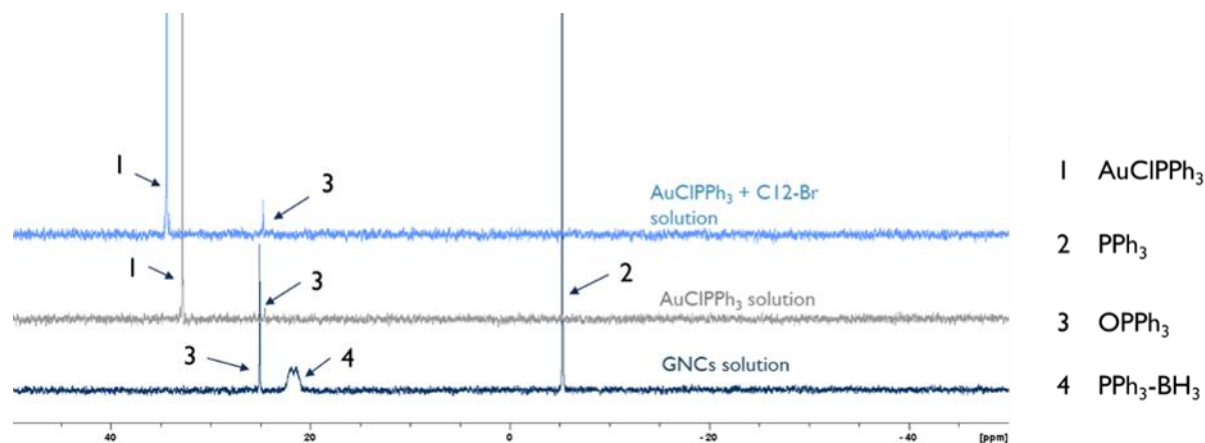


Figure III-7 ³¹P NMR spectra of gold source and C12-Br, gold source alone, and NCs suspension.

A solution of the gold precursor (AuCIPPh₃) and C12-Br ligand was analyzed (Figure III-7, light blue) and signals corresponding to AuCIPPh₃, PPh₃ and OPPh₃ were seen. The same were found in the solution of gold precursor alone (grey). In AuNCs suspension (dark blue), no AuCIPPh₃ was found which means all the gold precursor reacted. There was still some PPh₃ and OPPh₃ in the NCs solution and around 22 ppm, PPh₃-BH₃ signal appeared. However, the supposed AuNCs-PPh₃ signal was not observed which could mean that there are no PPh₃ capped NCs in solution (Figure III-7).

III.B.2. Mass spectrometry (MS) analysis

III.B.2.a. Instrumentation and software

Samples produced from AuClPPh₃, imidazolium salts and NaBH₄ in EtOH were analyzed by mass spectrometry (MS) to further identify the nature and the structure of NCs which are synthesized. The analyses were done using several mass spectrometer to confirm the results and to prevent a potential influence of the mass analyzer on the as-obtained structures.

As a reminder from chapter II, one of the analyzers is a Fourier-transform ion cyclotron resonance mass spectrometry (FT-ICR). This technology of mass spectrometer is used to determine the mass-to-charge ratio (m/z) of ions based on the cyclotron frequency of the ions in a fixed magnetic field. We also used ESI-TOF (Electrospray Ionization Time-of-Flight), TIMS-TOF (Trapped Ion Mobility Time-of-Flight) and MALDI-TOF (Matrix Assisted Laser Desorption Ionization Time-of-Flight). Time-of-flight mass spectrometry is a method in which an ion's m/z is determined by a time-of-flight measurement.

These methods allow us to get mass spectra where patterns can be attributed to molecules or NCs in an analyzed suspension. A study of the m/z value was conducted and the isotopic pattern were compared to see if they fit with a precise formula. At the beginning of this study, the rebuilding of the formula was done by “hand” but given the great number of NCs per single solution and the complexity of the structures, our team developed an analysis algorithm. Chapter II of this manuscript has in depth information on the mass spectrometry analysis methodology.

III.B.2.b. Analysis of synthesis with imidazolium iPr-Br

We first analyzed the samples coming from the reaction between AuClPPh₃, iPr-Br and NaBH₄ in EtOH. A study of the composition of the suspensions by ESI-MS just after purification was carried out (Figure III-8). Then, aging of the suspension and stability over time at room temperature was followed. We observed a polydisperse solution of cationic AuNCs of different formulas with gold number going from 6 to 40 (Figure III-8).

| Au NCS Formula | Nbr Au | m/z | Au NCS Formula | Nbr Au | m/z |
|--|--------|-----------|---|--------|-----------|
| Au ₆ (PPh ₃) ₅ Br ⁺ | 6 | 2573,1737 | Au ₁₁ (PPh ₃) ₇ (iPr)Br ²⁺ | 11 | 4314,2404 |
| Au ₆ (PPh ₃) ₆ Br ⁺ | 6 | 2835,2656 | Au ₂₀ (PPh ₃) ₁₂ H ₃ ³⁺ | 20 | 2363,1512 |
| Au ₈ (PPh ₃) ₆ ²⁺ | 8 | 1574,6408 | Au ₂₁ (PPh ₃) ₁₁ Br ²⁺ | 21 | 3550,6115 |
| Au ₈ (PPh ₃) ₇ Br ⁺ | 8 | 3491,2906 | Au ₂₁ (PPh ₃) ₁₁ Cl ²⁺ | 21 | 3528,1369 |
| Au ₉ (PPh ₃) ₇ H ²⁺ | 9 | 1804,6736 | Au ₃₈ (PPh ₃) ₁₅ Br ³⁺ | 38 | 3833,0073 |
| Au ₉ (PPh ₃) ₈ H ²⁺ | 9 | 1935,7192 | [Au ₄₀ (PPh ₃) ₁₄ Br ₄] ²⁺ | 40 | 5935,3079 |
| Au ₁₀ (PPh ₃) ₈ Br ⁺ | 10 | 4147,3154 | | | |
| Au ₁₁ (PPh ₃) ₈ H ²⁺ | 11 | 2132,6857 | | | |
| Au ₁₁ (PPh ₃) ₈ Br ₂ ⁺ | 11 | 4424,2003 | | | |
| Au ₁₁ (PPh ₃) ₉ H ²⁺ | 11 | 2263,7313 | | | |

Figure III-8 List of mixed PPh₃ only (red) and mixed PPh₃-iPr capped AuNCs (green) obtained by ESI-MS analysis of samples synthesized from AuClPPh₃, iPr-Br and NaBH₄, 5 hours after the synthesis.

The suspensions were composed of mostly a mixture of numerous PPh₃ capped AuNCs and only one specie with iPr-Br NHC ligand in its formula (Figure III-9 a)). This last one corresponds to Au₁₁(PPh₃)₇(iPr)Br₂⁺. It means that there are no clusters with more than one NHC ligand on the surface of the gold core that is formed. The nanocluster Au₁₁(PPh₃)₇(iPr)Br₂⁺ pattern was almost not detected at t = 0 but after 1 week, it was the nanocluster of highest intensity and relative abundancy.

Concerning single PPh₃ capped AuNCs, some structures had already been reported few years ago and others more recently.¹⁰ Indeed, an overview of the literature shows that there are very few articles describing the evolution of the species in suspension after synthesis. Most of the time, they specifically studied the most stable NCs structure or manage to crystallize one NCs structure, that is not necessarily the most representative in number of the species present in solution. Moreover, even if recent studies in the literature have demonstrated the existence of specific gold nanoclusters with a precise description of their chemical composition and structure, the complexity of the real mixture in terms of cluster diversity by their nuclearity and by the nature of the ligands has not yet been plenty addressed.

Figure III-9 a) Abundance of the number of gold nanoclusters identified for each ligand. b) Comparison of the number of gold atoms in identified nanoclusters to the number of ligands. The area of each dot is proportional to the number of different nanoclusters containing the same number of gold atoms and ligands. c) Bar chart histogram showing the number of nanoclusters identified depending on the number of gold atoms (red for PPh₃ only capped AuNCs and green for mixed iPr and PPh₃ capped AuNCs). All for samples at t = 0.

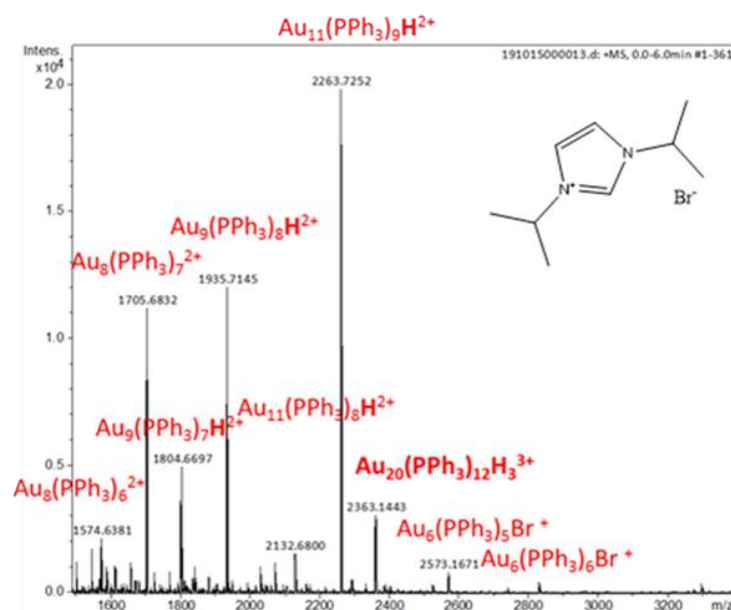


Figure III-10 FT-ICR MS spectra of NCs suspension synthesized from AuClPPh₃, NaBH₄ and *i*Pr-Br just after purification (at *t*₀). Not all PPh₃ capped AuNCs species are reported on this cf Figure III-8 for complete list).

When plotting the variation of the number of ligands with nuclearity (Figure III-9 b), it was observed that for smaller structures (Au₆ to Au₉) the number of ligands, *n*, is usually equal to the number of gold atoms, *x*, or to the number of gold atoms minus 1, *x*-1. We have a ligand:gold atom ratio of approximatively 1 in this experiment for smaller nanoclusters. This tendency was observed in the literature for the synthesis of nanoclusters Au₆(PPh₃)₆²⁺,¹¹ Au₈(PPh₃)₇²⁺,¹² Au₉(PPh₃)₈]H²⁺¹³ (Figure III-11).



Figure III-11 Schematic structural representation of Au₆(PPh₃)₆²⁺,¹⁰ Au₈(PPh₃)₇²⁺,¹¹ and Au₉(PPh₃)₈]H²⁺¹² (from left to right respectively).

However, from Au₁₁ to Au₂₁, this linear tendency changes, with a maximum of 12 ligands for all nanoclusters in this nuclearity range. It implies that there is a size range at which there is no more linear addition of ligands with increasing number of gold atoms in the nanoclusters structure. For larger PPh₃ protected gold nanoclusters, a study of the literature shows the same results with a nonlinear evolution of the number of ligands with the number of gold atoms. Various examples were reported such as for nanoclusters, Au₂₀(PPh₃)₁₂H₃³⁺¹⁴ or Au₅₅(PPh₃)₁₂Cl₆.¹⁵ These differences in the ligand to gold ratio may be due to the ligand coordination pattern (as PPh₃ is a monodentate ligand) and also to the nanoclusters core geometry. This will be discussed later. Then, by studying the number of identified nanoclusters correlated to the number of gold atoms, it appears that Au₁₁ nanocluster is the most common cluster size (Figure III-9 b and c). It means that the Au₁₁ structure stabilizes better various nanoclusters than the other structures of different nuclearity. Not only it is the most common

Syntheses of n-heterocyclic carbene stabilized gold nanoclusters from imidazolium salts and AuClPPh₃

size but it is also the most prominent when observing the intensity on the ESI-MS spectra at $t = 0$. Indeed, nanocluster $\text{Au}_{11}(\text{PPh}_3)_9[\text{H}^+]$ is highly detected (Figure III-10). It is followed by Au_9 and Au_8 nanoclusters that are also present in high intensity in ESI-MS spectra (Figure III-10). While it is well-known that nanoclusters in the Au_6 to Au_9 range are most abundant in syntheses of PPh_3 capped AuNCs,^{6,12} this synthesis highlights Au_{11} nanoclusters. XRD analysis of Au_{11} nanoclusters, $[\text{Au}_{11}(\text{PPh}_3)_8\text{Cl}_2]\text{Cl}$, unveiled an undecagold with eight phosphines and two chloride in the ligand shell and one outer sphere chloride.¹⁶ The effect of the NHC on the suspensions has then to be discussed.

In order to discuss about the stability of these different clusters, a study of the suspensions aged one week was carried out by ESI-TOF-MS and ESI-FTICR-MS. A strong evolution in the spectra of the fresh suspensions and 1 week after ageing can be seen (Figure III-12). At $t = 0$ (day 1), a dozen of patterns corresponding to single PPh_3 capped NCs with various formulas are clearly identified (Figure III-10). After one week ageing, the MS analysis showed that some of the PPh_3 capped NCs pattern disappeared from the spectra and the intensity of some other increased: only five types of PPh_3 capped NCs were still visible on the spectra (Figure III-12). It was observed that nanocluster $\text{Au}_5(\text{PPh}_3)_5^+$ was detected (which was not the case at $t = 0$). But we could not conclude if it was newly formed or if abundance increased allowing better detection. Also, there is a high increasing of a NCs with $i\text{Pr}-\text{Br}$ at the surface, $\text{Au}_{11}(\text{PPh}_3)_7(i\text{Pr})\text{Br}_2^+$. The intensity of the signals corresponding to this particular NCs was very low at $t = 0$. The $\text{Au}_{11}(\text{PPh}_3)_7(i\text{Pr})\text{Br}_2^+$ cluster has the highest pattern intensity over all the other NCs structures after few days and the tendency is confirmed when the analysis is conducted on the same suspension after 2 months. The experiment was repeated 6 times to ensure the reliability of this result. Looking at the low masses, $\text{Au}(i\text{Pr})_2$ monometallic complexes pattern intensity increase was also detected in the suspension after 1 week. It probably means that the less stable NCs dissolve to form more stable molecular complexes whereas the more stable clusters just remain in the suspension.

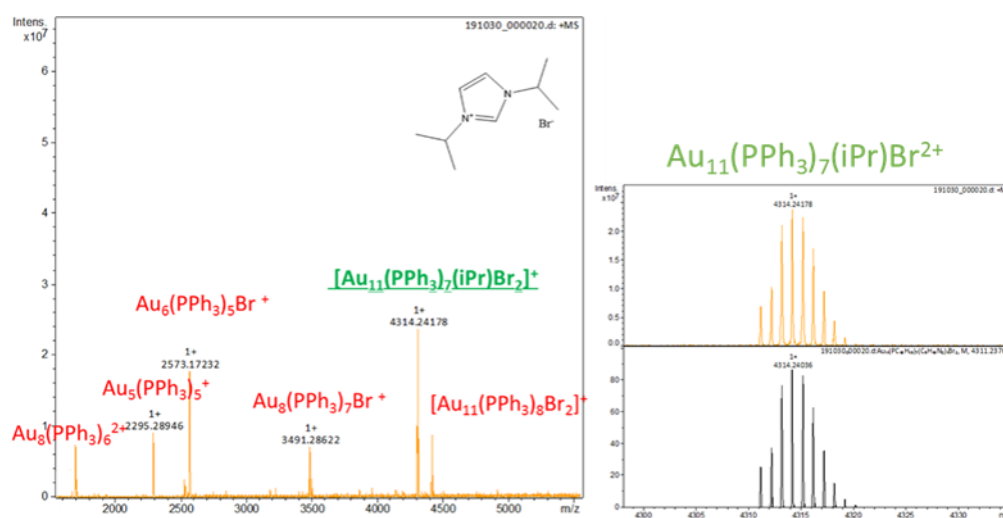


Figure III-12 FT-ICR MS spectra of NCs suspension synthesized from AuClPPh_3 , NaBH_4 and $i\text{Pr}-\text{Br}$ after 1 week (left). Theoretical (black) and experimental (yellow) isotopic patterns for $\text{Au}_{11}(\text{PPh}_3)_7(i\text{Pr})\text{Br}_2^+$.

Thus, we make the hypothesis that there is potentially a redistribution of clusters with an increase in the number of stable clusters due to a shift in equilibrium in solution. Another

Syntheses of n-heterocyclic carbene stabilized gold nanoclusters from imidazolium salts and AuClPPh₃

information can be extracted from the ESI-MS spectra (Figure III-10 and Figure III-12). There is a clear disappearance of the PPh₃-H⁺ cluster on the spectra between t = 0 and 1 week. Since PPh₃ protected nanoclusters synthesis has been reported through HCl etching and growth effects,⁶ in similar reaction conditions, it is possible that in our case H⁺ has an etching effect on some of the nanoclusters to form other nanoclusters. Also, it has recently been reported that small hydrogen-containing intermediate “building blocks” (e.g., Au₂(PPh₃)₂H⁺, Au₄(PPh₃)₄H⁺, and Au₇(PPh₃)₇H₅²⁺) are responsible for the growth of larger gold clusters (e.g., Au₆(PPh₃)₆²⁺ and Au₈(PPh₃)₇²⁺) in solution.¹⁷ Previous studies indicated that hydrogens may have a promotional effect on gold cluster reactivity.¹⁸ Takano *et. al.* demonstrated that a hydride-doped Au₉(PPh₃)₈H²⁺ cluster may contain hydrogen as a placeholder for subsequent addition of gold atoms from solution. The Au₉(PPh₃)₈H²⁺ cluster was also found to decrease in abundance over time.¹³

Same experiment was done with other imidazolium salts to determine the influence of NHC type on the distribution of the various clusters.

Syntheses of n-heterocyclic carbene stabilized gold nanoclusters from imidazolium salts and AuClPPh₃

III.B.2.c. Analysis of synthesis with imidazolium C12-Br

We analyzed the samples coming from the reaction between AuClPPh₃, C12-Br and NaBH₄ in EtOH. A study of the composition of the suspension by ESI-MS just after purification was carried out. Then, aging of the suspension and stability over time at room temperature was followed. We observed a polydisperse solution of cationic PPh₃ and NHC-ligated-gold AuNCs with different nuclearities from 5 to 129 gold atoms. We obtained mostly a mixture of single PPh₃ capped AuNCs, few species with mixed PPh₃ and NHC ligands and two species with only C12-Br NHC ligand at the surface (Figure III-13).

| Au NCS Formula | Nbr Au | m/z | Au NCS Formula | Nbr Au | m/z | Au NCS Formula | Nbr Au | m/z | Au NCS Formula | Nbr Au | m/z |
|--|--------|-----------|--|--------|-----------|--|--------|-----------|---|--------|------------|
| Au ₅ (PPh ₃) ₅ ⁺ | 5 | 2295,288 | Au ₈ (PPh ₃) ₆ Br ⁺ | 8 | 3229,1988 | Au ₁₀ (PPh ₃) ₇ Br ₃ ⁺ | 10 | 4045,0587 | Au ₁₂ (PPh ₃) ₈ BrCl ₂ ⁺ | 12 | 4612,1862 |
| Au ₅ (C12) ₄ ⁺ | 5 | 2603,4878 | Au ₈ (PPh ₃) ₇ ²⁺ | 8 | 1705,6864 | Au ₁₀ (PPh ₃) ₈ H ⁺ | 10 | 4068,4054 | Au ₁₂ (PPh ₃) ₈ Br ₂ H ⁺ | 12 | 4622,1747 |
| Au ₅ (C12) ₅ ⁺ | 5 | 3007,9008 | Au ₈ (PPh ₃) ₇ Cl ⁺ | 8 | 3446,3422 | Au ₁₀ (PPh ₃) ₈ Cl ⁺ | 10 | 4102,3665 | Au ₁₂ (PPh ₃) ₈ Br ₂ Cl ⁺ | 12 | 4657,1349 |
| Au ₅ (PPh ₃)(C12) ₄ ⁺ | 5 | 2865,5789 | Au ₈ (PPh ₃) ₇ Br ⁺ | 8 | 3491,2906 | Au ₁₀ (PPh ₃) ₈ Br ⁺ | 10 | 4147,3154 | Au ₁₂ (PPh ₃) ₈ Br ₃ ⁺ | 12 | 4701,0837 |
| Au ₅ (PPh ₃) ₂ (C12) ₃ ⁺ | 5 | 2723,257 | [Au ₈ (PPh ₃) ₅ (C12)Br] ⁺ | 8 | 3371,521 | Au ₁₀ (PPh ₃) ₈ ²⁺ | 10 | 2033,6985 | Au ₁₃ (PPh ₃) ₉ Br ₂ ⁺ | 13 | 5081,2254 |
| Au ₅ (PPh ₃) ₃ (C12) ₂ ⁺ | 5 | 2580,9351 | [Au ₈ (PPh ₃) ₆ (C12)Br] ⁺ | 8 | 3633,6128 | Au ₁₀ (PPh ₃) ₈ Br ₂ H ²⁺ | 10 | 2074,1614 | Au ₁₄ (PPh ₃) ₉ ²⁺ | 14 | 2558,6772 |
| Au ₅ (PPh ₃) ₄ (C12) ⁺ | 5 | 2438,6132 | Au ₉ (PPh ₃) ₇ H ²⁺ | 9 | 1804,6736 | [Au ₁₀ (PPh ₃) ₆ (C12)Br ₃] ⁺ | 10 | 4187,3815 | Au ₁₅ (PPh ₃) ₉ H ²⁺ | 15 | 2657,6644 |
| Au ₆ (PPh ₃) ₅ Br ⁺ | 6 | 2573,1737 | Au ₉ (PPh ₃) ₇ Br ²⁺ | 9 | 1844,1283 | Au ₁₀ (PPh ₃) ₇ (C12)H ⁺ | 10 | 4210,721 | Au ₁₆ (PPh ₃) ₁₀ ²⁺ | 16 | 2886,6894 |
| Au ₆ (PPh ₃) ₆ Br ⁺ | 6 | 2835,2656 | Au ₉ (PPh ₃) ₇ ClH ⁺ | 9 | 3644,3166 | Au ₁₁ (PPh ₃) ₈ H ²⁺ | 11 | 2132,6857 | Au ₂₀ (PPh ₃) ₁₂ H ₂ ²⁺ | 20 | 3544,2232 |
| Au ₇ (PPh ₃) ₆ ⁺ | 7 | 2952,3156 | Au ₉ (PPh ₃) ₇ BrH ⁺ | 9 | 3689,265 | Au ₁₁ (PPh ₃) ₈ Cl ₂ ⁺ | 11 | 4335,3019 | Au ₂₀ (PPh ₃) ₁₂ H ₃ ³⁺ | 20 | 2363,1512 |
| Au ₇ (PPh ₃) ₇ ⁺ | 7 | 3214,4068 | Au ₉ (PPh ₃) ₇ BrCl ⁺ | 9 | 3723,2252 | Au ₁₁ (PPh ₃) ₈ BrH ⁺ | 11 | 4345,2898 | Au ₂₁ (PPh ₃) ₁₁ Cl ²⁺ | 21 | 3528,1369 |
| Au ₇ (PPh ₃) ₅ (C12) ⁺ | 7 | 3094,6375 | Au ₉ (PPh ₃) ₇ Br ₂ | 9 | 3768,1757 | Au ₁₁ (PPh ₃) ₈ BrCl ⁺ | 11 | 4380,2513 | Au ₂₁ (PPh ₃) ₁₁ Br ²⁺ | 21 | 3550,6115 |
| Au ₇ (PPh ₃) ₄ (C12) ₂ ⁺ | 7 | 3236,9594 | Au ₉ (PPh ₃) ₈ H ²⁺ | 9 | 1935,7192 | Au ₁₁ (PPh ₃) ₈ Br ₂ ⁺ | 11 | 4424,2003 | Au ₃₈ (PPh ₃) ₁₅ Br ³⁺ | 38 | 3833,0073 |
| Au ₇ (PPh ₃) ₆ (C12) ⁺ | 7 | 3356,7287 | Au ₁₀ (PPh ₃) ₇ Br ⁺ | 10 | 3885,2237 | Au ₁₁ (PPh ₃) ₉ H ²⁺ | 11 | 2263,7313 | Au ₄₀ (PPh ₃) ₁₄ Br ₄ ²⁺ | 40 | 5935,3079 |
| Au ₈ (PPh ₃) ₆ ²⁺ | 8 | 1574,6408 | Au ₁₀ (PPh ₃) ₇ Br ₂ H ⁺ | 10 | 3966,1501 | [Au ₁₁ (PPh ₃) ₇ (C12)Br ₂] ⁺ | 11 | 4566,5224 | Au ₁₂₉ (PPh ₃) ₂₄ ³⁺ | 129 | 10567,7906 |

Figure III-13 List of mixed PPh₃ only (red), mixed PPh₃-C12 capped AuNCs (green) and single C12 (blue) capped AuNCs obtained by ESI-MS analysis of samples synthesized from AuClPPh₃, C12-Br and NaBH₄, 5 hours after the synthesis.

Syntheses of n-heterocyclic carbene stabilized gold nanoclusters from imidazolium salts and AuClPPh₃

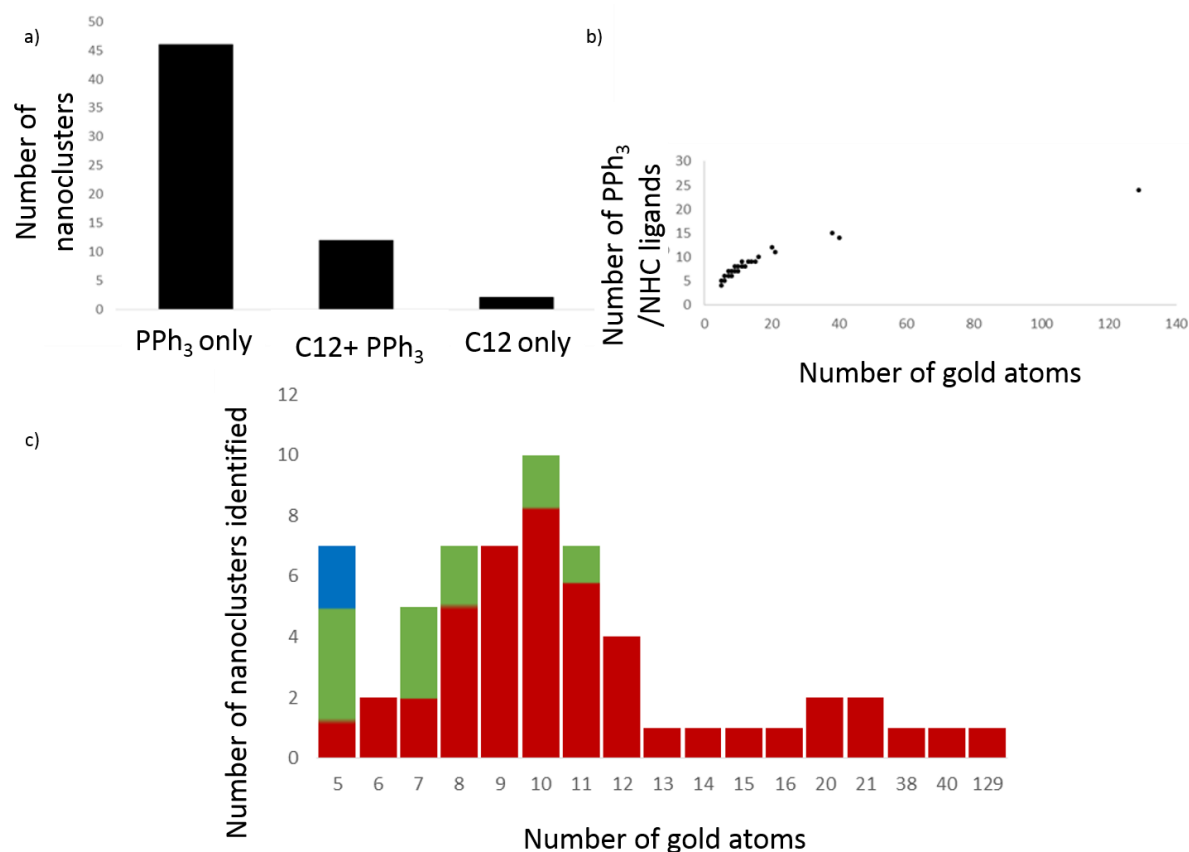


Figure III-14 a) Abundance of the number of gold nanoclusters identified for each ligand. b) Comparison of the number of gold atoms in identified nanoclusters to the number of ligands. c) Bar chart histogram showing the number of nanoclusters identified depending on the number of gold atoms (red for PPh₃ only capped AuNCs, green for mixed C12 and PPh₃ capped AuNCs, blue for only C12 capped AuNCs). All for samples at *t*₀.

Through ESI-MS spectra analysis, we could obtain some information on the chemical composition of the nanoclusters. There are 46 patterns corresponding to PPh₃ capped NCs with various formulas. There are also 12 patterns associated with mixed PPh₃ and C12-Br capped AuNCs with varying number of ligands. Moreover, there are only 2 AuNC structures capped only by C12-Br: Au₅(C12)₅⁺ and Au₅(C12)₄⁺ (Figure III-14 a). With ligand C12, there is a higher diversity of PPh₃, mixed PPh₃ and C12 and C12 capped nanoclusters that are formed than with ligand iPr. When plotting the variation of the number of ligands with nuclearity (Figure III-14 b), a curve with a logarithmic tendency is observed. For smaller structures (Au₆ to Au₉) the number of ligands evolves linearly with the number of gold atoms. The ligand:Au atom ratio is ca. 1 in this experiment for smaller nanoclusters and when the number of gold atoms is above 10, this tendency disappears. The use of different NHC ligand did not affect this parameter that is also observed when using ligand iPr. Finally, the number of identified nanoclusters as a function of the number of gold atoms shows that Au₁₁, Au₈ and Au₉ nanoclusters are quite common cluster sizes that are found when using C12-Br imidazolium salt as a NHC precursor. However, with ligand C12, Au₁₀ nanocluster is the most common cluster size (Figure III-14 c). Another nanocluster type appeared here with ligand C12, which is common to high number of nanoclusters, Au₅ nanoclusters. When observing the relative

Syntheses of n-heterocyclic carbene stabilized gold nanoclusters from imidazolium salts and AuClPPh₃

intensity of the patterns in the ESI-MS spectra at $t = 0$, the pattern corresponding to nanocluster $\text{Au}_5(\text{C12})_5^+$ was the most intense and relatively abundant with a ligand:Au stoichiometry of 1:1 (Figure III-15) inside the cluster.

It means that the nature of the ligand does not influence the ligand:Au ratio tendency but it does influence which clusters are abundant in solution regarding the number of Au atoms. The use of C12 ligand stabilized smaller nanoclusters with high relative abundance but also bigger nanoclusters (with low relative abundance). Indeed, the number of PPh₃ capped AuNCs is higher with C12-Br ligand and the nuclearity reaches 129 gold atoms in this case. At this step, there is a large panel of gold nanoclusters nuclearities. It means there is a clear influence of the type of NHC ligand on the PPh₃ capped AuNCs. With ligand C12-Br, we observe more diversity in the obtained nanoclusters. There is more both PPh₃ capped AuNCs species and mixed PPh₃-NHC capped AuNCs species. There is also more NHC capped AuNCs as well. In fact, we see that the coordination of C12-Br is more competitive than that of iPr. It could be due to various effects such as a stronger donor effect or the steric effects of the alkyl chains. We made the hypothesis that the longer side chains (iPr vs C₁₂H₂₅) allowed a better stabilization of various PPh₃ capped AuNCs. Indeed, studies showed that ligand length has a strong effect on particle spacing. Adding ligands to the core works as an isolation layer to the core and difference in relative energies is reduced. For longer ligands, the difference is increased in comparison to shorter ligands, but also to unprotected cores.¹⁹ It was also reported thanks to natural bond orbital analyses that steric effects play an important role in determining final cluster architectures.²⁰

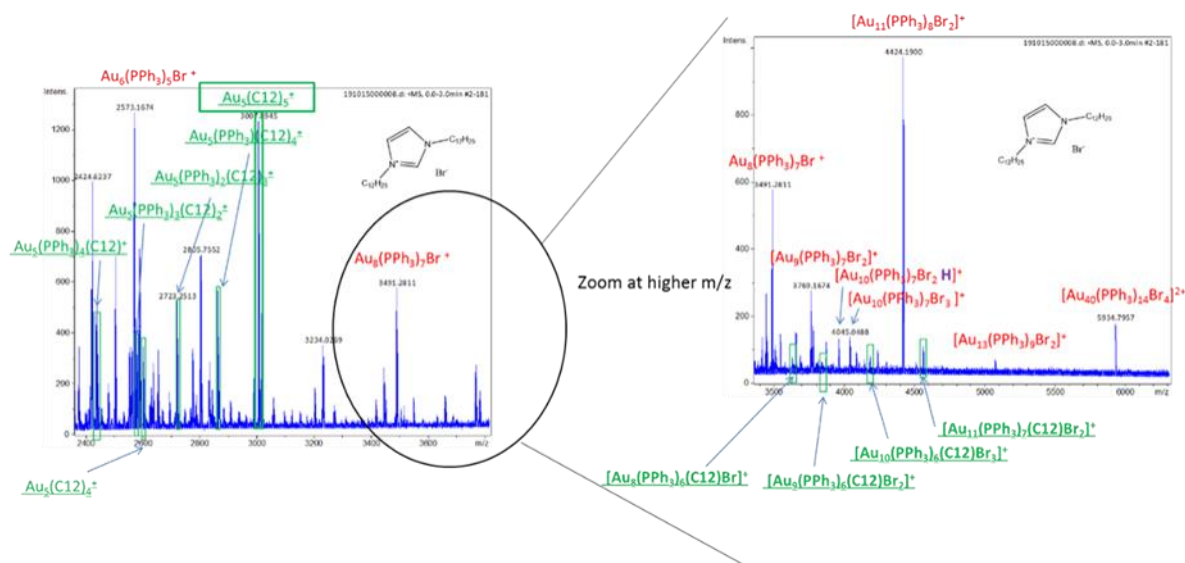


Figure III-15 FT-ICR MS spectra of NCs suspension synthesized from AuClPPh₃, NaBH₄ and C12-Br just after purification (at t_0). Not all PPh₃ capped AuNCs species are reported on this cf Figure III-14 for complete list.

After one week, the ESI-MS analysis showed that many of the PPh₃ capped NCs patterns disappeared from the spectra. The only PPh₃ capped nanoclusters that remained were: $\text{Au}_8(\text{PPh}_3)_7^{2+}$, $\text{Au}_9(\text{PPh}_3)_8\text{H}^{2+}$, $\text{Au}_5(\text{PPh}_3)_5^+$, $\text{Au}_6(\text{PPh}_3)_5\text{Br}^+$, $\text{Au}_{10}(\text{PPh}_3)_8\text{Br}^+$, $\text{Au}_8(\text{PPh}_3)_7\text{Br}^+$, $\text{Au}_{11}(\text{PPh}_3)_8\text{BrCl}^+$, and $\text{Au}_{11}(\text{PPh}_3)_8\text{Br}_2^+$ (Figure III-16). The intensity of some other patterns increased as for $\text{Au}_{11}(\text{PPh}_3)_7(\text{C12})\text{Br}_2^+$ (similar to what we observed with the samples with iPr-Br). In this case, all the patterns corresponding to mixed or single NHC capped AuNCs structures disappeared after 1 week except from one: $\text{Au}_{11}(\text{PPh}_3)_7(\text{C12})\text{Br}_2^+$ (Figure III-16). As

Syntheses of n-heterocyclic carbene stabilized gold nanoclusters from imidazolium salts and AuClPPh₃

we observed for the synthesis with iPr-Br ligand, for the PPh₃ capped AuNCs, there is an evolution of NCs composition over time in the suspension. The NCs structures which are unstable disappear whereas the most stable species stay stable over time. As for the NHC (ligand C12-Br) capped AuNCs, only one structure seems to remain stable over time: Au₁₁(PPh₃)₇(C12)Br₂⁺. Indeed, others C12-Br capped NCs patterns disappear with ageing of the suspensions. The nanocluster Au₁₁(PPh₃)₇(C12)Br₂⁺ is the same formula that was obtained and remained stable with ligand iPr-Br (Au₁₁(PPh₃)₇(iPr)Br₂⁺). However, with ligand C12, the nanocluster Au₁₁(PPh₃)₇(NHC)Br₂⁺ relative abundancy in ESI-MS is not the highest (high but lower than Au₁₁(PPh₃)₈Br₂⁺).

Similarly to the synthesis with ligand iPr, various PPh₃ capped AuNCs structures remain stable over time in the suspension (Figure III-16). The number of gold atoms goes from 5 to 11 with only one Au11 structure incorporating 1 NHC. However, the stabilization of only NHC capped AuNCs does not happen in these conditions.

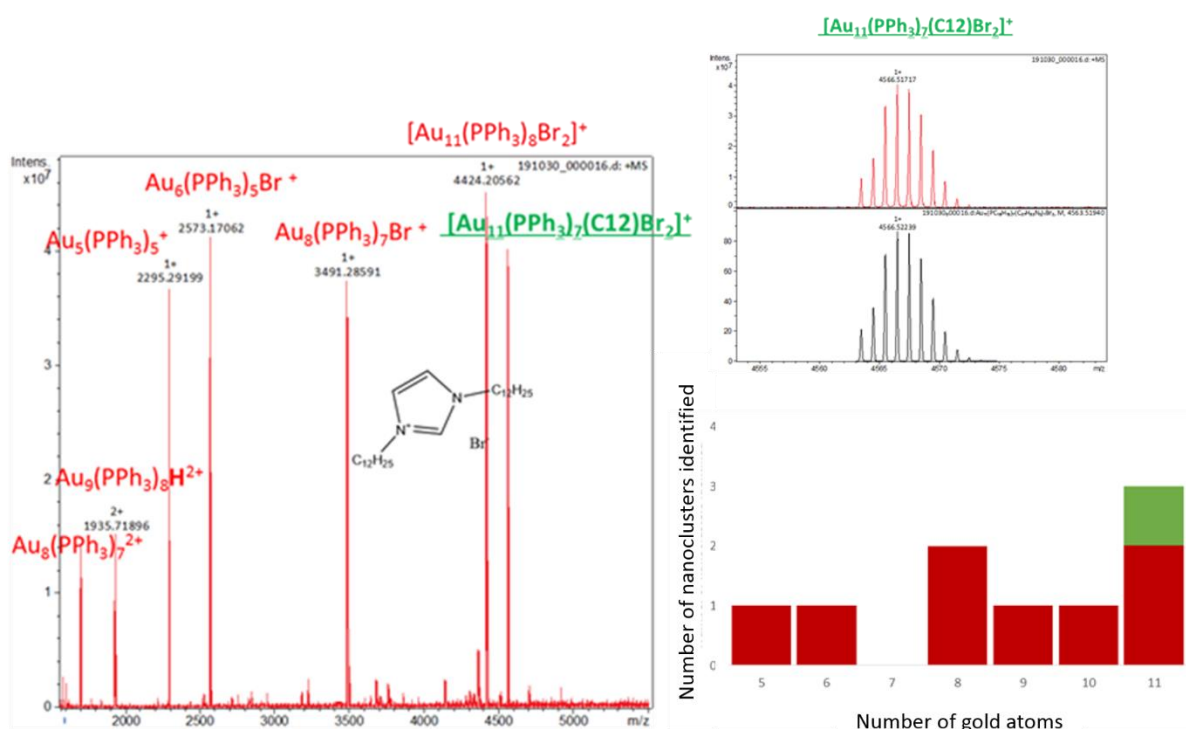


Figure III-16 FT-ICR MS spectra of NCs suspension synthesized from AuClPPh₃, NaBH₄ and C12-Br after 1 week (left). Bar chart histogram showing the number of nanoclusters identified depending on the number of gold atoms (red for PPh₃ only capped AuNCs, green for mixed C12 and PPh₃ capped AuNCs) for sample at 1 week (right).

There is also a clear disappearance of the PPh₃-H⁺ cluster on the spectra between t = 0 and 1 week (exception for Au₉(PPh₃)₈H₂²⁺ which did not disappear but intensity decreased). It is probably due to the same H⁺ growth effect explained previously.¹⁷ The main differences between the iPr and C12 ligand synthesis were observed at t = 0, just after synthesis. It seems to be a clear effect of the ligand on the different clusters abundancy. However, after one week,

Syntheses of n-heterocyclic carbene stabilized gold nanoclusters from imidazolium salts and AuClPPh₃

the stabilized nanoclusters are similar for both ligands unveiling a common reactivity mechanism.

III.B.2.d. Synthesis with imidazolium bC12-Br

We analyzed the samples coming from the reaction between AuClPPh₃, bC12-Br and NaBH₄ in EtOH. A study of the composition of the suspension by ESI-MS was also done just after purification. Then aging of the suspensions and stability over time at room temperature was followed. AuNCs with different formulas were obtained with a nuclearity going from 5 to 129. A mixture of PPh₃ capped AuNCs was mostly synthesized. Actually it was the same structures that were obtained for the synthesis with ligand C12-Br (Figure III-17, Figure III-18 a). A few species with mixed PPh₃ and NHC ligands were also obtained and one with only bC12 ligand at the surface was synthesized (Figure III-17).

For this ligand, the AuNCs structure with NHC in its formula with the biggest number of gold atoms was detected with a very low intensity: Au₂₁(PPh₃)₁₀(bC12)₆Br²⁺ (Figure III-17).

| Au NCS Formula | Nbr Au | m/z | Au NCS Formula | Nbr Au | m/z | Au NCS Formula | Nbr Au | m/z | Au NCS Formula | Nbr Au | m/z |
|---|--------|-----------|--|--------|-----------|---|--------|-----------|--|--------|-----------|
| Au ₅ (PPh ₃) ₅ ⁺ | 5 | 2295,288 | | | | Au ₁₀ (PPh ₃) ₈ Br ⁺ | 10 | 4147,3154 | Au ₁₂ (PPh ₃) ₈ Br ₃ ⁺ | 12 | 4701,0837 |
| Au ₅ (PPh ₃)(bC12) ₄ ⁺ | 5 | 3065,6415 | | | | Au ₁₀ (PPh ₃) ₈ ²⁺ | 10 | 2033,6985 | Au ₁₃ (PPh ₃) ₉ Br ₂ ⁺ | 13 | 5081,2254 |
| Au ₅ (PPh ₃) ₂ (bC12) ₃ ⁺ | 5 | 2873,304 | | | | Au ₁₀ (PPh ₃) ₈ Br ₂ H ²⁺ | 10 | 2074,1614 | Au ₁₄ (PPh ₃) ₉ ²⁺ | 14 | 2558,6772 |
| Au ₅ (bC12) ₄ ⁺ | 5 | 3257,9791 | Au ₉ (PPh ₃) ₇ H ²⁺ | 9 | 1804,6736 | Au ₁₁ (PPh ₃) ₈ H ²⁺ | 11 | 2132,6857 | Au ₁₅ (PPh ₃) ₉ H ²⁺ | 15 | 2657,6644 |
| Au ₆ (PPh ₃) ₅ Br ⁺ | 6 | 2573,1737 | Au ₉ (PPh ₃) ₇ Br ²⁺ | 9 | 1844,1283 | Au ₁₁ (PPh ₃) ₈ Cl ₂ ⁺ | 11 | 4335,3019 | Au ₁₆ (PPh ₃) ₁₀ ²⁺ | 16 | 2886,6894 |
| Au ₆ (PPh ₃) ₆ Br ⁺ | 6 | 2835,2656 | Au ₉ (PPh ₃) ₇ ClH ⁺ | 9 | 3644,3166 | Au ₁₁ (PPh ₃) ₈ BrH ⁺ | 11 | 4345,2898 | Au ₂₀ (PPh ₃) ₁₂ H ₂ ²⁺ | 20 | 3544,2232 |
| Au ₇ (PPh ₃) ₆ ⁺ | 7 | 2952,3156 | Au ₉ (PPh ₃) ₇ BrH ⁺ | 9 | 3689,265 | Au ₁₁ (PPh ₃) ₈ BrCl ⁺ | 11 | 4380,2513 | Au ₂₀ (PPh ₃) ₁₂ H ₃ ³⁺ | 20 | 2363,1512 |
| Au ₇ (PPh ₃) ₇ ⁺ | 7 | 3214,4068 | Au ₉ (PPh ₃) ₇ BrCl ⁺ | 9 | 3723,2252 | Au ₁₁ (PPh ₃) ₈ Br ₂ ⁺ | 11 | 4424,2003 | [Au ₂₁ (PPh ₃) ₁₀ (bC12) ₆ Br ₂] ⁺ | 21 | 3646,7804 |
| Au ₈ (PPh ₃) ₆ (bC12)Br ⁺ | 7 | 2952,3156 | Au ₉ (PPh ₃) ₇ Br ₂ | 9 | 3768,1757 | Au ₁₁ (PPh ₃) ₉ H ²⁺ | 11 | 2263,7313 | Au ₂₁ (PPh ₃) ₁₁ Cl ²⁺ | 21 | 3528,1369 |
| Au ₈ (PPh ₃) ₆ ²⁺ | 8 | 1574,6408 | Au ₉ (PPh ₃) ₈ H ²⁺ | 9 | 1935,7192 | [Au ₁₁ (PPh ₃) ₇ (bC12)Br ₂] ⁺ | 11 | 4616,5381 | Au ₂₁ (PPh ₃) ₁₁ Br ²⁺ | 21 | 3550,6115 |
| Au ₈ (PPh ₃) ₆ Br ⁺ | 8 | 3229,1988 | Au ₁₀ (PPh ₃) ₇ Br ⁺ | 10 | 3885,2237 | [Au ₁₁ (PPh ₃) ₇ (bC12) ₂ Br ₂] ⁺ | 11 | 4809,8764 | Au ₃₈ (PPh ₃) ₁₅ Br ³⁺ | 38 | 3833,0073 |
| Au ₈ (PPh ₃) ₇ ²⁺ | 8 | 1705,6864 | Au ₁₀ (PPh ₃) ₇ Br ₂ H ⁺ | 10 | 3966,1501 | [Au ₁₁ (PPh ₃) ₇ (bC12)Br ₃ H] ⁺ | 11 | 4697,463 | Au ₄₀ (PPh ₃) ₁₄ Br ₄ ²⁺ | 40 | 5935,3079 |
| Au ₈ (PPh ₃) ₇ Cl ⁺ | 8 | 3446,3422 | Au ₁₀ (PPh ₃) ₇ Br ₃ ⁺ | 10 | 4045,0587 | Au ₁₂ (PPh ₃) ₈ BrCl ₂ ⁺ | 12 | 4612,1862 | Au ₁₂₉ (PPh ₃) ₂₄ ³⁺ | 129 | 10567,791 |
| Au ₈ (PPh ₃) ₇ Br ⁺ | 8 | 3491,2906 | Au ₁₀ (PPh ₃) ₈ H ⁺ | 10 | 4068,4054 | Au ₁₂ (PPh ₃) ₈ Br ₂ H ⁺ | 12 | 4622,1747 | | | |
| | | | Au ₁₀ (PPh ₃) ₈ Cl ⁺ | 10 | 4102,3665 | Au ₁₂ (PPh ₃) ₈ Br ₂ Cl ⁺ | 12 | 4657,1349 | | | |

Figure III-17 List of mixed PPh₃ only (red), mixed PPh₃-bC12 capped AuNCs (green) and single bC12 (blue) capped AuNCs obtained by ESI-MS analysis of samples synthesized from AuClPPh₃, bC12-Br and NaBH₄, 5 hours after the synthesis.

When plotting the variation of the number of ligands with nuclearity (Figure III-18 b)), it was observed that for smaller structures, the number of ligands is usually equal to the number of gold atoms as for the other previous ligands. The results for the ligand:Au ratio for bigger nanoclusters are the same as with the other ligands. It shows that the nature of the NHC ligand seems to have very neglecting effect on this parameter. Then, a study of the number of identified

Syntheses of n-heterocyclic carbene stabilized gold nanoclusters from imidazolium salts and AuClPPh₃

nanoclusters as a function of the number of gold atoms shows that Au₁₁, Au₁₀ and Au₉ nanoclusters are quite common cluster sizes that are found when using ligand bC12. With ligand bC12, Au₁₁ nanocluster is the most common cluster size, similarly to the synthesis with iPr (Figure III-18 c). When observing the relative intensity of the patterns in the ESI-MS spectra at $t = 0$, only one nanocluster with 100% bC12 ligand was detected Au₅(bC12)₄⁺. This cluster is similar to the one found with ligand C12 but it did not remain stable in the suspension over time (as it was the case of ligand C12). It confirms the ability of longer alkyl chains NHC to stabilize smaller NCs. As the PPh₃ capped nanoclusters formed are the same than with ligand C12, our interest will focus on mixed stabilized species (green on Figure III-18 c). In the case of ligand bC12, we were able to stabilize a lower variety of species. Au₅, Au₈, Au₁₁ were commonly stabilized by both C12 and bC12 ligands, however C12 ligand was limited to the stabilization of Au₁₁ nanocluster when bC12 could also stabilize Au₂₁ type nanoclusters. It probably means that bC12 can stabilize bigger sized nanoclusters. One explanation of the fact that C12 stabilizes a higher variety of clusters can be due to the mesomeric effects brought by the benzimidazolium ring. Ligand bC12 is probably less good at electrodonation than ligand C12. Finally, the nature of the ligand does not influence on the ligand:Au ratio tendency. The use of bC12 ligand stabilized nanoclusters similar to the one with C12 with few differences. Indeed, the number of NHC+PPh₃ capped AuNCs is higher with C12-Br ligand. At this step, there is a large panel of gold nanoclusters nuclearities and study of the suspensions ageing could help in seeing a difference among the ligands.

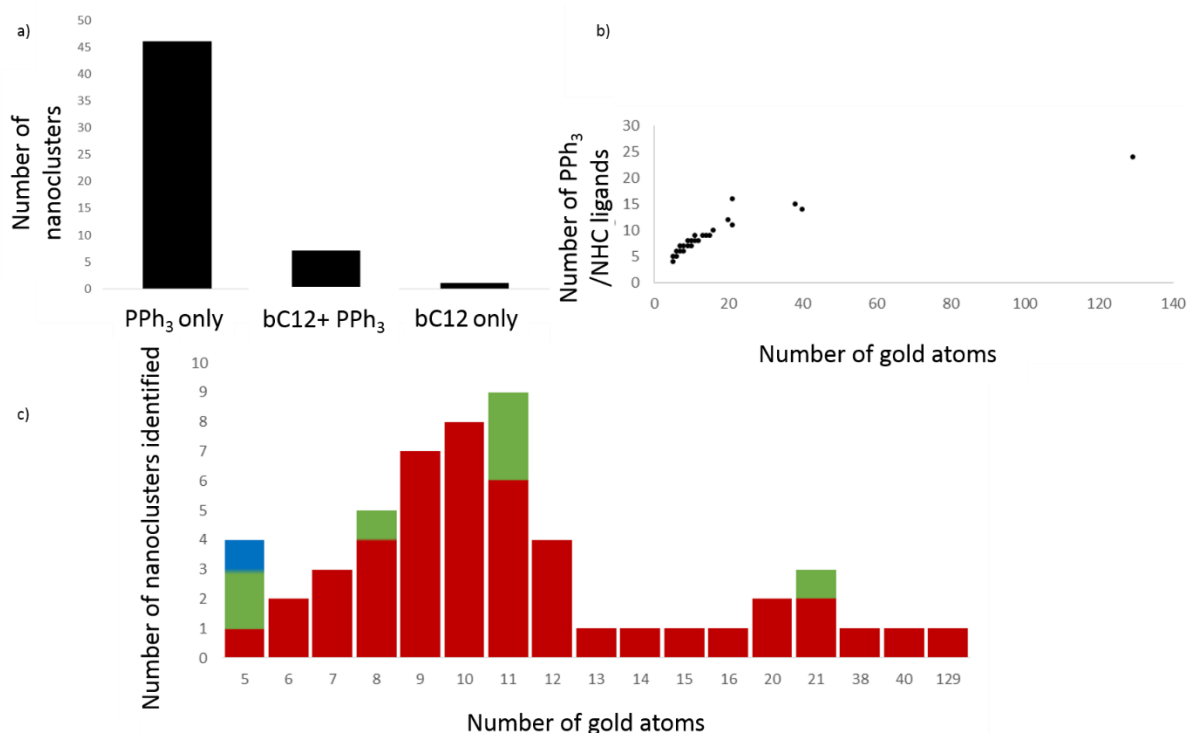


Figure III-18 a) Abundance of the number of gold nanoclusters identified for each ligand. b) Comparison of the number of gold atoms in identified nanoclusters to the number of ligands. c) Bar chart histogram showing the number of nanoclusters identified depending on the number of gold atoms (red for PPh₃ only capped AuNCs, green for mixed bC12 and PPh₃ capped AuNCs, blue for only bC12 capped AuNCs). All for samples at t_0 .

Syntheses of n-heterocyclic carbene stabilized gold nanoclusters from imidazolium salts and AuClPPh₃

In this case, we obtained around 46 patterns corresponding to PPh₃ capped AuNCs, 7 PPh₃ and bC12-Br capped AuNCs structures and 1 AuNCs which is only capped with bC12-Br ligand. In regards to bC12-Br capped AuNCs, two structures stayed stable over time: Au₁₁(PPh₃)₇(bC12)Br₂⁺ and Au₁₁(PPh₃)₆(bC12)₂Br₂⁺. Their relative intensity in ESI-MS is quite similar and way lower than Au₁₁(PPh₃)₇(iPr)Br₂⁺ and Au₁₁(PPh₃)₇(C12)Br₂⁺ pattern observed in the previous 1 week spectra. With this ligand, two types of NHC remained stable over time compared to synthesis using C12-Br and iPr-Br when only one structure with NHC at the surface showed great stability: it can explain the lower intensity (equilibrium between the two structures) (Figure III-19).

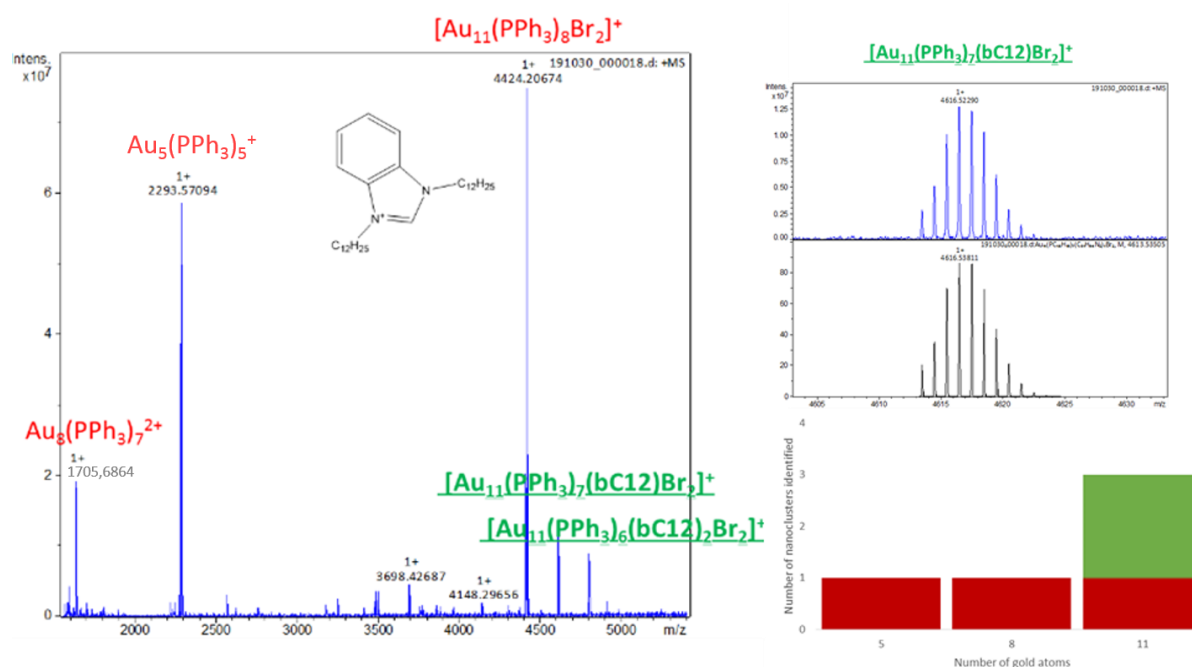


Figure III-19 FT-ICR MS spectra of NCs suspension synthesized from AuClPPh₃, NaBH₄ and bC12-Br after 1 week. Theoretical (black) and experimental (blue) isotopic patterns for Au₁₁(PPh₃)₇(bC12)Br₂⁺. Bar chart histogram showing the number of nanoclusters identified depending on the number of gold atoms (red for PPh₃ only capped AuNCs, green for mixed bC12 and PPh₃ capped AuNCs, blue for only bC12 capped AuNCs) for samples after 1 week.

Also, most PPh₃ capped AuNCs did disjoint over time as for the other ligands. This time, it seems like there are less PPh₃ capped NCs after 1 week remaining in the suspensions (only 3 structures) (Figure III-19). These differences can be attributed to a difference in bulkiness of ligand bC12-Br compared to C12-Br and iPr-Br if we suppose that it affects the NCs formation process. It could also be attributed to potential mesomeric effects due to the addition of a carbon cycle on bC12-Br compared to C12-Br, for example. Indeed, electronics can be altered by changing the nature of the azole ring: benzimidazole is inferior to imidazole in electron donating power.²¹ Similarities can be found when comparing the MS spectra obtained from the bC12-Br synthesis with the spectra of the synthesis carried out with the other ligands: the structures Au₅(PPh₃)₅⁺, Au₈(PPh₃)₇²⁺ and Au₁₁(PPh₃)₈Br₂⁺ are detected when analyzing the suspensions after 1 week (Figure III-19). It shows that in these reaction conditions, the formation of some stable PPh₃ capped AuNCs is not completely correlated to the presence of the NHC ligands in

Syntheses of n-heterocyclic carbene stabilized gold nanoclusters from imidazolium salts and AuClPPh₃

the suspension. However, there is a clear effect of the type of NHC ligand on the nature clusters that are formed and their stability over time.

III.B.2.e. ESI-MS results discussion

ESI-MS study allowed us to not only demonstrate that a high diversity of NCs structures and chemical compositions are obtained in our synthesis conditions but also that ageing of the cationic gold clusters suspensions put light onto the structures that are the most stable. These experiments were done many time and are reproducible in terms of NCs species formed and NCs species that are stable over time. Here, it was possible to conclude that the type of ligand has a direct influence on the NCs that are synthesized as different structures were stabilized depending on the ligand. However, for all the ligands, the mixed PPh₃ and NHC capped AuNCs Au₁₁(NHC)₇(NHC)Br₂⁺ signal in mass spectrometry was particularly stable over time. Indeed, ESI-MS study done on the sample after one month and three months show that they remain in the suspensions (see appendix). Moreover, ESI-MS analysis of the heated suspensions showed no degradation of the Au₁₁(NHC)₇(NHC)Br₂⁺ nanocluster. Also, some PPh₃ capped AuNCs structure showed great stability in all the samples using the three kinds of imidazolium salts.

A study of the theoretical analysis done in the literature could help us in understanding the dynamics between the phosphine and NHC ligands and also understand the better stability of some NCs structures in comparison to the others. Indeed, ESI-MS analysis showed the preferential stabilization of phosphine capped NCs over NHC capped NCs with the exception of a structure containing only 1 NHC.

NHC and phosphine ligands are both neutral and do not change the oxidation state or cluster charge to accompany an exchange reaction. Phosphine stabilized clusters do not have a layer of Au(I) atoms on the exterior, as it is the case for thiolate-stabilized clusters. Also, phosphines are monodentate ligands in comparison to thiolate for example (no staple pattern). It means that in our reaction conditions, ligand exchange could be favorable. However, Crudden *et al.* reported ligand exchange reaction to form mixed PPh₃ and NHC capped gold nanoclusters from [Au₁₁(PPh₃)₈Cl₂]Cl.²² As previously said, Au₁₁ is one of the most stable PPh₃ capped AuNC. DFT (Density functional theory) calculations showed that exchange of phosphines with iPr type NHC ligands is energetically favorable on almost all the phosphines positions. However, mostly one NHC was favorably exchanged experimentally. It proves that even though DFT-predicted favorable exchange reaction of seven phosphines out of eight, phosphine capped AuNCs are very stable and kinetic effects favors the exchange of only one NHC.

Another recent article reported a comparison of NHC capped NCs formation with their phosphine-protected analogues from DFT calculations. Wei *et al.*, used in particular an iPr NHC as a model.²³ They compared two AuNCs: [Au₁₁(PPh₃)₈Cl₂]⁺ (**Au11Cl2-P**) and [Au₁₁(NHC)₈Cl₂]⁺ (**Au11Cl2-C**) (Figure III-20). The geometries of the phosphine-protected AuNCs and their NHC homologues were optimized and compared (Figure III-20).

They also compared the energetic data associated with nanocluster bonding, major TD-DFT-computed UV-Vis excitation energies and TD-DFT-Computed fluorescence emission energies. It was concluded that the hypothetical NHC-protected AuNCs exhibited similar structural chemistry to that of the experimentally characterized phosphine-protected analogues. There is a similarity in the bond distances and results showed similar thermodynamic stability.

Syntheses of n-heterocyclic carbene stabilized gold nanoclusters from imidazolium salts and AuClPPh₃

This was confirmed by evaluating the Au–P and Au–C bonding energies in these species, with the Au–C being slightly stronger than the Au–P bond by a few kcal.mol⁻¹. There were also comparable HOMO–LUMO gaps which means they have comparable kinetic stability (Figure III-20). These results showed that phosphine protected AuNCs and NHC protected AuNCs are similarly stable with still better results for NHC ligands. It means that PPh₃ can stabilize as well as iPr ligand the AuNCs. For gold source AuClPPh₃, the fact that PPh₃ are already linked to the gold would make it difficult to favor the formation of NHC capped NCs. However, the addition of a NHC in the structure seems to provide better stability to the Au₁₁ NCs.

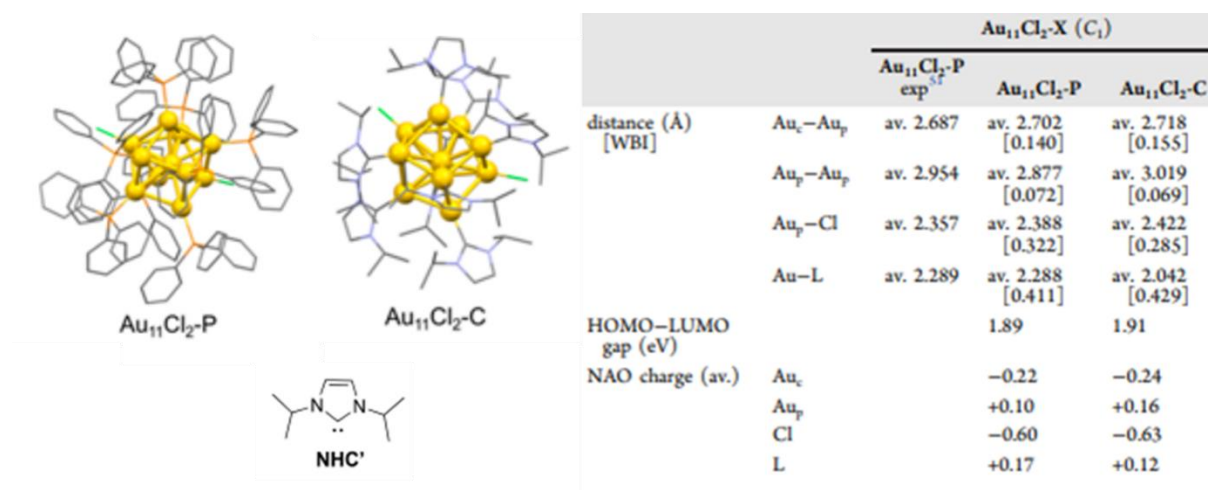


Figure III-20 $[Au_{11}(PPh_3)_8Cl_2]^+$ ($Au_{11}Cl_2-P$) and $[Au_{11}(NHC)_8Cl_2]^+$ ($Au_{11}Cl_2-C$) represented by DFT and relevant computed data for $[Au_{11}Cl_2L_8]^+$ Clusters [$L = PPh_3$ ($Au_{11}Cl_2-P$) and NHC ($Au_{11}Cl_2-C$)].

The versatility in the electronic properties of the NHC's family compared to phosphines could increase the gap (structural, reactivity, properties, etc.) between both types of stabilized AuNCs. Even though phosphine protected AuNCs are very stable and display interesting properties (cf Chapter I), the gain obtained by the use of NHC ligands could be tremendous. Indeed, the two types of clusters, PPh₃ and NHC protected clusters, are almost identical from a thermodynamic point of view.²³ In our case as we start from an AuClPPh₃ precursor, the formation of PPh₃ clusters is kinetically favored hence the majority of PPh₃ clusters formed at the end.

Moreover, another discussion can be made from the results that were obtained. Indeed, we highlighted the fact that the evolution of the suspensions composition over time could be due to H⁺ responsible for the growth of larger gold nanoclusters but another parameter can be taken into account. Indeed, PPh₃ ligands during AuNCs formation can have a dual role: as a stabilizer and proactive etching agent. These conclusions were based upon a study of cluster size populations, Au₈, Au₉ and Au_x (10 < x < 13).²⁴ Pettibone *et al.* showed that growth and etching occur allowing the narrowing of cluster dispersity. We have been wondering why it is mostly the NCs structures with 11 gold atoms that display high stability over time. One of the hypotheses is that this 11 gold atoms structure is highly stable toward etching and promotes the integration of one NHC ligand in its organization. Also, there is probably an effect of the AuNCs core structure. It was reported that Au₁₃NC is in the transition region between planar and three-dimensional nanostructures probably due to increased internal coordination. In the case of Au₁₃ NCs a single central gold atom is coordinated by 12 outer gold atoms to form “one-

Syntheses of n-heterocyclic carbene stabilized gold nanoclusters from imidazolium salts and AuClPPh₃

shell". When 42 gold atoms are packed to the 12 outer atoms, a two-shell Au₅₅ NC is formed. Full-shell clusters are favored for small nanoclusters.²⁵ Au₁₁ nanoclusters structure is composed of an undecagold surrounded by ligands. The ligand:Au ratio follows the same tendency among monodentate PPh₃ and NHC protected clusters due to core geometries and ligand coordination patterns.

The association of the reagents effects, the thermodynamic stability of the ligands and the kinetics effects due to the gold source structure allows the formation of stable small single PPh₃ nanoclusters and highly stable mixed PPh₃ and NHC protected Au₁₁ nanoclusters.

III.C. Conclusion

In this chapter we were able to synthesize NHC capped AuNCs, mixed NHC and PPh₃ capped AuNCs and PPh₃ capped AuNCs. Gold nanoclusters with various nuclearity going from 5 to 129 were formed. Also, the number of stabilizing ligands varied from 4 to 24 ligands depending on the nanoclusters. More importantly, we were able to study the different AuNCs that can be formed during the synthesis and their stability over time. In a first part, the nature of the NHC ligand did not seem to have any influence on the NCs morphology and size. However, given their extra small size and molecular behavior, NCs are difficult to study only by UV-Vis spectroscopy analysis and TEM observation. The influence of the reducing agent was also assessed since it was shown that a strong reducing agent is necessary to stabilize AuNCs in these conditions.

Synthesis in other solvents such as toluene and DCM were performed to assess a possible effect of the solvent (this time NaBH₄ was dissolved in water) but it did not really change the nature of the AuNCs we obtained. Actually, when using these organic solvents, we had formation of emulsions that made some of our analysis difficult since it made the purification steps harder to proceed. Thus, ethanol was kept as solvent for this part of our studies.

ESI-MS has been a technic of choice to analyze our sample and study the synthesized NCs structures and relative stability. We observed that bulkier ligands could stabilize temporarily AuNCs capped by NHC only in our reaction media, like Au₅(NHC)₄⁺. But their thermodynamically unfavorable structure made them unstable over time. The notion of thermodynamically favorable AuNCs structures was introduced there. With all the NHC ligands used only one specie could incorporate an NHC in its structure: Au₁₁(PPh₃)₇(NHC)Br₂⁺. Also, nanocluster Au₁₁(PPh₃)₈Br₂⁺ was the most stable and abundant nanocluster. We could conclude that Au₁₁ nanocluster are also very stable with only PPh₃ as stabilizing ligand probably due to the structure that give Au₁₁ nanoclusters higher thermodynamical stability. Several phosphine capped AuNCs were synthesized and remained stable over time in the various suspensions. Moreover, the only NHC capped AuNCs that were stable over time, were the one with a majority of phosphine ligands in their structures. The synthesis kinetic aspects are favorable to PPh₃ nanoclusters because PPh₃ are already coordinated with gold in the precursor (AuClPPh₃).

Our next goal is to perform a reaction, which does not involve a competitive ligand such as PPh₃, and to study the NCs synthesized when only NHC are the ligands. For this purpose, we developed a synthesis pathway using gold complex HAuCl₄.3H₂O as gold source.

References

- (1) Ozin, G. A.; Mitchell, S. A. Ligand-free Metal Clusters. *Angew. Chem. Int. Ed. Engl.* **1983**, *22* (9), 674–694.
- (2) Duan, H.; Nie, S. Etching Colloidal Gold Nanocrystals with Hyperbranched and Multivalent Polymers: A New Route to Fluorescent and Water-Soluble Atomic Clusters. *J. Am. Chem. Soc.* **2007**, *129* (9), 2412–2413.
- (3) Li, Y.; Liu, S.; Yao, T.; Sun, Z.; Jiang, Z.; Huang, Y.; Cheng, H.; Huang, Y.; Jiang, Y.; Xie, Z.; Pan, G.; Yan, W.; Wei, S. Controllable Synthesis of Gold Nanoparticles with Ultrasmall Size and High Monodispersity via Continuous Supplement of Precursor. *Dalton Trans.* **2012**, *41* (38), 11725–11730. <https://doi.org/10.1039/C2DT31270K>.
- (4) MacLeod Carey, D.; Muñoz-Castro, A. Evaluation of N-Heterocyclic Carbene Counterparts of Classical Gold Clusters; Bonding Properties of Octahedral CAu₆, Icosahedral Au₁₃Cl₂, and Bi-Icosahedral Au₂₅Cl₂ Cores from Relativistic DFT Calculations. *J. Phys. Chem. C* **2019**, *123* (19), 12466–12473. <https://doi.org/10.1021/acs.jpcc.9b01254>.
- (5) Hippolyte, L. New Syntheses of N-Heterocyclic Carbene-Stabilized Gold Nanoparticles, Sorbonne université, 2018.
- (6) Huang, -Ting; Sun, -Zhi-hu; Pan, -Guo-qiang. - Selective Synthesis of Different-Sized Gold Nanoclusters through HCl-Etching and -Growth Effect. - *Chinese Journal of Chemical Physics*, 2018, *31*, 223.
- (7) Ji, X.; Song, X.; Li, J.; Bai, Y.; Yang, W.; Peng, X. Size Control of Gold Nanocrystals in Citrate Reduction: The Third Role of Citrate. *J. Am. Chem. Soc.* **2007**, *129* (45), 13939–13948.
- (8) Jin, R.; Qian, H.; Wu, Z.; Zhu, Y.; Zhu, M.; Mohanty, A.; Garg, N. Size Focusing: A Methodology for Synthesizing Atomically Precise Gold Nanoclusters. *J. Phys. Chem. Lett.* **2010**, *1* (19), 2903–2910. <https://doi.org/10.1021/jz100944k>.
- (9) Wang, L.; Peng, J.; Tang, Z.; Kang, X.; Fu, M.; Chen, S. Styrene Oxidation Catalyzed by Au₁₁(PPh₃)₇Cl₃ and [Au₁₁(PPh₃)₈Cl₂]Cl Nanoclusters: Impacts of Capping Ligands, Particle Size and Charge State. *Appl. Catal. Gen.* **2018**, *557*, 1–6. <https://doi.org/10.1016/j.apcata.2018.03.001>.
- (10) Hewitt, M. A.; Hernández, H.; Johnson, G. E. ESI-MS Identification of the Cationic Phosphine-Ligated Gold Clusters Au₁–22: Insight into the Gold–Ligand Ratio and Abundance of Larger Clusters. *J. Am. Soc. Mass Spectrom.* **2021**, *32* (1), 237–246. <https://doi.org/10.1021/jasms.0c00293>.
- (11) Huang, T.; Huang, L.; He, W.; Song, X.; Sun, Z.; Jiang, Y.; Pan, G.; Wei, S. Ammonia-Induced Size Convergence of Atomically Monodisperse Au₆ Nanoclusters. *J. Phys. Chem. C* **2018**, *122* (11), 6405–6411. <https://doi.org/10.1021/acs.jpcc.7b12422>.
- (12) Huang, T.; Huang, L.; Jiang, Y.; Hu, F.; Sun, Z.; Pan, G.; Wei, S. Direct Self-Focusing Synthesis of Monodisperse [Au₈(PPh₃)₇]²⁺ Nanoclusters. *Dalton Trans.* **2017**, *46* (36), 12239–12244. <https://doi.org/10.1039/C7DT02657A>.
- (13) Takano, S.; Hirai, H.; Muramatsu, S.; Tsukuda, T. Hydride-Doped Gold Superaatom (Au₉H)₂⁺: Synthesis, Structure, and Transformation. *J. Am. Chem. Soc.* **2018**, *140* (27), 8380–8383. <https://doi.org/10.1021/jacs.8b03880>.
- (14) Yuan, S.-F.; Li, J.-J.; Guan, Z.-J.; Lei, Z.; Wang, Q.-M. Ultrastable Hydrido Gold Nanoclusters with the Protection of Phosphines. *Chem. Commun.* **2020**, *56* (51), 7037–7040. <https://doi.org/10.1039/D0CC02339F>.
- (15) Schmid, G. The Relevance of Shape and Size of Au₅₅ Clusters. *Chem. Soc. Rev.* **2008**, *37* (9), 1909–1930. <https://doi.org/10.1039/B713631P>.
- (16) McKenzie, L. C.; Zaikova, T. O.; Hutchison, J. E. Structurally Similar Triphenylphosphine-Stabilized Undecagolds, Au₁₁(PPh₃)₇Cl₃ and [Au₁₁(PPh₃)₈Cl₂]Cl, Exhibit Distinct Ligand Exchange Pathways with Glutathione. *J. Am. Chem. Soc.* **2014**, *136* (38), 13426–13435. <https://doi.org/10.1021/ja5075689>.

Syntheses of n-heterocyclic carbene stabilized gold nanoclusters from imidazolium salts and AuClPPh₃

- (17) Hewitt, M. A.; Hernández, H.; Johnson, G. E. Light Exposure Promotes Degradation of Intermediates and Growth of Phosphine-Ligated Gold Clusters. *J. Phys. Chem. C* **2020**, *124* (5), 3396–3402. <https://doi.org/10.1021/acs.jpcc.9b10920>.
- (18) Jena, N. K.; Chandrakumar, K. R. S.; Ghosh, S. K. Beyond the Gold–Hydrogen Analogy: Doping Gold Cluster with H-Atom–O₂ Activation and Reduction of the Reaction Barrier for CO Oxidation. *J. Phys. Chem. Lett.* **2011**, *2* (12), 1476–1480. <https://doi.org/10.1021/jz2006435>.
- (19) Milowska, K. Z.; Stolarczyk, J. K. Role of Ligand–Ligand vs. Core–Core Interactions in Gold Nanoclusters. *Phys. Chem. Chem. Phys.* **2016**, *18* (18), 12716–12724. <https://doi.org/10.1039/C5CP06795B>.
- (20) Dufour, F.; Fresch, B.; Durupthy, O.; Chaneac, C.; Remacle, F. Ligand and Solvation Effects on the Structural and Electronic Properties of Small Gold Clusters. *J. Phys. Chem. C* **2014**, *118* (8), 4362–4376. <https://doi.org/10.1021/jp409019z>.
- (21) Glorius, F. N-Heterocyclic Carbenes in Catalysis—An Introduction. **2006**.
- (22) Narouz, M. R.; Osten, K. M.; Unsworth, P. J.; Man, R. W. Y.; Salorinne, K.; Takano, S.; Tomihara, R.; Kaappa, S.; Malola, S.; Dinh, C.-T.; Padmos, J. D.; Ayoo, K.; Garrett, P. J.; Nambo, M.; Horton, J. H.; Sargent, E. H.; Häkkinen, H.; Tsukuda, T.; Crudden, C. M. N-Heterocyclic Carbene-Functionalized Magic-Number Gold Nanoclusters. *Nat. Chem.* **2019**, *11* (5), 419–425. <https://doi.org/10.1038/s41557-019-0246-5>.
- (23) Wei, J.; Halet, J.-F.; Kahlal, S.; Saillard, J.-Y.; Munoz-Castro, A. Toward the Formation of N-Heterocyclic-Carbene-Protected Gold Clusters of Various Nuclearities. A Comparison with Their Phosphine-Protected Analogues from Density Functional Theory Calculations. *Inorganic Chemistry*, 2020, *59*, 15240–15249.
- (24) Pettibone, J. M.; Hudgens, J. W. Gold Cluster Formation with Phosphine Ligands: Etching as a Size-Selective Synthetic Pathway for Small Clusters? *ACS Nano* **2011**, *5* (4), 2989–3002. <https://doi.org/10.1021/nn200053b>.
- (25) Xia, X.; Shao, Y. Quantum Mechanical Studies of Full-shell Noble Metal Nanoclusters in Water. *Int. J. Quantum Chem.* **2018**, *118* (20), e25709.

CHAPTER IV: SYNTHESIS OF N-HETEROCYCLIC CARBENE STABILIZED GOLD NANOCLUSTERS FROM IMIDAZOLIUM SALTS AND $\text{HAuCl}_4 \cdot 3\text{H}_2\text{O}$

In this chapter, we will describe a study of NHC capped AuNCs synthesis using imidazolium salts and a gold precursor that does not contain a strong stabilizing ligand such as PPh_3 in order to obtain full NHC nanoclusters. Indeed, using AuClPPh_3 , the strong coordination of PPh_3 to Au(I) before the reduction step is not displaced to the benefit of NHC, and at the best only one NHC is present in the chemical structure of gold nanoclusters. To avoid this competition between ligands, we studied the synthesis with another gold precursor.

First, syntheses with AuClTHT (Chloro(tetrahydrothiophene)gold(I)) and AuClSMe_2 (Chloro(dimethyl sulfide)gold(I)) were tested. For these preliminary tests, gold precursors (0.05 mmol, 1 equiv.) were dissolved in 2.5 ml of ethanol, then a C12-Br imidazolium salt (4 equiv.) solution in 2.5 ml of ethanol was added. Finally, NaBH_4 (10 equiv.) in 1 ml of ethanol was added. The reaction was left under stirring for 5 hours. Then, the suspensions were centrifuged to remove excess NaBH_4 (10 min, 10000 rpm), and the solvent was evaporated. 5 ml of benzene (to remove potential unreacted starting material) was added and the mixture was sonicated 1 min. After decantation, the benzene solution was removed and the beige solid was removed. Benzene was evaporated and the resulting brown solid redispersed in ethanol for further analysis. The syntheses using both gold sources gave similar results. Brown suspensions were obtained and aggregation occurred within an hour. Unpurified suspensions also went through aggregation within an hour. Mass spectrometry analysis of the suspensions showed no nanocluster signals. The same reaction was reproduced with the addition of NaH (2 equiv. / imidazolium salt, 6 minutes before adding NaBH_4) to promote a better deprotonation of the imidazolium salt. However, the same results were obtained since quick aggregation of the suspensions occurred. The reaction in organic solvents gave gold nanoparticles suspensions, similarly to the syntheses reported by Hippolyte *et al.*¹

Then synthesis with another gold source, Hydrogen tetrachloroaurate(III) trihydrate ($\text{HAuCl}_4 \cdot 3\text{H}_2\text{O}$) was tested. In this chapter we will describe a study of NHC capped AuNCs synthesis using imidazolium salts and $\text{HAuCl}_4 \cdot 3\text{H}_2\text{O}$ as gold source.

IV.A. Non water dispersible nanoclusters using $\text{HAuCl}_4 \cdot 3\text{H}_2\text{O}$

IV.A.1. Imidazolium salts synthesis

In this chapter, we used the same imidazolium salts that were previously reported: iPr-Br, C12-Br, bC12-Br. We also worked with a wider range of ligand precursors and extended the selection to: Allyl-Br, bAllyl-Br, Benzyl-Br, and bBenzyl-Cl. The interest was to study a maximum the influence of the nature of the ligand on the obtained NCs and on the suspensions overall stability. The following parameter were assessed to choose the ligands: long carbonyl chains (C12-Br) versus small chains (iPr-Br, Allyl-Br), imidazolium (C12-Br/Allyl-Br) vs benzimidazolium ring (bC12-Br/bAllyl-Br), and nature of the anion (Cl^- vs Br^-). These parameters are very important since, for example, the use of imidazolium salts with an iodide anion led to the precipitation of the suspensions into aggregates, regardless of the imidazolium used.

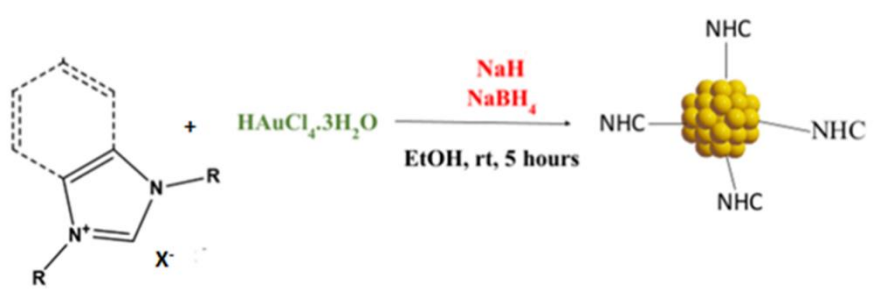
A previous study from 2016 reported the effect of the side-group of benzimidazole-2-ylidene on the size of NPs.² They demonstrated that ligand exchange reactions between thioethers and benzimidazol-2-ylidenes occurred at the surface of AuNPs. The team reported that benzimidazol-2-ylidenes bearing methyl, n-hexyl and phenyl groups on the N atoms, led to significant etching of the NPs, thus decrease in size. Actually, the NPs went from $5.8 (\pm 1.2)$ nm to $2.8 (\pm 0.6)$ nm when ligand exchange was done with benzimidazol-2-ylidenes bearing methyl groups. For benzimidazol-2-ylidenes bearing phenyl groups the NPs went from $5.8 (\pm 1.2)$ nm to $3.4 (\pm 0.8)$ nm. On the other hand, n-hexyl group led to a more moderate size decrease going from $5.8 (\pm 1.2)$ nm to $5.1 (\pm 1.0)$ nm. It is probably due to the fact that long alkyl chains of the n-hexyl interact better with each other leading to increased stabilization and decreased etching. Indeed, the long alkyl chains form a protective layer around the particles preventing aggregation and surface degradation.

The syntheses for NHC precursor's Allyl-Br, bAllyl-Br, Benzyl-Br, bBenzyl-Cl are the same as for iPr-Br, C12-Br and bC12-Br. In a round flask NaH (1 equiv.) is introduced under N_2 . Then, distilled THF (40 ml) is added, followed by (benz)imidazole addition (1 equiv., 30 mmol) at 0°C . The corresponding alkyl bromide (2 equiv.) is added and the reaction media is left under stirring for 1 hour. Then, the reaction media is heated at 75°C for 24 hours (or 48 hours depending on the ^1H NMR spectra). The imidazolium salts were analyzed by ^1H NMR and IR spectroscopy to confirm their synthesis (see appendix).

IV.A.2. Non water dispersible nanoclusters synthesis

As stated previously, our focus here was to use a gold source that did not bear strong stabilizing ligands in its structure that could compete with NHC.

A solution of $\text{HAuCl}_4 \cdot 3\text{H}_2\text{O}$ (0.05 mmol) in 2.5 ml of ethanol is mixed with a solution of imidazolium salt in 2.5 ml of ethanol for 20 minutes. Then, NaH (2 equiv. / imidazolium salt) is added as a base for imidazolium deprotonation. Finally, six minutes after, a solution of reducing agent NaBH_4 (10 equiv.) in 1 ml of ethanol is added and yields brown suspensions (Scheme IV-1). The reaction is left under stirring for 5 hours. The suspensions are centrifuged (10 min, 10000 rpm) to remove the excess of NaBH_4 that has not completely solubilized, then the solvent is evaporated. Then, the suspensions were centrifuged to remove excess NaBH_4 (10 min, 10000 rpm), and the solvent was evaporated. 5 ml of benzene (to remove potential unreacted starting material) was added and the mixture was sonicated 1 min. After decantation, the benzene solution was removed and the beige solid was removed. Benzene was evaporated and the resulting brown solid redispersed in ethanol for further analysis.



Scheme IV-1 Synthesis of NHC capped AuNCs using gold source $\text{HAuCl}_4 \cdot 3\text{H}_2\text{O}$ and imidazolium salts.

The suspensions were observed by TEM and analyzed by UV spectroscopy. Also, stability over time of the suspensions using various NHC precursors was studied. Syntheses with 4 equiv., 5 equiv. and 10 equiv. of ligand iPr-Br, bC12-Br and C12-Br were performed. No significant effect of the imidazolium salt/Au ratio was observed. Thus, the results for the synthesis with 4 equiv. of imidazolium salt will be presented in the next part.

IV.A.2.a. Effect of the ligand

IV.A.2.a.i. Effect of the ligand on the suspension stability

In this part, the following imidazolium salts were used: C12-Br, bC12-Br, iPr-Br, Allyl-Br, bAllyl-Br, Benzyl-Br and bBenzyl-Cl. The same synthesis protocol as in part IV.A.1.b was followed. By using various ligands in our reaction conditions, we saw a real influence on the formation of AuNCs since we observed clear differences in suspensions stability over time.

When the synthesis was performed with imidazolium salts like Allyl-Br and bAllyl-Br, we observed a direct and complete aggregation when adding the reducing agent in the reaction media. Indeed, upon addition of NaBH_4 , a black precipitate formed in the bottom of the flask

Synthesis of n-heterocyclic carbene stabilized gold nanoclusters from imidazolium salts and $\text{HAuCl}_4 \cdot 3\text{H}_2\text{O}$

and the solution above was clear. Several reactions parameters were modified to see if we could obtain AuNCs: the imidazolium salt/Au ratio was increased up to 10, the NaH/imidazolium salt was increased up to 5, the reaction media was cooled at 0°C or heated to 70°C . However, these two type of NHCs did not stabilize neither AuNCs nor AuNPs.

Then, the imidazolium salts, iPr-Br and Benzyl-Br were used. We observed brown suspensions with a little bit of aggregation. These NHC ligands were able to temporary stabilize NCs as observed by TEM (Figure IV-1). When using imidazolium salt iPr-Br, particles sized $1.7 (\pm 0.4)$ nm were formed. When using imidazolium salt Benzyl-Br, particles sized $0.9 (\pm 0.2)$ nm were formed. It means that the benzyl rings on the N atoms favors the formation of smaller particles.

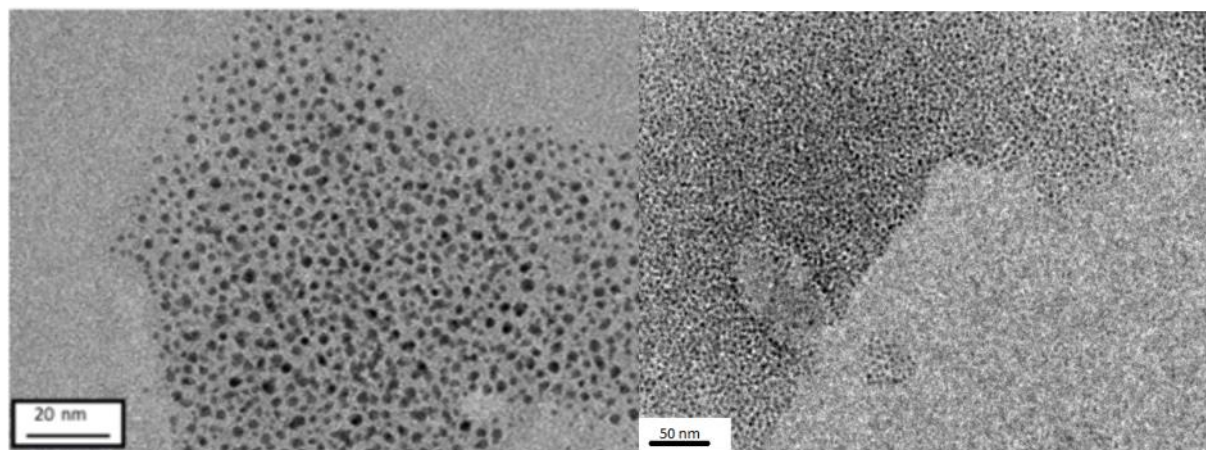


Figure IV-1 TEM images of AuNCs synthesized using NHC precursors iPr-Br (left) and Benzyl-Br (right).

However, stability over time of the suspensions was extremely low. After two hours, strong aggregation of the suspensions and the formation of gold mirror on the container wall were observed. After 4 hours, the suspensions were not colored anymore and the gold mirror quantity increased. A few hypotheses could be made on these results. Since, particles were primary formed but did aggregate later, there is probably instability of the particles. Also, the formation of the gold mirror probably indicates etching process that could happen in our reaction conditions. Further analysis of these suspensions will be presented in the next part to understand what did happen.

Results were different with the other NHC precursors used: C12-Br, bC12-Br, bBenzyl-Cl.

After synthesis, brown suspensions were obtained. This time no aggregation was observed nor gold mirror with aging of the suspensions. The differences in suspensions stability, for the synthesis with these three imidazolium salts, started showing after weeks. After 2 weeks, the samples from bBenzyl-Cl showed signs of aggregation and after 1 month, aggregation and gold mirror appeared. For the samples with bC12-Br, lightening of the suspensions color appeared after 1 month. As for the synthesis with ligand C12-Br, no aggregation was detected after several months when stored at room temperature. The suspensions were observed by TEM (Figure IV-2) and UV spectroscopy analysis was conducted (see appendix). It showed no noticeable plasmon band on the spectra. The synthesis using imidazolium salt C12-Br gave NPs

Synthesis of n-heterocyclic carbene stabilized gold nanoclusters from imidazolium salts and $\text{HAuCl}_4 \cdot 3\text{H}_2\text{O}$

of size $1.9 (\pm 0.3)$ nm. The one using benzimidazolium salt bC12-Br gave NPs of size $1.2 (\pm 0.2)$ nm. The one using benzimidazolium salt bBenzyl-Cl gave NPs of size $1.6 (\pm 0.3)$ nm (Figure IV-2).

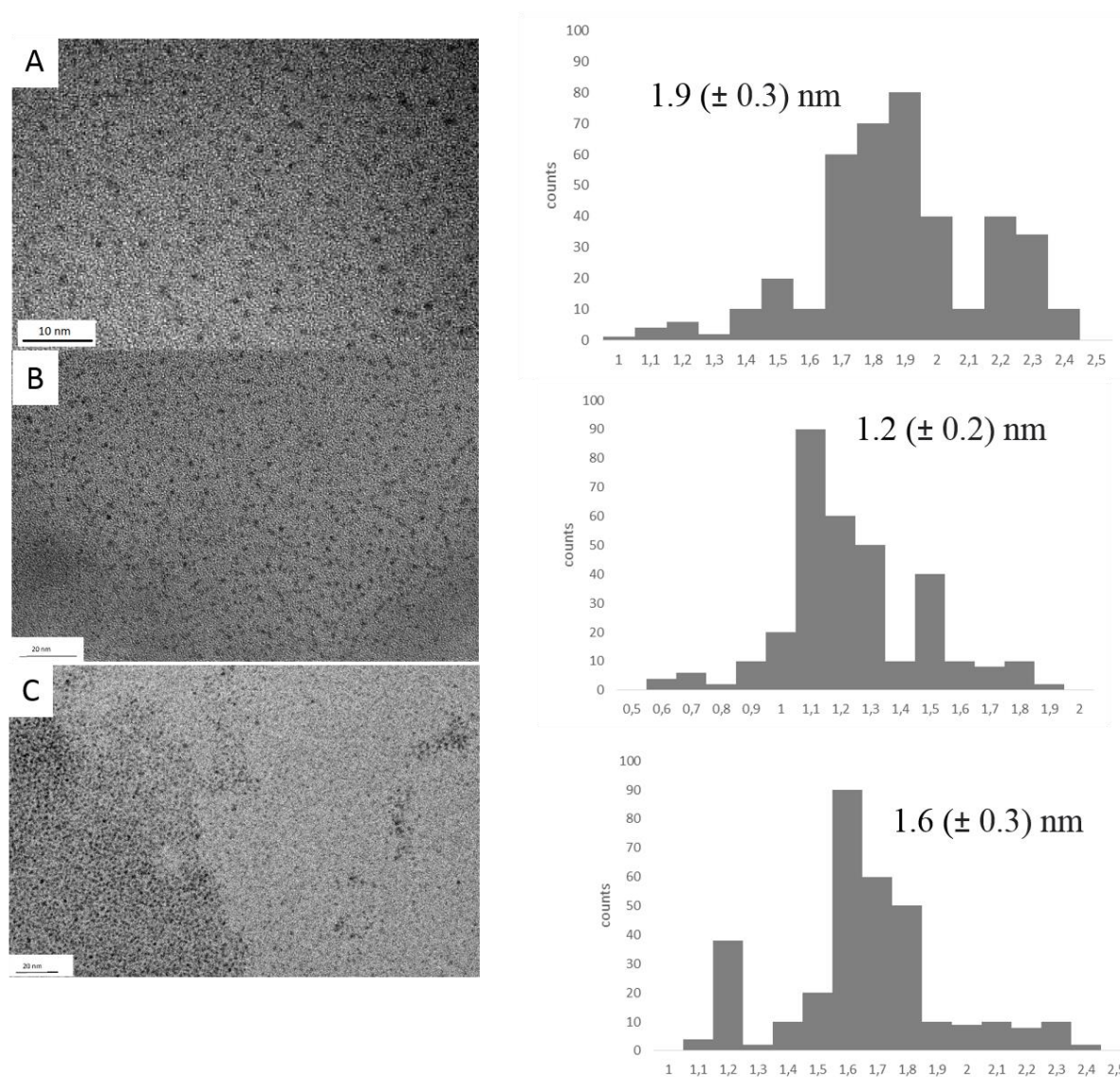


Figure IV-2 TEM images of AuNCs synthesized from $\text{HAuCl}_4 \cdot 3\text{H}_2\text{O}$ using NHC precursors C12-Br (A), bC12-Br (B) and bBenzyl-Cl (C).

TEM observation of the suspensions confirmed the synthesis of extra small NCs for the three ligands. The size of the particles synthesized using benzimidazolium salt bC12-Br was significantly smaller than the size of the particles synthesized using the two other imidazolium salts. It could be due to synergetic effects of the benzimidazolium ring and the long C12 alkyl chains. Discussing the effect of the ligand on the size at the scale of the NCs is very difficult since the average NCs size is 1-2 nm. Thus, we need to determine the composition of the nanoclusters formed.

In order to determine the exact nature of the synthesized AuNCs, a study of the suspensions and their potential evolution over time by mass spectrometry was conducted. Indeed, we will

Synthesis of n-heterocyclic carbene stabilized gold nanoclusters from imidazolium salts and $\text{HAuCl}_4 \cdot 3\text{H}_2\text{O}$

look at the population of nanoclusters formed, see if there are stable formulas, and if there is a difference in nanocluster populations for the three ligands.

IV.A.2.a.ii. Mass spectrometry analysis of the suspensions

First the samples obtained from the synthesis using imidazolium salt iPr-Br and Benzyl-Br were analyzed. The samples will be referred to as iPr-AuNC and Benzyl-AuNC. Given the instability of the suspensions over time, it was very difficult to see if AuNCs were formed before aggregation and formation of gold mirrors for both samples. Analysis of the samples showed mostly a high intensity pattern corresponding to $[\text{Au}(\text{NHC})_2]^+$ molecular complex for both iPr-AuNC and Benzyl-AuNC samples. Although computational studies show that the binding energy between NHCs (such as iPr) and gold is high enough to ensure AuNCs stability, the absence of secondary interactions between NHCs substituents on the N atoms (such as van der Waals interactions) can explain the poor stability of the suspensions. The strength of the NHC-Au bonds leads to formation of highly thermodynamically stable molecular complex $[\text{Au}(\text{NHC})_2]^+$. However, AuNPs stabilized by NHCs bearing isopropyl chains and benzyl chains on the N atoms have been reported.^{3,4} The differences may come from the fact that they used benzimidazol-2-ylidenes NHCs and not imidazol-2-ylidenes. Indeed, the benzene ring bring additional stabilization through p-p stacking. It means that the nature the length of the side chains is not the only parameter driving the ability of NHCs to stabilize AuNCs.

Mass spectrometry analysis were also conducted on the samples C12-AuNCs, bC12-AuNCs and bBenzyl-AuNCs. For sample C12-AuNCs, the analysis of the suspension at t=0 (just after washing), showed multiple patterns corresponding to different Au_{13} NHC capped AuNCs structures (Figure IV-3). In this case, we have several C12 stabilizing ligand in the nanoclusters outer shell and the nuclearity does not vary.

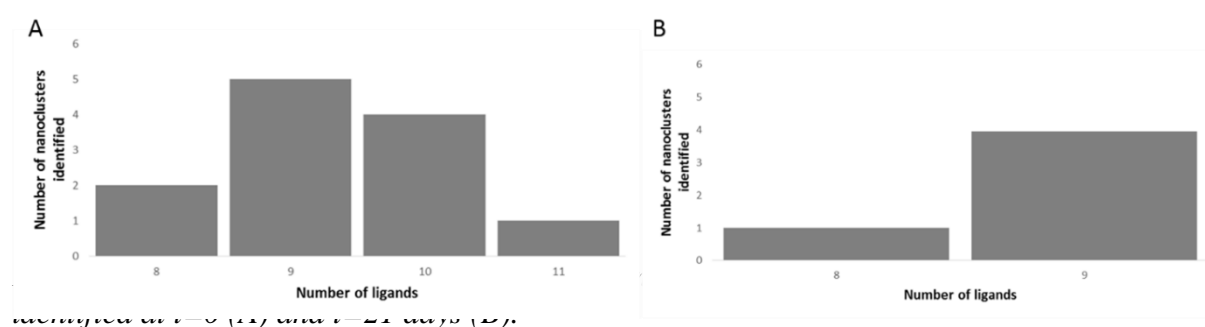
| Au NCS Formula | Nbr Au | m/z |
|--|--------|-----------|
| $\text{Au}_{13}(\text{C12})_9\text{Br}(\text{CH}_3)_2^{2+}$ | 13 | 3156,1265 |
| $\text{Au}_{13}(\text{C12})_9\text{Br}_2\text{H}^{2+}$ | 13 | 3181,5659 |
| $\text{Au}_{13}(\text{C12})_9\text{Br}_2\text{CH}_3^{2+}$ | 13 | 3188,5738 |
| $\text{Au}_{13}(\text{C12})_9\text{Br}_2\text{Cl}^{2+}$ | 13 | 3199,0454 |
| $\text{Au}_{13}(\text{C12})_9\text{Br}_3^{2+}$ | 13 | 3221,0208 |
| $\text{Au}_{13}(\text{C12})_{10}\text{Br}(\text{CH}_3)_2\text{H}^{2+}$ | 13 | 3255,1137 |
| $\text{Au}_{13}(\text{C12})_{10}\text{Br}_3\text{H}_2^{2+}$ | 13 | 3424,7359 |
| $\text{Au}_{13}(\text{C12})_{10}\text{Br}_3\text{CH}_3\text{H}^{2+}$ | 13 | 3431,7437 |
| $\text{Au}_{13}(\text{C12})_{10}\text{Br}_4\text{H}^{2+}$ | 13 | 3464,1906 |
| $\text{Au}_{13}(\text{C12})_{11}\text{Br}_5\text{H}^{2+}$ | 13 | 3706,8602 |
| $\text{Au}_{13}(\text{C12})_8\text{Br}_3\text{CH}_3^+$ | 13 | 6052,6518 |
| $\text{Au}_{13}(\text{C12})_8\text{Br}_4^+$ | 13 | 6117,5458 |

Synthesis of n-heterocyclic carbene stabilized gold nanoclusters from imidazolium salts and $\text{HAuCl}_4 \cdot 3\text{H}_2\text{O}$

Some of the nanoclusters formula attracted our attention $\text{Au}_{13}(\text{C12})_9\text{Br}(\text{CH}_3)_2^{2+}$, $\text{Au}_{13}(\text{C12})_9\text{Br}_2\text{CH}_3^{2+}$, $\text{Au}_{13}(\text{C12})_{10}\text{Br}(\text{CH}_3)_2\text{H}^{2+}$, $\text{Au}_{13}(\text{C12})_{10}\text{Br}_3\text{CH}_3\text{H}^{2+}$, $\text{Au}_{13}(\text{C12})_8\text{Br}_3\text{CH}_3^+$. Indeed, the presence of a CH_3 in the nanocluster structure was surprising. But verification of the masses and comparison of the experimental and theoretical isotopic patterns confirmed these formula. Also, analysis of samples synthesized with various batches of $\text{HAuCl}_4 \cdot 3\text{H}_2\text{O}$, ethanol and imidazolium salt confirmed these results. It means that it probably comes from the mass spectrometer (preparation of the sample for analysis or device). When looking at the interference's and contaminants encountered in mass spectrometry ⁵, it shows that presence of solvents such as acetonitrile or methanol can results in contamination in the samples. Since some of our ESI-MS samples have been done in MeOH and we also did MeOH washing sometimes, the contamination probably comes from MeOH in the mass spectrometer. The binding mode of these CH_3 is still a mystery. Review of the literature did not show similar structures. Given the Au_{13} icosahedral structure, ligands are usually bonded to the 12 orbital gold atoms. Maybe, CH_3^- is formed in the gas phase as reported by Ellison *et al.*⁶

The number of NHC ligands in the NCs composition varies from eight to eleven at $t=0$. We note that the population of NC with nine C12 ligands is the most represented. Following aging of the suspensions, we observed that most NCs patterns intensity decrease over time, some even disappear. After 3 weeks, only the nanoclusters with eight and nine C12 ligands are detected in *Figure IV-3 Listing of nanoclusters synthesized from C12-Br and $\text{HAuCl}_4 \cdot 3\text{H}_2\text{O}$ in EtOH at $t=0$.*

the suspensions (Figure IV-4). It means that for Au_{13} nanoclusters, the structures with eight to nine NHC ligands are the most thermodynamically stable. Indeed, nine C12 ligands were able to stabilize the highest number of nanoclusters and these nanoclusters are detected in the suspensions 3 weeks after. However, the relative intensity of the nanoclusters is not the same depending on the composition as we will see later.



If we summarize, after 3 weeks of aging, there are only 5 nanoclusters that are present in the suspensions (Figure IV-5).

Synthesis of n-heterocyclic carbene stabilized gold nanoclusters from imidazolium salts and $\text{HAuCl}_4 \cdot 3\text{H}_2\text{O}$

| Au NCS Formula | Nbr Au | m/z |
|--|---------------|----------------------|
| $\text{Au}_{13}(\text{C12})_9\text{Br}(\text{CH}_3)_5^{2+}$ | 13 | 3156,1265 |
| $\text{Au}_{13}(\text{C12})_9\text{Br}_2\text{H}^{2+}$ | 13 | 3181,5659 |
| $\text{Au}_{13}(\text{C12})_9\text{Br}_2\text{CH}_3^{2+}$ | 13 | 3188,5738 |
| $\text{Au}_{13}(\text{C12})_9\text{Br}_2\text{Cl}^{2+}$ | 13 | 3199,0454 |
| $\text{Au}_{13}(\text{C12})_9\text{Br}_3^{2+}$ | 13 | 3221,0208 |
| $\text{Au}_{13}(\text{C12})_{10}\text{Br}(\text{CH}_3)_4\text{H}^{2+}$ | 13 | 3255,1137 |
| $\text{Au}_{13}(\text{C12})_{10}\text{Br}_3\text{H}_2^{2+}$ | 13 | 3424,7359 |
| $\text{Au}_{13}(\text{C12})_{10}\text{Br}_3\text{CH}_3\text{H}^{2+}$ | 13 | 3431,7437 |
| $\text{Au}_{13}(\text{C12})_{10}\text{Br}_4\text{H}^{2+}$ | 13 | 3464,1906 |
| $\text{Au}_{13}(\text{C12})_{11}\text{Br}_5\text{H}^{2+}$ | 13 | 3706,8602 |
| $\text{Au}_{13}(\text{C12})_8\text{Br}_3\text{CH}_3^{+}$ | 13 | 6052,6518 |
| $\text{Au}_{13}(\text{C12})_8\text{Br}_4^{+}$ | 13 | 6117,5458 |

Figure IV-5 Listing of nanoclusters synthesized from C12-Br and $\text{HAuCl}_4 \cdot 3\text{H}_2\text{O}$ in EtOH at $t = 21$ days.

The intensity of all NCs pattern drastically decrease after 21 days except for one: $\text{Au}_{13}(\text{C12})_9\text{Br}_3^{2+}$ (named $\text{Au}_{13}(\text{C}_{27}\text{H}_{52}\text{N}_2)_9\text{Br}_3^{2+}$ in Figure IV-7). From $t = 0$ to $t = 21$ days, nanocluster $\text{Au}_{13}(\text{C12})_9\text{Br}_3^{2+}$ has the highest pattern intensity. If we consider that this nanocluster intensity is of 100 % in the example of Figure IV-7 at $t = 21$ days, we can calculate the other nanoclusters relative intensity. This was done on 5 mass spectrometry spectra obtained from ESI-TOF and ESI-FTICR experiments on samples C12-AuNCs. The results obtained in term of relative intensity of nanoclusters were very similar. If we take nanocluster $\text{Au}_{13}(\text{C12})_9\text{Br}_3^{2+}$ as a reference, nanocluster $\text{Au}_{13}(\text{C12})_8\text{Br}_4^{+}$ pattern had a relative intensity of 9% in all the experiments. Nanoclusters $\text{Au}_{13}(\text{C12})_9\text{Br}_2\text{CH}_3^{2+}$, $\text{Au}_{13}(\text{C12})_9\text{Br}_2\text{H}^{2+}$ and $\text{Au}_{13}(\text{C12})_9\text{Br}_2\text{Cl}^{2+}$ had a relative pattern intensity of 30%, 5% and 15% respectively in all experiments. Although we did not conduct quantitative experiments, there is a clear decrease in the nanoclusters intensity that are detected with aging except for $\text{Au}_{13}(\text{C12})_9\text{Br}_3^{2+}$. Indeed, at $t = 0$, compared to nanocluster $\text{Au}_{13}(\text{C12})_9\text{Br}_3^{2+}$, the relative pattern intensities are 15%, 70%, 25% and 35% for nanoclusters $\text{Au}_{13}(\text{C12})_8\text{Br}_4^{+}$, $\text{Au}_{13}(\text{C12})_9\text{Br}_2\text{CH}_3^{2+}$, $\text{Au}_{13}(\text{C12})_9\text{Br}_2\text{H}^{2+}$ and $\text{Au}_{13}(\text{C12})_9\text{Br}_2\text{Cl}^{2+}$ respectively (Figure IV-6). Most of the remaining nanoclusters after 3 weeks have nine C12 ligands in their composition except for $\text{Au}_{13}(\text{C12})_8\text{Br}_4^{+}$ which has eight ligands. Indeed, we can see that it is detected in the suspensions over time but the intensity of the corresponding pattern decreases in all the experiments.

Synthesis of n-heterocyclic carbene stabilized gold nanoclusters from imidazolium salts and $\text{HAuCl}_4 \cdot 3\text{H}_2\text{O}$

| Nanoclusters | Relative intensity at t = 0 (%) | Relative intensity at t = 21 days (%) |
|---|---------------------------------|---------------------------------------|
| $\text{Au}_{13}(\text{C12})_9\text{Br}_3^{2+}$ | 100 | 100 |
| $\text{Au}_{13}(\text{C12})_8\text{Br}_4^+$ | 15 | 9 |
| $\text{Au}_{13}(\text{C12})_9\text{Br}_2\text{CH}_3^{2+}$ | 70 | 30 |
| $\text{Au}_{13}(\text{C12})_9\text{Br}_2\text{H}^{2+}$ | 25 | 5 |
| $\text{Au}_{13}(\text{C12})_9\text{Br}_2\text{Cl}^{2+}$ | 35 | 15 |

Figure IV-6 Pattern relative intensity of nanoclusters stable in suspensions just after washing and after 3 weeks with intensity = 100 % for the most intense nanocluster pattern.

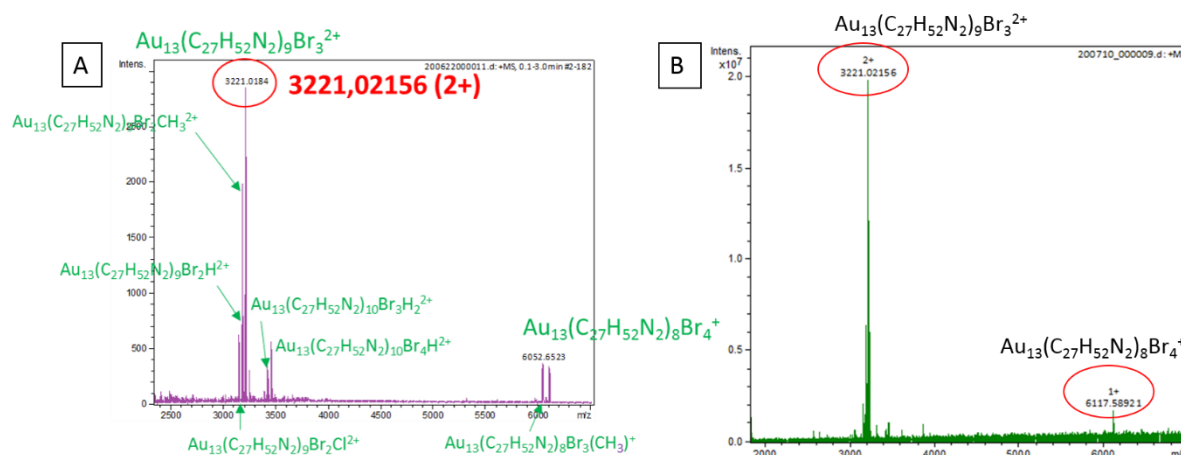


Figure IV-7 ESI-TOF mass spectrometry spectra of C12-AuNCs suspensions in EtOH at t = 0 (A) and t = 21 days (B).

After 3 weeks there are 5 nanoclusters species identified by ESI mass spectrometry (Figure IV-8). They all have the same number of gold atoms, 13. Four of them have nine C12 NHC ligands in their composition whereas only one has eight C12 NHC ligands in its composition. Also, after heating of the sample at 65°C for 5 hours, the suspensions were still stable and ESI-MS spectra showed that the spectra are similar to the one obtained in Figure IV-7 B but the peak for $\text{Au}_{13}(\text{C12})_9\text{Br}_3^{2+}$ is highly detected on the spectra compared to the others which are detected at a very low intensity.

Synthesis of n-heterocyclic carbene stabilized gold nanoclusters from imidazolium salts and $\text{HAuCl}_4 \cdot 3\text{H}_2\text{O}$

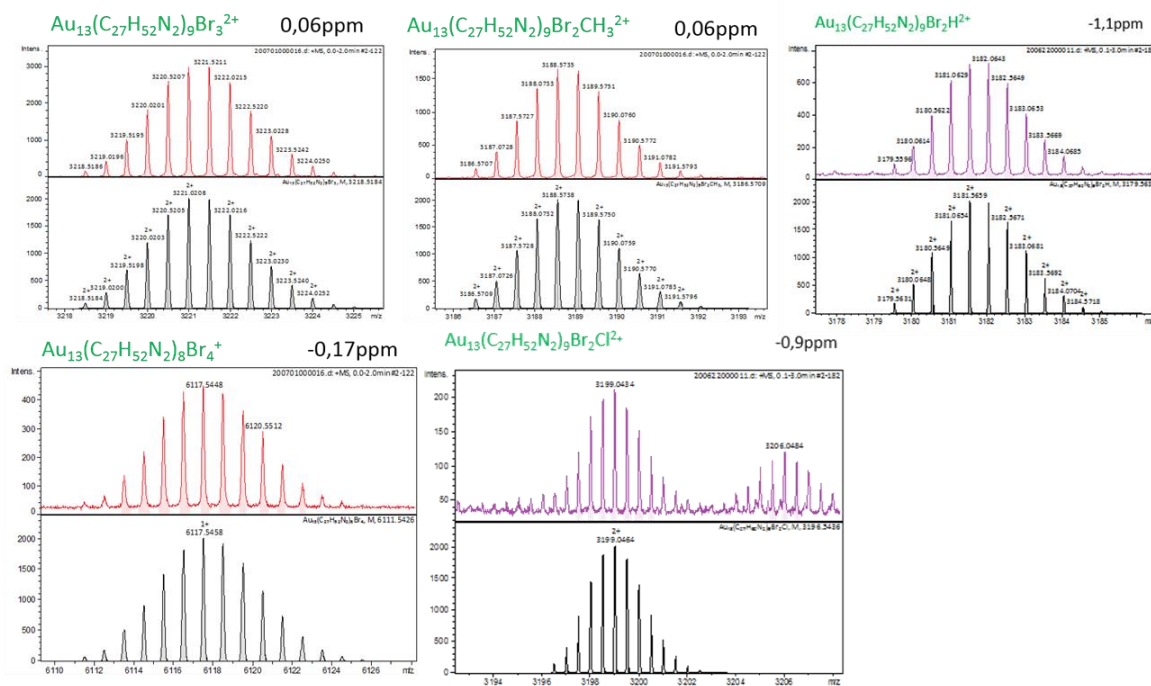


Figure IV-8 Experimental (red) and theoretical (black) patterns for the nanoclusters stable in suspensions after 3 weeks in the C12-AuNCs samples.

The question of what do happen to the nanoclusters that are not stable over aging is raised. Two main hypotheses have been made. One is that etching of the most unstable nanoclusters into small molecular complexes occurs. The other is that there is a decomposition of the most unstable nanoclusters followed by recombination into more stable nanoclusters. Our team leans toward the second hypothesis since there was no significant increase of molecular complex $\text{Au}(\text{NHC})_2^+$ detected in our suspension but an increase of $\text{Au}_{13}(\text{C12})_9\text{Br}_3^{2+}$ pattern intensity.

The MS analysis confirmed the synthesis of NHC capped AuNCs and gave us the precise structures. Similarly to the previous chapter, we saw that multiples NCs are formed during the synthesis but only the most stable ones remain with aging of the suspensions. Actually, nanocluster $\text{Au}_{13}(\text{C12})_9\text{Br}_3^{2+}$ is the most stable (no decreasing of the peak intensity with time compared to the other nanoclusters which peaks intensity is only decreasing). This type of nanocluster, $\text{Au}_{13}(\text{NHC})_9\text{X}_3^{2+}$, is similar to the one reported by Narouz *et al.* through crystallization of the nanoclusters obtained from 1,3-Dibenzyl-1H-benzo[d]imidazol-2-ylidene)gold(I) chloride reduction. Since we did not make a selection by crystallization, we see more species as well as their evolution in time.

The same experiments were conducted for the suspensions obtained with imidazolium salts bC12-Br and bBenzyl-Cl (bC12-AuNCs, bBenzyl-AuNCs).

The results were very different compared to those obtained for samples C12-AuNCs. First, for samples bC12-AuNCs the analysis of the samples showed that various NCs were formed. However, we did not only get Au_{13} NCs but mostly very small molecular complexes such as $\text{Au}_2(\text{bC12})_4\text{Br}^+$, $\text{Au}_2(\text{bC12})_5\text{Br}_2\text{H}^+$, $\text{Au}_3(\text{bC12})_6\text{Br}_2^+$ and $\text{Au}_4(\text{bC12})_8\text{Br}_3^+$. There were also $\text{Au}_8(\text{bC12})_7^{2+}$, $\text{Au}_{11}(\text{bC12})_8\text{Br}_2^+$, $\text{Au}_{15}(\text{bC12})_{10}\text{Br}_3^{2+}$, $\text{Au}_{15}(\text{bC12})_9\text{Br}_4^+$, $\text{Au}_{16}(\text{bC12})_9\text{BrH}^+$

Synthesis of n-heterocyclic carbene stabilized gold nanoclusters from imidazolium salts and $\text{HAuCl}_4 \cdot 3\text{H}_2\text{O}$

$\text{Au}_{18}(\text{bC12})_9\text{Br}_3^+$ and $\text{Au}_{20}(\text{bC12})_{11}\text{Br}_2^{2+}$ nanoclusters (Figure IV-9). The variability of NCs structures is higher for ligand bC12-Br since the number of gold atoms in the NCs goes from 2 to 20.

| Au NCS Formula | Nbr Au | m/z |
|--|--------|-----------|
| $\text{Au}_2(\text{bC12})_4\text{Br}^+$ | 2 | 2292,568 |
| $\text{Au}_2(\text{bC12})_5\text{Br}_2\text{H}^+$ | 2 | 2827,9236 |
| $\text{Au}_3(\text{bC12})_6\text{Br}_2^+$ | 3 | 3479,3123 |
| $\text{Au}_4(\text{bC12})_8\text{Br}_3^+$ | 4 | 4666,0561 |
| $\text{Au}_8(\text{bC12})_7^{2+}$ | 8 | 2379,3695 |
| $\text{Au}_{11}(\text{bC12})_8\text{Br}_2^+$ | 11 | 5964,9048 |
| $\text{Au}_{15}(\text{bC12})_{10}\text{Br}_3^{2+}$ | 15 | 3870,7789 |
| $\text{Au}_{15}(\text{bC12})_9\text{Br}_4^+$ | 15 | 7367,0352 |
| $\text{Au}_{16}(\text{bC12})_9\text{BrH}^+$ | 16 | 3662,6284 |
| $\text{Au}_{18}(\text{bC12})_9\text{Br}_3^+$ | 18 | 7878,0175 |
| $\text{Au}_{20}(\text{bC12})_{11}\text{Br}_2^{2+}$ | 20 | 3930,3057 |

Figure IV-9 Listing of nanoclusters synthesized from bC12-Br and $\text{HAuCl}_4 \cdot 3\text{H}_2\text{O}$ in EtOH at $t=0$.

An analysis of the spectra was done on samples bC12-AuNCs (Figure IV-10). The number of bC12 ligands increased with the number of gold atoms in a logarithmic way (Figure IV-10, A). The highest number of ligands was of 11 for nanocluster $\text{Au}_{20}(\text{bC12})_{11}\text{Br}_2^{2+}$. There was no gold nuclearity that was clearly more represented than the other in term of population of nanoclusters (Figure IV-10, B). Moreover, it was mostly nanoclusters with nine NHC ligands in their composition that were synthesized (Figure IV-10, C). The analysis of the bC12-AuNCs shows that there is more variety of NCs structures that are stabilized with this ligand in comparison with C12-Br. Also, no Au_{13} nanocluster structure was synthesized. When it comes to the patterns intensities in the spectra at $t = 0$, the species that had high patterns intensities were $\text{Au}_2(\text{bC12})_4\text{Br}^+$, $\text{Au}_8(\text{bC12})_7^{2+}$, $\text{Au}_{16}(\text{bC12})_9\text{BrH}^+$ and $\text{Au}_{11}(\text{bC12})_8\text{Br}_2^{2+}$.

Synthesis of n-heterocyclic carbene stabilized gold nanoclusters from imidazolium salts and $\text{HAuCl}_4 \cdot 3\text{H}_2\text{O}$

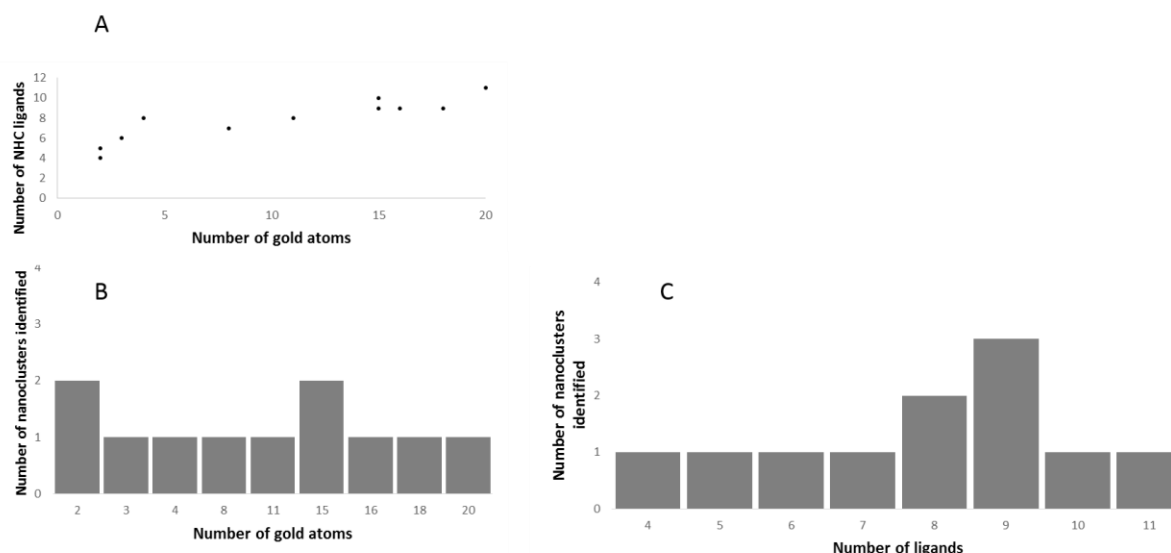


Figure IV-10 A) Comparison of the number of gold atoms in identified nanoclusters to the number of bC12 ligands. B) Bar chart histogram showing the number of nanoclusters identified depending on the number of gold atoms. C) Bar chart showing the number of nanoclusters identified depending on the number of bC12 ligands.

MS following of the suspensions evolution over time showed that after 1 month there was not significant change on the suspensions composition. There was mostly molecular complex $\text{Au}_2(\text{bC12})_4\text{Br}^+$. The intensity of some peaks associated to the AuNCs decreased over time but we could still detect some traces of them especially $\text{Au}_8(\text{bC12})_7^{2+}$, $\text{Au}_{11}(\text{bC12})_8\text{Br}_2^{2+}$, $\text{Au}_{16}(\text{bC12})_9\text{BrH}^{2+}$ in the samples. We can note that this time purification did not remove excess $\text{Au}_2(\text{bC12})_4\text{Br}^+$ complexes that were highly detected in the samples. In comparison to imidazol-2-ylidenes, the presence of the benzene ring fused to the positions 3 and 4 may induce further stabilization through p-p stacking at the surface of the NCs.⁷ It is a first explanation on the ability of this ligand to stabilize more types of AuNCs.

It means also that depending on the ligand, we could be able to stabilize some AuNCs or not and it directly plays a role in the nature of NCs structures. Some ligands may be able to fit better for the formation of stable AuNCs than the others.

Same ESI-MS experiments were done with synthesis using imidazolium salt bBenzyl-Cl (samples bBenzyl-AuNCs).

Results showed a high intensity pattern for $\text{Au}_2(\text{bBenzyl})_4\text{Cl}^+$ specie. Other NCs were detected with lower intensity: $\text{Au}_{12}(\text{bBenzyl})_8\text{Cl}_3^+$, $\text{Au}_{13}(\text{bBenzyl})_8\text{Cl}_4^+$, $\text{Au}_{15}(\text{bBenzyl})_9\text{Cl}_4^+$ and $\text{Au}_{15}(\text{bBenzyl})_{10}\text{Cl}_3^{2+}$ (Figure IV-11).

Synthesis of n-heterocyclic carbene stabilized gold nanoclusters from imidazolium salts and $\text{HAuCl}_4 \cdot 3\text{H}_2\text{O}$

At $t = 0$, the evolution of the number of ligands depending on the number of gold atoms profile is similar to what we have previously seen for the other ligands (Figure IV-12, A). This time we were able to stabilize species with a number of gold atoms going from two to fifteen. Only five species were stabilized with two of them having fifteen gold atoms in their composition (Figure IV-12, B). As for the number of stabilizing ligands, the highest number was ten ligands for nanocluster $\text{Au}_{15}(\text{bBenzyl})_{10}\text{Cl}_3^{2+}$. Two species had eight stabilizing ligands in their composition (Figure IV-12, C).

| Au NCS Formula | Nbr Au | m/z |
|---|--------|-----------|
| $\text{Au}_2(\text{bBenzyl})_4\text{Cl}^+$ | 2 | 1621,4894 |
| $\text{Au}_{12}(\text{bBenzyl})_8\text{Cl}_3^+$ | 12 | 4856,6846 |
| $\text{Au}_{13}(\text{bBenzyl})_8\text{Cl}_4^+$ | 13 | 5088,6194 |
| $\text{Au}_{15}(\text{bBenzyl})_{10}\text{Cl}_3^{2+}$ | 15 | 3021,9394 |
| $\text{Au}_{15}(\text{bBenzyl})_9\text{Cl}_4^+$ | 15 | 5744,7240 |

Figure IV-11 Listing of nanoclusters synthesized from *bBenzyl-Cl* and $\text{HAuCl}_4 \cdot 3\text{H}_2\text{O}$ in EtOH at $t=0$.

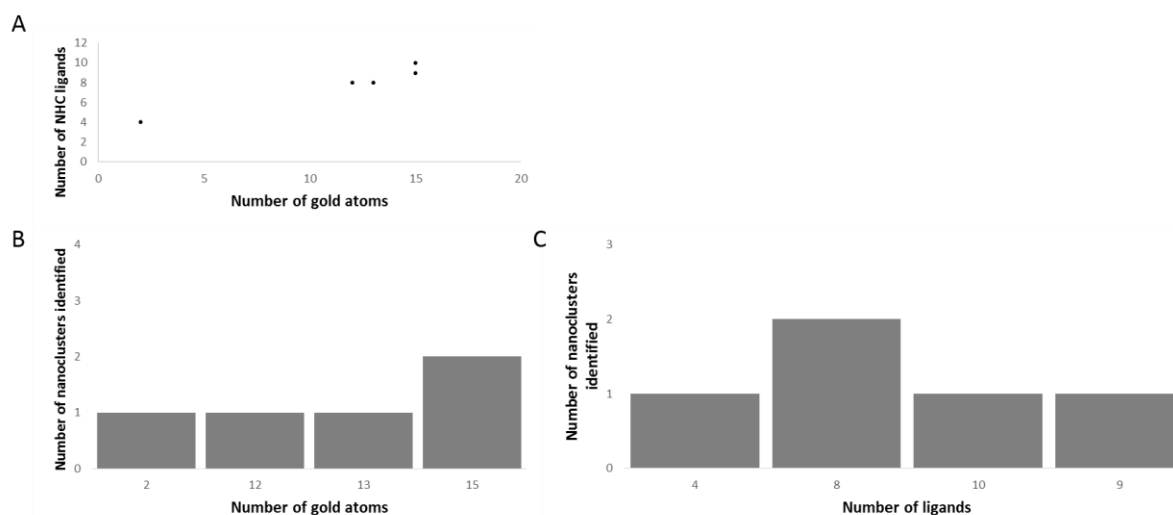


Figure IV-12 A) Comparison of the number of gold atoms in identified nanoclusters to the number of *bBenzyl* ligands. B) Bar chart histogram showing the number of nanoclusters identified depending on the number of gold atoms. C) Bar chart showing the number of nanoclusters identified depending on the number of *bBenzyl* ligands.

Synthesis of n-heterocyclic carbene stabilized gold nanoclusters from imidazolium salts and $\text{HAuCl}_4 \cdot 3\text{H}_2\text{O}$

After 1 month, most of the peak intensity did decrease except for $\text{Au}_2(\text{bBenzyl})_4\text{Cl}^+$. Also, gold-NHC molecular complex $[\text{Au}(\text{bBenzyl})_2]^+$ was detected in the suspension. What is surprising is that we did not detect the $[\text{Au}_{13}(\text{NHC})_9\text{Cl}_3]^{2+}$ that Narouz *et al.*³ isolated while it is with the same NHC (from 1,3-dibenzylbenzimidazolium) and the same anion (Cl^-). There is different hypothesis that can be made on that subject. First, maybe the nanocluster $[\text{Au}_{13}(\text{NHC})_9\text{Cl}_3]^{2+}$ is synthesized but obtained in very large minority thus not detected by ESI-MS. This hypothesis is very unlikely to be true since we were able to detect gold nanoclusters with very low intensity signals. Then, we can see that we were able to detect $[\text{Au}_{13}(\text{NHC})_8\text{Cl}_4]^+$ in the samples at $t = 0$ and after 1 month aging. If we draw an analogy with the syntheses of PPh_3 capped AuNCs, we can see that nanoclusters $\text{Au}_{13}(\text{PPh}_3)_8^+$ ⁸ and $\text{Au}_{13}(\text{PPh}_3)_{10}\text{HNaCl}^{2+}$ ⁹ were synthesized by different teams with similar reagents, solvent and concentrations (5mM solution of AuClPPH_3 mixed with a 5mM solution of NaBH_4). However, the teams did not obtain the same results since the first one obtained $\text{Au}_{13}(\text{PPh}_3)_8^+$ and the second one obtained $\text{Au}_{13}(\text{PPh}_3)_{10}\text{HNaCl}^{2+}$. It means that it is not only the ligand that drives the structure of a nanoclusters but also other reaction conditions such as the reaction time and the purification method. This could explain why with similar NHC ligand (from 1,3-dibenzylbenzimidazolium), our team and other team synthesized two different NHC capped Au_{13} nanoclusters.

Some of the results obtained when analyzing bBenzyl-AuNCs samples are similar to the one obtained with samples bC12-Br. Indeed, the nuclearity of the nanoclusters stabilized does vary (not only Au_{13} NCs are obtained). Also, the thermodynamical stability of the suspensions goes over time toward the formation of very small molecular complexes. Some bigger nanoclusters are synthesized such as Au_{15} NCs and they are still detected after 1 month. However, their relatively low pattern intensity makes us believe that they are not synthesized in high quantity when using ligand bC12-Br or bBenzyl-Cl. Also, our hypothesis here goes toward etching of the nanoclusters toward the formation of smaller, more stable, molecular complexes given the formation of $[\text{Au}(\text{bBenzyl})_2]^+$ over time.

Ligand C12-Br has shown to be a ligand of choice for the synthesis of stable NHC capped Au_{13} NCs. The suspensions were verified after 3 months and the $\text{Au}_{13}(\text{C12})_9\text{Br}_3^{2+}$ NC did not decompose into molecular complexes. The high stability of the C12-AuNCs samples can be explained by the strong binding of the NHC to gold and by the interactions between the long alkyl chains that occur simultaneously.¹⁰ For the ligands, bC12-Br and bBenzyl-Cl, the benzene ring may allow further stabilization of nanoclusters with various number of gold atoms but the drawback is that it increases the formation of unstable nanoclusters. These nanoclusters will then decompose into molecular complexes with ageing of the suspensions. Thus, the use of an imidazol-2-ylidenes ligand with long stabilizing chains is then recommended for size focusing synthesis of highly stable nanoclusters.

Some attempt to crystallize the NCs were done so that characterization techniques such as XRD could be performed but, unfortunately, we could not crystallize them (probably due to the bulkiness of the long alkyl chains).

For most of the syntheses, we could observe that a significant amount of molecular complex $[\text{Au}(\text{NHC})_2]^+$ was formed. It was formed in crude product but also with the ageing of the purified suspensions. The mechanism for the formation of Au-NHC complexes was previously studied for ligand exchange reactions on AuNPs.² According to the results, the binding of NHC to gold is more favorable than the binding of thioethers to gold which leads to the ligand

Synthesis of n-heterocyclic carbene stabilized gold nanoclusters from imidazolium salts and $\text{HAuCl}_4 \cdot 3\text{H}_2\text{O}$

exchange. However, a high quantity of $[\text{Au}(\text{NHC})_2]^+$ in the suspension makes us suppose that the strength of the Au-NHC bond leads to the formation of Au-NHC complexes on the surface. Indeed, the strength of the Au-NHC bond leads to a delocalization of the electrons toward the ligand (because the NHC-Au bonds compete with the Au-Au bonds). It results in gold atoms being detached from the metallic core. The NHC-Au fragments released from the surface can react with the NHC ligands in solution, leading to the formation of $[\text{Au}(\text{NHC})_2]^+$ complexes and thereby to the erosion of the AuNCs. Similar phenomena were observed with other ligands such as phosphines.¹¹ It means that we have to find the right compromise between a ligand that binds to the surface but not too much so as not to lead to dissolution. Some comparison of the binding energy of NHCs to metals such as Ruthenium or Nickel, depending on the NHCs being saturated or unsaturated or being more or less bulky, have been done.¹² It was reported that for the less bulky NHC-metal complexes, the saturated NHC ligands are predicted to bind more strongly than the unsaturated NHC ligands, whereas for the bulkier NHC-Metal complexes, the saturated NHC ligands binds less strongly than the unsaturated NHC ligands. For example, for complexes $\text{Ru}(\text{NHC})\text{Cl}$, the bond dissociation energies are higher in the complexes without substituents in the ortho positions of the NHCs. Other example, for complex $\text{Ni}(\text{CO})_3(\text{NHC})$, with the less bulky NHCs ligands the complexes are stable, whereas with the bulky NHC ligands the complexes are destabilized. Thus, the steric and electronic contributions of the various NHCs to the NHC-metal bonding has a direct effect on the stability on the structures that we want to synthesize. Imidazol-2-ylidenes ligands with long stabilizing alkyl chains on the N atoms seem to be good ligands for nanoclusters stabilization because it focuses the size of the particles synthesized (Au_{13} in our case) and stabilize them on the long run. Also, it could help in increasing the synthesis yields (no decomposition into molecular complexes).

As we found why for some ligands there were mostly gold complexes $[\text{Au}(\text{NHC})_2]^+$ with aggregation, there is still the question of the formation of gold mirror from samples iPr-AuNCs and Benzyl-AuNCs. It could be due to insufficient quantity of NHC ligand. However, analysis of the samples with increased ratio of NHC ligand (NHC: Au ratio of 10:1) revealed again only $[\text{Au}(\text{NHC})_2]^+$ complexes in the suspensions. Yet, after 1 month, gold mirror is still formed. It means that the $[\text{Au}(\text{NHC})_2]^+$ complex is reduced. There could be a photodegradation phenomenon due to light exposure in these samples since there is normally no more reducing agent in the samples at this stage. Indeed, it was recently reported that intermediate degradation and nanocluster growth are shown to be dependent on irradiation of the reacting solution with light in PPh_3 capped nanoclusters synthesis.¹³

Surprisingly the only ligand that did clearly stabilize an AuNCs species over time in suspension is C12-Br. We could have imagined that we would get the same results for bC12-Br but that is not the case. Indeed, ligand bC12-Br did stabilize AuNCs but the tendency went toward the formation of small complexes $[\text{Au}(\text{NHC})_2]^+$ and $[\text{Au}_2(\text{NHC})_4]^+$ with the aging of the suspensions. Our first hypothesis is that the benzene on the benzimidazolium compared to imidazolium does influence the interactions between the alkyl side chains. Our second hypothesis is that p-p stacking interactions are so strong that they lead to stronger Au-NHC bond thus to detachment of gold atoms from the NCs surface. With aging, it could lead to slow surface recombination and reaction of NHC-Au moieties with NHC in the suspensions. It could explain the low intensity of the high nuclearity AuNCs in our reaction conditions. Au_{25} and Au_{13} NCs synthesized from benzimidazolium have been reported^{4,3} but it was the product of crystallization of the nanoclusters. It means that there was no study of the nanocluster stability

Synthesis of n-heterocyclic carbene stabilized gold nanoclusters from imidazolium salts and $\text{HAuCl}_4 \cdot 3\text{H}_2\text{O}$

toward aging of the suspensions (when in suspension with other gold nanoclusters and remaining NHC). Also, these reported studies did not present if low masses Au-NHC molecular complexes were synthesized and how they evolve. We can have two contributions: strength of complexation and intermolecular interactions of the chains on the surface.

Some additional experiments were conducted by adding PPh_3 in the reaction medium. Indeed, the last chapter showed that when using AuClPPh_3 gold source we obtained mostly PPh_3 capped AuNCs and mixtures and NHC and PPh_3 capped AuNCs. The experiment was done as followed. A solution of $\text{HAuCl}_4 \cdot 3\text{H}_2\text{O}$ (0.05 mmol) in 2 ml ethanol is mixed with a solution of imidazolium salt (4 equiv.) in 2ml ethanol and a solution of PPh_3 (4 equiv.) in 1 ml ethanol for 20 minutes. Then, NaH (2 equiv. / imidazolium salt) is added as a base for imidazolium salt deprotonation. Finally, six minutes after, a solution of reducer NaBH_4 (10 equiv.) in 1 ml ethanol is added to give brown suspensions. The reaction is left under stirring for 5 hours. The suspensions are centrifuged (10 min, 10000 rpm) to remove excess NaBH_4 , then solvent is evaporated. Then, the suspensions were centrifuged to remove excess NaBH_4 (10 min, 10000 rpm), and the solvent was evaporated. 5 ml of benzene (to remove potential unreacted starting material) was added and the mixture was sonicated 1 min. After decantation, the benzene solution was removed and the beige solid was removed. Benzene was evaporated and the resulting brown solid redispersed in ethanol for further analysis. ESI-MS analyses of these samples showed no traces of PPh_3 capped nanoclusters on the spectra. The obtained spectra are similar to the ones obtained for samples C12-AuNCs. Thus, when PPh_3 is not already linked to gold, the competition between the ligands goes toward the formation of C12 capped AuNCs which is a first proof of the better stabilization of the NHCs compared to PPh_3 .

IV.A.2.b. Effect of the use of NaH and influence of the reactions solvent

Other reaction parameters were tested to optimize the reactions conditions. First, the removal of NaH as a base was tested since previous results on AuNPs showed that NaBH_4 , the reducing agent, was basic enough to deprotonate the imidazolium and at the same time reduce the initial gold complex to form AuNPs.

The synthesis was performed using $\text{HAuCl}_4 \cdot 3\text{H}_2\text{O}$ (0.05 mmol) as a gold source and NHC precursors (4 equiv.) bC12-Br and C12-Br in 5 ml of ethanol. However, this time only a solution of NaBH_4 (10 equiv.), which acts as reducing agent and strong base, was added. The synthesis was performed for 5 hours at room temperature. The suspensions was centrifuged (10 min, 10000 rpm) to remove the excess of NaBH_4 , then solvent was evaporated. 1 ml of benzene was added and the mixture was sonicated 1 min. After decantation, benzene was removed and the solid was redispersed in ethanol for further analysis.

These reactions conditions lead to direct aggregation for all the samples when adding the reducing agent. It means that, in EtOH, NaBH_4 does reduce the gold source but does not deprotonate the imidazolium salt to give NHC. It is probably due to the formation kinetics of the free NHC or its recombination with the protons of the solution to give back the imidazolium.

Synthesis of n-heterocyclic carbene stabilized gold nanoclusters from imidazolium salts and $\text{HAuCl}_4 \cdot 3\text{H}_2\text{O}$

It could also be due to secondary reactions between NaBH_4 and EtOH , which is a solvent likely to give a proton, lowering the basic character of NaBH_4 . It seems like the basic character of NaBH_4 is more or less pronounced depending on the solvent. Thus, in this reactions conditions adding a base (here NaH) to ensure proper generation of the NHC ligands is mandatory. To overcome this limitation, we decided to dissolve the reducing agent in water and then to add the NaBH_4 water solution to the ethanol solution containing the gold source and the imidazolium salt. The same aggregation problem was observed. We were looking for a solvent that can increase the life of the free NHC by limiting recombination into imidazolium. We did the hypotheses that the reverse protonation of the NHC is slower and that NaBH_4 basic character is stronger in in organic solvents.

In this aim, imidazolium salt (4 equiv.) was dissolved in toluene with the gold source $\text{HAuCl}_4 \cdot 3\text{H}_2\text{O}$ (0.05 mmol). Then, a solution of NaBH_4 prepared in water was added (10 equiv. in 1ml). We obtained directly red suspensions for both ligands and TEM observation associated with UV spectra analysis confirmed that AuNPs were formed (Figure IV-13). These results are similar to what was obtained by Hippolyte *et al.* for NHC capped gold nanoparticle synthesis.¹⁴ Mean size of the NPs were $7.8 (\pm 1.8)$ nm for bC12-Br capped AuNPs and $8.3 (\pm 0.5)$ nm for C12-Br capped NPs. In addition, a clear UV plasmon band could be observed on the spectra around 535 nm for both ligands.

The same reaction conditions were done but this time NaH was added in the toluene solution containing the gold source and imidazolium salt. TEM observation showed that we also obtained AuNPs with similar sizes as for the synthesis without NaH . In this case, toluene and water are non-miscible solvents and maybe the slow diffusion of the reducer into the organic phase allows deprotonation of the imidazolium and reduction of the gold source. Also, it prevents the reverse protonation of the NHCs.

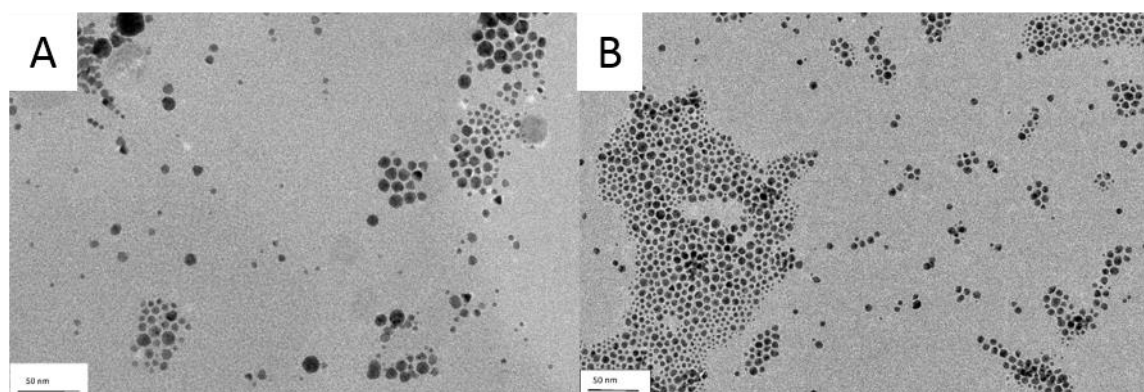


Figure IV-13 TEM images of AuNPs synthesized in toluene from $\text{HAuCl}_4 \cdot 3\text{H}_2\text{O}$, NaBH_4 and using bC12-Br (A) and C12-Br (B) ligands.

There is a clear equilibrium between deprotonation of the imidazolium and reduction that pushes the reaction toward the formation of NCs or NPs depending on the reaction conditions. Indeed, when the reaction medium is EtOH and that there is no other base than NaBH_4 , the reaction lean toward complete aggregation of the species. However, when a base is added before the reducer, the reaction leans towards the formation of AuNCs. It means that in our reaction conditions, the use of NaBH_4 alone is not able to generate neither stable AuNCs nor AuNPs.

Synthesis of n-heterocyclic carbene stabilized gold nanoclusters from imidazolium salts and $\text{HAuCl}_4 \cdot 3\text{H}_2\text{O}$

Studies on the pK_a at 25°C for imidazolium cations to give the corresponding imidazol-2-yl carbenes in water have been conducted.¹⁵ They calculated pK_a between 21.2 and 23.8 for four different imidazolium and benzimidazolium salts (1,3-bis-((S)-1-phenylethyl)benzimidazolium, 1,3-dimethylimidazolium, 1,3-dimethylbenzimidazolium and imidazolium cation). These values of pK_a show that these imidazolium cations are relatively weak carbon acids thus they can be easily deprotonated. However, when the imidazolium salt is deprotonated to form a carbene, it either goes back to its original state through hydrogen transfer in water or it undergoes reorganization by dielectric relaxation of the solvent. Indeed, it was evidenced that the reverse protonation of carbenes by water is limited by solvent reorganization and occurs with a rate constant of $k_{\text{reorg}} = 10^{11} \text{ s}^{-1}$. Also, it was shown that even carbenes with a very highly basic carbon lone pair undergo proton transfer from hydroxylic solvents that is limited by solvent reorganization with a rate constant on the order of 10^{11} s^{-1} . It means that in ethanol, even if proton transfer to reform imidazolium salts occurs very rapidly, the solvent reorganization rate can allow to stabilize the carbenic form for a certain amount of time. Kinetics play a major role in the stabilization of the NHC form. With NaH ($\text{pK}_a = 35$ in water), the hydride is almost “free” because the bond with Na^+ is very weak and it is very quickly available to play his role as a base. With NaBH_4 , it remains bound to boron, making it difficult for it to snatch protons. The kinetic of deprotonation being longer with NaBH_4 , reprotonation of the NHCs occurs way more rapidly than deprotonation. Thus, stabilization of particles cannot happen. With NaH, the kinetic of deprotonation and the solvent reorganization rate allow the NHC to be stabilized long enough to react with gold and stabilize gold nanoclusters.

When the reaction is done in toluene and water, there is formation of NPs with or without NaH. It indicates that in toluene, NaBH_4 can be used as a base so the addition of NaH as a base is not necessary because there is slow reverse protonation of the imidazolium salt in organic solvents.

Finally, we concluded that to be able to form and stabilize AuNCs, ethanol is a solvent of choice and the use of a strong base is mandatory in our conditions.

IV.A.2.c. Effect of redispersion in organic solvent

The NCs synthesis being carried out in ethanol, we tried to redisperse the AuNCs in an organic solvent for purification reasons. Indeed, most of the starting materials are soluble in ethanol. However, we obtained very interesting results on their stability toward solvent transfer.

After synthesis in ethanol (as reported in the previous parts), the samples C12-AuNCs and bC12-AuNCs were purified and the solvent was evaporated. The black solid obtained was redispersed in toluene. The suspensions colors went from dark brown to red very quickly. After TEM observation and UV spectroscopy, it was confirmed that gold NPs were formed. TEM images of the suspensions after transfer in toluene showed that, for both ligands, there were two populations of particles. Indeed, we could still observe some extra small particles (especially for synthesis with ligands C12-Br). The samples of synthesis with C12-Br gave particles of mean size $1.9 (\pm 0.5)$ nm in EtOH to $3.1 (\pm 2.2)$ nm after transfer in toluene. For ligand bC12, the particles size went from $1.1 (\pm 0.3)$ nm in EtOH to $3.5 (\pm 1.1)$ nm (Figure IV-14).

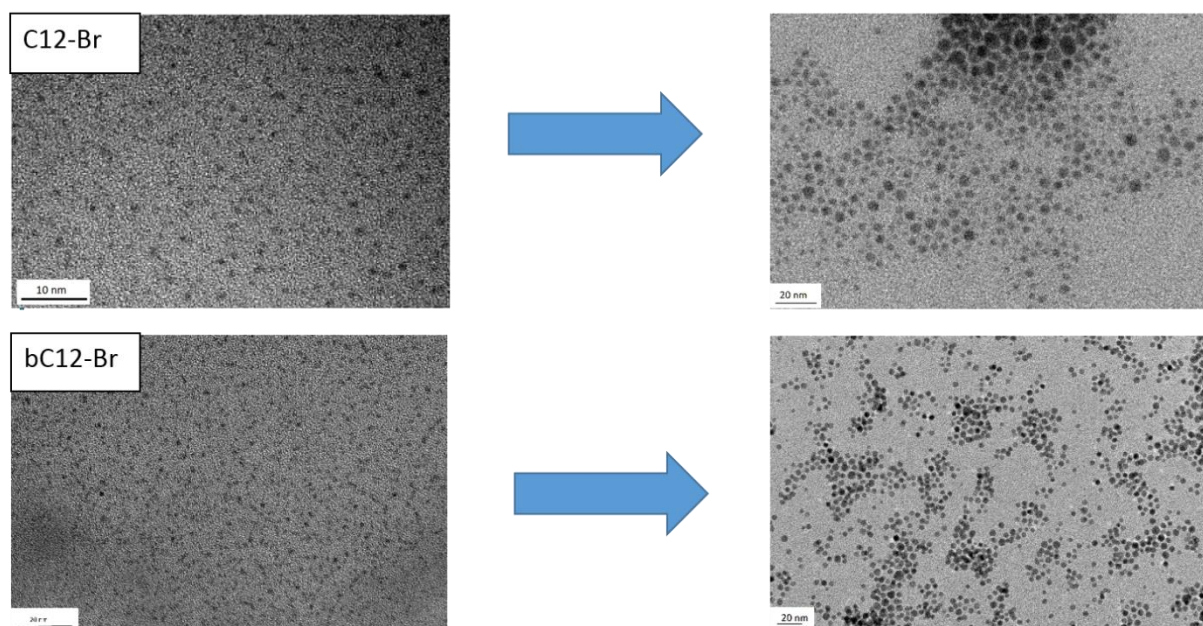


Figure IV-14 TEM images of samples C12-AuNCs and bC12-AuNCs in EtOH (left) and after redispersion in toluene (right).

In addition, UV spectra of samples C12-AuNCs and bC12-AuNCs showed both plasmon absorption bands around 530 nm. This also confirmed the reorganization of the NCs into NPs when dispersed into toluene. The suspensions were also analyzed by ESI-MS and we could not observe the patterns corresponding to AuNCs anymore. Another experiment was done. This time, toluene was directly added to samples C12-AuNCs and bC12-AuNCs in ethanol before purification of the samples. The coloration of the suspension was a mixture of brown and red. Upon addition of toluene there is a shift of the NCs equilibrium toward formation of AuNPs.

Other organic solvents like dichloromethane (DCM) and tetrahydrofuran (THF) were tested.

Synthesis of n-heterocyclic carbene stabilized gold nanoclusters from imidazolium salts and $\text{HAuCl}_4 \cdot 3\text{H}_2\text{O}$

Samples C12-AuNCs and bC12-AuNCs were purified, then solvent was evaporated and the black solids were redispersed in either DCM or THF. For both solvents, we obtained similar results as for toluene (Figure IV-15). Indeed, the suspensions turned red when solvent transfer was done. TEM observation and UV spectroscopy confirmed the formation of AuNPs. In DCM NPs of $4.2 (\pm 1.2)$ nm were obtained after transfer and in THF NPs of $3.6 (\pm 1.3)$ nm. As for the UV spectra the plasmon band was around 530 nm for both solvents similarly to toluene.

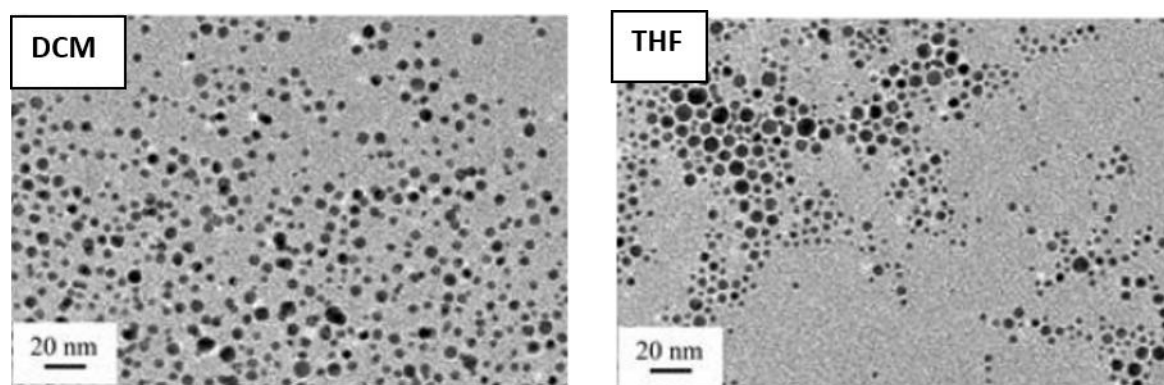


Figure IV-15 TEM images of samples C12-AuNCs and bC12-AuNCs after redispersion in DCM and THF.

We concluded that when dissolved in organic solvents, the higher solubility of the stabilizing ligands, changed their conformation. It probably induces a destabilization of the NCs which then reorganize into AuNPs. It seems that in these conditions, NPs are more thermodynamically stable structures than NCs. Thus, conservation of our samples in EtOH was chosen to preserve the stability of our AuNCs and allow further characterization.

In this part, we were able to study the formation of gold nanoclusters stabilized by various NHC ligands. The use of $\text{HAuCl}_4 \cdot 3\text{H}_2\text{O}$ gold source allowed stabilization of AuNCs with NHC in the outer shell. We were able to confirm by ESI-MS analysis that various nanoclusters are synthesized and not only one species. There is a great interest in looking at the whole solution by ESI-MS and not only at a NC isolated by crystallization. We are able to observe which nanoclusters structures are synthesized and to follow their stability toward aging. One of the nanoclusters formula that we observed had already been reported, $\text{Au}_{13}\text{NHC}_9\text{Cl}_3^{2+}$. Au_{13} nanoclusters synthesized from 1,3-Dibenzyl-1H-benzo[d]imidazol-2-ylidene)gold(I) chloride and 1,3-Bis(naphthalen-2-ylmethyl)-1H-benzo[d]imidazol-2-ylidene)gold(I)chloride reduction were crystallized and observed through single crystal diffraction. The crystals were further characterized after (in particular by ESI-MS) and found to be highly emitting at 730 nm.³ These

Synthesis of n-heterocyclic carbene stabilized gold nanoclusters from imidazolium salts and $\text{HAuCl}_4 \cdot 3\text{H}_2\text{O}$

nanoclusters synthesized from 1,3-Dibenzyl-1H-benzo[d]imidazol-2-ylidene)gold(I) chloride and 1,3-Bis(naphthalen-2-ylmethyl)-1H-benzo[d]imidazol-2-ylidene)gold(I)chloride reduction reported by Narouz *et al.*, showed great thermal stability similarly to the nanocluster $\text{Au}_{13}(\text{C}_{12})_9\text{Br}_3^{2+}$ we obtained. The team reported the synthesis of other NHC Au_{13} nanoclusters however, they did not publish the ESI-MS spectra to assess the composition of the suspensions. Since the only ESI-MS spectra that were reported are the one obtained from the dissolution of the crystals, it means we do not know which nanoclusters were exactly present in the suspensions.

Moreover, the influence of the nature of the NHC ligand was shown through the differences in the suspensions stabilities, in the nature of the AuNCs formed and in the evolution of the suspension composition toward aging. Our study showed that Imidazol-2-ylid type ligands, with long carbonyl chains (C12-Br), favored more stable suspension over time, size focusing on the nanoclusters formed and aging toward stable NC form. Shorter or less bulky substituents on the N atoms were not able to really stabilize gold NCs. Steric hindrance and the donor character of the ligand is essential to avoid the formation of small molecular species and favor the stabilization of clusters. Moreover, we were able to discuss the importance of the deprotonation kinetics of the NHC ligand in comparison to the reduction of gold. Given the reverse protonation of the NHC ligands in EtOH, the use of a strong base such as NaH is mandatory to allow both deprotonation of the NHC ligand and gold reduction (by NaBH_4). Finally, the equilibrium of formation of gold nanoclusters is fragile because they can either decompose and form molecular complexes (as seen previously) or decompose to form more stable nanoparticles as seen when redispersed in organic solvent. All of these parameters explain the very low synthesis yields that are observed when NHC capped gold nanoclusters are synthesized since it is actually very difficult to stabilize them.

Our team interest then focused on synthesizing water dispersible NHC capped gold nanoclusters aiming at future applications.

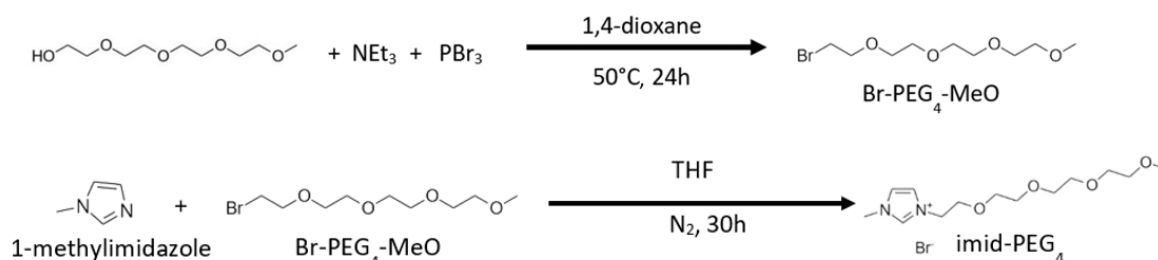
IV.B. NHC stabilized water dispersible nanoclusters using $\text{HAuCl}_4 \cdot 3\text{H}_2\text{O}$

IV.B.1. Water soluble imidazolium salt synthesis

Our team aim was to develop a synthesis of water dispersible AuNCs. We wanted to have a functionalization that allows to obtain aqueous dispersions of NHC capped Au clusters in a single step (no step of solvent transfer that can destabilize the NCs) for biological applications. The synthesis of an imidazolium salt with a polyethyleneglycol (PEG) chain was developed. PEGylated ligands are widely used for the functionalization of nanoparticles of interest for diagnosis (optical imaging probe, contrast agent for MRI, etc.) or for therapy (radiosensitizing particles, for therapeutic hyperthermia, etc.).¹⁶

For imidazolium salt imid-PEG₄, we synthesized at first the MeO-PEG₄-Br. In a round flask, MeO-PEG₄-OH was dried under vacuum at 120°C overnight. Then, anhydrous 1,4-dioxane was added at room temperature and under N₂ to the reaction medium. The mixture was frozen in liquid nitrogen then put under vacuum then it was left to warm up at room temperature (3 cycles). The suspension was finally cooled in an ice bath and Et₃N and PBr₃ were added under stirring and N₂ atmosphere. Finally, the mixture was left 24h at 50°C (scheme IV-2). The 1,4-dioxane is removed by evaporation under vacuum and the crude oil obtained was dissolved in water (50 ml) and treated with Na₂CO₃ 5 % (20 ml) until the pH of the mixture is neutral. The aqueous and the organic layer were separated. Then, the organic layer was dried over MgSO₄, filtered and put under vacuum. An oil was obtained with a yield of 87 %. The yield can be increased by extraction of the aqueous layer with CHCl₃ (3 x 20 ml) up to 95 %. ¹HNMR analysis in CDCl₃ displayed signals (ppm): 3.78 (t, 2H, OCH₂CH₂Br), 3.6 (m, 12H, O-CH₂CH₂-O), 3.44 (t, 2H, OCH₂CH₂Br), 3.33 (s, 3H, OCH₃).

Then, we used MeO-PEG₄-Br to synthesize the imidPEG₄ ($20 \cdot 10^{-3}$ mol) by reaction with 1-methylimidazole ($20 \cdot 10^{-3}$ mol) in 10 ml THF under N₂ for 30h at reflux. We obtained a yellow oil with a yield of 98% (Scheme IV-2). The imidazolium salt was analyzed by NMR spectroscopy to make sure the good molecule was obtained and to verify its purity (Figure IV-16).



Scheme IV-2 Synthesis of PEG bromide MeO-PEG₄-Br and imid-PEG₄.

Synthesis of n-heterocyclic carbene stabilized gold nanoclusters from imidazolium salts and $\text{HAuCl}_4 \cdot 3\text{H}_2\text{O}$

| Imid PEG ₄ ($^1\text{H}/^{13}\text{C}$) | Assignments |
|--|--|
| 9.61 (dd) / 136.8 | N-C(H)-N |
| 7.58 (dd) / 123.1 7.47 (dd) / 122.9 | N-CH=CH-N |
| 4.37 (t) / 49.2 | N-CH ₂ -CH ₂ -O |
| 3.87 (s) / 36.3 | H ₃ C-N |
| 3.67 (t) / 68.5 | N-CH ₂ -CH ₂ -O |
| 3.4 (m) / 69.9 | -O-CH ₂ -CH ₂ -O |
| 3.30 (t) / 71.4 | -CH ₂ -O-CH ₃ |
| 3.11 (s) / 58.5 | -CH ₂ -O-CH ₃ |

Figure IV-16 ^1H NMR and ^{13}C NMR signal assignments for Imid PEG₄ in CDCl_3 .

Assignments were made based on chemical shifts and multiplicity of ^1H signals, with the help of ^1H - ^{13}C HSQC and ^1H - ^{13}C HMBC experiments.

IV.B.2. Water soluble nanoclusters synthesis

In the meantime our team worked on developing a synthesis of water dispersible AuNCs. Our work was inspired by the synthesis of amphiphilic NHC capped AuNPs performed by Crudden's team. They used a NHC-gold(I) complex (Figure IV-17).¹⁷ To obtain the target amphiphilic AuNPs they synthesized a benzimidazolium precursor that is asymmetrically functionalized with triethylene glycol as the hydrophilic chain and a dodecyl alkyl group as the hydrophobic segment. Then, excess NaBH_4 in a water and CH_2Cl_2 biphasic solvent was added to induce reduction and nanoparticles production.

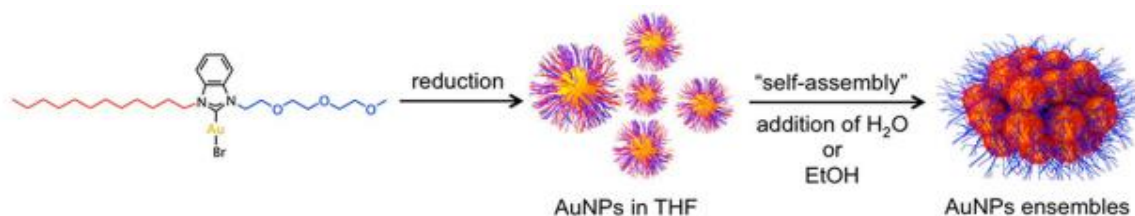
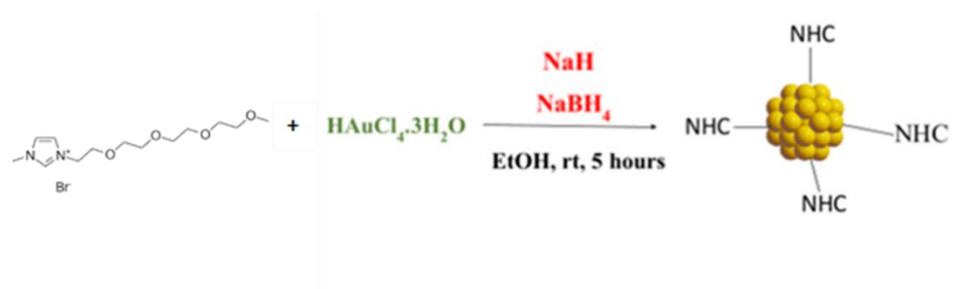


Figure IV-17 Amphiphilic AuNPs formation and their self-assembly in polar solvents.¹⁰

As part of this thesis, we synthesized an imidazolium salt bearing a PEG chain; imidPEG₄. We kept the same strategy as previously. The gold source, $\text{HAuCl}_4 \cdot 3\text{H}_2\text{O}$ (0.05 mmol), was dissolved in 2.5 ml EtOH with 4 equiv. of the imidazolium salt (4 equiv.). Then, NaH (2 equiv./imid PEG₄) and NaBH_4 (10 equiv.) were subsequently added in the reaction media (Scheme IV-3).

Synthesis of n-heterocyclic carbene stabilized gold nanoclusters from imidazolium salts and $\text{HAuCl}_4 \cdot 3\text{H}_2\text{O}$



Scheme IV-3 Synthesis of NHC capped AuNCs in ethanol using gold source $\text{HAuCl}_4 \cdot 3\text{H}_2\text{O}$ and imidPEG₄.

Brown suspensions in EtOH were obtained. The suspensions were then put in a dialysis cassette, with a molecular weight cut-off of 7 kDa, and immersed in deionized water overnight to remove unreacted molecules and ions. The brown suspensions were analyzed by TEM and UV spectroscopy. TEM observation showed that ultra-small particles were obtained with a mean size of 0.9 (\pm 0.4) nm. Also, UV spectroscopy showed no visible plasmon band on the spectra (Figure IV-18). These first results lean toward the formation of AuNCs suspension in EtOH using the same reaction conditions as previously.

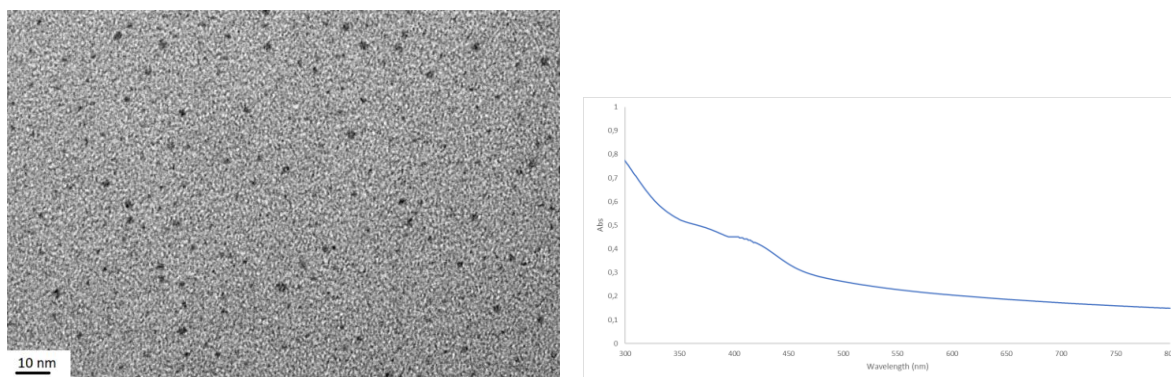


Figure IV-18 TEM image and UV spectra of AuNCs synthesized from imid PEG₄ and HAuCl₄.3H₂O in EtOH 1 hour after dialysis.

Then, the samples were analyzed by ESI-MS. With this ligand, we did not observe high nuclearity AuNCs as we were expecting. The samples were mostly composed of $\text{Au}_2(\text{imidPEG}_4)_4\text{Br}^+$. Also, the study of crude products (before dialysis) showed that gold complex $\text{Au}(\text{imidPEG}_4)_2^+$ was also produced. There was no trace of imidazolium salt in the low masses. These results were very surprising given the TEM observation results. As no higher nuclearity AuNCs structures were detected (even when screening higher m/z), our first hypothesis is that we synthesized ultra-small nanoparticles but no nanoclusters. The nanoparticles were probably going through growing stages (e.g. Oswald ripening). Then, we questioned the stability of our suspensions. Indeed, some of our previous experiences showed

Synthesis of n-heterocyclic carbene stabilized gold nanoclusters from imidazolium salts and $\text{HAuCl}_4 \cdot 3\text{H}_2\text{O}$

that $\text{Au}_2(\text{NHC})_4\text{Br}^+$ can be synthesized in majority but present low stability over time. Indeed, the samples produced from synthesis with bBenzyl-Cl imidazolium salt displayed low stability after 1 month (formation of gold mirror and aggregation). The samples imidPEG₄-AuNCs turned dark red after 24 hours in EtOH when stored at room temperature. TEM observations showed that the extra small particles grew to much bigger ones with a mean size of $3.6 (\pm 0.9)$ nm. The size of the particles has been multiplied by 4 over the course of 24 hours. Moreover, UV spectra changed from spectra with no significant observable band to spectra with a plasmon band around 525 nm (Figure IV-19).

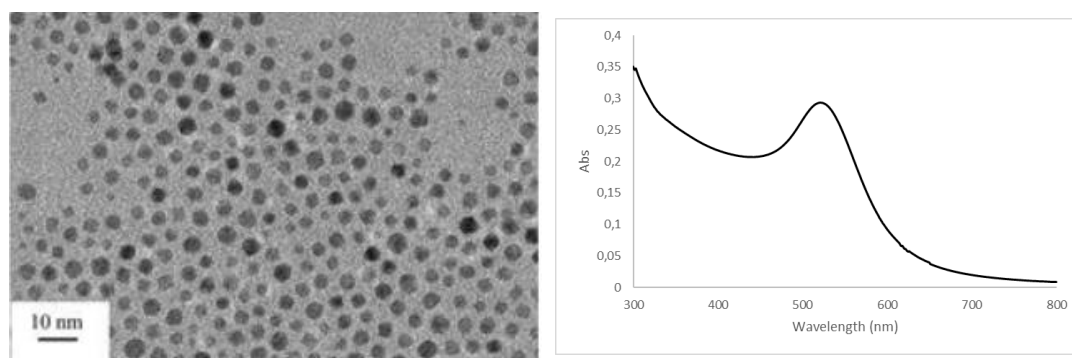


Figure IV-19 TEM image and UV spectra of AuNCs synthesized from imidPEG₄ and $\text{HAuCl}_4 \cdot 3\text{H}_2\text{O}$ in EtOH after 24 hours.

The results showed that even though the experiment is highly reproducible the ultra-small particles which are formed are not stable: the suspensions evolve toward the formation of AuNPs over time. Since after purification there is no more reducing agent and that the samples have been protected from light, these nanoparticles probably come from the reaction between $[\text{Au}_2(\text{NHC})_4\text{Br}]^+$ and the ultra-small nanoparticles. It means that in these reaction conditions the most thermodynamically favorable situation is neither the formation of AuNCs nor the formation of gold-NHC molecular complexes but the formation of gold nanoparticles. The AuNPs that are formed are highly stable over time in ethanol. No aggregation nor evolution of the suspensions was observed over time. Not only the suspensions did stay red but TEM observation also confirmed these results since no aggregation or particles size changes occurred. Also, ESI-MS analysis showed no evolution of the composition over time (no apparition of molecular specie in washed samples).

We studied the effect of the ligand/Au ratio to see if we could form stable AuNCs structures in these conditions.

IV.B.2.a. Effect of the ligand/Au ratio

The same synthesis protocol as in the previous part was done. However, this time it was carried out with varying equivalents of imidazolium salt imidPEG₄. We performed it with 1 equiv., 4 equiv., 10 equiv., 15 equiv. and 20 equiv. of imidPEG₄.

Just with visual observation of the suspensions, we were able to see that the synthesis with 1 equiv. of imidazolium, directly gave pink-red suspensions that became dark red after a few hours. However, these suspensions were not very stable over time (two days) and gold mirror formed in the flask. It probably means that there was not enough ligand to stabilize

Synthesis of n-heterocyclic carbene stabilized gold nanoclusters from imidazolium salts and $\text{HAuCl}_4 \cdot 3\text{H}_2\text{O}$

nanoparticles in these conditions. The synthesis using 4 equiv. of imidazolium gave brown suspensions that became red 24h after. The red suspensions were very stable over time (more than 2 weeks). The synthesis using 10 equiv., 15 equiv. and 20 equiv. of ligand gave similar results. We obtained brown suspensions that changed color to red 2 days after purification when stored at room temperature. The red suspensions were also stable over time. It seems like adding more imidazolium salt, thus more NHC ligand, stabilize the NCs form longer (up to 1 day longer). We note that these results were reproducible.

TEM observation and UV spectra were done on the samples when the suspensions were brown and when the suspensions turned red. When looking at the TEM images, a few observations could be made. For the samples when the suspension is still brown we obtained extra small particles but no conclusion could be made on the influence of the ligand/Au ratio. However, when the suspensions turned red (NPs suspensions), it seems like adding more ligand leads to smaller NPs. Indeed, the synthesis with 20 equiv. of imidPEG₄ gave $3.1 (\pm 0.6)$ nm NPs whereas the one using 10 equiv. and 4 equiv. gave $6.5 (\pm 0.5)$ nm and $7.1 (\pm 1.1)$ nm respectively. This decrease in size with the increase of the quantity of imidazolium introduced had already been observed for the synthesis of NP in organic medium.¹⁴ For the one using 1 equiv. we had two populations one of 30 nm and the other of 6 nm approximatively. In addition, the synthesis with 1 equivalent of imidPEG₄, evolves over time to bigger NPs (Figure IV-20). We repeated the experiment a few times, however, this result was not always reproducible. Indeed, the decrease in size with the increase in imidazolium salt ratio did not always happen. Even though this result is not always reproducible, the fact that the suspensions color always takes more time to turn red with 10, 15 and 20 equiv. than with 1 and 4 equiv. of imidPEG₄ is a hint to the influence of the ligand quantity regarding the NPs growth control.

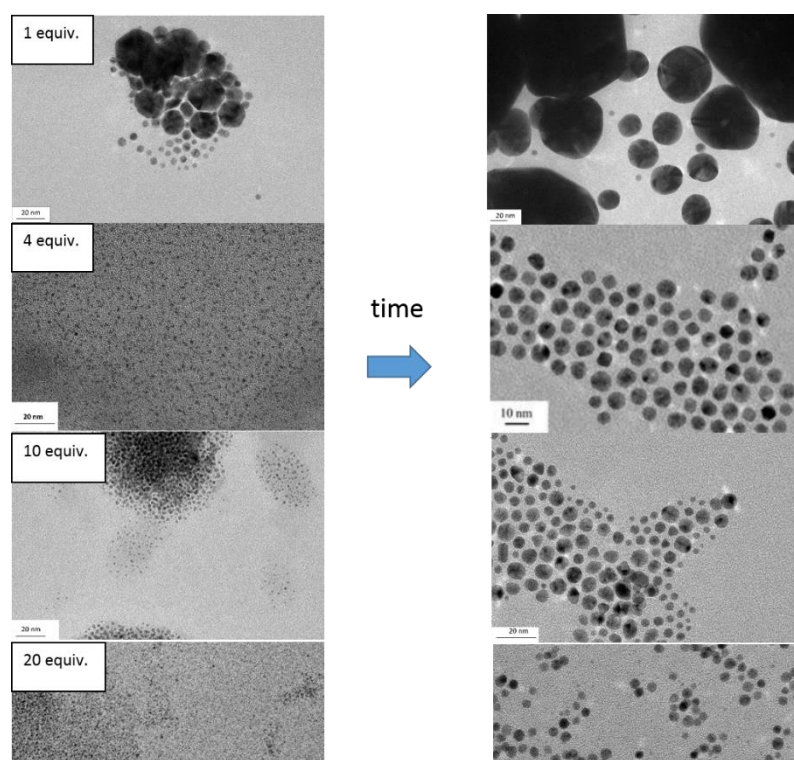


Figure IV-20 TEM images of suspensions of samples imidPEG₄-AuNCs in EtOH using various equivalents of imidPEG₄ (1, 4, 10, 20 equiv.) over time.

Even though there seem to have an influence of the ligand/Au ratio in the synthesis, it is not enough to stabilize AuNCs. However, we are able to obtain stable NPs with a ligand dependent effect on the size. We also studied the effect of the solvent on the synthesis. Indeed, we tried to carry on the synthesis in organic solvents and in water.

IV.B.2.b. Effect of the solvent

The synthesis was reproduced in toluene, DCM and in water instead of ethanol.

First, $\text{HAuCl}_4 \cdot 3\text{H}_2\text{O}$ (0.05 mmol) was dissolved in 2.5 ml toluene and mixed with a 2.5 ml toluene solution of imidPEG₄ (4 equiv.). Then, NaH (2 equiv/imidPEG₄) was added followed by addition of an aqueous (1 ml) solution of NaBH_4 (10 equiv.). A red suspension of AuNPs was obtained but NPs slowly started to aggregate and form gold mirror over time when left into toluene. The same results were observed when synthesis was done in DCM. We believed aggregation occurred maybe due to poor solubility of imidPEG₄ in organic solvents which lower the availability of NHCs, thus we decided to try to transfer the NPs in water. Water was added to the NPs suspensions (in toluene and in DCM), then the solvents were mixed through 30 seconds stirring. Then, the flask are left for an hour to allow transfer of the NPs. Almost complete discoloration of the organic solvent phase (light pink color) happened during transfer of the NPs in water (became red). However, the stability was of 24-48 hours. The results were surprising since we assumed that the NPs should be stable in water with a ligand bearing a PEG chain. TEM observation shows that the size of the NPs grows after transfer in water. A hypothesis is that when particles are placed in water, there is an equilibrium which is established between ligand coordinated at the NPs surface and ligands in solution (Figure IV-21). The passage of ligand towards the water solution leads to destabilization of the particles and to their growth to decrease the surface to volume ratio towards a new state of equilibrium.

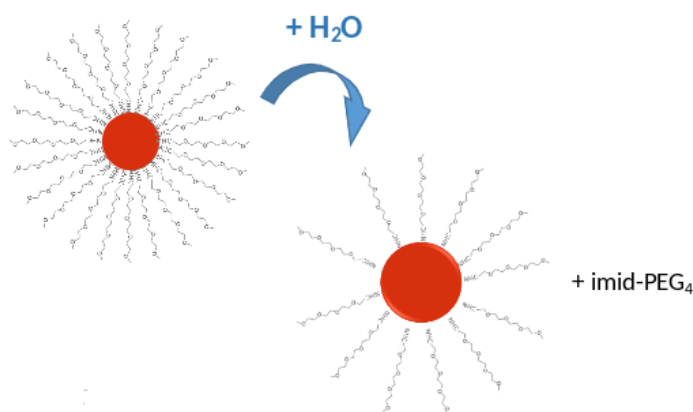


Figure IV-21 Transfer of NHC-PEG₄ stabilized AuNPs into water.

Synthesis of n-heterocyclic carbene stabilized gold nanoclusters from imidazolium salts and $\text{HAuCl}_4 \cdot 3\text{H}_2\text{O}$

The same reaction was done in water but unfortunately it directly led to the formation of aggregates. It is probably due to the fact that in water NaH reacts to give NaOH thus it does not deprotonate the ligand. Also, in water, reverse protonation of the NHC happen very fast, which prevents the stabilization of the carbene form long enough. In these reaction conditions, NaBH_4 deprotonation kinetics is not efficient.

We decided to do further characterization of the suspensions to see if we could find traces of AuNCs in the red suspensions (24 hours after purification) synthesized in EtOH.

IV.B.2.c. Analysis by Mass Spectrometry, NMR and XPS

We previously analyzed the suspensions synthesized from $\text{HAuCl}_4 \cdot 3\text{H}_2\text{O}$ and imidPEG₄ (4 equiv.) in EtOH just after purification when they were still brown. Here, the samples were analyzed 24 hours after purification, when they turned red. The samples were analyzed by mass spectrometry to find if AuNCs were detected. ESI-MS spectra showed that we obtained mostly molecular complex $\text{Au}(\text{imidPEG}_4)_2^+$ (Figure IV-22). Regardless of the number of equivalent of imidPEG₄, the MS results were the same. We tried to find traces of NCs structures but we could not. Given that the samples were purified it means that the only thing that can be detected by ESI-MS in the samples is indeed these molecular complexes. We can conclude that no gold nanoclusters are stabilized in these reaction conditions. The brown color of the suspensions in the beginning comes from extra small nanoparticles that grow in size over 48 hours and then stabilize in size (red suspensions).

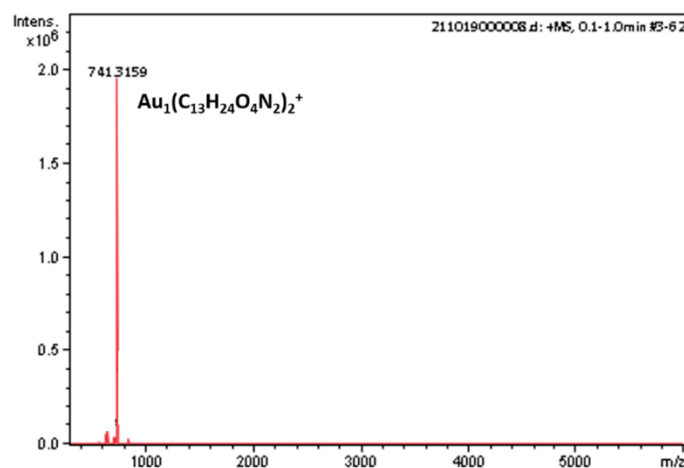


Figure IV-22 ESI-MS spectrum of synthesis from $\text{HAuCl}_4 \cdot 3\text{H}_2\text{O}$ and 4 equiv. of imidPEG₄ in EtOH.

Also, we did ^1H NMR experiments in CDCl_3 to detect the carbene form in the suspensions and maybe to see if we could have information on the gold surface – ligand interaction. No signal

Synthesis of n-heterocyclic carbene stabilized gold nanoclusters from imidazolium salts and $\text{HAuCl}_4 \cdot 3\text{H}_2\text{O}$

corresponding to the proton of the free imidazolium salt was observed. It confirmed the results obtained by ESI-MS, where no signal associated to imidazolium salt was found. Also, no signal corresponding to the NHC ligands linked to gold NPs was detected. This is probably due to the broadening of the signal when molecules are close to the NP surface. Indeed, the lower rotational mobility of the ligands when attached to the surface, and their distribution on the NP's surface induce a loss of the signals of the ligands.

XPS (X-ray photoelectron spectrometry) experiments were performed on the samples $\text{NHCPEG}_4\text{-AuNCs}$ synthesized in EtOH after purification (red suspensions). Results showed that the formation of metallic gold is evidenced by the $\text{Au}4f$ signal composed of only 2 peaks at 83.7 and 87.6 eV, which correspond to spin orbit coupling $\text{Au}4f_{7/2}$ and $\text{Au}4f_{5/2}$, respectively (Figure IV-23).. The binding energies and difference between the two components energies (3.9 eV) is characteristic of metallic gold (Au^0).¹⁸ Also, no peak is observed in the 185-210 and 65-72 eV regions which indicates an absence of bromine and chlorine in the sample. This result was surprising since we know thanks to ESI-MS analysis that there is some remaining $[\text{Au}(\text{NHCPEG}_4)_2]^+$ and $[\text{Au}_2(\text{NHCPEG}_4)_4\text{Br}]^+$ complexes in the suspension. The $\text{N}1s$ spectrum shows two signals. One minor signal towards the higher energies at 402.6 eV suggesting an electrostatic interaction. Some of this electrostatic component could be explained by insufficient washing of the NPs, however, the absence of detected bromide does not follow this assumption. It is probably due to electrostatic interaction between the ligand and the NPs. The other major signal, corresponds to a covalent interaction at 400.5 eV. These results confirms the formation of AuNPs stabilized covalently by the NHCPEG_4 ligand.

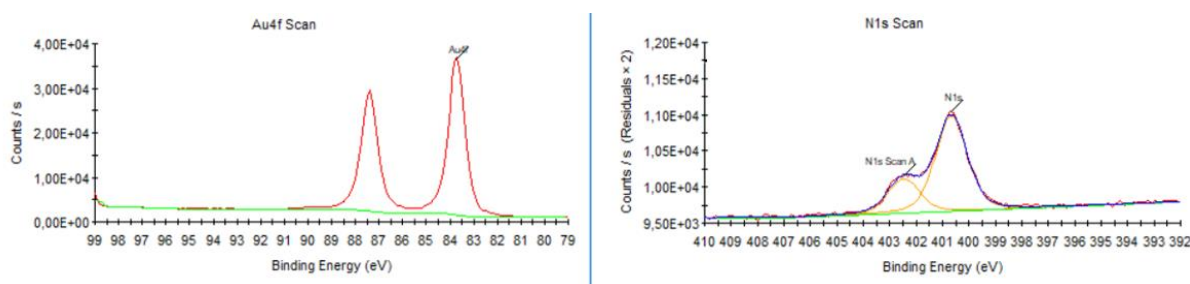


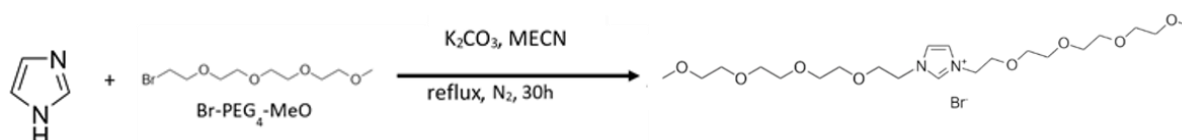
Figure IV-23 XPS $\text{N}1s$ and $\text{Au}4f$ spectra of nanoparticles synthesized from $\text{HAuCl}_4 \cdot 3\text{H}_2\text{O}$, 4 equiv. of imidPEG_4 , NaH and NaBH_4 in EtOH.

After analysis of the samples the results showed that with the ligand imidPEG_4 , we were only able to stabilize AuNPs. In an attempt to obtain similar results as the one obtained with ligand $\text{C}12\text{-Br}$, we decided to try the experiment with two PEG side chains instead of one (to get closer to $\text{C}12\text{-Br}$ structure). Maybe this time we could obtain stable gold NCs.

Synthesis of n-heterocyclic carbene stabilized gold nanoclusters from imidazolium salts and $\text{HAuCl}_4 \cdot 3\text{H}_2\text{O}$

IV.B.2.d. Attempt with another water soluble ligand

The following reaction was performed to obtain the ligand imidBisPEG₄. Imidazole (436 mg, 2 mmol), K_2CO_3 (3 mmol), Br-PEG₄-OMe (4 mmol) and 7 ml MeCN were put in a sealed flask and heated at reflux for 30 hours under stirring (Scheme IV-4). The solvent was evaporated and the residue was dissolved in DCM and filtered. The filtrate was evaporated under reduced pressure, triturated in Et₂O and decanted. We obtained an oil with a yield of 78%.



Scheme IV-4 Synthesis of imidazolium salt imidBisPEG₄.

The imidazolium salt was analyzed by ^1H NMR and ^{13}C NMR to confirm its synthesis and purity. ^1H NMR (400 MHz, CDCl_3) δ 9.57 (t, 1H), 7.68 (d, 2H), 7.47 (d, 2H), 7.2 (m, 2H), 4.38 (m, 4H), 3.79 (m, 4H), 3.56 (m, 17H), 3.36 (s, 6H), 2.28 (s, 3H). ^{13}C NMR (101 MHz, CDCl_3) δ 143.8, 139.3, 138.2, 128.5, 126.8, 122.7, 71.6, 70.1, 70.09, 70.02, 68.7, 58.7, 49.3, 21.4.

There should therefore be only one signal corresponding to the ethylene protons of the heterocycle. These different signals (7.68 (d, 2H), 7.47 (d, 2H)), could indicate the presence of by product imidazole-PEG (only one functionalization).

The imidazolium salt was used for AuNCs synthesis in EtOH. We kept the same strategy as previously. The gold source $\text{HAuCl}_4 \cdot 3\text{H}_2\text{O}$ was dissolved in EtOH with 4 equiv. of the imidazolium salt. Then NaH and NaBH_4 were subsequently added in the reaction media. Purification through 7kDa dialysis cassettes against water overnight was done.

We obtained brown suspension in EtOH and TEM observation showed extra small particles. In addition, UV spectroscopy analysis showed no plasmon band. However, after 2 days of storing at room temperature, the suspensions turned red. We were hoping that it will have the same behavior as synthesis with ligand C12-Br but ESI-MS results showed us that we mostly obtained molecular complexes similarly to what is obtained with ligand imidPEG₄. Also, TEM and UV spectroscopy after 2 days showed the formation of gold NPs in EtOH. Since we could not obtain AuNCs in these conditions, we still tried to test the stability of AuNPs toward transfer in water. Indeed, adding another PEG chain could improve the solubility in water and the stability of the NPs. Results showed that with 2 PEG side chains the stability in water was of a few days. It was not very different from the results obtained with ligand imidPEG₄.

Finally, we were not able to stabilize water dispersible AuNCs by using PEGylated water soluble imidazolium salt. However, stable NHC-PEG₄ NPs were synthesized in ethanol. Upon transfer in water, the particles were stable up to a week. Then, formation of gold mirror on the flask appeared. Increasing the ligand/Au ratio did not prevent this phenomenon. Also, the synthesis of an imidazolium salt with both N atoms bearing PEG chains did not change the results. Our outlook would be the synthesis of an imidazolium salt with longer PEG chains. It could allow the stabilization of AuNCs, if not it could improve the stability of the formed AuNPs in water for potential biological applications.

IV.C. Conclusion

This chapter described different attempts to synthesize stable NHC capped gold nanoclusters. First, a method using various imidazolium salts, $\text{HAuCl}_4 \cdot 3\text{H}_2\text{O}$ as gold source, NaH as base and NaBH_4 as reducing agent was developed. We were able to obtain non water dispersible AuNCs with various nuclearity depending on the type of ligand used. We confirmed that the improved stability of the NHC coated AuNCs can be explained by strength of the NHC-Au bond and by the interactions between the long alkyl chains that occur simultaneously. Indeed, the strength of the bond has to be high but not too much to avoid the formation of Au-NHC molecular complexes. Because the Au-NHC bond is strong it can lead to a delocalization of electrons towards the ligands (with Au-NHC bond being stronger than Au-Au bond), resulting in a gold atom detached from the metallic structure. Thus, imidazole-2-ylidene with long alkyl chains were better candidate than benzimidazole-2-ylidene NHCs in our reaction conditions for AuNCs formation (less $\text{Au}(\text{NHC})_2$ complexes formed) and stabilization in complex environments (without separation of the nanoclusters crystals). Also, the presence of long stabilizing alkyl chains increased the nanoclusters stability over time drastically. Indeed, the NHC ligands with smaller substituents on the N atoms performed poorly at stabilizing AuNCs on a long period of time. The equilibrium between deprotonation of the imidazolium salt to form carbenes and gold reduction were also studied. Our synthesis being in ethanol, the use of NaH was mandatory to be able to deprotonate the imidazolium salt with a high rate and avoid quick reverse protonation of the NHCs. Finally, the ESI-MS analysis method developed in the previous chapter showed here again great efficiency since we were able to analyze very quickly mixtures of nanoclusters and follow their stability toward aging.

Moreover, an attempt to develop a synthesis of water dispersible AuNCs was done. The method used PEGylated imidazolium salts, $\text{HAuCl}_4 \cdot 3\text{H}_2\text{O}$ as gold source, NaH as base and NaBH_4 as reducing agent in ethanol. However, we were not able to stabilize AuNCs in these conditions which was surprising given the similarities between imidazolium C12-Br and the PEGylated imidazolium salts. A line of thought, would be that the PEG chain interacts differently than the C12 chains. Maybe the hydrophilic character of the PEG chains induce interactions with the solvent that give them different spatial conformation compared to the hydrophobic C12 chains. What is interesting is that we were able to synthesize stable gold nanoparticles with this method. It highlights the thin line that lies between the synthesis methods of gold nanoparticles and gold nanoclusters. Further development could be made to try to shift the synthesis of water dispersible AuNPs toward AuNCs. Finding an efficient etching agent could permit the formation of gold NCs from these AuNPs.

The following of our work will focus on the synthesis of NHC stabilized particles that are formed through precipitation of Ag^+ and S^{2-} ions, Ag_2S . This study will extend the scope on the ability of NHC to stabilize particles of interest at the nanometric scale.

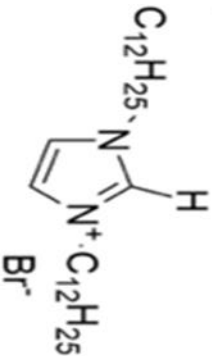
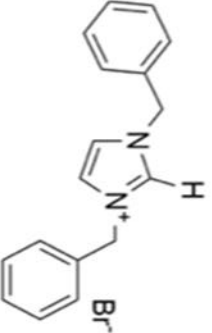
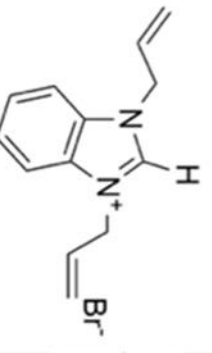
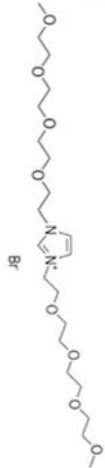
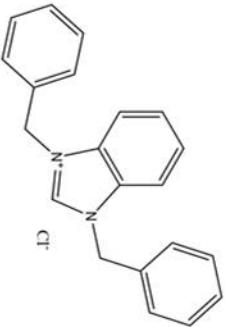
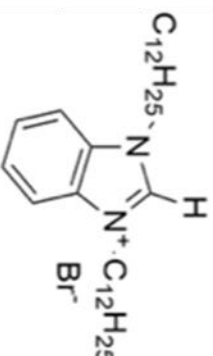
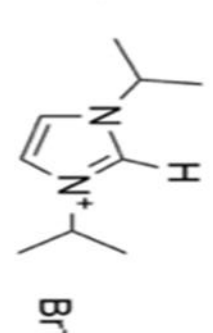
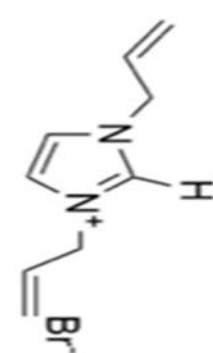
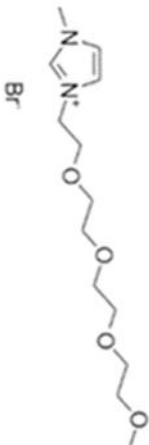
References

- (1) Hippolyte, L. New Syntheses of N-Heterocyclic Carbene-Stabilized Gold Nanoparticles, Sorbonne université, 2018.
- (2) Rodríguez-Castillo, M.; Lugo-Preciado, G.; Laurencin, D.; Tielens, F.; van der Lee, A.; Clément, S.; Guari, Y.; López-de-Luzuriaga, J. M.; Monge, M.; Remacle, F. Experimental and Theoretical Study of the Reactivity of Gold Nanoparticles Towards Benzimidazole-2-ylidene Ligands. *Chem. Eur. J.* **2016**, *22* (30), 10446–10458.
- (3) Narouz, M. R.; Takano, S.; Lummis, P. A.; Levchenko, T. I.; Nazemi, A.; Kaappa, S.; Malola, S.; Yousefalizadeh, G.; Calhoun, L. A.; Stampelcoskie, K. G.; Häkkinen, H.; Tsukuda, T.; Crudden, C. M. Robust, Highly Luminescent Au₁₃ Superatoms Protected by N-Heterocyclic Carbenes. *J. Am. Chem. Soc.* **2019**, *141* (38), 14997–15002. <https://doi.org/10.1021/jacs.9b07854>.
- (4) Shen, H.; Deng, G.; Kaappa, S.; Tan, T.; Han, Y.-Z.; Malola, S.; Lin, S.-C.; Teo, B. K.; Häkkinen, H.; Zheng, N. Highly Robust but Surface-Active: An N-Heterocyclic Carbene-Stabilized Au₂₅ Nanocluster. *Angew. Chem. Int. Ed.* **2019**, *58* (49), 17731–17735. <https://doi.org/10.1002/anie.201908983>.
- (5) Keller, B. O.; Sui, J.; Young, A. B.; Whittall, R. M. Interferences and Contaminants Encountered in Modern Mass Spectrometry. *Anal. Chim. Acta* **2008**, *627* (1), 71–81. <https://doi.org/10.1016/j.aca.2008.04.043>.
- (6) Ellison, G. B.; Engelking, P. C.; Lineberger, W. C. An Experimental Determination of the Geometry and Electron Affinity of Methyl Radical. *J. Am. Chem. Soc.* **1978**, *100* (8), 2556–2558. <https://doi.org/10.1021/ja00476a054>.
- (7) Favier, I.; Massou, S.; Teuma, E.; Philippot, K.; Chaudret, B.; Gómez, M. A New and Specific Mode of Stabilization of Metallic Nanoparticles. *Chem. Commun.* **2008**, No. 28, 3296–3298.
- (8) Huang, -Ting; Sun, -Zhi-hu; Pan, -Guo-qiang. - Selective Synthesis of Different-Sized Gold Nanoclusters through HCl-Etching and -Growth Effect. - *Chinese Journal of Chemical Physics*, 2018, *31*, 223.
- (9) Hewitt, M. A.; Hernández, H.; Johnson, G. E. ESI-MS Identification of the Cationic Phosphine-Ligated Gold Clusters Au₁–22: Insight into the Gold–Ligand Ratio and Abundance of Larger Clusters. *J. Am. Soc. Mass Spectrom.* **2021**, *32* (1), 237–246. <https://doi.org/10.1021/jasms.0c00293>.
- (10) Visbal, R.; Laguna, A.; Gimeno, M. C. Simple and Efficient Synthesis of [MCl(NHC)] (M = Au, Ag) Complexes. *Chem. Commun.* **2013**, *49* (50), 5642–5644. <https://doi.org/10.1039/C3CC42919A>.
- (11) Sharma, R.; Holland, G. P.; Solomon, V. C.; Zimmermann, H.; Schifffenhaus, S.; Amin, S. A.; Buttry, D. A.; Yarger, J. L. NMR Characterization of Ligand Binding and Exchange Dynamics in Triphenylphosphine-Capped Gold Nanoparticles. *J. Phys. Chem. C* **2009**, *113* (37), 16387–16393. <https://doi.org/10.1021/jp905141h>.
- (12) Cavallo, L.; Correa, A.; Costabile, C.; Jacobsen, H. Steric and Electronic Effects in the Bonding of N-Heterocyclic Ligands to Transition Metals. *Carbene Chem.* **2005**, *690* (24), 5407–5413. <https://doi.org/10.1016/j.jorganchem.2005.07.012>.
- (13) Hewitt, M. A.; Hernández, H.; Johnson, G. E. Light Exposure Promotes Degradation of Intermediates and Growth of Phosphine-Ligated Gold Clusters. *J. Phys. Chem. C* **2020**, *124* (5), 3396–3402. <https://doi.org/10.1021/acs.jpcc.9b10920>.
- (14) Bridonneau, N.; Hippolyte, L.; Mercier, D.; Portehault, D.; Murr, M.; Marcus, P.; Fensterbank, L.; Chanéac, C.; Ribot, F. N-Heterocyclic Carbene-Stabilized Gold Nanoparticles with Tunable Sizes. *Dalton Trans.* **2018**, *47*. <https://doi.org/10.1039/C8DT00416A>.
- (15) Amyes, T. L.; Diver, S. T.; Richard, J. P.; Rivas, F. M.; Toth, K. Formation and Stability of N-Heterocyclic Carbenes in Water: The Carbon Acid PKa of Imidazolium Cations in Aqueous Solution. *J. Am. Chem. Soc.* **2004**, *126* (13), 4366–4374. <https://doi.org/10.1021/ja039890j>.

Synthesis of n-heterocyclic carbene stabilized gold nanoclusters from imidazolium salts and H₂HAuCl₄·3H₂O

- (16) Zhang, X.-D.; Wu, D.; Shen, X.; Liu, P.-X.; Yang, N.; Zhao, B.; Zhang, H.; Sun, Y.-M.; Zhang, L.-A.; Fan, F.-Y. Size-Dependent in Vivo Toxicity of PEG-Coated Gold Nanoparticles. *Int. J. Nanomedicine* **2011**, *6*, 2071–2081. <https://doi.org/10.2147/IJN.S21657>.
- (17) Narouz, M. R.; Li, C.-H.; Nazemi, A.; Crudden, C. M. Amphiphilic N-Heterocyclic Carbene-Stabilized Gold Nanoparticles and Their Self-Assembly in Polar Solvents. *Langmuir ACS J. Surf. Colloids* **2017**, *33* (50), 14211–14219. <https://doi.org/10.1021/acs.langmuir.7b02248>.
- (18) Chastain, J.; King Jr, R. C. Handbook of X-Ray Photoelectron Spectroscopy. *Perkin-Elmer Corp.* **1992**, *40*, 221.

Synthesis of n-heterocyclic carbene stabilized gold nanoclusters from imidazolium salts and $\text{HAuCl}_4 \cdot 3\text{H}_2\text{O}$

| | | | | |
|---|---|--|---|---|
| C12-Br (1,3-didodecylimidazolium bromide) | Benzyl-Br (1,3-dibenzylimidazolium bromide) | bAllyl-Br (1,3-diallylbenzimidazolium bromide) | imidBisPEG₄ (1,3-ditetraethyleneglycolimidazolium bromide) | bBenzyl-Cl (1,3-dibenzylimidazolium chloride) |
|  |  |  |  |  |
| bC12-Br (1,3-didodecylbenzimidazolium bromide) | iPr-Br (1,3-diisopropylimidazolium bromide) | Allyl-Br (1,3-diallylimidazolium bromide) | imidPEG₄ (1-methyl, 3-tetraethyleneglycolimidazolium bromide) | |
|  |  |  |  | |

PART II - NHC STABILIZED SILVER SULFIDE NANOPARTICLES: A STUDY ON SYNTHESIS AND CHARACTERIZATION

CHAPTER V: SYNTHESIS OF N-HETEROCYCLIC CARBENE STABILIZED SILVER SULFIDE NANOPARTICLES

This chapter reports on the synthesis of Ag₂S nanoparticles. Our interest on Ag₂S nanoparticles grew because it is an ionic solid formed by precipitation of Ag⁺ and S²⁻ ions. It allows to overcome the competition of reduction and complexation reactions as observed with gold nanoclusters. The main interest was not only to study the reaction conditions to produce stable NHC protected Ag₂S NPs but also to obtain Ag₂S NPs with photoluminescence (PL) properties of interest especially for nanothermometry.

V.A. Introduction on silver sulfide nanoparticles

Silver sulfide nanoparticles, Ag₂S, have been studied for their ability to emit mainly in the second infrared window (1000–1350 nm). But other emission values are also observed depending on synthesis conditions. Such materials are extensively studied as optical probes for early diagnostic in vivo in nanomedicine. Optical property allows imaging deeper biological tissues without a few drawbacks that we will discuss later. Also, they can be considered as environmentally stable alternatives to heavy metals. Studies have demonstrated the cytotoxic nature of silver (in silver nanoparticles or Ag⁺ form). This metal is also used as an additive in bandages for burns or wounds as an antibacterial. Indeed, α-Ag₂S is one of the most insoluble silver minerals known. The very low solubility product of the Ag₂S phase ($K_s = 6.3 \times 10^{-50}$) prevents the release of toxic Ag⁺ ions within biological media.¹ Ag-S binding energy being very high (200 kJ.mol⁻¹), it allows better stability of Ag₂S in biological media. Moreover, it was reported that Ag₂S NPs internalized within cells are not subjected to significant oxidative stress. Indeed, the acid pH within the endosomes does not lead to an increase in the toxicity of the Ag₂S NPs internalized in the cells.² Ag₂S NPs are then less reactive than Ag⁰ NPs (thus less toxic).^{3,4} However, the nature of the surface ligand also plays a role in the toxicity induced by Ag₂S nanoparticles. Depending on the type of ligand the affinity to cells membrane or the oxidative stress induced on the cells may vary.⁵ In this context, the use of NHCs as stabilizing ligands is interesting.

V.A.1. Ag₂S nanoparticles for applications

Ag₂S NPs can be interesting for various applications such as semiconductor materials or photocatalyst agents for example.⁶ Actually, the monoclinic bulk α -Ag₂S is one of the oldest known semiconductor materials, discovered by Michael Faraday. He saw that Ag₂S behaved as insulator at room temperature and is highly conductive at elevated temperatures.⁷ Ag₂S NPs are also prime candidates for theranostic applications. Because of their high-performance optical properties and to the possibility to functionalize their surfaces, there gave promising results for in vivo imaging and cellular temperature measurement.⁸ Due to their ability to absorb in the NIR-I and to emit in the NIR-II, they exhibit a high penetration depth in tissues (Figure V-1).⁹ Indeed, in this window there is a minimization of tissues autofluorescence, of diffusion for a better spatial resolution and of biological component extinction coefficients. It also allows improved contrast image at increased tissue depth. In addition to their photophysical performances, these NPs show the unique asset of being made of a highly stable and nontoxic material, which lets imagine that they could be suitable for in vivo applications.

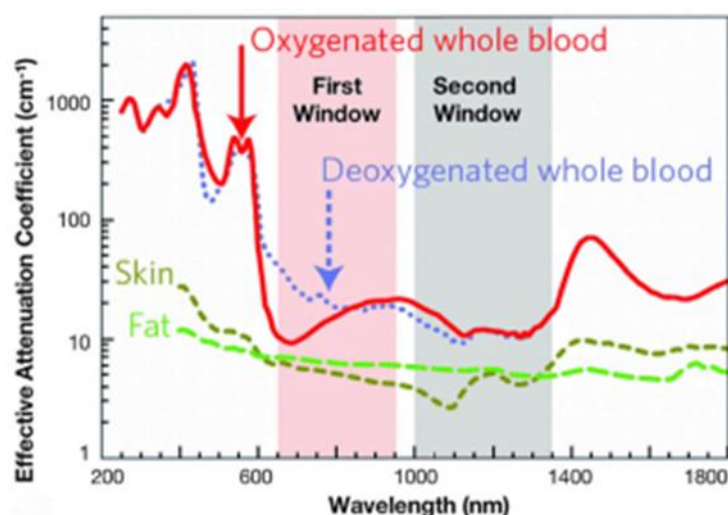


Figure V-1 NIR-I and NIR-II optical transparency windows in some biological tissues and fluids.⁹

Cytotoxic studies have shown that Ag₂S has no toxicity in terms of cell proliferation, apoptosis, necrosis, and genetic damage as has been a good candidate for the development of NPs in biological applications. In a toxicological study, it was reported that MPEG-SH (thiol-terminated methyl polyethylene glycol) capped Ag₂S NPs showed no cytotoxic and genotoxic effects on cells exposed during 24h to NPs concentrations of 0.01, 0.1, 1, 10 and 50 μ g/ml.¹⁰ No cellular death was observed for the majority of concentrations, except for 50 μ g/ml with $13.4 \pm 1.7\%$ with respect to control (in comparison CdS NPs showed 100% cytotoxicity at this concentration). These characteristics suggest a great potential for the use of Ag₂S NPs for biomedical applications. Indeed, it has been shown that Ag₂S NPs have a great potential for in vivo imaging, disease detection and cancer diagnosis. Studies on Ag₂S in NIR spectrometry have been carried out to use them for molecular imaging of living cells. The results of this research have shown that Ag₂S are attractive for medical studies with high efficiency and biocompatibility.¹¹ A few example of these NPs used for bioimaging, drug delivery or biosensors have been reported. For example, a study showed pegylated Ag₂S NPs synthesis

exhibiting high stability. They acted as fluorescent emitting in the NIR-II (1200 nm). It enabled *in vivo* monitoring of lymphatic drainage and vascular networks with deep tissue penetration and high spatial and temporal resolution. It also allowed *in vivo* tracking of angiogenesis mediated by a tiny tumor. Results showed that they could be useful in surgical treatments such as sentinel lymph node (SLN) dissection as well as in evaluating blood supply in tissues and organs and screening of anti-angiogenic drugs.¹² Ag₂S NPs exhibit very interesting properties that make them good candidates in biomedical applications. Researchers are still trying to improve their development due to the challenges associated with biological media.

V.A.2. Ag₂S crystalline structure

If we look at the Ag-S phase diagram, Ag₂S can have different crystalline forms depending on the temperature: it has three stable forms between room temperature and its melting point. These results were confirmed by measurements of the thermal expansion and heat capacity of Ag₂S, combined with high-temperature XRD. Results have shown that reversible phase transformations take place during heating and cooling of Ag₂S. The crystal structures are monoclinic α -Ag₂S (acanthite), cubic β -Ag₂S (argentite) and cubic γ -Ag₂S (Figure V-2).¹³ Taking into account the temperature in our reaction conditions, the formation of α -Ag₂S or acanthite nanoparticles is expected. Ag₂S is formed at an average of 33.33 atomic % sulfur.¹⁴ This phase accepts a wide range of silver or sulfur sub-stoichiometry.

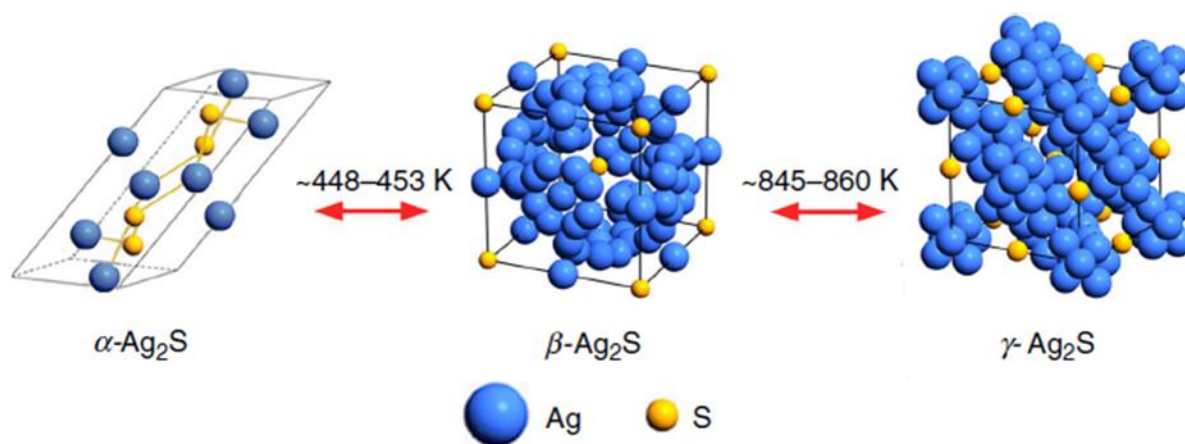


Figure V-2 Change in silver sulfide crystal structure during reversible phase transformations.¹³

Ag₂S nanocrystals are semiconductor crystals that are often called Ag₂S quantum dots (QD). A semiconductor crystal which has a radius (r) that is inferior to its excitonic Bohr radius (r_B) is called quantum dot. By modifying the size of the QDs, it is possible to modulate the width of the gap and therefore the energy of the photoluminescence emission peak. The smaller the nanoparticles, the greater the photoluminescence emission energy (therefore the weaker the wavelength of the associated emission peak).¹⁵ It was reported that the Bohr radius at room temperature (300K) is 2.2 nm for Ag₂S QDs.¹⁶ The size-dependent optical properties of Ag₂S QDs were restricted in the range of 2.4 to 4.4 nm. The energy of the photoluminescence emission peak increases (shift towards low wavelengths) when the size of the nanoparticles decreases. The Ag₂S QDs optical properties depend on particle size and on the surface state. It

is important to find synthesis methods that will allow stabilization of different sizes of nanoparticles in order to modulate the emission wavelength. Furthermore, the optical properties can be strongly influenced by surface effects, especially by the nature of the stabilizing ligands. It is therefore interesting to test new ligands such as NHCs.

V.A.3. Ag₂S synthesis pathway. State of the art.

Ag₂S NPs have been synthesized by various methods, such as sol–gel method, conventional heating method, microwave method, hydrothermal method, etc. Every method has both advantages and disadvantages, so we aim at choosing the best procedure for our NPs.

Two pathways can be distinguished: organic and aqueous synthesis pathway.

Organic synthesis pathway is mostly done by conventional heating and gives more monodisperse nanoparticles. Du *et.al* reported in 2010 the synthesis of monodisperse Ag₂S NIR emitting NPs from a single source precursor: Ag(DDTC), Silver diethyldithiocarbamate. Ag(DDTC) hydrate, oleic acid, octadecylamine and octadecene (ODE) were heated to 100 °C to remove water and oxygen, thus forming a homogeneous brown solution. Then, the resulting mixture was heated to 200 °C under N₂ atmosphere for 30 min, affording a dark colloidal solution. Nanoparticles are formed with a size of approximatively 10 nm and presented NIR emission at 1058 nm under 785 nm excitation.¹⁷ Later, Zhang *et al.* also reported a monodisperse Ag₂S NPs synthesis from Ag(DDTC) and dodecanethiol (DT).¹⁶ They were able to obtain emission-tunable NIR Ag₂S NPs by varying reaction temperature and reaction time. For example, for 30 min at 200°C (similar reaction conditions as Du *et al.*), they obtained NPs of 4.4 nm with photoluminescence (PL) emission at 1175 nm when excited at 785 nm. For 2 min at 140°C, they obtained NPs of 2.8 nm with PL emission at 1052 nm when excited at 785 nm. Size-dependent optical properties of Ag₂S NPs were observed in the range from 2.4 to 4.4 nm. But no size-dependence of the optical property was observed when the size of Ag₂S NPs was larger than 4.4 nm. They concluded that it is mostly due to strong quantum confinement effects at smaller sizes. Other reaction conditions were explored to broaden the PL emission range of Ag₂S NPs by Jiang *et.al*. They reported the synthesis of emission-tunable NIR Ag₂S NPs with sizes ranging from around 1.5 to 4.6 nm. This domain of size is smaller than the Bohr radius, thus there is an effect on the width of the gap and a strong effect on the energy of the photoluminescence emission. A seed-assisted synthesis method in two-step was performed to prepare different-sized Ag₂S NPs. Seed of 1.5 nm in size were synthesized by injecting hexamethyldisilathiane ((TMS)₂S) into a mixture of silver acetate, myristic acid, 1-octylamine (OA), and 1-octadecene at a given temperature under argon atmosphere. Ag₂S NPs were synthesized in a second step by dropwise addition of Ag(OA) solution (AgNO₃ and OA in toluene) and sulfur solution (sulfur powder in toluene) into a toluene solution containing the previously synthesized Ag₂S seeds. The NPs photoluminescence did cover a range from 690 to 1227 nm depending on the hot-injection temperature and growth time. The emissions shifted to higher wavelength by increasing the growth time (larger NPs size): For an injection temperature of 50 °C and growth time of 3 seconds the PL emission peak was at 690 nm. For an injection

temperature of 50 °C and growth time of 30 min the PL emission peak was at 730 nm.¹⁸ The Ag₂S nanoparticles synthesis method in organic solvents by thermal degradation is an approach of choice due to the ability to easily solubilize the reactants, to tune the NPs size thus the PL activity by making effortless changes (temperature, silver precursor, reaction time, etc), to obtain monodisperse NPs. However, some of the difficulties are that the reactions are very sensitive to air due to low stability of the silver precursors when exposed to O₂. The transfer of the Ag₂S NPs from organic solvents to biocompatible solvents for potential applications is also a critical step. To overcome this last issue, synthesis in organic biocompatible solvents and in aqueous solvents have been developed. Jiang *et al.* synthesized in 2012 Ag₂S NPs using AgNO₃ and 3-mercaptopropionic acid (MPA) dispersed in ethylene glycol and heated 110°C then 145°C. They obtained NPs with size ranging from 1.5 nm to 6.3 nm and with photoluminescence emissions tuned in the range from 510 to 1221 nm, respectively, by modulating the AgNO₃/MPA ratio and the growth time. Ag₂SNPs emitting in the second infrared window were obtained for particular reaction conditions corresponding to: 5mM of AgNO₃ at 145 ° C for 60 min.¹⁹ Nevertheless, a few drawbacks appeared when it comes to synthesis in ethylene glycol. Indeed, synthesis in ethylene glycol usually requires high reaction temperatures compared to another biocompatible and green solvent like water.

For the synthesis in aqueous solvents, Brelle *et al.* prepared Ag₂S NPs capped with cysteine or glutathione for the first time in water. Cysteine and glutathione are thiol containing biomolecules that form high-affinity silver-ligand complexes. These metal-biomolecule complexes can then serve as excellent matrixes during the process of silver sulfide nucleation. Indeed, these biomolecules have the ability to compete for metal binding sites and thus restrict the incorporation of inorganic sulfide during nucleation. In a two-step procedure silver acetate was added to a solution containing dissolved glutathione or cysteine to form the corresponding Ag-cysteine or Ag-glutathione complexes. Then, a solution of Na₂S was injected in the solutions of Ag-cysteine or Ag-glutathione at pH 10.5. The team was able to synthesize nanoparticles of approximatively 9 nm.²⁰ However, no emission was detected at room temperature for any of the samples. Later, Acar *et.al* reported the synthesis of Ag₂S NPs by conventional heating. They carried out the synthesis using 2-mercaptopropionic acid (2-MPA) as surfactant. The NPs size and the emission wavelength of these NPs could be tuned by varying the Ag/S and 2-MPA/Ag ratios, the reaction temperature and the reaction time. They obtained NPs with varying size from 2.3 to 3.1 nm (small size variation) and emission varying from 780 to 950 nm.²¹ By heating at relatively low temperatures (30, 60 and 90°C) in water and using 2-MPA as a surfactant they were able to obtain highly luminescent NIR-emitting Ag₂S NPs even though the PL emission is lower than those obtained when synthesis are carried out in organic solvents. Conventional heating was proven to be an efficient method for the synthesis of NIR-II emitting Ag₂S NPs in both organic and aqueous solvents. This method is quite easy to implement however, temperature regulation can be difficult, especially when precise temperature ramp must be achieved to control the size of the nanoparticles. Also, reaction's time are usually prolonged when heating by conventional heating.

Another method better at temperature controlling method was explored for the synthesis of aqueous Ag₂S NPs: microwave synthesis. One of the examples is the synthesis of Ag₂S NPs from AgNO₃ and D-penicillamine (DPA) in water through a microwave assisted method reported by Wang *et al.* Ag₂S NCs with tunable PL emission from visible region to NIR region were produced with highest wavelength at 802 nm for 2.33 ± 0.85 nm NPs. A shift toward

Synthesis of n-heterocyclic carbene stabilized silver sulfide nanoparticles

higher wavelength of the PL emission was observed with size increase of the particles however no emission in the NIR-II window was achieved.²² Compared with the conventional heating method, microwave irradiation method has a rapid temperature elevation and homogeneous heating ability. Moreover, the reactions times are usually very low (3 min in the previous example).

To summarize, conventional heating in organic solvents is a method that showed great results in Ag₂S NPs synthesis with high monodispersity and high photoluminescence activity. However, this method requires high temperatures and transfer in biocompatible solvents for some applications. Another method is microwave heating in aqueous solvents. This method allows homogeneous and fast heating at lower temperatures. However, emission in the second window of the NIR seems harder to reach with this method. Interestingly, there is no evident correlation between NPs size and emission wavelength showing the importance of diversifying the synthesis methods of Ag₂S NPs for a better control of their optical properties.

To conclude, our main goal is to synthesize stable monodisperse Ag₂S NPs stabilized by our ligands of interest: NHCs. The literature on synthesis of NHC capped Ag₂S NPs is quite recent and poor. Brutchey *et al.*, reported Ag₂S synthesis performed by conventional heating.^{23,24,25} These studies showed that NHC ligands are strongly bounded to the NPs, which provides excellent colloidal stability and prevents room-temperature ligand exchange reactions with traditional long-chain oleylamine or oleic acid ligands. We did explore conventional heating and microwave irradiation synthesis methods of NHC capped Ag₂S NPs.

V.B. Synthesis of Ag₂S NPs by conventional heating

One of the pathways to obtain NHC capped Ag₂S NPs is conventional heating in organic solvents. A study of the literature highlighted synthesis using dodecanethiol as a solvent, sulfur precursor and silver acetate as a silver source.²⁶ Also, one of our co-worker Lise Abiven,²⁷ developed and optimized Ag₂S NPs synthesis from silver diethyldithiocarbamate (AgDDT) in octadecene by conventional heating. From these results, we attempted a NHC capped Ag₂S NPs synthesis in dodecanethiol.

First, a silver complex was synthesized using a solution of sodium diethyldithiocarbamate (0.15 mmol, 1 equiv.) in 100 ml of water mixed with a solution of AgNO₃ (0.15 mmol, 1 equiv.) in 100 ml of water at room temperature giving as a resulting product silver diethyldithiocarbamate (AgDDT). Imidazolium salt C12-Br (40 equiv., 4mmol) was dissolved in dodecanethiol (10 mL) with NaH under stirring and N₂. Then, AgDDT (0.1 mmol) was added to the reaction mixture. The reagents were left under stirring until complete dissolution then the temperature was increased up to 160°C gradually. A black suspension was obtained. TEM observation unveiled NPs of 4.2 (± 0.3) nm (Figure V-3).

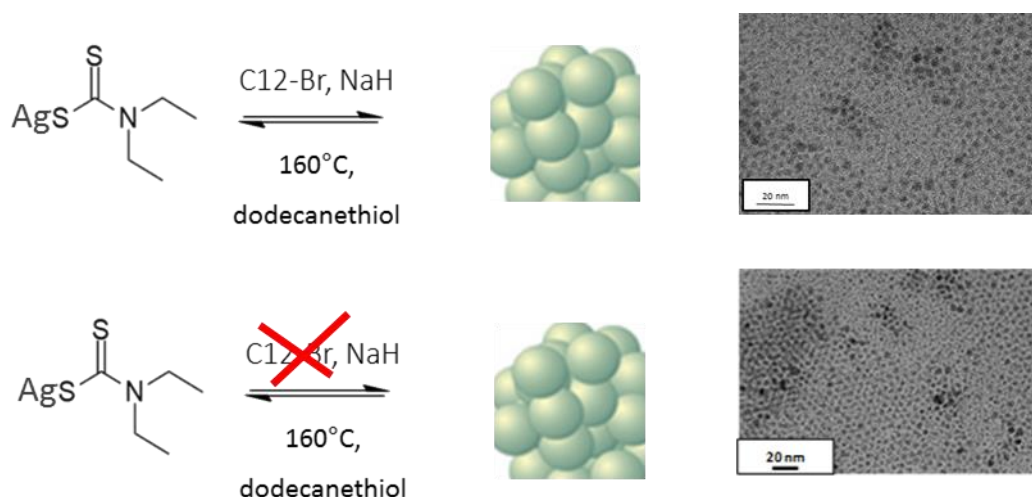


Figure V-3 Synthesis of Ag₂S NPs in dodecanethiol by conventional heating with and without C12-Br NHC capping ligand. TEM images of as obtained NPs.

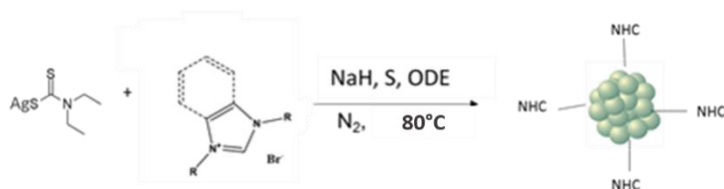
However, NPs were also synthesized when the synthesis was performed without the imidazolium salt. The reaction without imidazolium salt produced a black suspension and TEM observation showed that NPs of 3.6 (± 0.2) nm were obtained (Figure V-3). Indeed, dodecanethiol does not only act as a solvent or sulfur source but also as ligand in these reaction conditions. Going back to the literature, syntheses of Ag₂S NPs in dodecanethiol without other source of ligand have been reported.²⁸ To see if the NHC ligand C12-Br had an influence on the nature of the stabilization of the NPs, other characterization technics need to be used.

In order to avoid the influence of the reaction solvent on the synthesis, octadecene (ODE), which does not react as a ligand, was used. In this next synthesis, AgDDT (0.1 mmol) was added in a solution of C12-Br (40 equiv.) and NaH (60 equiv.) in ODE (10 mL) under N₂. The suspensions were heated up to 160 °C. It gradually colored to black. However, no further

Synthesis of n-heterocyclic carbene stabilized silver sulfide nanoparticles

characterization of these suspensions was pursued because a few drawbacks did appear. First, solubilization of the imidazolium salt in ODE was very difficult. We obtained a non-homogeneous black paste. Also, the particles did not redisperse in organic solvents (toluene, DCM, THF) after washing with ethanol or acetone.

With the intention of obtaining stable Ag₂S NPs, the synthesis method was modified. Increasing of the reaction temperature to 200°C was done, but a gray aggregated paste was obtained. Then, the quantity of imidazolium salt was decreased to 10 equiv. It allowed better solubilization of the imidazolium salt in octadecene. The resulting product was black and less pasty than for the synthesis with 40 equiv. of imidazolium salt. However, after washing the NPs did completely aggregate. Then, another approach was developed. Indeed, after study of the literature, it was reported that some Ag₂S NPs syntheses occurred at much lower temperature and with addition of an external sulfur source (other than the sulfur in the silver complex).²⁴ Thus, we decided to add an additional sulfur source and decrease the temperature. AgDDT silver complex (0.1 mmol) was mixed with an imidazolium salt (10 equiv.) and NaH in ODE (10 mL). The suspensions were put under stirring and N₂ at 80°C for 1 hour. Then, sulfur powder was added. The reaction media were left in the same conditions for 2 hours (Scheme V-1). It gave dark brown suspensions. The suspensions were washed with ethanol, then redispersed in toluene for analysis.



Scheme V-1 Synthesis of NHC capped Ag₂S NPs in ODE with S (sulfur powder).

For this synthesis two type of imidazolium salts were used: C12-Br (1,3-didodecylimidazoliumbromide) and Benzyl-Br (1,3-dibenzylimidazoliumbromide). TEM observation showed that NPs with ligand dependent sizes were obtained. Synthesis using benzyl-Br imidazolium salt gave small NPs of 2.4 (± 0.7) nm and the one using C12-Br imidazolium salt gave NPs of size 5.5 (± 1.1) nm (Figure V-4). The expectations were that ligand C12-Br with its long alkyl chain would give smaller NPs. Indeed, it was reported that Ag₂S nanoparticles size obtained from synthesis with different alkyl chain lengths in the coating decrease with the increase of the chain lengths.²⁹ We made the hypothesis that it probably depends on the C12 chains conformation on the surface compared to the benzyl rings on benzyl-Br.

Synthesis of n-heterocyclic carbene stabilized silver sulfide nanoparticles

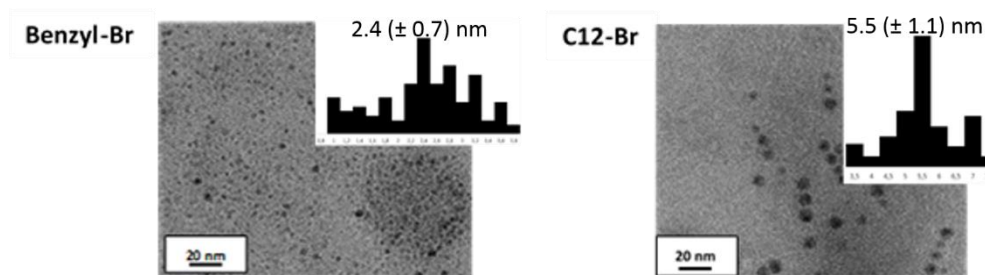


Figure V-4 TEM images of NHC (benzyl-Br and C12-Br) capped Ag₂S NPs synthesized in ODE.

After synthesis and washing with ethanol or acetone, we observed stability problems. Indeed, the suspensions aggregated only 2 hours after purification. No further characterization was pursued on these samples due to their very low stability. It may be due to the decrease of the stabilizing agent quantity (10 equiv. of imidazolium salt vs 40 equiv. of ligand in the literature). However, increasing of the imidazolium salt quantity leads to solubility issues.

The synthesis pathway by conventional heating still needs to be improved so that further characterization can be done on the NPs. The reflections are going toward doing the synthesis in mixed organic solvents such as ODC (octadecene)/DCM (dichloromethane) or in organic solvents that do not evaporate at higher temperature such as DMSO. Changing the synthesis solvents could improve the solubility of the imidazolium salts and NaH. It could also give us more stable Ag₂S NPs. As of today, we were not able to resolve the problem of the NPs stability after purification. Moreover, stabilization of the temperature by conventional heating at low temperature (80°C) was difficult. Indeed, for conventional heating method, the thermal energy is brought by heat convection through an oil bath or a heating mantle. The temperature rise ramps are slow and poorly controlled, probably due to heat transfer limitations.

V.C. Synthesis of Ag₂S NPs by using imidazolium salt: imid-PEG₄

In parallel, our team developed a microwave assisted synthesis of water soluble NHC capped Ag₂S NPs. The main goal was to synthesize stable water soluble Ag₂S NPs that could emit in the NIR-II window of interest. Thus, in the following, the imidazolium salt imid-PEG₄ is used as NHC precursor.

All the microwave assisted synthesis are performed in microwave Anton Paar Monowave 300. Indeed, microwave displays a fast and homogeneous heating leading to unique step of particle nucleation for a narrow size distribution.

V.C.1. Choice of the heating method and of the ligand.

V.C.1.a. Microwave-assisted heating

Microwave-assisted syntheses were chosen for the continuation of our studies. Indeed, this method has advantages compared to conventional heating synthesis method. The microwave synthesis method allows a better control of the temperature. The microwave energy is directly transmitted to the molecules and the ions contained in the reaction medium allowing “in core” heating. It allows a uniform temperature rise compared to conventional heating. Microwaves can lead to much higher heating rates than those which are achieved through conventional heating. A high temperature can be applied on a very short time.³⁰ This reducing of the synthesis time can help in avoiding ligand thus nanoparticles degradation exposed to high temperatures. Also, it allows a homogeneous nucleation of the NPs in the reactor through homogeneous heating. However, microwave-assisted synthesis has also drawbacks. It was reported that one of the limitations of microwave is the restricted penetration depth of irradiation into the molecules and ions in the reaction media. This means that reagents in the center of large reaction vessel are heated by convection and not by direct “in core” dielectric heating. Thus, the size of the reactor is limited if homogeneous heating is to be achieved.³¹ The microwave our team used is an Anton Paar Monowave 300. This microwave can contain only 1 reactor at a time and has a total volume ability of 16 mL. It can heat up to 300°C with a pressure up to 30 bars. Most of our syntheses were performed at 100°C for 5 minutes (microwave power of 300 W). The temperature rises to 100°C in a few seconds then a temperature plateau is maintained for 5 min. Then, there is cooling of the reactor through pressurized air. The only parameters that were modified on the microwave setting during this thesis are the temperature and the reaction's time.

V.C.1.b. Choice of the ligand

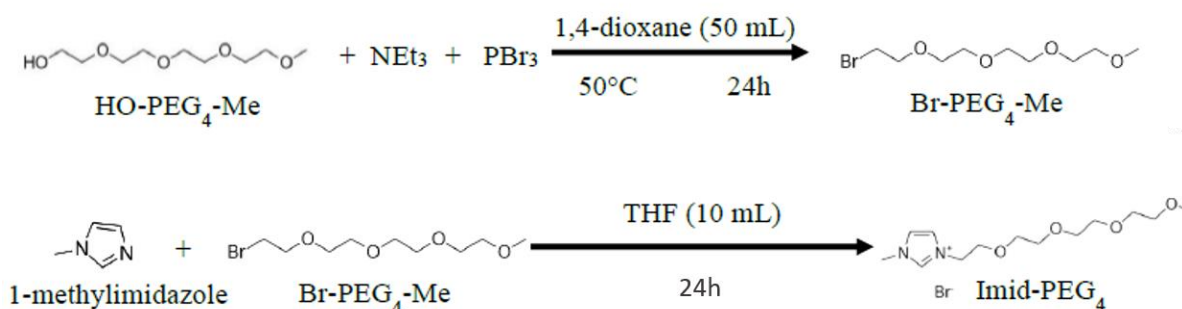
The ligand allows the control of the growth of the nanoparticles and their colloidal stability in suspension.³² Ishisone *et al.* reported the synthesis of Ag₂S NPs capped with two types of azobenzene-derivatized alkanethiol differing in chain length (called 2AM10SH and 8AM5SH). They successfully controlled the reversible aggregation–dispersion behavior for Ag₂S NPs of 8.1 nm capped with ligand 2AM10SH but could not with 8AM5SH capped Ag₂S

Synthesis of n-heterocyclic carbene stabilized silver sulfide nanoparticles

NPs of 8.1 nm. Indeed, the later were extremely stable regardless of the ligand conformation. It shows that the length of the spatial structure of the ligand (in this article chain length or cis/trans conformation) does influence the NPs stability. Other parameters have an influence, such as the affinity of the ligand with the Ag^+ cation or the ligand concentration. It has a direct influence on the reaction kinetics and the morphology and optical properties of Ag_2S NPs.³³

Our work being based on the use of NHC ligands to control the growth and colloidal stability of the synthesized nanoparticles, we tried to find a suitable imidazolium salt (as NHC precursor) to synthesize. Actually, it was reported that NHC– Ag_2S nanocrystals displayed a very high colloidal stability.²⁴ Since, our first goal was to develop a synthesis in aqueous media, it goes without saying that we synthesized a water soluble imidazolium salt. Moreover, thinking about future applications, the incorporation of a polyethylene glycol (PEG) chain in the imidazolium salt seems interesting. Indeed, it was reported that PEG ligand can allow longer circulation time of the nanoparticles in the bloodstream, which increases the probability of the nanoparticles to reach their biological target.³⁴ Moreover, since it seems like the ligand steric hindrance can improve the monodispersity and the optical properties of the nanoparticles produced,³³ we hoped that the PEG chain on the NHC could help in this direction. With these criteria, the imidazolium salt, that we will call imidPEG₄ in the following parts, was synthesized.

First, poly(ethylene glycol) methyl ether bromide (1 equiv.) is synthesized then it is mixed with 1-Methylimidazole (20 mmol) in 10 mL THF under N_2 . The mixture is left under stirring overnight. A yellow oil is obtained and the remaining solvent is evaporated under vacuum. Then, the product is washed with ether. The imidPEG₄ imidazolium salt is obtained with a 100% yield (Scheme V-2).



Scheme V-2 Synthesis of PEGylated imidazolium salt ImidPEG₄.

This imidazolium salt is stable when stored at room temperature under air. The use of an efficient stabilizing ligand is mandatory in our reaction conditions. Without ligand source (only silver precursor and sulfur), precipitation will probably happen. This phenomenon will be addressed later.

V.C.2. Microwave assisted synthesis pathway

The synthesis is inspired by previous synthesis done in our laboratory by Lise Abiven.²⁷ She synthesized 11-Mercaptoundecanoic acid (11-MUA) capped Ag_2S NPs by microwave. This

Synthesis of n-heterocyclic carbene stabilized silver sulfide nanoparticles

synthesis was reproduced mixing a solution of AgNO_3 (5 mM, $25 \cdot 10^{-5}$ mol, 42.5 mg, 1 equiv.) in water and a solution of 11-MUA (5 equiv., 16.2 mg) in water. Then, a solution of $\text{Na}_2\text{S} \cdot 9\text{H}_2\text{O}$ (0.5 equiv., 30 mg) in water is added just before heating. The suspensions were still colorless at this stage. The crystallization of Ag_2S was carried out in microwave at 100°C for 5 min. The following optimized reaction conditions were chosen here: $\text{Ag}/\text{S} = 2$ and $11\text{-MUA}/\text{Ag} = 5$. Black suspensions were obtained after microwave heating and purified by centrifugation in ethanol. TEM observation showed that Ag_2S spherical NPs with a mean size of $6.3(\pm 1.6)$ nm were obtained (Figure V-5).

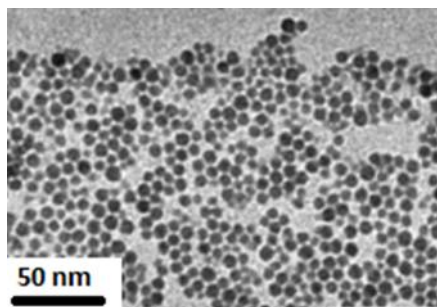


Figure V-5 TEM image of 11-MUA capped Ag_2S nanoparticles synthesized by microwave.²⁶

After successfully synthesizing these NPs, this synthesis was reproduced by replacing 11-MUA with a water-soluble imidazolium salt (imid-PEG₄ as NHC precursor) in the presence of a base.

V.C.2.a. Effect of the reaction solvent on stability and morphology

The syntheses were carried out in various solvents with different results. The first synthesis test was carried out in water. Water as a solvent facilitates waste management aiming at developing greener synthesis for better environment safety.

First, a solution of imid-PEG₄ and NaH in water was mixed with a solution of AgNO_3 in water. Then, a solution of $\text{Na}_2\text{S} \cdot 9\text{H}_2\text{O}$ in water was added just before heating in microwave. The synthesis was carried out in microwave at 100°C for 5 min. Various Ag/S and ligand/ Ag ratio were tested (table V-1). In all these conditions, no NPs were observed and only a metallic silver aggregate is observed in the bottom of the reactor. The synthesis was carried out without ligand and it gave the same results (Table V-1, sample Ag_2S -5). This shows that rather than deprotonating the imid-PEG₄, NaH probably reacts preferentially with water to produce sodium hydroxide.

Synthesis of n-heterocyclic carbene stabilized silver sulfide nanoparticles

Table V-1 Synthesis of Ag₂S NPs in water by using ImidPEG₄ and Na₂S.9H₂O.

| sample | solvent | [Ag] mM | Ag/S | Ligand/Ag | T (°C) | t (min) | results |
|---------------------|---------|------------|------|-----------|--------|---------|-------------|
| Ag ₂ S-1 | water | 5 | 1 | 5 | 100°C | 5 | aggregation |
| Ag ₂ S-2 | water | 5 | 1 | 25 | 100°C | 5 | aggregation |
| Ag ₂ S-3 | water | 5 | 2 | 5 | 100°C | 5 | aggregation |
| Ag ₂ S-4 | water | 5 | 2 | 25 | 100°C | 5 | aggregation |
| Ag ₂ S-5 | water | 5 | 2 | 0 | 100°C | 5 | aggregation |

We precise the synthesis protocol for sample Ag₂S-2. 593.5 mg of ImidPEG₄ (25 equiv.) were dissolved in 10 ml of water, then NaH (80.6 mg, 2equiv. / ImidPEG₄) was dissolved in 4 mL water and added to the ImidPEG₄ solution. The resulting suspension was left under stirring for 5 minutes approximatively. Then, 11.4 mg of AgNO₃ (67.10⁻⁶ mol), dissolved in 1 ml of water, were added. The solution was stirred for 10 minutes, protected from light. After, 16 mg of Na₂S.9H₂O (1 equiv.), dissolved in 4 mL of water, were added to the solution. Immediately afterwards, the reaction medium was transferred into a monomodal microwave cavity and heated to 100° C (300 W) for 5 min, with magnetic stirring. After microwave heating, all the particles were aggregated at the bottom of the reactor. The reaction medium was dialyzed with dialysis cassette, the molecular weight threshold of which is 10 kDa. This cassette was immersed in deionized water for 24 h to eliminate unreacted molecules and ions. For sample Ag₂S-2, washing did not change anything to the aggregated state of the sample.

Thus, when the reaction is done in water, it proceeds as if there was no stabilizing ligand in the suspensions and everything does precipitate. It is certainly due to the formation of NaOH from NaH in water. It prevents NaH to react as a base for the imidazolium salt. To overcome this problem other synthesis solvents were tested.

First, synthesis in ethylene glycol (EG) that is a good organic biocompatible solvent was performed. Same protocol as for the synthesis in water was applied (Table V-2). Although Ag₂S syntheses in EG are usually performed a higher temperature we tried to see if it could work in our chosen heating settings.

Table V-2 Synthesis of Ag₂S NPs in ethylene glycol by using ImidPEG₄ and Na₂S.9H₂O.

| sample | solvent | [Ag] mM | Ag/S | Ligand/Ag | T (°C) | t (min) | results |
|---------------------|---------|------------|------|-----------|--------|---------|-------------|
| Ag ₂ S-6 | EG | 5 | 1 | 5 | 100°C | 5 | aggregation |
| Ag ₂ S-7 | EG | 5 | 1 | 25 | 100°C | 5 | aggregation |
| Ag ₂ S-8 | EG | 5 | 2 | 5 | 100°C | 5 | aggregation |
| Ag ₂ S-9 | EG | 5 | 2 | 25 | 100°C | 5 | aggregation |

A slight coloration of the suspensions after microwave was observed but it did not last. Indeed, after 30 min all the particles were aggregated. Washing by dialysis did not allow redispersion of the aggregate.

Synthesis of n-heterocyclic carbene stabilized silver sulfide nanoparticles

Other synthesis temperatures were tested (115°C, 125°C) to get closer to what is done in the literature for Ag₂S NPs synthesis. Unfortunately, it gave similar results with aggregation of the particles. The use of NaH in protic solvents to perform this synthesis was disregarded. It was decided to use polar aprotic solvents instead. Our choice went to dimethylsulfoxide (DMSO). Indeed, not only DMSO is a polar aprotic solvent but also all of the reagents are soluble in this solvent. Also, literature indicates that NaH deprotonation of imidazolium to obtain NHC is possible in DMSO (pK_a \approx 20-23).³⁵

A solution of imid-PEG₄ and NaH in DMSO was mixed with a solution of AgNO₃ in 10 ml of the same solvent. Then, a solution of Na₂S.9H₂O in DMSO was added just before heating in microwave (Table V-3).

Table V-3 Synthesis of Ag₂S NPs in DMSO by using ImidPEG₄ and Na₂S.9H₂O.

| sample | solvent | [Ag] mM | Ag/S | Ligand/Ag | T (°C) | t (min) | results |
|----------------------|---------|------------|------|-----------|--------|---------|------------------------|
| Ag ₂ S-10 | DMSO | 5 | 1 | 5 | 100°C | 5 | Black/brown suspension |
| Ag ₂ S-11 | DMSO | 5 | 1 | 25 | 100°C | 5 | Black/brown suspension |
| Ag ₂ S-12 | DMSO | 5 | 2 | 5 | 100°C | 5 | Black/brown suspension |
| Ag ₂ S-13 | DMSO | 5 | 2 | 25 | 100°C | 5 | Black/brown suspension |

The syntheses were carried out in microwave at 100°C for 5 min. Ag/S ratio of 1 and 2 were tested. Ligand/Ag ratios of 5 and 25 were also tested (Table V-3). The solvent solubilized well all the reagents and a dark brown (almost black) suspension was obtained after microwave.

We precise the synthesis protocol for sample Ag₂S-11. 593.5 mg of ImidPEG₄ (25 equiv.) were dissolved in 10 ml of DMSO, then NaH (80.6 mg, 2 equiv. / ImidPEG₄) was dissolved in 4mL DMSO and added to the ImidPEG₄ solution. The resulting suspension was left under stirring for 5 minutes approximatively. Then, 11.4 mg of AgNO₃, dissolved in 1 ml of DMSO, were added. The solution was stirred for 10 minutes, protected from light. After, 16 mg of Na₂S.9H₂O, dissolved in 4 mL of DMSO, were added to the solution. Immediately afterwards, the reaction medium was transferred into a monomodal microwave cavity and heated to 100°C (300 W) for 5 min, with magnetic stirring. After microwave heating, the suspension was dialyzed with dialysis cassette, the molecular weight threshold of which is 10 kDa. This cassette was immersed in deionized water for 24 h to eliminate unreacted molecules and ions. A black/dark brown stable suspension was obtained.

TEM observations showed that 6.0 (\pm 2.2) nm NPs were obtained for sample Ag₂S-10 and 5.9 (\pm 1.5) nm NPs for sample Ag₂S-11 (Figure V-6). The samples were polydisperse and it seems like there are two populations with different sizes. There was no drastic effect on the NPs size when increasing the quantity of ligand which was very surprising. Thus, we decided to keep the Ligand/Ag ratio to 5 as optimized Ligand/Ag ratio in DMSO.

Synthesis of n-heterocyclic carbene stabilized silver sulfide nanoparticles

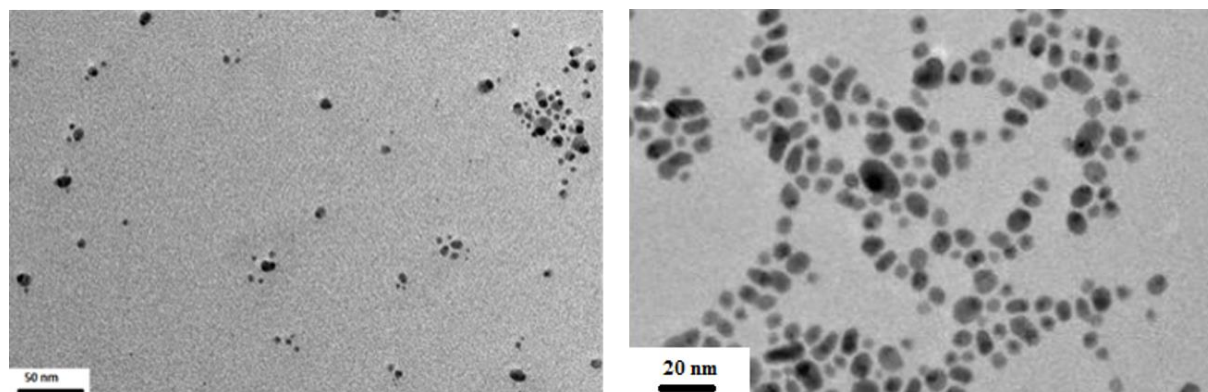


Figure V-6 TEM images of NPs synthesized from AgNO_3 , imid-PEG₄, NaH and $\text{Na}_2\text{S} \cdot 9\text{H}_2\text{O}$ in DMSO after microwave heating at 100°C for samples Ag₂S-10 (left) and Ag₂S-11 (right).

Table V-4 Synthesis of Ag₂S NPs in DMSO without ImidPEG₄ or Na₂S · 9H₂O.

| sample | solvent | [Ag] mM | Ag/S | Ligand/Ag | T (°C) | t (min) | results |
|----------------------|---------|------------|-------|-----------|--------|---------|------------------------|
| Ag ₂ S-14 | DMSO | 5 | 1 | 0 | 100°C | 5 | aggregate |
| Ag ₂ S-15 | DMSO | 5 | S = 0 | 5 | 100°C | 5 | Black/brown suspension |

The synthesis in the same reaction conditions was performed but without the imid-PEG₄ (Table V-4, sample Ag₂S-14). This experiment was done as a first proof of the stabilizing effect of the NHC ligand in DMSO. The reaction produced aggregated suspensions, which proves the stabilizing effect of the NHC. Also, the experiment was carried out without the sulfur source Na₂S · 9H₂O (Table V-4, sample Ag₂S-15). In this case, we obtained stable brown suspensions. Also, TEM images confirmed the formation of NPs with a mean size of 6.4 (±2.9) nm (Figure V-7). The obtention of nanoparticles without the sulfur source in the reaction media, means that Ag₂S NPs were not formed but another type of particles (probably silver NPs). We will later discuss why we think that in our previous synthesis (Figure V-6), we could have synthesized both NHC-PEG₄-Ag NPs and NHC-PEG₄-Ag₂S NPs.

Synthesis of n-heterocyclic carbene stabilized silver sulfide nanoparticles

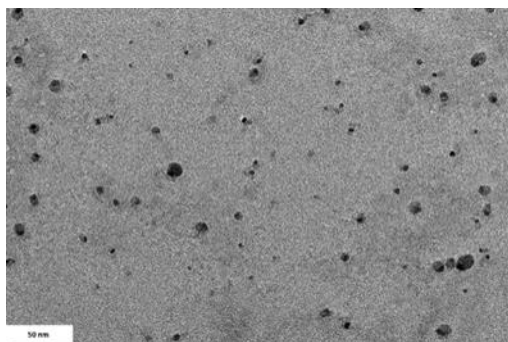


Figure V-7 TEM images of NPs synthesized from AgNO_3 , imid-PEG₄ and NaH in DMSO after microwave heating at 100°C (Ag₂S-15).

Synthesis in DMSO showed that stable NPs suspensions were obtained in these reactions conditions. However, another solvent was tested as synthesis solvent. The main goal was to compare the results with the synthesis in DMSO. Also, an article reported explosion hazards of NaH in DMSO.³⁶ The organic solvent dichloromethane (DCM) was chosen due to high solubility of the reagents in it. In order to get rid of unwanted interactions as much as possible, anhydrous DCM was also used. This is important since the presence of water in the solvents could lead to formation of aggregates in the suspensions. A solution of imid-PEG₄ and NaH in DCM was mixed with a solution of AgNO_3 in DCM. Then, a solution of $\text{Na}_2\text{S} \cdot 9\text{H}_2\text{O}$ in DCM was added just before heating in microwave. The syntheses were carried out in microwave at 100°C for 5 min. The chosen ligand/Ag ratio was 5 (Table V-5).

Table V-5 Synthesis of Ag₂S NPs in DCM by using ImidPEG₄ and $\text{Na}_2\text{S} \cdot 9\text{H}_2\text{O}$.

| sample | solvent | [Ag] mM | Ag/S | Ligand/Ag | T (°C) | t (min) | results |
|----------------------|---------|------------|------|-----------|--------|---------|------------------------|
| Ag ₂ S-16 | DCM | 5 | 1 | 5 | 100°C | 5 | Black/brown suspension |
| Ag ₂ S-17 | DCM | 5 | 2 | 5 | 100°C | 5 | Black/brown suspension |

After microwave heating, brown suspensions were obtained. TEM images unveiled NPs of mean size 6 (± 0.5) nm coexisting with bigger ones of 19 (± 2.5) nm size (sample Ag₂S-16, Figure V-8). The use of DCM as a reaction solvent gave stable suspensions at room temperature for both Ag/S ratios. Also, the use of DCM seems safer than DMSO in our reaction conditions.

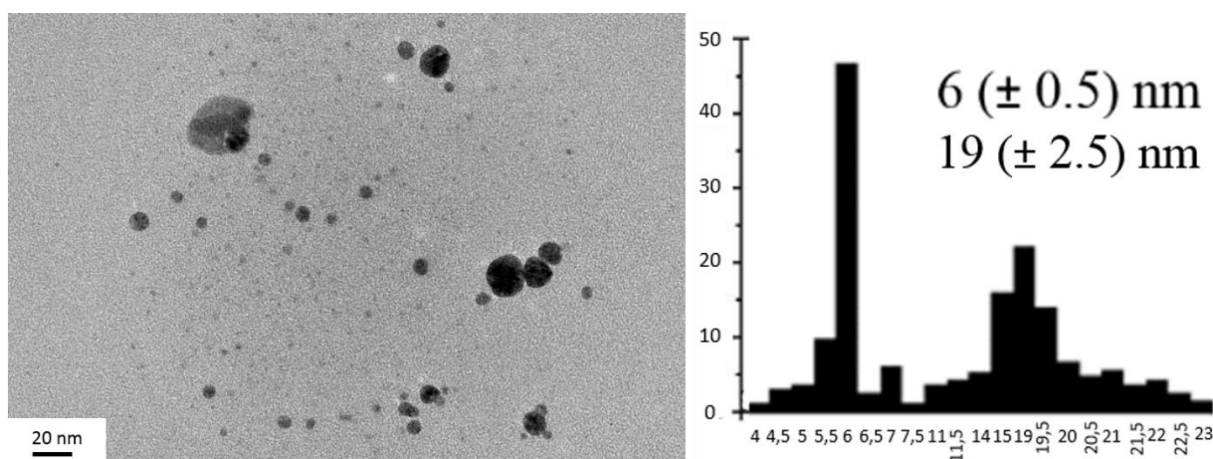


Figure V-8 TEM of NPs synthesized from AgNO_3 , imid-PEG₄, NaH and $\text{Na}_2\text{S} \cdot 9\text{H}_2\text{O}$ in DCM (sample Ag₂S-16).

To conclude on the effect of the solvent, we were able to successfully obtain stable nanoparticles suspensions synthesized in organic solvents. The synthesis in “greener” solvents such as water and ethylene glycol did not work. We realized that the conversion of imidazolium to NHC using NaH as a base is a limiting step. Indeed, the reactivity of NaH in the different solvents has resulted in choosing to do the synthesis in an organic solvent when we initially had planned to do it in water to get closer of the green chemistry principles. After screening different synthesis solvents, we tried to understand how the synthesis without sulfur source produced NPs. A first hypothesis is that Ag-NHC NPs are formed in these reaction conditions. Further characterization will be performed to assess this hypothesis.

However, it means that even when a sulfur source is added in the reaction media, both Ag-NHC NPs and Ag₂S-NHC NPs could be synthesized in these conditions. In the next part, we decided to use a different sulfur source to further study this hypothesis.

V.C.2.b. Influence of the sulfur source on synthesis

In the previous part, it was shown that the synthetic pathways of Ag₂S NPs gave surprising results. A study of the different electrochemical potentials gives a hint about the reactions that can take place (Figure V-9).

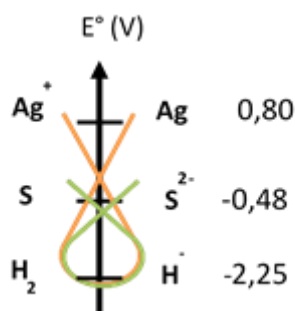


Figure V-9 Diagram of electrochemical potentials for our reagents (Ag^+/Ag , S/S^{2-} , H_2/H^-).

The formation of Ag_2S NPs usually occurs through NPs precipitation.³⁷ In our case, the ligand interacts with Ag^+ metal ions to form Ag-Ligand molecular complexes. The introduction of the anion into the reaction medium, S^{2-} , triggers the formation of molecular clusters. Through condensation of clusters, small polynuclear entities called germs are formed. It happens when the concentration of clusters exceeds a value C_{min} , greater than the molar solubility of the solid formed. This is nucleation according to LaMer's model. The more reactive the precursors, the greater the number of clusters formed in the reaction medium will be. Also, the nucleation will be triggered faster. The third stage of the model proposed by LaMer is the growth of germs. It leads to the rapid decrease of clusters concentration within the reaction medium. If the concentration of the clusters goes below the threshold C_{min} , the formation of new germs is blocked. The seeds formed during nucleation capture the clusters present in the reaction medium to form larger particles. The fourth stage is ageing. It determines the final characteristics of the particles. Indeed, the particles formed in the previous steps are in a metastable state with respect to their size, crystal structure or morphology. Solid-state reorganizations and dissolution/crystallization equilibria can occur during the aging stage.

The orange pathway (Figure V-9) shows that Ag^+ (from AgNO_3) can be reduced by H^- ions (from NaH), which would allow the formation of NHC capped metallic Ag^0 nanoparticles (Ag-NHCPEG_4) in the presence of imid- PEG_4 . Furthermore, the green pathway indicates that the consumption of excess NaH by S^0 could lead to formation of S^{2-} . These S^{2-} could then react with Ag^+ and lead to the precipitation of Ag_2S NPs. H^- ions, which were supposed to deprotonate the imidazolium salt, can also reduce the Ag^+ ions opening a second reaction pathway. Thus, this synthesis can possibly produce both Ag_2S NPs and Ag NPs. Other hypothesis in the literature show that, upon heating and in presence of a sulfur (S^0) source, Ag NPs can be transformed into Ag_2S NPs, probably by sulfur insertion into the Ag NPs structure.²⁴

The previous synthesis done with $\text{Na}_2\text{S} \cdot 9\text{H}_2\text{O}$ were reproduced but using sulfur powder S^0 to compare the results and see the influence of the sulfur source. A solution of imid- PEG_4 and NaH in ethylene glycol was mixed with a solution of AgNO_3 in the same solvent. Then, a solution of sulfur powder in ethylene glycol was added just before heating. The synthesis was carried out in microwave at 100°C for 5 min. The Ag/S ratio was 1 and Ligand/ Ag ratio was 5 (Table V-6, sample $\text{Ag}_2\text{S-18}$).

Synthesis of n-heterocyclic carbene stabilized silver sulfide nanoparticles

Table V-6 Synthesis of Ag₂S NPs in EG, DMSO, DCM by using ImidPEG₄ and sulfur powder.

| sample | solvent | [Ag] mM | Ag/S | Ligand/Ag | T (°C) | t (min) | results |
|----------------------|---------|------------|------|-----------|--------|---------|------------------------|
| Ag ₂ S-18 | EG | 5 | 1 | 5 | 100°C | 5 | aggregate |
| Ag ₂ S-19 | DMSO | 5 | 1 | 5 | 100°C | 5 | Black/brown suspension |
| Ag ₂ S-20 | DCM | 5 | 1 | 5 | 100°C | 5 | Black/brown suspension |

The coloration of the suspensions was darker than with Na₂S.9H₂O but aggregation still occurred quite rapidly (Figure V-10).

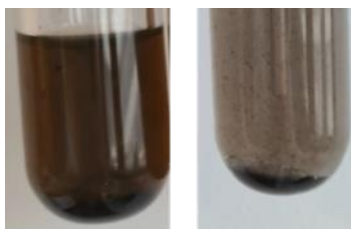


Figure V-10 Microwave assisted Ag₂S NPs (left) suspension when sulfur powder is used for synthesis in ethylene glycol (right) and suspension when Na₂S.9H₂O is used for synthesis in ethylene glycol.

The same synthesis was performed in DMSO and stable brown suspensions were obtained (Table V-6, sample Ag₂S-19).

We precise the synthesis protocol for sample Ag₂S-19. 118.5 mg of ImidPEG₄ (5 equiv.) were dissolved in 10 ml of DMSO, then NaH (16.1 mg, 2 equiv. / ImidPEG₄) was dissolved in 4mL DMSO and added to the ImidPEG₄ solution. The resulting suspension is left under stirring for 5 minutes approximatively. Then, 11.4 mg of AgNO₃, dissolved in 1 ml of DMSO, was added. The solution was stirred for 10 minutes, protected from light. After, 2.1 mg of S⁰, dissolved in 4 mL of DMSO, were added to the solution. Immediately afterwards, the reaction medium was transferred into a monomodal microwave cavity and heated to 100° C (300 W) for 5 min, with magnetic stirring. After microwave heating, the suspension was dialyzed with dialysis cassette, the molecular weight threshold of which was 10 kDa. This cassette was immersed in deionized water for 24 h to eliminate unreacted molecules and ions. A black/dark brown stable suspension is obtained.

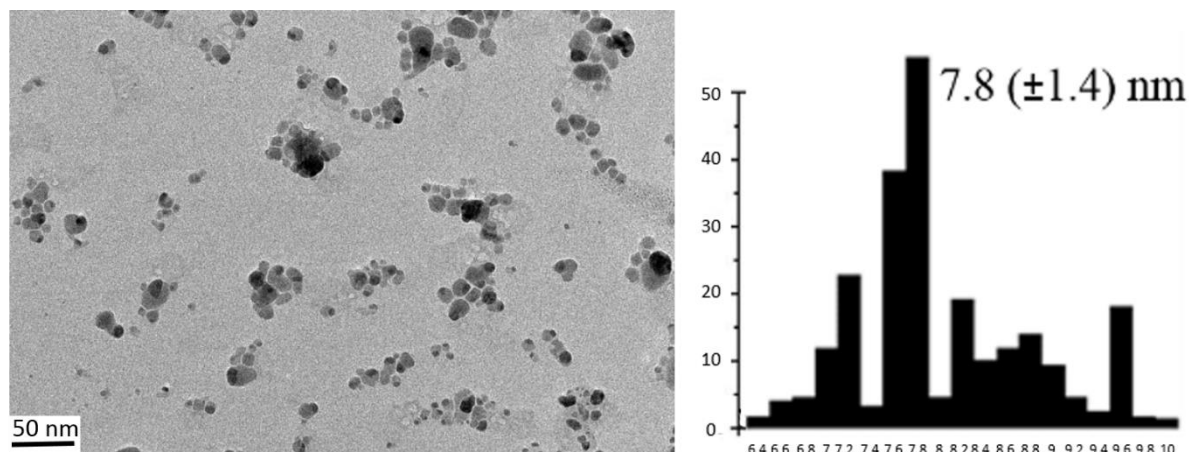


Figure V-11 TEM images of NPs synthesized from AgNO_3 , imid-PEG₄, NaH and S^0 in DMSO with microwave (sample Ag₂S-19).

TEM observation showed 7.8 (± 1.4) nm NPs (Figure V-11). In comparison with previous synthesis using $\text{Na}_2\text{S} \cdot 9\text{H}_2\text{O}$, it gave slightly bigger NPs but still polydispersed. We can see different contrasts on the particles. It is in agreement with the fact that we have two types of NPs (Ag_2S and Ag NPs). In terms of morphology and average size of NPs, the change of sulfur source did not lead to drastic changes when synthesis is performed in DMSO.

We decided to see if the same tendency was followed in DCM. The synthesis performed in DCM led to stable brown suspensions (Table V-6, sample Ag₂S-20). NPs with a mean size of 9.6 (± 1.7) nm were observed by TEM (Figure V-13). In the case of synthesis in DCM, we observed bigger NPs size when using S^0 compared to $\text{Na}_2\text{S} \cdot 9\text{H}_2\text{O}$ as sulfur source (Figure V-12).

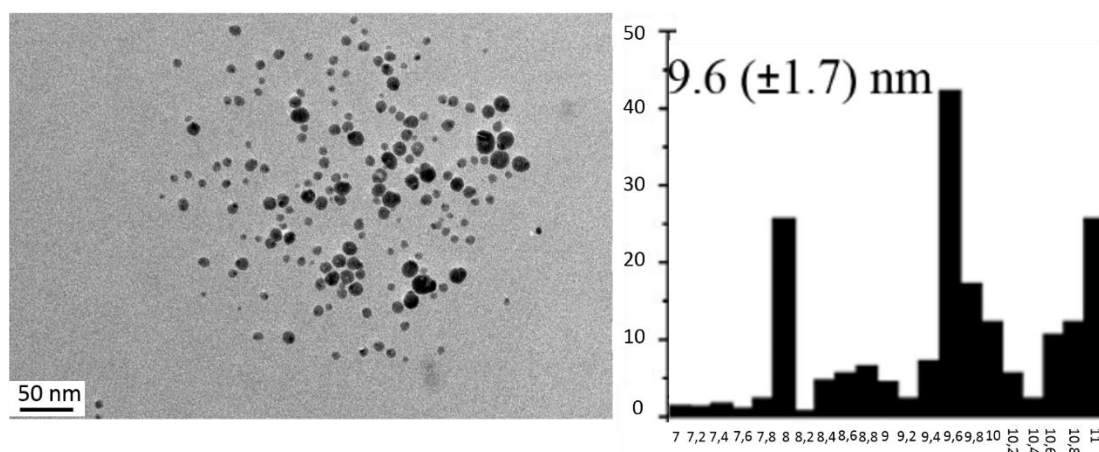


Figure V-12 TEM images of NPs synthesized from AgNO_3 , imid-PEG₄, NaH and S^0 in DCM (sample Ag₂S-20).

Concerning the effect of the sulfur source on suspension stability, NPs size and morphology, we did not see considerable changes. The small effects we saw could be due to a better solubility of S^0 in organic solvents compared to $Na_2S \cdot 9H_2O$. According to electrochemical potentials, two different reduction pathways could happen leading to either $Ag(0)$ NPs or Ag_2S NPs. UV-Vis spectroscopy analysis was done to see if it could bring more information on the NPs by studying the absorption peaks.

V.C.2.c. UV-Vis spectroscopy study

A study of the literature was done to see if Ag_2S NPs and Ag NPs had characteristic absorption bands as it is the case for gold NPs, for example. For Ag NPs, various articles reported an absorption band around 430 nm in UV-Vis spectroscopy.^{38,39,40} An observation of the UV-Vis spectra of suspensions after synthesis with both sulfur sources showed two absorption bands: one just below 300 nm and the other around 360 nm (Figure V-13).

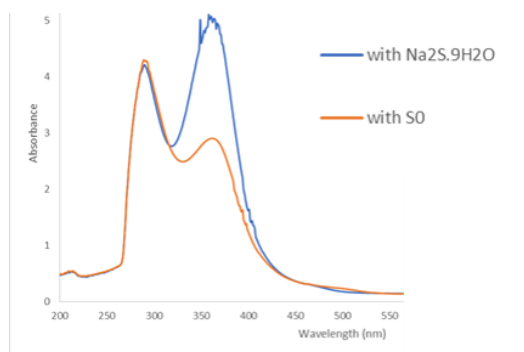


Figure V-13 UV-Vis spectra of NPs stabilized by imidPEG₄ synthesized in DMSO with Na_2S (blue curve) and S (orange curve). Samples Ag_2S -10 in Table V-3 and Ag_2S -19 in table V-6 respectively.

At the same time, it was noticed that when the imid-PEG₄ is added to NaH in DMSO to initiate the deprotonation, the suspension color changes (Figure V-14). This phenomenon was followed by UV-Vis spectroscopy. In fact, this color change could mean that the ligand has an effect on the UV-Vis spectra of NPs suspensions. A high intensity peak at 280 nm and a broad peak at 350 nm was observed. It is similar to the results obtained for the NPs UV-Vis spectra in DMSO (Figure V-13). However, in the case of the ligand spectrum, second peak (350 nm) is very broad compared to the one on the NPs spectrum. This peak has also lower intensity than the one of the NPs spectra. Very broad absorption spectra are usually indicative of a charge transfer.⁴¹

Synthesis of n-heterocyclic carbene stabilized silver sulfide nanoparticles

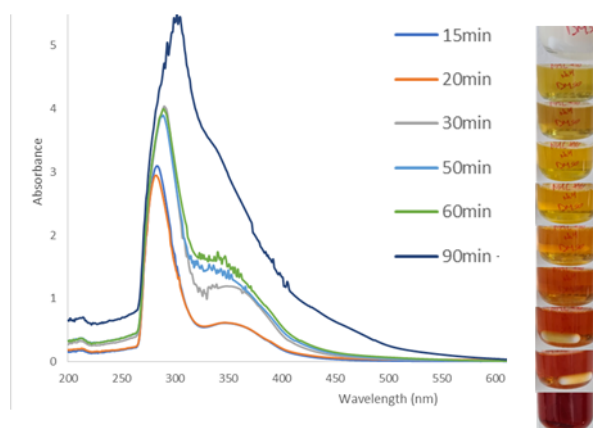


Figure V-14 UV spectroscopy following of the imidazolium mixed with NaH in DMSO over time.

Over time the second peak around 350 nm on the “ligand” spectrum flattens and tend to disappear. The sole study of UV-Vis spectra cannot give complete information on the nature of the synthesized particles. In fact, some of the peaks that are seen on the NPs UV spectra, could be attributed to the ligand. It can be noted that no peak at 430-450 nm was observed as it is usually the case for Ag NPs of this size.

To gain more information on the NPs nature, HRTEM-EDX experiments were conducted on samples presented in the previous parts. Also, the influence of the sulfur source on the samples composition can be assessed.

V.C.2.d. HRTEM-EDX characterization for chemical composition

Samples of interest were analyzed by High Resolution Transmission Electron Microscopy and Energy Dispersive X-Ray Analysis (HRTEM-EDX). They were synthesized with characteristics listed in Table V-7.

Table V-7 Ag₂S NPs synthesized in DCM by using ImidPEG₄ and sulfur source (Na₂S.9H₂O or sulfur powder).

| Particles in samples | solvent | [Ag] mM | Ag/S | Sulfur source | Ligand/Ag | T (°C) | t (min) |
|----------------------|---------|---------|------|-------------------------------------|-----------|--------|---------|
| Ag ₂ S-21 | DCM | 5 | 1 | Na ₂ S.9H ₂ O | 5 | 100°C | 5 |
| Ag ₂ S-22 | DCM | 5 | 1 | S | 5 | 100°C | 5 |
| Ag ₂ S-23 | DCM | 5 | 2 | Na ₂ S.9H ₂ O | 5 | 100°C | 5 |
| Ag ₂ S-24 | DCM | 5 | 2 | S | 5 | 100°C | 5 |
| Ag-21 | DCM | 5 | 1 | Na ₂ S.9H ₂ O | 5 | 100°C | 5 |
| Ag-22 | DCM | 5 | 1 | S | 5 | 100°C | 5 |
| Ag-23 | DCM | 5 | 2 | Na ₂ S.9H ₂ O | 5 | 100°C | 5 |
| Ag-24 | DCM | 5 | 2 | S | 5 | 100°C | 5 |

When observed in HRTEM, the samples showed similarities. Two types of NPs could be observed for all of them. The first type of NPs were spherical NPs completely crystalline in lower proportion (Figure V-15). The second type of NPs were spherical NPs with a heart/shell organization in much higher proportion (Figure V-16). For this second type of particles, the heart is much more crystalline than the shell. We can hypothesize that the heterogeneity of the core/shell NPs comes from two phases: silver sulfide and metallic silver. It has been reported in the literature in the case of Ag_2S nanoparticles that the high redox potential of silver ions and the high temperature used during synthesis can lead to the formation of a metallic silver core. To minimize the formation of the metallic silver core different strategies have been proposed but it led to NPs with low quantum yields and photoluminescence lifetimes.⁴²

EDX analysis (Table V-8, Ag-21, Ag-22, Ag-23, Ag-24) on these samples for elements Ag and S showed that the first category of NPs, which are uniformly crystalline, are composed of Ag (oxygen and azote from the ligand were also detected). However, 0% of sulfur atoms were found. As for the second category of NPs, which have a core/shell organization, they were composed of Ag and sulfur (in the proportion reported in table V-8). Oxygen and azote from the ligand were also detected. It means that both NHC capped Ag NPs and NHC capped Ag_2S NPs were synthesized. It confirms the hypotheses that were raised in the previous parts about the samples NPs composition. Since, both types of NPs were found in all the samples, it means that there are various way leading to the synthesis of a NP mixture since the mechanism involved when using sulfur powder and $\text{Na}_2\text{S} \cdot 9\text{H}_2\text{O}$ are very different. However, it also means that changing the sulfur source did not help in resolving the issue of two NPs types synthesis.

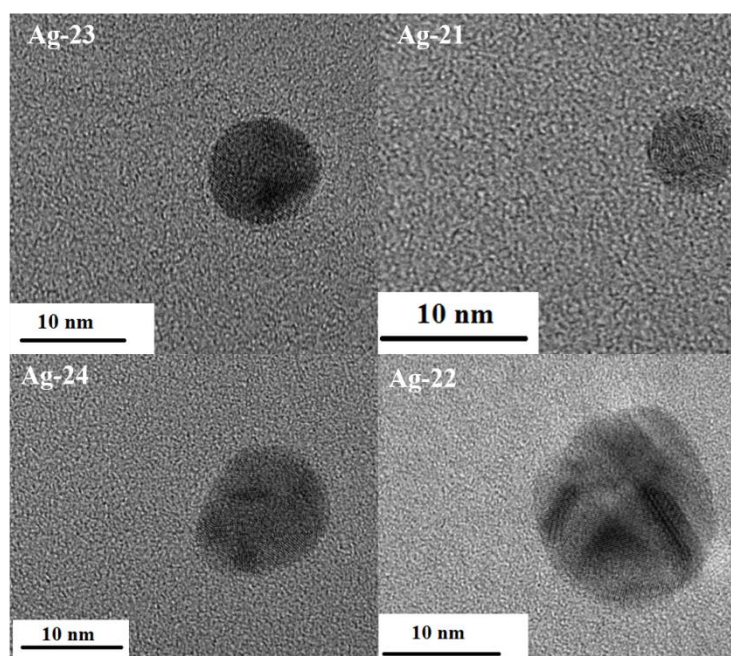


Figure V-15 HRTEM images of crystalline NHC capped Ag NPs in samples Ag-21, Ag-22, Ag-23 and Ag-24.

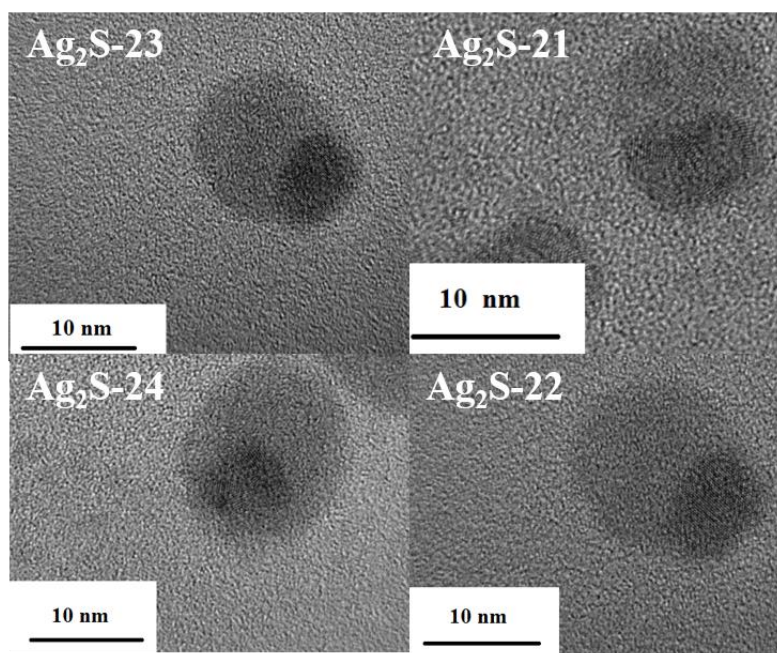


Figure V-16 HRTEM images of crystalline NHC capped Ag_2S NPs in samples $\text{Ag}_2\text{S-21}$, $\text{Ag}_2\text{S-22}$, $\text{Ag}_2\text{S-23}$ and $\text{Ag}_2\text{S-24}$.

Table V-8 Sizes and Ag/S ratio (mean size based only on Ag_2S NPs) for samples synthesized in DCM from AgNO_3 and sulfur source ($\text{Na}_2\text{S} \cdot 9\text{H}_2\text{O}$ or sulfur powder).

| sample | Ag/S | Sulfur source | Ligand/Ag | Size TEM (nm) | Ag/S MET-EDX |
|--------------------------|------|---|-----------|--------------------------------|--------------|
| $\text{Ag}_2\text{S-21}$ | 1 | $\text{Na}_2\text{S} \cdot 9\text{H}_2\text{O}$ | 5 | $6 (\pm 0.5)$ / $19 (\pm 2.5)$ | 1.62 |
| $\text{Ag}_2\text{S-22}$ | 1 | S | 5 | $9.6 (\pm 1.7)$ | 1.68 |
| $\text{Ag}_2\text{S-23}$ | 2 | $\text{Na}_2\text{S} \cdot 9\text{H}_2\text{O}$ | 5 | $7.8 (\pm 1.8)$ | 2 |
| $\text{Ag}_2\text{S-24}$ | 2 | S | 5 | $9.5 (\pm 1.4)$ | 2.25 |

The mean Ag/S ratio were calculated for Ag_2S NPs in various grids for all the samples (Table V-8). It showed that when the starting reagents Ag/S ratio is of 1, the final Ag/S ratio of the NPs is sub stoichiometric, below 2 (1.62 when using $\text{Na}_2\text{S} \cdot 9\text{H}_2\text{O}$ and 1.68 when using sulfur powder). On the contrary, when the starting reagents Ag/S ratio is of 2, the final Ag/S ratio of the NPs is stoichiometric or above stoichiometry (2 when using $\text{Na}_2\text{S} \cdot 9\text{H}_2\text{O}$ and 2.25 when

Synthesis of n-heterocyclic carbene stabilized silver sulfide nanoparticles

using sulfur powder). The Ag/S ratio is controlled by the amount of $\text{Na}_2\text{S} \cdot 9\text{H}_2\text{O}$ introduced into the reaction medium. The Ag/S ratio decreases with an increase in the amount of $\text{Na}_2\text{S} \cdot 9\text{H}_2\text{O}$. Thus, the ionic strength increases by increasing the quantity of cations (Na^+) present in the medium. When the ionic strength is high, the nucleation of the Ag_2S NPs is triggered by the addition of sulfur to the reaction medium before introduction into the microwave. This is probably the case when $\text{Ag/S} = 1$. Indeed, it was reported that ionic strength is one of the factors which affect silver nanowires sulfidation to form Ag_2S . The four electrolytes Na^+ , K^+ , Mg^{2+} and Ca^{2+} promoted sulfidation, leading to significantly increased rate constants compared to reaction without any electrolyte.⁴³ It means the resulting NPs are going to be more polydisperse in size. When $\text{Ag/S} = 2$, the nucleation is triggered by microwave irradiation. It means the seeds are formed over a very short period. The particles grow at the same time which reduces the polydispersity of the population of nanoparticles obtained (Ag_2S -21 vs Ag_2S -23).

To conclude this synthesis method produces two types of NPs: NHC capped Ag NPs and NHC capped Ag_2S NPs. Even though there are much more Ag_2S NPs in all the samples, we could not move the equilibrium toward the synthesis of Ag_2S NPs completely. One of the lines of thought would be to increase the synthesis time from 5 minutes to 10 or 15 minutes to allow further formation of Ag_2S NPs. However, these syntheses have not been done yet. Also, analysis of the Ag/S ratio in the NPs by HRTEM-EDX shows an effect of the initial Ag/S ratio introduced through the reagents. It does not seem to impact the overall morphology of the NPs except for the polydispersity but it could have a higher impact on the resulting properties. The effect on the photoluminescence of the NPs will be presented in the next part.

Measurement of emission and PL activity were performed to see if characteristic NIR-II Ag_2S NPs emission could be measured.

V.C.3. Photoluminescence properties of Ag_2S nanoparticles

V.C.3.a. Theory and optical set up

Our main interest for Ag_2S NPs comes from their ability to emit in the NIR-II window, which could be a great asset for temperature measurement at the cellular scale, for example. To obtain the NPs PL information, an Ag_2S NPs suspension in water is placed in a cell under stirring and then, the suspension is excited by a 730 nm laser. The system is connected to an optical filter which collects the emitted photons using a NIR(II) camera (InGaS detector) (Figure V-17).

After asserting that the NPs emit in the window of interest, the future goal would be to extract temperature information from PL data. PL parameters need to be extracted from hyperspectral data. When the PL parameter is measured then the temperature is calculated with the calibration model resulting from the experimental data. One of our team members, Lise Abiven, developed a calibration curve obtained from Ag_2S NPs dispersed in D_2O . The relative sensitivity (S_r) is obtained thanks to the material-parameter couple and expressed in $\% \cdot ^\circ\text{C}^{-1}$.²⁷

Synthesis of n-heterocyclic carbene stabilized silver sulfide nanoparticles

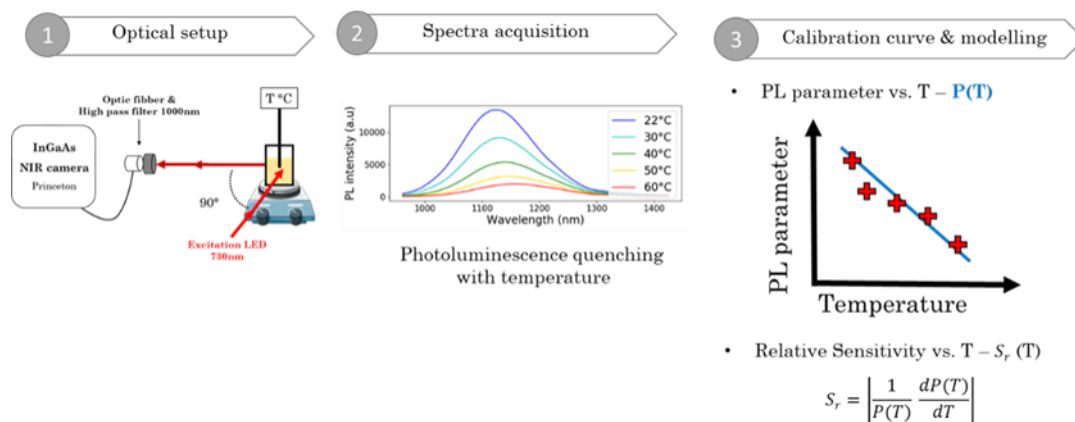


Figure V-17 Optical set up for PL measurement activity and modelling of PL parameter as a function of temperature.

Samples of NPs synthesized in DCM were used for PL intensity measurements. After drying of DCM solvent, redispersion in water of the samples was done to wash them through dialysis. Then, the PL curves were recorded. The sample were subjected to excitation at 730 nm and a high pass filter 1000 nm was used.

V.C.3.b. Photoluminescence of Ag₂S NPs

PL of NPs synthesized in DCM using two different sulfur sources, S and Na₂S.9H₂O in the microwave, were first studied. An emission peak between 1050 nm and 1100 nm seem to appear for both samples (Figure V-18). Unfortunately, the signal/noise ratio is very low in the window of interest. This means that the NPs excited at 730 nm emit very few photons between 1000nm and 1400nm (our window of interest). This may be related to the Ag/S ratio since the samples were concentrated.

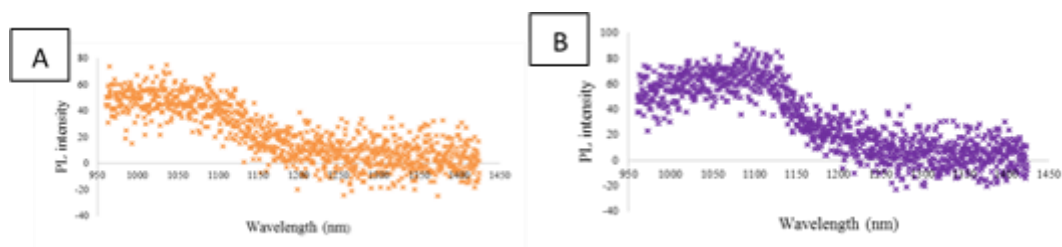


Figure V-18 Emission spectra in water of silver sulfide NPs synthesized with (A) S0 (B) Na₂S.9H₂O with microwave for Ag/S ratio = 1.

Synthesis of n-heterocyclic carbene stabilized silver sulfide nanoparticles

The influence of the Ag/S ratio on the NPs emission was explored by changing the ratio from 1 to 2. We wanted to see if it did improve the signal/noise ratio and thus the number of photons emitted in the NIR-II window. The previous synthesis was reproduced in DCM. NPs of size 5.5 (± 2.6) nm were obtained for the synthesis with $\text{Na}_2\text{S} \cdot 9\text{H}_2\text{O}$. For the synthesis with S, TEM observations showed two populations: $\approx 4\text{ nm}$ NPs and $\approx 15\text{ nm}$ NPs. Emission spectra were also measured and it actually gave better signal/noise ratio with the change of Ag/S ratio to 2 instead to 1 (Figure V-19). The analysis of the sample synthesized from $\text{Na}_2\text{S} \cdot 9\text{H}_2\text{O}$ displays on the PL spectrum a very broad peak whereas the one synthesized from S is sharper.

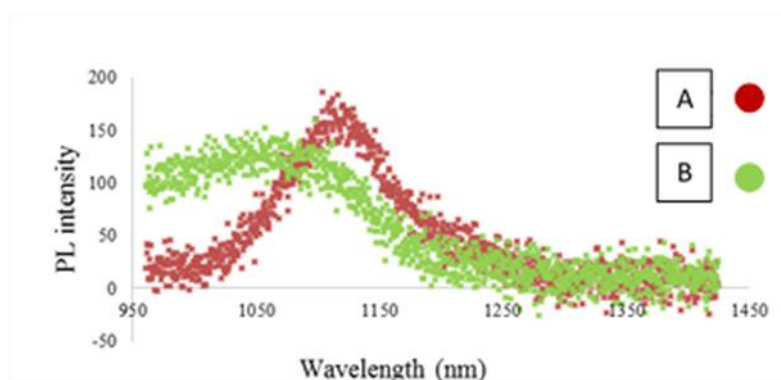


Figure V-19 Emission spectra in water of silver sulfide NPs synthesized with (A) S and (B) $\text{Na}_2\text{S} \cdot 9\text{H}_2\text{O}$ using microwave heating for Ag/S ratio = 2.

V.C.3.c. Dependence of the Ag_2S photoluminescence with temperature

A study was performed on sample (A). This study consisted of heating the sample over time to see if a change in temperature implies changes in the emission properties of the materials. First, the temperature is kept stable at 19°C for 5 min. Then, a rise in temperature of $5^\circ\text{C}/\text{min}$ is applied from 19°C to 40°C . Then, there is a decrease of temperature from 40°C to 19°C during approximately 5 minutes. Finally, the temperature is back at 19°C for 5 minutes. This experiment is applied as a cycle and the NPs PL emission is measured at the same time. By recording the evolution of the photoluminescence intensity as a function of time (Figure V-20), and therefore of the temperature variation, an extinction of the PL can be observed. Indeed, the PL peak intensity is stable from 0 to 5 minutes when the temperature is at 19°C . Then, from 5 minutes to 15 minutes, corresponding to the temperature variation window, the PL intensity decrease proportionally to the increase in temperature. When the temperature goes back to the initial temperature of 19°C , the PL intensity goes back at its maximum. This quenching of PL as a function of temperature allows nanomaterials to potentially be used as nanothermometers.

Synthesis of n-heterocyclic carbene stabilized silver sulfide nanoparticles

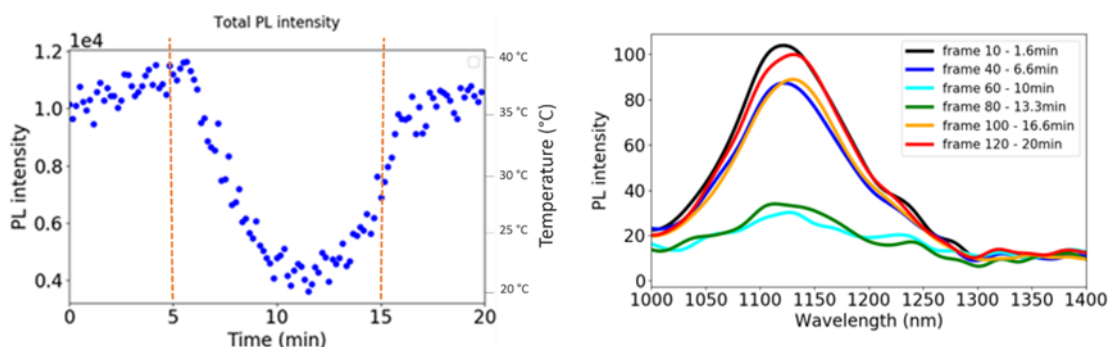


Figure V-20 Evolution of PL intensity as a function of time and temperature for silver sulfide NPs suspension synthesized from AgNO_3 , imid-PEG₄, NaH and S in DCM (Ag_2S -24). Red dotted line corresponds to switching on (5 min) and turning off (15 min) of the heating.

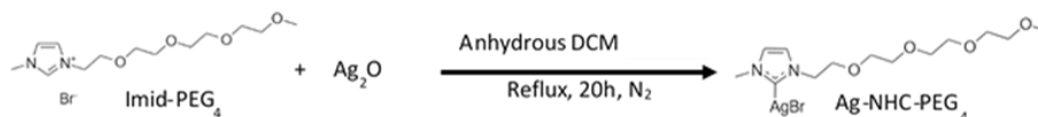
The photoluminescence bands observed below 1150 nm indicates the presence of the silver sulfide phase in our samples (Figure V-19). Indeed, silver nanoparticles do not emit in the wavelength window that we detect with the hyperspectral camera that we used in this study.⁴⁴

The synthesis of Ag_2S NPS from imidazolium-PEG₄, allowed better understanding of the synthesis mechanisms involved, as well as the importance of the choice of solvents. In the current reaction conditions, DCM was the best solvent we tested for the reagents solubility and reactivity. The influence of the Ag/S ratio was confirmed here with particles emitting in the NIR-II window being in greater number in the samples synthesized with $\text{Ag/S} = 2$. The influence of the sulfur source on the reaction mechanisms was also demonstrated, even though it did not have a huge impact on NPs morphology it seems like it does influence the final NPs emission properties giving better resolution spectra. The use of some of the reagents complicated the synthesis pathway (NaH). Therefore, to overcome these problems, it was chosen to explore another synthetic route that uses Ag-NHC-PEG₄ as a reagent.

V.D. Synthesis using Ag-NHC complex: Ag-NHC-PEG₄

V.D.1. Synthesis of complex Ag-NHC-PEG₄

In this part the Ag-NHC-PEG₄ complex was produced to free ourselves from the step of in situ generation of the NHC-PEG₄. The synthesis consists of dissolving the imid-PEG₄ in DCM and then add an excess of silver oxide (Ag₂O). The synthesis is carried out at reflux for 20 h under N₂ (Scheme V-3). After 20 hours, the reaction suspension is filtered, the solvent is evaporated and the crude product is washed with ethyl acetate. It gives us the complex as a brown oil with a yield >75%.



Scheme V-3 Synthesis of complex Ag-NHC-PEG₄.

In order to confirm the formation of this compound, ¹H and ¹³C NMR analysis were performed in CDCl₃ and compared with the spectra that we previously obtained from the analysis of imid-PEG₄. ¹H-¹³C HSQC and ¹H-¹³C HMBC complementary experiments helped in doing the attributions. A study of the chemical shift (¹³C) [ppm] value for the samples, shows that the potential “carbenic carbon” is around 181 ppm. It is similar to chemical shifts of known carbenic carbons. This value is different from the corresponding carbon in the imidazolium salt which has a lower chemical shift around 137 ppm. The comparison of the ¹H NMR spectra of Imid-PEG₄ and Ag-NHC-PEG₄ (Figure V-21) also give information on the formation of the complex. One of the proof of the complex formation is that all the proton peaks are similar except the signal labelled 11 at 9.6 ppm (“imidazolium peak”). The signal disappears in the Ag-NHC-PEG₄ form. The complex was kept in air and remained stable over time.

Synthesis of n-heterocyclic carbene stabilized silver sulfide nanoparticles

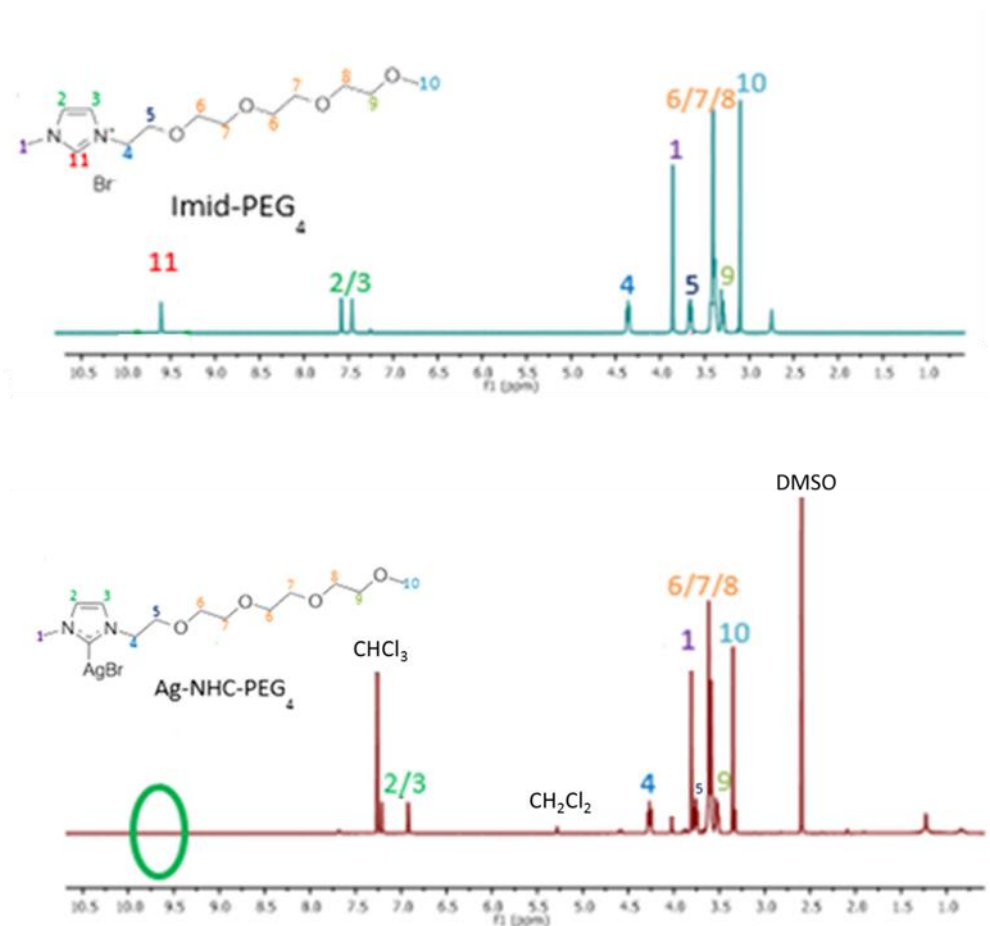


Figure V-21 ^1H NMR spectra of Ag-NHC-PEG₄ and Imid-PEG₄ in CDCl₃.

V.D.2. Microwave assisted NPs synthesis

The ligand Ag-NHC-PEG₄ was used as NHC and silver source here. All the microwave assisted synthesis were performed in a microwave Anton Paar Monowave 300 (Figure V-22).

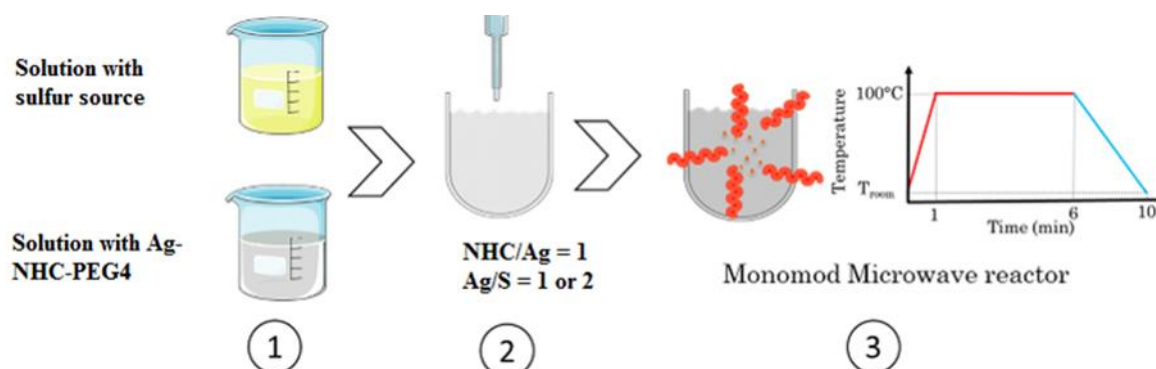


Figure V-22 Microwave assisted Ag₂S NPs synthesis pathway using silver-NHC complex.

Synthesis of n-heterocyclic carbene stabilized silver sulfide nanoparticles

V.D.2.a. Influence of the solvent

Since NaH was not needed in this part, the NPs synthesis was again performed in water. To a solution of Ag-NHC-PEG₄ in water, a solution of Na₂S.9H₂O in water was added just before heating. The synthesis was carried out in microwave at 100°C for 5 min (Table V-9, Ag₂S-a and Ag₂S-b).

Table V-9 Ag₂S NPs synthesized in water and DCM by using Ag-NHC-PEG₄ and Na₂S.9H₂O.

| sample | solvent | [Ag] mM | Ag/S | Sulfur source | Ligand/Ag | T (°C) | t (min) |
|---------------------|---------|------------|------|-------------------------------------|-----------|--------|---------|
| Ag ₂ S-a | water | 5 | 1 | Na ₂ S.9H ₂ O | 1 | 100°C | 5 |
| Ag ₂ S-b | water | 5 | 2 | Na ₂ S.9H ₂ O | 1 | 100°C | 5 |
| Ag ₂ S-c | DCM | 5 | 1 | Na ₂ S.9H ₂ O | 1 | 100°C | 5 |
| Ag ₂ S-d | DCM | 5 | 2 | Na ₂ S.9H ₂ O | 1 | 100°C | 5 |

No NPs were observed as we obtained a silver aggregate in the bottom of the flask. Aiming at understanding why the synthesis did not proceed in water, ¹H NMR of Ag-NHC-PEG₄ in D₂O (90%) H₂O (10%) was carried out. At the very moment the complex is added into water, the suspension becomes blurry, then everything precipitates. We tried to see if degradation of the complex occurred and when it did happen. There was no difference between the spectra of the complex in D₂O/H₂O after 10 min or after 24h (only after 24h the suspension was clear and everything was at the bottom of the tube). Thus, it means the degradation occurs very rapidly. We have been able to observe that the carbene reprotonates itself in water and reform the imidazolium. The absence of the ¹H imidazolium signal and of the associated carbon (137.3 ppm) on the HSQC map was also observed. It comes from the fact that the reaction is carried out in a medium mainly consisting of D₂O (90%). It is therefore the deuterated form of imidazolium which is obtained by hydrolysis of Ag-NHC-PEG₄. This synthetic route is therefore not possible in water solvent since there the Ag-NHC-PEG₄ complex is hydrolyzed. To avoid such hydrolysis reaction and the destruction of the Ag-NHC-PEG₄ complex, the synthesis was done in an organic solvent.

DCM was then chosen as a solvent for the synthesis. To a solution of Ag-NHC-PEG₄ in DCM, a solution of Na₂S.9H₂O in DCM was added just before heating. The synthesis was carried out in microwave at 100°C for 5 min. Also, synthesis with both Ag/S ratio of 1 and 2 were achieved (Table V-9, Ag₂S-c and Ag₂S-d).

TEM observation showed that Ag₂S NPs sized 9.5 (±1.9) nm were synthesized for Ag/S = 1 (Ag₂S-c). Ag₂S NPs sized 8.9 (±2.3) nm were synthesized for Ag/S = 2 (Ag₂S-d) (Figure V-23).

We precise the synthesis protocol for sample Ag₂S-c. 30.4 mg of Ag-NHC-PEG₄ (1 equiv.) were dissolved in 8 ml of DCM and the resulting suspension was left under stirring for 5 minutes approximatively. Then, Na₂S.9H₂O (16 mg, 1 equiv.) was dissolved in 4mL of DCM and added to the Ag-NHC-PEG₄ solution. Immediately afterwards, the reaction medium was transferred into a monomodal microwave cavity and heated to 100° C (300 W) for 5 min, with magnetic

Synthesis of n-heterocyclic carbene stabilized silver sulfide nanoparticles

stirring. After microwave heating, the suspension was dialyzed with dialysis cassette, the molecular weight threshold of which was 10 kDa. This cassette was immersed in deionized water for 24 h to eliminate unreacted molecules and ions. A black/dark brown stable suspension is obtained.

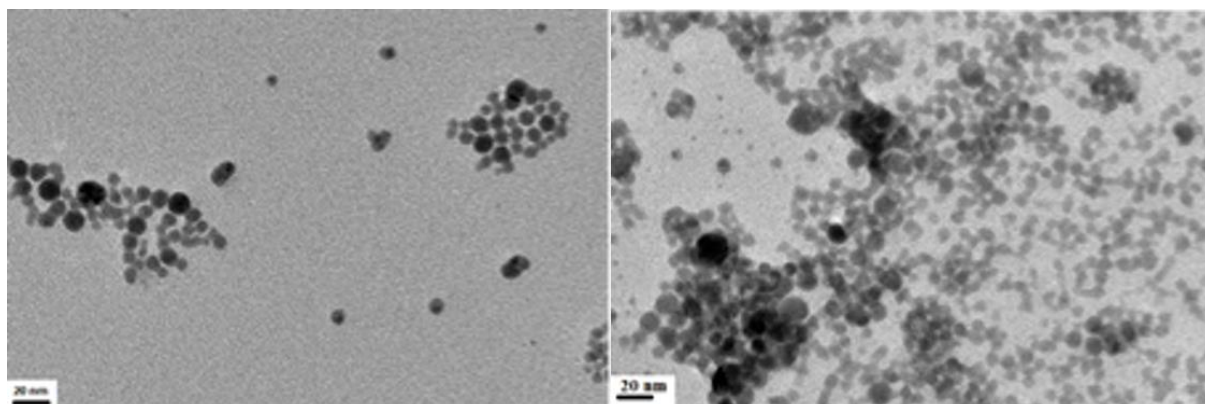


Figure V-23 TEM images of Ag₂S NPs synthesized in DCM with microwave from Ag-NHCPEG₄ + Na₂S.9H₂O with Ag/S ratio of 1 (left) and Ag/S ratio of 2 (right).

These results led to conclude that the Ag/S ratio did not tremendously influence the morphology nor the size of the NPs. UV-Vis spectroscopy did not give us much more information especially due to the NHC ligand absorption. Then, PL analysis has been carried out on the reported synthesis.

V.D.2.b. Photoluminescence of Ag₂S-NHC PEG₄ NPs

The PL emission spectra were recorded for synthesis with Ag/S = 1 and Ag/S = 2 (sample Ag₂S-c and Ag₂S-d). For the sample Ag₂S-c, a slight broad peak is observed between 1050 nm and 1150 nm. However, the intensity is extremely low meaning that very few photons are emitted in the NIR-II window. For the sample Ag₂S-d, there was a large emission peak between 1000 nm and 1150 nm with much higher intensity. These experiments confirmed some of the results obtained. There is an influence of the Ag/S ratio on the NPs PL curves signal/noise ratio. It seems like even though stable Ag₂S NPs are synthesized with an Ag/S ratio of 1, there is not enough photons that are emitted in the NIR-II in these conditions. Better signal/noise is observed for the PL curves of the samples synthesized when ratio Ag/S = 2 (Figure V-24). The presence of a shoulder on the spectrum may mean that we synthesize two populations of

Synthesis of n-heterocyclic carbene stabilized silver sulfide nanoparticles

particles however previous characterizations (HRTEM-EDX) did not suggest two populations of particles.

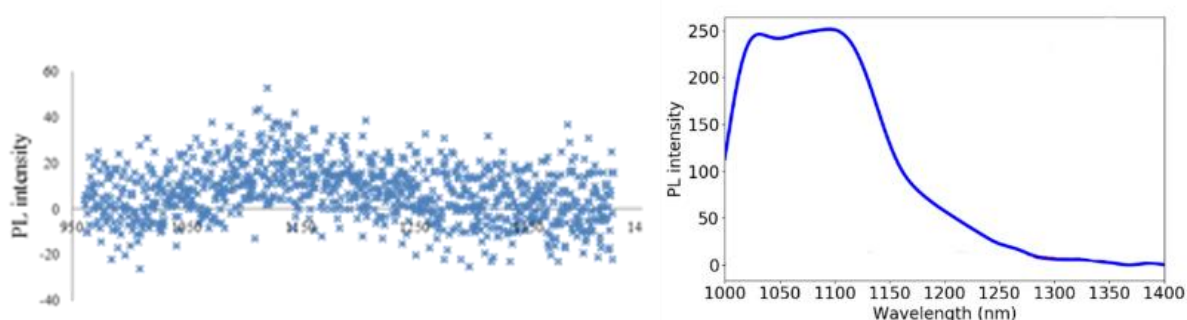


Figure V-24 Emission spectra in water of Ag₂S NPs synthesized with Ag-NHCPEG₄ and Na₂S·9H₂O in DCM with Ag/S ratio = 1 (left, sample Ag₂S-c) and Ag/S ratio = 2 (right sample Ag₂S-d).

The Ag/S ratio is a determining factor for obtaining an emission in our window of interest with our Ag₂S NPs. This synthesis pathway can give stable suspensions of NIR-II emitting Ag₂S NPs under certain conditions (Ag/S = 2). One of the downfalls is that the ligand/Ag ratio cannot be modulated here. Also, great experiment would be to measure the influence of temperature on PL intensity for these samples to confirm the possibility to use them as potential future nanothermometers. To understand the differences in PL emission properties further characterization were performed on the samples.

V.D.3. Further characterization of Ag₂S NPs

V.D.3.a. HRTEM-EDX characterization for chemical composition

Samples of interest were analyzed by High Resolution Transmission Electron Microscopy and Energy Dispersive X-Ray Analysis (HRTEM-EDX). They were synthesized with characteristics listed in Table V-10.

Table V-10 Sizes and Ag/S ratio (mean size based only on Ag₂S NPs) for samples synthesized from Ag-NHC-PEG₄ and Na₂S.9H₂O.

| sample | Ag/S | Size TEM (nm) | Ag/S MET-EDX |
|---------------------|------|---------------|--------------|
| Ag ₂ S-c | 1 | 9.5 (±1.9) | 1.87 |
| Ag ₂ S-d | 2 | 8.9 (±2.3) | 2 |

The results confirmed the presence of Ag and S atoms. It also showed oxygen and azote atoms coming from the NHC ligand. NPs with a slight sub stoichiometric Ag/S atomic ratio (1.87) for sample Ag₂S-c were observed. HRTEM observation showed a core/shell organization with the core that is more crystalline as seen in previous part (Figure V-25).

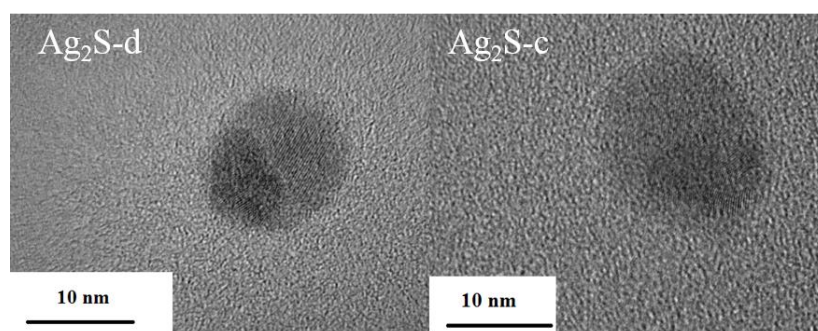


Figure V-25 HRTEM images of crystalline NHC capped Ag₂S NPs in samples Ag₂S-c and Ag₂S-d.

The HRTEM analysis confirmed the obtaining of Ag₂S NPs but did not give us much information on the differences between the NPs synthesized with Ag/S ratio 2 or 1. Indeed, the synthesis of Ag₂S NPs with Ag/S atomic ratios of less than 2 has been reported in several studies.^{42,45} Further analysis have been performed on samples Ag₂S-d to gain more information

V.D.3.a. XPS Analysis

X-ray photoelectron spectroscopy (XPS) was used to study the silver-sulfur interaction at the nanoparticles surface. XPS spectra are obtained by irradiating of materials with a beam of X-rays. Simultaneously the kinetic energy and number of electrons that escape from the analyzed surface (up to 10 nm depth) is measured. The material is placed in a high vacuum chamber. Thanks to XPS we can determine the chemical state of an analyzed surface and also give the material elementary composition. XPS can also give the binding mode of the ligand on the metallic surface when analyzing NPs. However, characterization can be challenging due to peaks widening for example.

XPS analysis was carried out on sample Ag₂S-d (Figure V-26). Spectra over a wide scan range of Ag₂S-d NPs depicting strong existence of Ag 3d, S 2p, C 1s, N 1s are shown in Figure V-26. The Ag 3d spectrum of Ag₂S-d NPs was characterized by two peaks, which were the result of spin orbital separation. It corresponds to the core levels of Ag 3d_{3/2} (at 374 eV) and Ag 3d_{5/2} (at 368 eV).⁴⁶ These values are characteristic of silver sulfide.⁴⁷ For S 2p, it was observed that the sulfur ions are in the S²⁻ state at binding energies 161 eV. These values are in good agreement with the previously reported values for Ag₂S NPs.⁴⁸ Moreover, analysis of elemental composition from XPS data unveiled an elemental ratio of approximately 2/1 for Ag/S, which also confirms the formation of Ag₂S NPs (Figure V-26). These values are in good agreement with results obtained from EDX analysis. For the ligand we calculated the theoretical ratio of total number of atoms divided by the number of carbon atoms in the ligand: $N(\text{total}) / C(\text{NHC-PEG}) = 0.15$. By XPS, we obtained a value of 0.13 which is in good agreement if we take into account the little contamination on the carbon spectrum. Also, to validate the covalent bonding of the ligand we did study the N 1s spectrum. NHC binding to the NPs surface was corroborated a N 1s peak at a binding energy at 401.5 eV.²³ (Figure V-26).

Synthesis of n-heterocyclic carbene stabilized silver sulfide nanoparticles

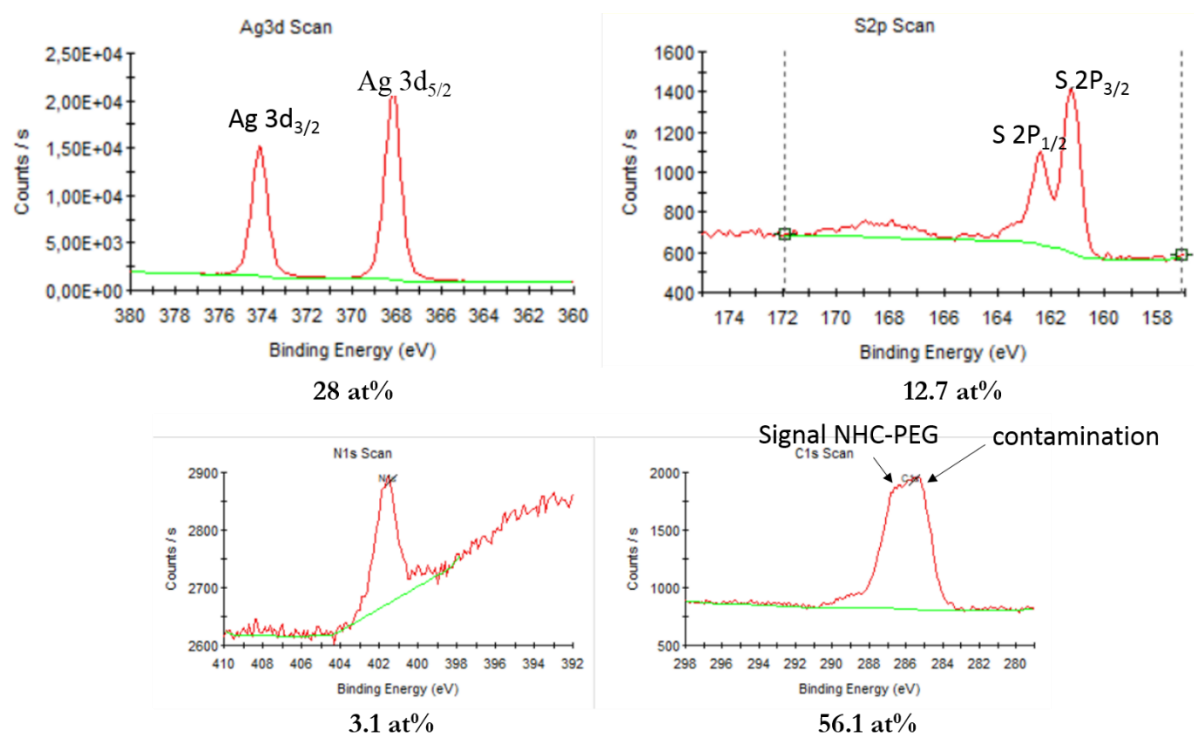


Figure V-26 Ag 3d, S 2p, C 1s, N 1s XPS spectra for the sample $\text{Ag}_2\text{S-d}$ and elemental composition.

Through XPS analysis, we were able to confirm the composition of the samples: Ag_2S NPs with a Ag/S ratio of 2. Also, the coordination of ligand NHC-PEG₄ to the NPs was assessed.

More surface characterization was performed. FT-IR analyses of the Ag-NHC-PEG₄ and of the sample $\text{Ag}_2\text{S-d}$ showed that both spectra display characteristic bands at 1105 cm^{-1} (C-O stretching) for the PEG chain and characteristic bands at approximately 1570 cm^{-1} and 1457 cm^{-1} (C-N stretching) for the NHC ring.

V.D.4. Low temperature synthesis

In this part, we tried to evaluate the influence of the solvent on the reaction's kinetic when the reaction is not assisted by microwave in various solvents. Indeed, it is possible to evaluate how solubility of the chemicals influence the reactions kinetics and the particles size. Also, it is possible to see how solubility is not the only parameter to take into account when choosing the solvent. Moreover, it is an example of how using microwave heating improves the reactions speed. For this synthesis, Ag-NHC-PEG₄ was mixed with Na₂S.9H₂O in solution using different solvents and the suspension was let under stirring at room temperature. The reagents ratios were Ag/S = 2 and NHC-PEG₄/Ag = 1. First, aggregation in the suspensions and color of the suspensions were observed and then their evolution was followed over time during 8 days (Figure V-27).














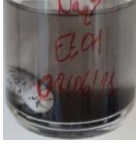






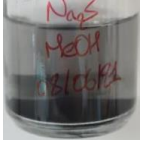



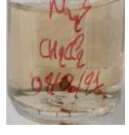


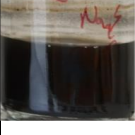
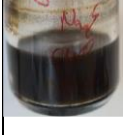

| time \ solvent | 5 minutes | 3 hours | 1 day | 2 days | 6 days | 8 days |
|-------------------------------|---|---|---|--|---|---|
| ACT (Acetonitrile) |  |  |  |  |  |  |
| THF (Tetrahydrofurane) |  |  |  |  |  |  |
| EtOH (Ethanol) |  |  |  |  |  |  |
| MeOH (Methanol) |  |  |  |  |  |  |
| DCM (Dichloromethane) |  |  |  |  |  |  |

Figure V-27 Evolution of Ag₂S suspensions synthesized from Na₂S.9H₂O and Ag-NHC-PEG₄ over time at room temperature in various solvents.

Syntheses that were carried out in EtOH and MeOH gave precipitated suspensions. Our hypothesis is that the same hydrolysis of the Ag-NHCPEG₄ complex, already observed in water

Synthesis of n-heterocyclic carbene stabilized silver sulfide nanoparticles

also happened in these other solvents. Despite the high solubility of the reagents in EtOH and MeOH, the reaction did not give stable NPs. The reaction in THF happened rapidly (after 5 minutes the suspension is already light brown) and after 1 day the suspension is completely dark brown. However, from day 1 to day 8, there are aggregates at the bottom of the flask (even when using anhydrous THF). When using ACT, aggregates did not form but the reaction kinetic (followed by color change) was very slow compared to THF for example. As for DCM, the reaction was finished after day 1 (no special evolution of suspension color or particles size from day 1 to day 8). No aggregates were noticed in the suspensions. We note that over time there was a strong evaporation of the solvent at room temperature. The NPs suspensions were observed after 8 days of ageing by TEM for the synthesis performed in ACT, DCM and THF. The mean sizes are respectively of 9.6 (± 2.5) nm, 12.7 (± 4.9) nm, 11.1 (± 3.8) nm (Figure V-28).

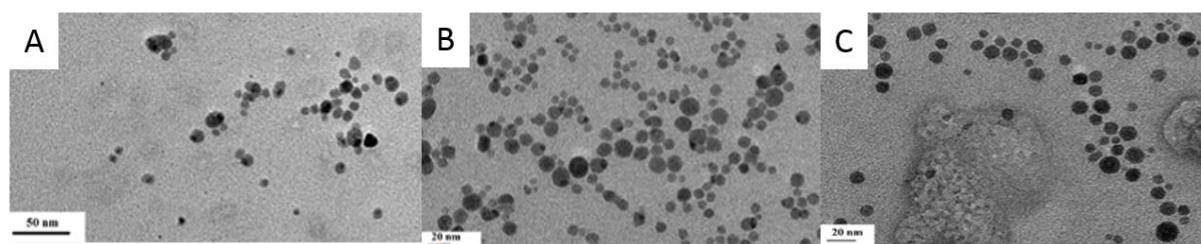


Figure V-28 TEM images of Ag_2S NPs synthesis from $\text{Na}_2\text{S} \cdot 9\text{H}_2\text{O}$ and Ag-NHC-PEG_4 in THF (A), DCM (B) and ACT (C) at room temperature.

Compared to the synthesis in microwave the particles were more polydisperse and slightly bigger in size. These results confirmed our choice of DCM as a reaction solvent. Indeed, the reaction is fast, there is a good solubility of the reagents and there is no sign of aggregation. It also confirmed that NPs synthesis can be performed at low temperature without microwave. Of course, microwave synthesis speeds up the reaction. Also, for the synthesis in DCM, these particles did not exhibit emission in the NIR-II as the one synthesized by microwave. Synthesis by microwave also seem to improve crystallization as observed by HRTEM.

Further studies could be performed on NHC capped Ag_2S NPs such as study of the crystalline structure which can have an influence on the band gap. Also, a study of the surface to determine the density of ligands (by Thermogravimetric analysis for example) could be conducted.

Synthesis in microwave in our reaction conditions was proven to be most effective regarding Ag_2S NPs PL properties. Also, using an NHC-metallic complex simplify the reaction conditions and prevents side reactions in an easy synthesis pathway.

V.E. CONCLUSION

To conclude, we were able to successfully synthesize water soluble NHC capped Ag₂S NPs using two methods. One consists in adding AgNO₃ in a suspension of imid-PEG₄ and NaH then add a sulfur source and initiate the reaction in microwave. Even though this pathway gave stable suspensions, the reactivity of some of the reagents induced undesired secondary reactions. HRTEM-EDX analysis allowed to see that both Ag and Ag₂S NPs are synthesized in our reaction conditions. Further improvement would be to shift the reaction equilibrium toward the formation of only Ag₂S NPs.

The second method relies on the reaction between sulfur source Na₂S.9H₂O and complex Ag-NHCPEG₄ in DCM. It is a simple and reproducible synthesis method for the formation of NHC capped Ag₂S NPs. The obtained NPs were NIR-II emitting for Ag/S reagents ratio of 2. In these conditions the ligand/Ag ratio is of 1. Knowing as the surfactant to silver ratio can be a determining parameter, we would like to develop synthesis with a ligand/Ag ratio superior to 1. Increasing the quantity of ligand could lead to a modification of the NPs optical properties.

To the best of our knowledge, it is the first synthesis of water soluble NHC capped Ag₂S NPs reported so far. The possibility of studies on this subject are wide and opened. Future advancements in the subject would be to change the parameters like the size of the PEG chain. Actually, a shorter or longer chain could modulate the size of the NPs but also their stability. Many other parameters could also be tested to tune the NPs PL properties aiming at emission in the NIR-II.

Other than microwave heating method, conventional heating was explored with little success. Indeed, we were able to obtain NPs but the suspensions were difficult to purify and unstable. This synthesis route parameters still need to be tuned to obtain more stable NPs suspensions.

The literature on NHC protected Ag₂S NPs is very slight. Thus, there is still a lot to do on this topic. By using the rich library of NHC ligands, it is possible to tune further the NPs size (thus the PL properties). Literature showed that the mean diameter of reported Ag₂S NPs displayed a linear correlation with the Tolman electronic parameter (which is a commonly employed parameter to compare electron-donating ability). It means that by using more or less electro-donating NHCs stabilizing ligands, it is possible to influence Ag₂S NPs mean diameter.²³

References

- (1) Zhang, Y.; Zhang, Y.; Hong, G.; He, W.; Zhou, K.; Yang, K.; Li, F.; Chen, G.; Liu, Z.; Dai, H. Biodistribution, Pharmacokinetics and Toxicology of Ag₂S near-Infrared Quantum Dots in Mice. *Biomaterials* 2013, 34 (14), 3639–3646.
- (2) Aydemir, D.; Hashemkhani, M.; Acar, H. Y.; Ulus, N. N. Evaluation of the Biocompatibility of the GSH-Coated Ag₂S Quantum Dots in Vitro: A Perfect Example for the Non-Toxic Optical Probes. *Mol. Biol. Rep.* 2020, 47 (6), 4117–4129.
- (3) Reinsch, B. C.; Levard, C.; Li, Z.; Ma, R.; Wise, A.; Gregory, K. B.; Brown, G. E.; Lowry, G. V. Sulfidation of Silver Nanoparticles Decreases Escherichia Coli Growth Inhibition. *Environ. Sci. Technol.* 2012, 46 (13), 6992–7000. <https://doi.org/10.1021/es203732x>.
- (4) Nowack, B. Nanosilver Revisited Downstream. *Science*, 2010, 330, 1054–1055.
- (5) Buchman, J. T.; Hudson-Smith, N. V.; Landy, K. M.; Haynes, C. L. Understanding Nanoparticle Toxicity Mechanisms to Inform Redesign Strategies to Reduce Environmental Impact. *Acc. Chem. Res.* 2019, 52 (6), 1632–1642.
- (6) Abbasi, M.; Rafique, U.; Murtaza, G.; Ashraf, M. A. Synthesis, Characterisation and Photocatalytic Performance of ZnS Coupled Ag₂S Nanoparticles: A Remediation Model for Environmental Pollutants. *SI Nanochemistry Mater.* 2018, 11 (6), 827–837. <https://doi.org/10.1016/j.arabjc.2017.12.017>.
- (7) Funke, K. Solid State Ionics: From Michael Faraday to Green Energy—the European Dimension. *Sci. Technol. Adv. Mater.* 2013, 14 (4), 043502. <https://doi.org/10.1088/1468-6996/14/4/043502>.
- (8) Hocaoglu, I.; Asik, D.; Ulusoy, G.; Grandfils, C.; Ojea-Jimenez, I.; Rossi, F.; Kiraz, A.; Doğan, N.; Acar, H. Y. Cyto/Hemocompatible Magnetic Hybrid Nanoparticles (Ag₂S–Fe₃O₄) with Luminescence in the near-Infrared Region as Promising Theranostic Materials. *Colloids Surf. B Biointerfaces* 2015, 133, 198–207. <https://doi.org/10.1016/j.colsurfb.2015.05.051>.
- (9) Gil, H. M.; Price, T. W.; Chelani, K.; Bouillard, J.-S. G.; Calaminus, S. D. J.; Stasiuk, G. J. NIR-Quantum Dots in Biomedical Imaging and Their Future. *iScience* 2021, 24 (3), 102189. <https://doi.org/10.1016/j.isci.2021.102189>.
- (10) Munari, M.; Sturve, J.; Frenzilli, G.; Sanders, M. B.; Brunelli, A.; Marcomini, A.; Nigro, M.; Lyons, B. P. Genotoxic Effects of CdS Quantum Dots and Ag₂S Nanoparticles in Fish Cell Lines (RTG-2). *Mutat. Res. Toxicol. Environ. Mutagen.* 2014, 775–776, 89–93. <https://doi.org/10.1016/j.mrgentox.2014.09.003>.
- (11) Zhang, Y.; Hong, G.; Zhang, Y.; Chen, G.; Li, F.; Dai, H.; Wang, Q. Ag₂S Quantum Dot: A Bright and Biocompatible Fluorescent Nanoprobe in the Second Near-Infrared Window. *ACS Nano* 2012, 6 (5), 3695–3702. <https://doi.org/10.1021/nn301218z>.
- (12) Li, C.; Zhang, Y.; Wang, M.; Zhang, Y.; Chen, G.; Li, L.; Wu, D.; Wang, Q. In Vivo Real-Time Visualization of Tissue Blood Flow and Angiogenesis Using Ag₂S Quantum Dots in the NIR-II Window. *Biomaterials* 2014, 35 (1), 393–400. <https://doi.org/10.1016/j.biomaterials.2013.10.010>.
- (13) Sadovnikov, S. I.; Gusev, A. I. Thermal Expansion, Heat Capacity and Phase Transformations in Nanocrystalline and Coarse-Crystalline Silver Sulfide at 290–970 K. *J. Therm. Anal. Calorim.* 2018, 131 (2), 1155–1164. <https://doi.org/10.1007/s10973-017-6691-8>.
- (14) Sharma, R. C.; Chang, Y. A. The Ag–S (Silver-Sulfur) System. *Bull. Alloy Phase Diagr.* 1986, 7 (3), 263–269. <https://doi.org/10.1007/BF02869003>.
- (15) Maldiney, T. Nanocristaux à Luminescence Persistante: Nouveaux Concepts Pour l'imagerie in Vivo, Université Pierre et Marie Curie-Paris VI, 2012.
- (16) Zhang, Y.; Liu, Y.; Li, C.; Chen, X.; Wang, Q. Controlled Synthesis of Ag₂S Quantum Dots and Experimental Determination of the Exciton Bohr Radius. *J. Phys. Chem. C* 2014, 118 (9), 4918–4923. <https://doi.org/10.1021/jp501266d>.
- (17) Du, Y.; Xu, B.; Fu, T.; Cai, M.; Li, F.; Zhang, Y.; Wang, Q. Near-Infrared Photoluminescent Ag₂S Quantum Dots from a Single Source Precursor. *J. Am. Chem. Soc.* 2010, 132 (5), 1470–1471. <https://doi.org/10.1021/ja909490r>.
- (18) Jiang, P.; Tian, Z.-Q.; Zhu, C.-N.; Zhang, Z.-L.; Pang, D.-W. Emission-Tunable Near-Infrared Ag₂S Quantum Dots. *Chem. Mater.* 2012, 24 (1), 3–5. <https://doi.org/10.1021/cm202543m>.

- (19) Jiang, P.; Zhu, C.-N.; Zhang, Z.-L.; Tian, Z.-Q.; Pang, D.-W. Water-Soluble Ag₂S Quantum Dots for near-Infrared Fluorescence Imaging in Vivo. *Biomaterials* 2012, 33 (20), 5130–5135. <https://doi.org/10.1016/j.biomaterials.2012.03.059>.
- (20) Brelle, M. C.; Zhang, J. Z.; Nguyen, L.; Mehra, R. K. Synthesis and Ultrafast Study of Cysteine- and Glutathione-Capped Ag₂S Semiconductor Colloidal Nanoparticles. *J. Phys. Chem. A* 1999, 103 (49), 10194–10201. <https://doi.org/10.1021/jp991999j>.
- (21) Hocaoglu, I.; Çizmeciyani, M. N.; Erdem, R.; Ozen, C.; Kurt, A.; Sennaroglu, A.; Acar, H. Y. Development of Highly Luminescent and Cytocompatible Near-IR-Emitting Aqueous Ag₂S Quantum Dots. *J. Mater. Chem.* 2012, 22 (29), 14674–14681. <https://doi.org/10.1039/C2JM31959D>.
- (22) Jia, X.; Li, D.; Li, J.; Wang, E. Water-Dispersible near-Infrared Ag₂S Nanoclusters with Tunable Fluorescence for Bioimaging Application. *RSC Adv.* 2015, 5 (99), 80929–80932. <https://doi.org/10.1039/C5RA18361H>.
- (23) Lu, H.; Brutchey, R. L. Tunable Room-Temperature Synthesis of Coinage Metal Chalcogenide Nanocrystals from N-Heterocyclic Carbene Synthons. *Chem. Mater.* 2017, 29 (3), 1396–1403. <https://doi.org/10.1021/acs.chemmater.6b05293>.
- (24) Lu, H.; Zhou, Z.; Prezhdoo, O. V.; Brutchey, R. L. Exposing the Dynamics and Energetics of the N-Heterocyclic Carbene–Nanocrystal Interface. *J. Am. Chem. Soc.* 2016, 138 (45), 14844–14847. <https://doi.org/10.1021/jacs.6b09065>.
- (25) Smock, S. R.; Alimento, R.; Mallikarjun Sharada, S.; Brutchey, R. L. Probing the Ligand Exchange of N-Heterocyclic Carbene-Capped Ag₂S Nanocrystals with Amines and Carboxylic Acids. *Inorg. Chem.* 2021, 60 (17), 13699–13706. <https://doi.org/10.1021/acs.inorgchem.1c02018>.
- (26) Wu, P.-J.; Yu, J.-W.; Chao, H.-J.; Chang, J.-Y. Silver-Based Metal Sulfide Heterostructures: Synthetic Approaches, Characterization, and Application Prospects. *Chem. Mater.* 2014, 26 (11), 3485–3494. <https://doi.org/10.1021/cm500959a>.
- (27) Abiven, L. Mesure de Température sans Contact, En Temps Réel et à l'échelle Cellulaire, Par Photoluminescence de Nanoparticules de Sulfure d'argent, Sorbonne Université, 2022.
- (28) Tang, A.; Wang, Y.; Ye, H.; Zhou, C.; Yang, C.; Li, X.; Peng, H.; Zhang, F.; Hou, Y.; Teng, F. Controllable Synthesis of Silver and Silver Sulfide Nanocrystals via Selective Cleavage of Chemical Bonds. *Nanotechnology* 2013, 24, 355602. <https://doi.org/10.1088/0957-4484/24/35/355602>.
- (29) Ma, Y.; Zhao, Z.; Xian, Y.; Wan, H.; Ye, Y.; Chen, L.; Zhou, H.; Chen, J. Highly Dispersed Ag₂S Nanoparticles: In Situ Synthesis, Size Control, and Modification to Mechanical and Tribological Properties towards Nanocomposite Coatings. *Nanomaterials* 2019, 9 (9), 1308.
- (30) Grant, E.; Halstead, B. J. Dielectric Parameters Relevant to Microwave Dielectric Heating. *Chem. Soc. Rev.* 1998, 27 (3), 213–224.
- (31) De La Hoz, A.; Alcázar, J.; Carrillo, J.; Herrero, M. A.; Muñoz, J. D. M.; Prieto, P.; De Cózar, A.; Diaz-Ortiz, A. Reproducibility and Scalability of Microwave-Assisted Reactions; IntechOpen, 2011.
- (32) Ishisone, T.; Endo, H.; Kawai, T. Reversible Dispersion and Aggregation of Ag₂S Nanoparticles Capped with Azobenzene-Derivatized Alkanethiols. *J. Nanosci. Nanotechnol.* 2012, 12 (1), 648–655.
- (33) Jing, L.; Kershaw, S. V.; Li, Y.; Huang, X.; Li, Y.; Rogach, A. L.; Gao, M. Aqueous Based Semiconductor Nanocrystals. *Chem. Rev.* 2016, 116 (18), 10623–10730.
- (34) Lu, F.; Ju, W.; Zhao, N.; Zhao, T.; Zhan, C.; Wang, Q.; Fan, Q.; Huang, W. Aqueous Synthesis of PEGylated Ag₂S Quantum Dots and Their in Vivo Tumor Targeting Behavior. *Biochem. Biophys. Res. Commun.* 2020, 529 (4), 930–935.
- (35) Li, Z.; Li, X.; Cheng, J.-P. An Acidity Scale of Triazolium-Based NHC Precursors in DMSO. *J. Org. Chem.* 2017, 82 (18), 9675–9681. <https://doi.org/10.1021/acs.joc.7b01755>.
- (36) Yang, Q.; Sheng, M.; Henkelis, J. J.; Tu, S.; Wiensch, E.; Zhang, H.; Zhang, Y.; Tucker, C.; Ejeh, D. E. Explosion Hazards of Sodium Hydride in Dimethyl Sulfoxide, N,N-Dimethylformamide, and N,N-Dimethylacetamide. *Org. Process Res. Dev.* 2019, 23 (10), 2210–2217. <https://doi.org/10.1021/acs.oprd.9b00276>.

- (37) Martínez-Castañón, G. A.; Sánchez-Loredo, M. G.; Dorantes, H. J.; Martínez-Mendoza, J. R.; Ortega-Zarzosa, G.; Ruiz, F. Characterization of Silver Sulfide Nanoparticles Synthesized by a Simple Precipitation Method. *Mater. Lett.* 2005, 59 (4), 529–534.
- (38) Bhui, D. K.; Bar, H.; Sarkar, P.; Sahoo, G. P.; De, S. P.; Misra, A. Synthesis and UV–Vis Spectroscopic Study of Silver Nanoparticles in Aqueous SDS Solution. *J. Mol. Liq.* 2009, 145 (1), 33–37. <https://doi.org/10.1016/j.molliq.2008.11.014>.
- (39) Maragoni, V.; Maragoni, V.; Ayodhya, D.-D.; Madhusudhan, A.; Amrutham, S.; Guttana, V.; Mangatayaru, K. A Novel Green Synthesis of Silver Nanoparticles Using Gum Karaya: Characterization, Antimicrobial and Catalytic Activity Studies. *J. Clust. Sci.* 2013, 25. <https://doi.org/10.1007/s10876-013-0620-1>.
- (40) Ahmad, M.; Abdel Wahab, E.; El-Maaref, A.; Rawway, M.; Shaaban, E. Irradiation of Silver and Agar/Silver Nanoparticles with Argon, Oxygen Glow Discharge Plasma, and Mercury Lamp. *SpringerPlus* 2014, 3, 443. <https://doi.org/10.1186/2193-1801-3-443>.
- (41) Akkoç, S.; Gök, Y.; İlhan, İ.; Kayser, V. N-Methylphthalimide-Substituted Benzimidazolium Salts and PEPPSI Pd-NHC Complexes: Synthesis, Characterization and Catalytic Activity in Carbon-Carbon Bond-Forming Reactions. *Beilstein J. Org. Chem.* 2016, 12, 81–88. <https://doi.org/10.3762/bjoc.12.9>.
- (42) Ortega-Rodríguez, A.; Shen, Y.; Zabala Gutierrez, I.; Santos, H. D.; Torres Vera, V.; Ximendes, E.; Villaverde, G.; Lifante, J.; Gerke, C.; Fernández, N. 10-Fold Quantum Yield Improvement of Ag₂S Nanoparticles by Fine Compositional Tuning. *ACS Appl. Mater. Interfaces* 2020, 12 (11), 12500–12509.
- (43) Zhang, Y.; Xia, J.; Liu, Y.; Qiang, L.; Zhu, L. Impacts of Morphology, Natural Organic Matter, Cations, and Ionic Strength on Sulfidation of Silver Nanowires. *Environ. Sci. Technol.* 2016, 50 (24), 13283–13290.
- (44) Jia, K.; Wang, P.; Yuan, L.; Zhou, X.; Chen, W.; Liu, X. Facile Synthesis of Luminescent Silver Nanoparticles and Fluorescence Interactions with Blue-Emitting Polyarylene Ether Nitrile. *J. Mater. Chem. C* 2015, 3 (15), 3522–3529.
- (45) Du, C.; Tian, J.; Liu, X. Effect of Intrinsic Vacancy Defects on the Electronic Properties of Monoclinic Ag₂S. *Mater. Chem. Phys.* 2020, 249, 122961.
- (46) Wagner, C. D. *Handbook of X-Ray Photoelectron Spectroscopy: A Reference Book of Standard Data for Use in x-Ray Photoelectron Spectroscopy*; Perkin-Elmer, 1979.
- (47) Nguyen, M. L.; Murphy, J. A.; Hamlet, L. C.; Lau, B. L. Ligand-Dependent Ag₂S Formation: Changes in Deposition of Silver Nanoparticles with Sulfidation. *Environ. Sci. Nano* 2018, 5 (5), 1090–1095.
- (48) Armelao, L.; Colombo, P.; Fabrizio, M.; Gross, S.; Tondello, E. Sol–Gel Synthesis and Characterization of Ag₂S Nanocrystallites in Silica Thin Film Glasses. *J. Mater. Chem.* 1999, 9 (11), 2893–2898.
- (49) D. Holbrey, J.; R. Seddon, K. The Phase Behaviour of 1-Alkyl-3-Methylimidazolium Tetrafluoroborates; Ionic Liquids and Ionic Liquid Crystals. *J. Chem. Soc. Dalton Trans.* 1999, No. 13, 2133–2140. <https://doi.org/10.1039/A902818H>.

Conclusion

This work is divided in two parts that focus on the synthesis of two different type of nanometric particles stabilized by N-heterocyclic carbenes (NHCs): gold nanoclusters (AuNCs) and silver sulfide nanoparticles (Ag₂S NPs). First, the main goals were to develop easy and reproducible synthesis methods by testing various synthesis tools, parameters and reagents for gold nanoclusters production. We also needed to ensure the stability of as-obtained nanoclusters and better understand the kinetic or thermodynamic origin of their formation. Then, the second objective was to find and develop efficient characterization methods to validate the composition of the nano-objects obtained, follow the effects of the synthesis settings and for some of these nanoclusters study their properties. Finally, we wished to extend the synthesis protocol developed for NHC-gold nanostructures to the formation other nanoparticles of interest, the silver sulfide. Ag₂S is a fluorophore that emits in the second near-infrared window (NIR-II, 1000-1700 nm), which allows for better in vivo imaging quality in terms of deeper tissue imaging, higher spatial resolution, and higher contrast due to minimal auto-fluorescence and tissue diffusion.

Chapter II

A preliminary and very important part of our work focused on the development of mass spectrometry methodology for the analysis of gold nanoclusters suspensions. The literature on the analysis of gold nanoclusters was large, however it was lacking since most of the characterization methods such as UV-Vis spectroscopy did not give much information on the nanoclusters chemical composition. This specific characterization technique provides information on nanoclusters optical properties through discrete electronic transition related to such superatomic units. UV-Vis spectroscopy can also bring out the effect of the different protecting ligands on the AuNCs optical properties. However, usually experimental spectra do not have well-defined enough features to do that much conclusions. Some other characterization methods give precise structural and chemical information such as X-Ray diffraction. Nevertheless, using this technic, only the species that crystallize can be observed. This is a limiting point, since we do not have access to the real composition of the species in suspension. In addition, formation of the crystal can be difficult, time consuming, and often based on luck. The last major characterization technique that drew our interest was mass spectrometry. Mass spectrometry (MS) analyses of gold nanoclusters had already been reported in the literature, especially ESI (electrospray ionization source)-MS, but it was limited by the number of nanoclusters and species in suspension that can be analyzed on the spectra. The more species, the more patterns on the spectra, and analysis of the spectra becomes quite impossible. It became mandatory for our team to develop in collaboration with Denis Lesage and François Simon (IPCM, SU), a software designed for the analysis of nanoclusters in a large range of nuclearity and in very complex mixtures. No such software was found on the market to our knowledge for the analysis of such nanoclusters. It became a rapid and efficient way to find the nanoclusters composition with high accuracy. This software is still in development to allow a faster processing of the data and to add more specificities. We aim at increasing the precision in the formulas that are proposed for a specific pattern on the spectra at a given m/z .

Chapter III

Then, we developed a synthesis of NHC stabilized gold nanoclusters from AuClPPh₃ as a gold source. Our approach was inspired by previously reported syntheses of NHC capped gold nanoparticles reported by one of our coworker, Laura Hippolyte.¹ The main goal has been the use of three imidazolium salts as NHCs precursors: 1,3-diisopropylimidazolium bromide (iPr-Br), 1,3-didodecylimidazolium bromide (C12-Br) and 1,3-didodecylbenzimidazolium bromide (bC12-Br). These imidazolium salts are different in the length of the chains on the N atoms and in the presence or absence of a benzene ring fused to the imidazolium ring. Density Functional Theory (DFT) calculations predicted that NHCs ligands generally formed stronger bonds than phosphine ligands to stabilize gold nanoclusters. However, the use of a gold source where gold is already bonded to PPh₃, made the synthesis of nanoclusters only stabilized by NHCs experimentally impossible. Our results showed that the competition between phosphine and NHCs as ligands is favored toward phosphines. Various nanoclusters with various nuclearities were formed. Most of them are PPh₃ capped AuNCs and mixed NHC-PPh₃ Au NCs are always in the minority of identified clusters. These results were common when using all three NHC precursors. However, there was still some differences between the syntheses depending on the type of NHC. When using iPr-Br NHC precursor, the only specie containing NHCs that was stable was Au₁₁(PPh₃)₇(iPr)Br₂⁺. However, when using ligands C12 or bC12, a greater diversity of clusters, in number, nuclearity and chemical composition, were formed. We were able to detect by ESI-MS analysis, in the samples after purification, nanoclusters stabilized by NHCs only (such as Au₅(NHC)₄⁺) but these nanoclusters did decompose with ageing of the suspensions. Nanoclusters stabilized by both NHCs and PPh₃ were also detected in the samples after purification, but all of them did not remain stable with ageing except for one, Au₁₁(PPh₃)₇(NHC)Br₂⁺. Moreover, nanoclusters stabilized by PPh₃ only were detected by ESI-MS analysis; some of them remained stable toward ageing of the samples and some of them did decompose. When analyzing the results obtained from using NHC precursor iPr-Br comparing to the result obtained when using NHC precursors C12-Br and bC12-Br, we can conclude that the length of the alkyl chains on the NHCs N atoms does influence the ability to form nanoclusters. Indeed, the composition of the samples after synthesis are very different. The variety of nanoclusters synthesized is way higher for imidazolium salts C12-Br and bC12-Br than for iPr-Br. It is probably due to steric effects of the long alkyl chains and through secondary weak interactions between the chains (such as Van der Waals). However, following of ageing of the samples by ESI-MS, showed that this effect of the ligand is limited to the thermodynamical stability of the nanocluster formed. Indeed, the only NHC containing nanocluster that did remain stable is the same for all NHC ligands: Au₁₁(PPh₃)₇(NHC)Br₂⁺. The thermodynamically favored binding of the NHC to gold atom compared to PPh₃ was not observed here. It confirmed limitations of most DFT calculations when it comes to predict the stabilization of gold nanoclusters since they do not take into account some kinetics parameters, more especially, the fact that PPh₃ ligands are already bonded to gold in AuClPPh₃ before the reduction step. The only stable NHC containing nanoclusters incorporated still one NHC, for all the NHC ligands tested in this study. This behavior was also observed by another team working on ligand exchange reactions between PPh₃ capped Au₁₁ gold nanoclusters and NHCs.²

Conclusion

Chapter IV

The following of this work focused on the synthesis of AuNCs stabilized only by NHCs. $\text{HAuCl}_4 \cdot 3\text{H}_2\text{O}$ was chosen as gold source to avoid a stronger complexation of gold atom and was used with seven imidazolium salts. We increased the variety of NHC precursors to have a better understanding of the ligand effects on the nanoclusters composition and stability. We found out that short substituted groups on the NHCs N atoms, decreased the suspensions stability and the ability to stabilize AuNCs such as for the syntheses with imidazolium salt Allyl-Br and bAllyl-Br. The syntheses using imidazolium salts C12-Br and bC12-Br showed that the long alkyl chains were not the only determining parameter for very stable nanoclusters synthesis. The benzene on the benzimidazolium ring of bC12 allows stabilization of more nanocluster species than with C12 ligand. The π - π stacking effects brought by the benzene ring are supposed to enhance the stabilizing ability of the ligands and strengthen the NHC-Au bond. Experimental data show that when imidazolium salt bC12-Br is used as NHC precursor, mostly $[\text{Au}(\text{NHC})_2]^+$ molecular complex is formed. It seems like the increased bond strength, brought by the benzene ring in bC12-Br, favors the formation of $[\text{Au}(\text{NHC})_2]^+$ molecular complex and also favors decomposition of some nanoclusters into $[\text{Au}(\text{NHC})_2]^+$ molecular complex with ageing of the samples. This tendency was also observed in the synthesis using imidazolium salt bBenzyl-Cl. It was then determined that ligand C12-Br allowed a good nanocluster stabilization through the long alkyl chains without promoting the formation of $[\text{Au}(\text{NHC})_2]^+$ molecular complexes. Also, with ligand C12-Br, the nuclearity was focused on the same number since only NHC capped Au_{13} nanoclusters were formed. Also, ageing of the suspensions went toward the thermodynamic stabilization of $[\text{Au}_{13}(\text{C12})_9\text{Br}_3]^{2+}$ nanocluster. Moreover, the kinetics effects of imidazolium salts deprotonation were studied. In protic solvents, reverse protonation of the NHC happens very rapidly, thus it was necessary to use NaH as a base since NaBH_4 deprotonation rate was too slow compared to reverse protonation in ethanol. Then, aiming at developing water dispersible AuNCs, water soluble imidazolium salts were synthesized (imidPEG₄, imidBisPEG₄). However, the results went toward the formation of stable nanoparticles in water solution for both ligands. We observed after synthesis and purification of the brown suspensions, the formation of extra small particles (size < 2 nm) by TEM (transmission electronic microscopy). However, the suspensions evolved toward the formation of larger particles in size and suspensions color changed from brown to red. ESI-MS analysis on samples with ultra-small particles (brown suspensions after purification) and on samples with larger particles (red suspensions after ageing) did not detect the formation of any nanoclusters and only Au-NHC molecular complexes were observed. The results were surprising, especially given the structural similarities between C12-Br and imidBisPEG₄ NHC precursors. It seems that other effects and parameters drive the synthesis toward the formation of AuNCs (probably chain conformation in a given solvent). Since it was confirmed that no AuNCs were formed, further analysis on the samples after ageing were done (red suspensions). XPS analysis confirmed the formation of NHC capped Au NPs and a localized surface plasmon band at 530 nm, characteristic of gold nanoparticles, was observed on UV-Visible spectra.

Conclusion

Chapter V

The final part of our work was the development of NHC capped silver sulfide nanoparticles. The interest of this ionic solid formed by precipitation of Ag^+ and S^{2-} ions, comes from its stability in biological media and its ability to emit in the second infrared window (NIR-II) when excited in the first infrared window. The literature on NHC capped Ag_2S being very light, we developed a synthesis designed for obtaining water dispersible Ag_2S NPs for biological applications (especially for *in vivo* imaging and for nanothermometry). Our syntheses were developed based on the work of Lise Abiven on contactless temperature measurements at the cellular scale, by photoluminescence (PL) of Ag_2S NPs.³ We first developed syntheses by conventional heating method using AgDDT (silver diethyldithiocarbamate) as silver source and imidazolium salts, which did not give expected results due to particles stability issues. Then, in collaboration with Thomas Naillon, we developed microwave assisted synthesis methods. The first method consisted in the use of AgNO_3 and an imidazolium salt, imidPEG₄, with NaH as a base and a sulfur source ($\text{Na}_2\text{S} \cdot 9\text{H}_2\text{O}$ or S^0). Various solvents and reagents ratios were tested to conclude on the optimized heating settings (5 min, 100°C) and reagents ratio ($\text{Ag}/\text{S} = 2$ and $\text{NHC}/\text{Ag} = 5$). Analysis by HRTEM-EDX (high resolution transmission electronic microscopy-energy dispersive x-ray) confirmed that both Ag_2S NPs and Ag NPs were synthesized through this synthesis method as already reported by Ortega-Rodriguez *et al.* who used thermal degradation of Ag(DDTC) in oleylamine and dodecanethiol.⁴ Even though the obtained Ag_2S NPs were emitting in the NIR-II, the inability to shift the synthesis completely toward the formation of Ag_2S NPs led to the development of a second synthesis method. This method uses Ag-NHCPEG₄ complex and $\text{Na}_2\text{S} \cdot 9\text{H}_2\text{O}$. We were able to obtain stable Ag_2S NIR-II emitting NPs dispersible in water. Various solvents and reagents ratios were tested to conclude on the optimized heating settings (5 min, 100°C) and reagents ratio ($\text{Ag}/\text{S} = 2$ and $\text{NHC}/\text{Ag} = 5$). We were also able to confirm a link between the photoluminescence activity and the temperature, which makes them potential candidates as nanothermometers.

Prospects on Part I

NHC capped AuNCs are structurally similar to PPh_3 capped AuNCs: they are thermodynamic analogues. It would be possible to play on the versatility of the N heterocycles of the NHC ligands to modulate their donor character. Then, it would be possible to associate the nuclearity of the nanoclusters formed to the donor character of the NHCs. It would also be great to conduct a comparative study of the results obtained by calculation methods (such as DFT) to experimentation. Moreover, increasing the ageing experiment time could allow further understanding on the stability of the various nanoclusters synthesized.

Moreover, we would like to develop an efficient separation method of all the nanoclusters for individual study. Several attempts by silica gel column chromatography did not succeed in this aim (except for $[\text{Au}_{13}(\text{C}_{12})_9\text{Br}_3]^{2+}$). PAGE (Polyacrylamide gel electrophoresis) chromatography or HPLC (High-performance liquid chromatography) could help in this goal. Then, we could do further surface characterization to study the gold-NHC interface XPS (X-ray photoelectron spectroscopy), SAXS (Small angle X-ray scattering), TGA (Thermogravimetric analysis), etc). Also, the nanoclusters properties could be studied such as catalytic properties or fluorescence properties.

Conclusion

Prospects on Part II

The first prospects would be to find a way to develop further the conventional heating synthesis method in organic solvents of Ag₂S NPs. The first ideas will be to work in mixed solvents environments to allow better solubility of the reagents and increase the quantity of the NHC ligand for a better stabilization of the NPs. Regarding the microwave assisted synthesis, the prospects would be to shift the first synthesis method toward the synthesis of Ag₂S NPs only. Indeed, this first synthesis produced both Ag NPs Ag₂S NPs. This shift could be done by increasing the reaction time, for example. Then, the synthesis of imidazolium salts with longer PEG chains could influence the PL of the particles as well as the NPs affinity to cells membrane or the oxidative stress induced on the cells. Testing a larger panel of water-soluble silver-NHC complexes could thus improve the resulting NPs overall properties. Finally, when it comes to properties, further PL tests could be performed followed by *in vivo* experiments to validate NPs stability or toxicity.

Conclusion

References

- (1) Hippolyte, L. New Syntheses of N-Heterocyclic Carbene-Stabilized Gold Nanoparticles, Sorbonne université, 2018.
- (2) Narouz, M. R.; Osten, K. M.; Unsworth, P. J.; Man, R. W. Y.; Salorinne, K.; Takano, S.; Tomihara, R.; Kaappa, S.; Malola, S.; Dinh, C.-T.; Padmos, J. D.; Ayoo, K.; Garrett, P. J.; Nambo, M.; Horton, J. H.; Sargent, E. H.; Häkkinen, H.; Tsukuda, T.; Crudden, C. M. N-Heterocyclic Carbene-Functionalized Magic-Number Gold Nanoclusters. *Nat. Chem.* **2019**, *11* (5), 419–425. <https://doi.org/10.1038/s41557-019-0246-5>.
- (3) Abiven, L. Mesure de Température sans Contact, En Temps Réel et à l'échelle Cellulaire, Par Photoluminescence de Nanoparticules de Sulfure d'argent, Sorbonne Université, 2022.
- (4) Ortega-Rodríguez, A.; Shen, Y.; Zabala Gutierrez, I.; Santos, H. D.; Torres Vera, V.; Ximendes, E.; Villaverde, G.; Lifante, J.; Gerke, C.; Fernández, N. 10-Fold Quantum Yield Improvement of Ag₂S Nanoparticles by Fine Compositional Tuning. *ACS Appl. Mater. Interfaces* **2020**, *12* (11), 12500–12509.

Appendix

A. ADDITIONAL EXPERIMENTAL DATA

A. Chapter II

Example of nanocluster formula finding with Labview software for nanocluster $[\text{Au}_{129}(\text{PPh}_3)_{24}]^{3+}$ (C27 = ligand C12 in Figure A-1)

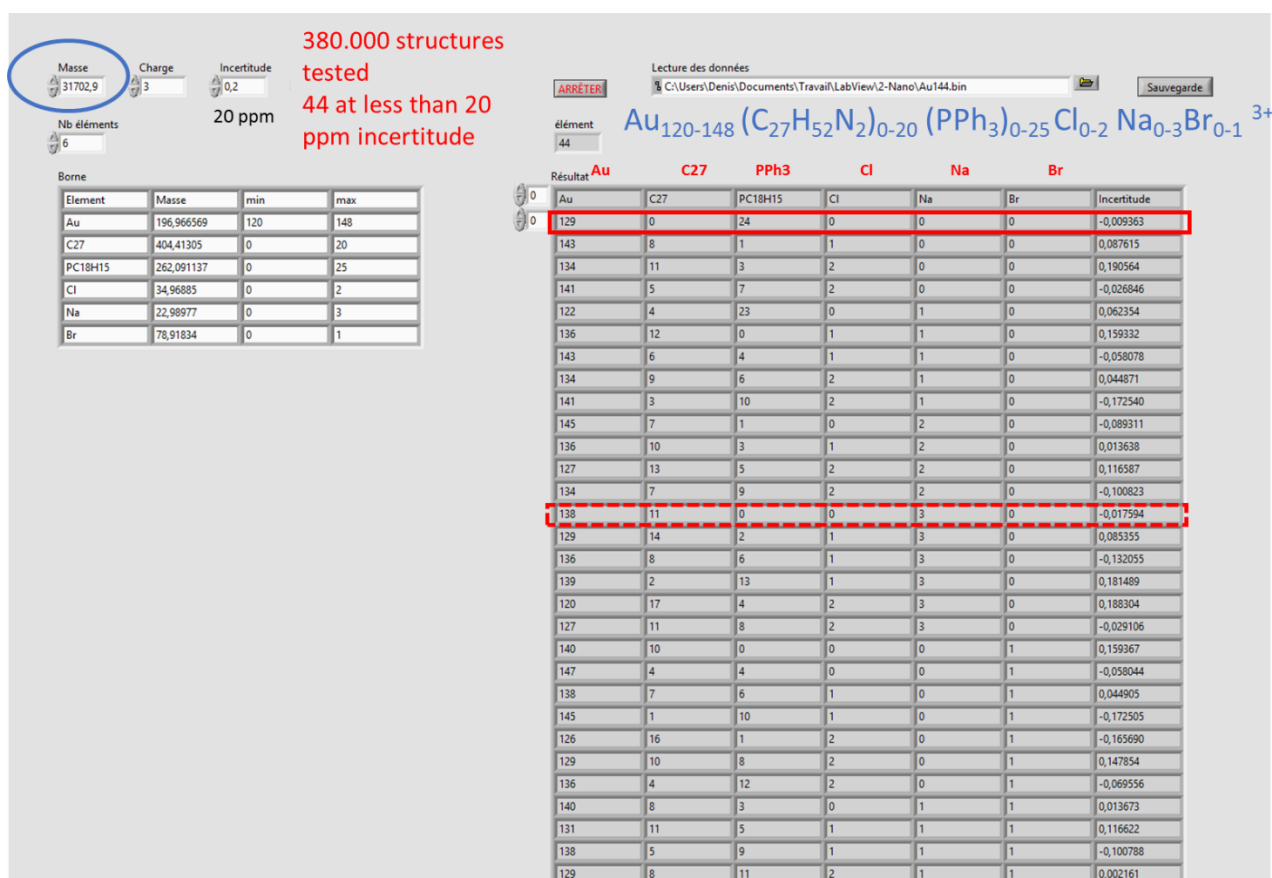


Figure A-1 Interface of Labview software for nanoclusters

One pattern is chosen on the spectra and the corresponding values are entered in the software. For all the 44 structures isotopical pattern were simulated on the Bruker mass spectrometer software. Out of all these structures only 1 theoretical isotopic pattern corresponded to the experimental isotopic pattern: the one from for $[\text{Au}_{129}(\text{PPh}_3)_{24}]^{3+}$. Below are presented examples of isotopic patterns for $[\text{Au}_{129}(\text{PPh}_3)_{24}]^{3+}$ and for $[\text{Au}_{138}(\text{C27})_{11}\text{Na}_3]^{3+}$.

Appendix

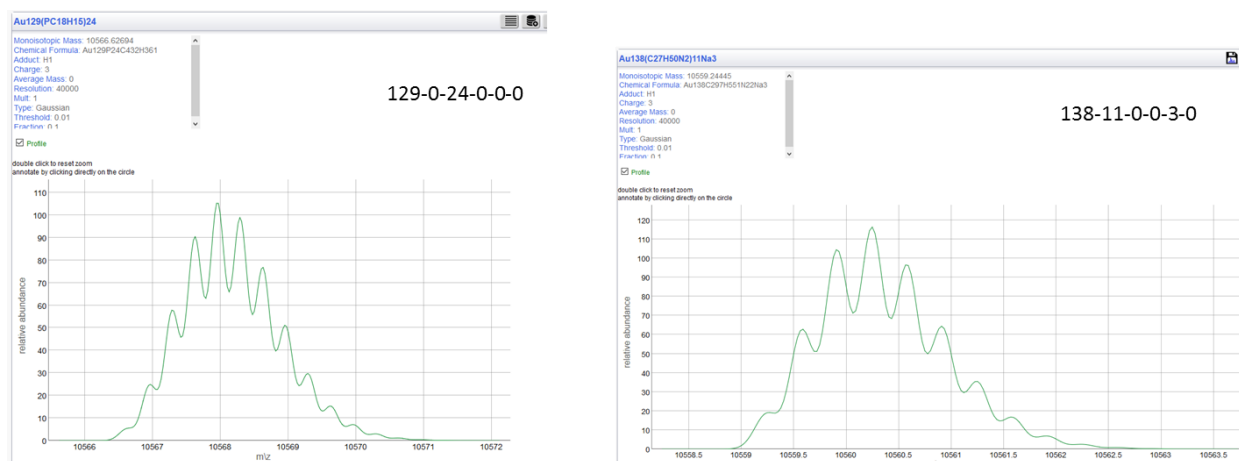


Figure A-2 Comparison of theoretical isotopic patterns for $[\text{Au}_{129}(\text{PPh}_3)_{24}]^{3+}$ and $[\text{Au}_{138}(\text{C}_{27}\text{H}_{50}\text{N}_2)_{11}\text{Na}_3]^{3+}$.

A. Chapter III

Synthesis and morphology. Effect of the ligand/Au ratio (Figure A-3)

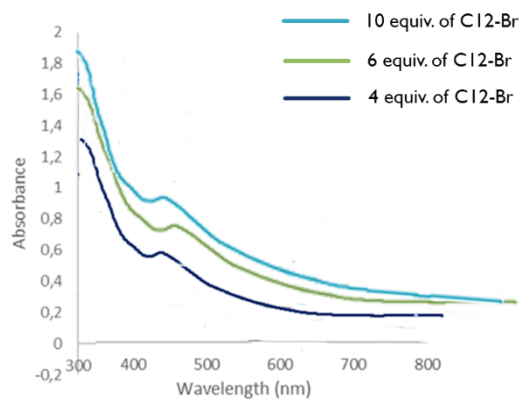


Figure A-3 UV-Vis spectra of AuNCs synthesized from AuClPPh_3 , imidazolium salt C12-Br (4, 5, 10 equiv.) and NaBH_4 in EtOH.

Appendix

Mass spectrometry (MS) analysis. ESI-MS results discussion Spectrum of the suspensions after 3 months showing little suspensions evolution except for nanoclusters having H^+ which disappeared on C12-AuNC sample spectrum (Figure A-4)

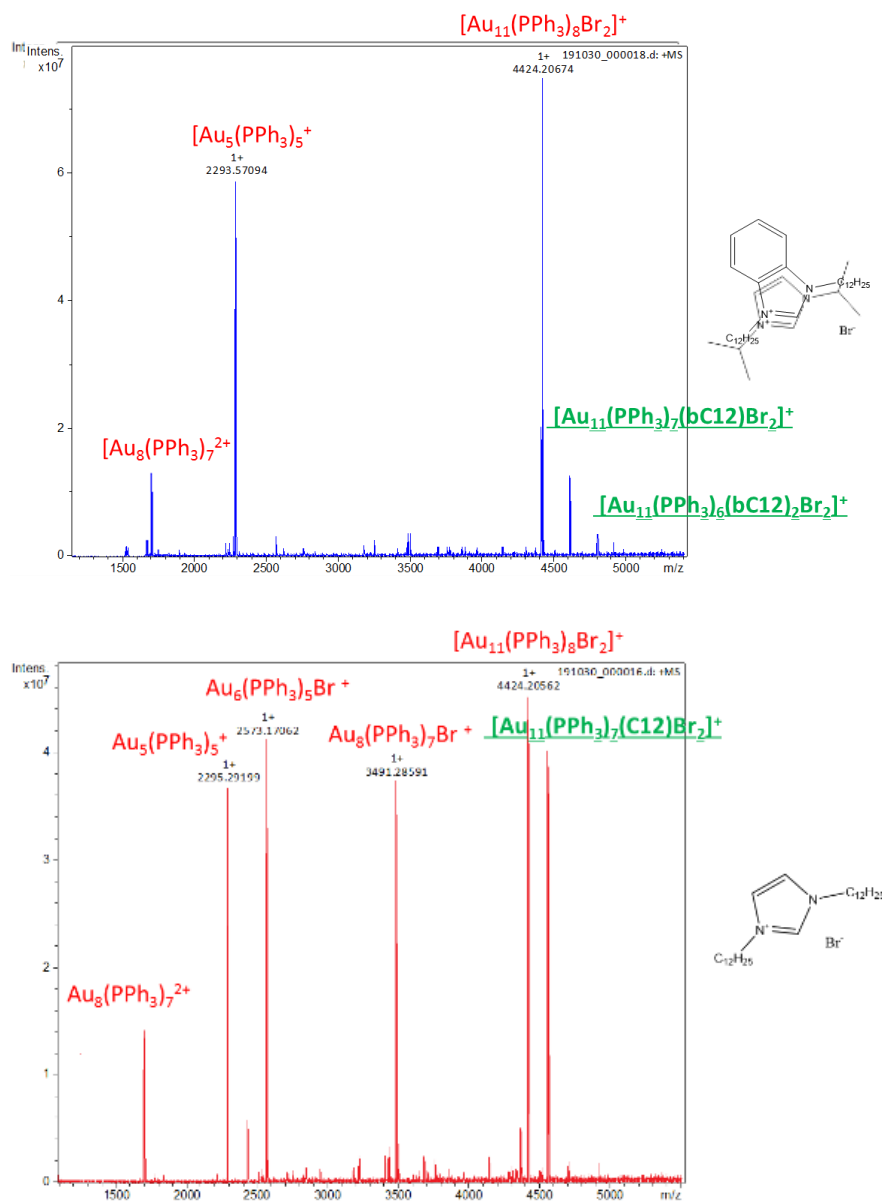
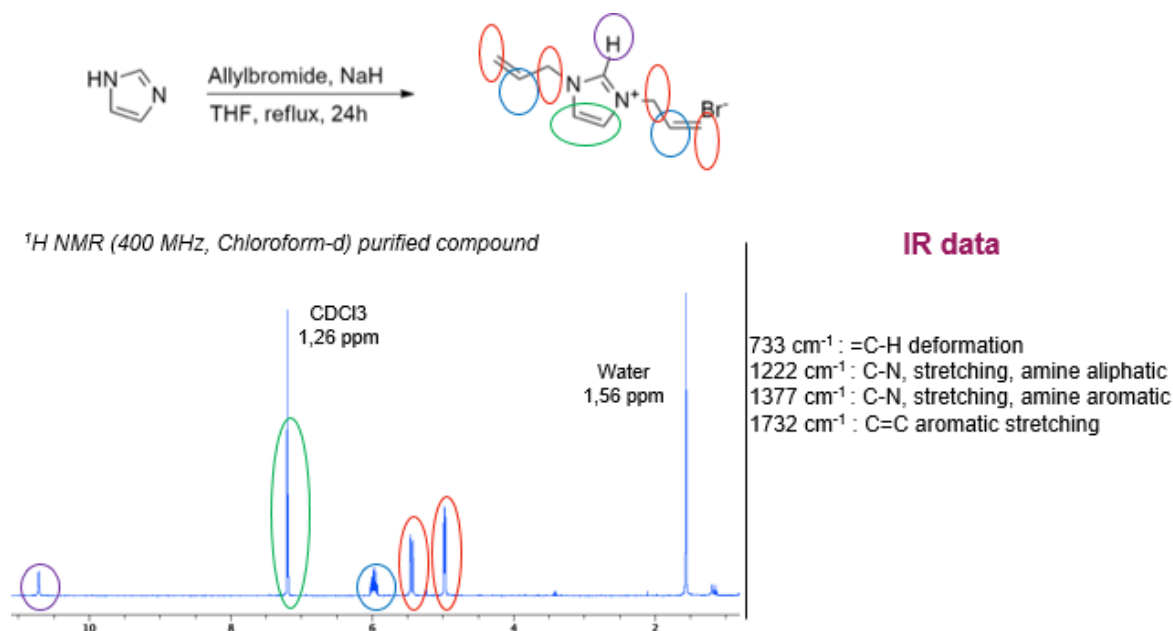
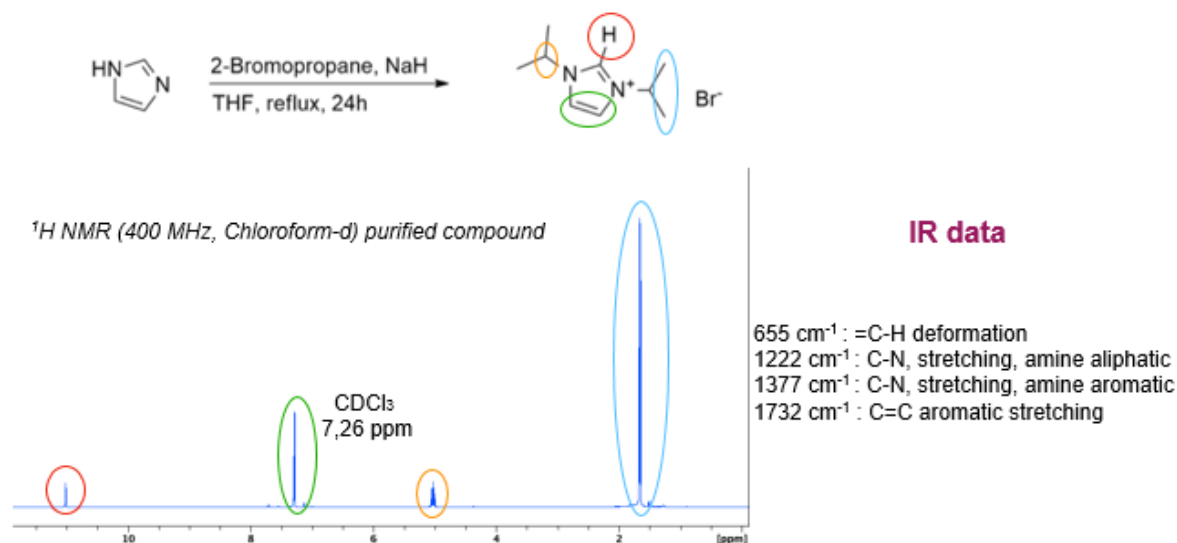


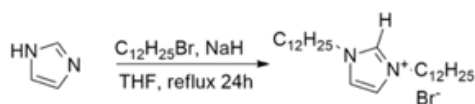
Figure A-4 ESI MS spectra of AuNCs synthesized from $AuClPPh_3$, imidazolium salts iPr-Br, C12-Br, bC12-Br (4equiv.) and $NaBH_4$ in EtOH after 3 months.

A. Chapter IV

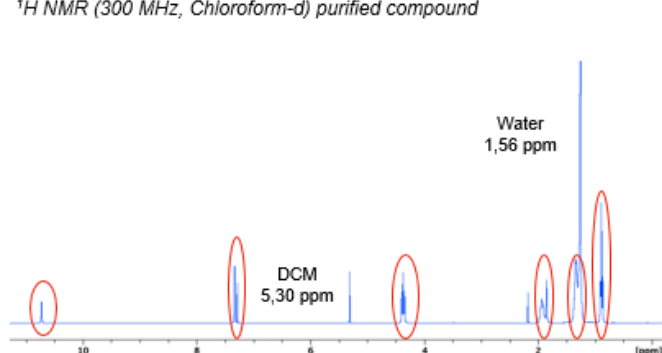
^1H NMR spectra and infrared data of imidazolium salts used in chapter IV to confirm formation and purification. Some impurities corresponding to residual solvents can be observed on ^1H NMR spectra



Appendix

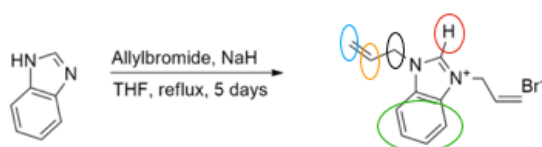


^1H NMR (300 MHz, Chloroform- d) purified compound

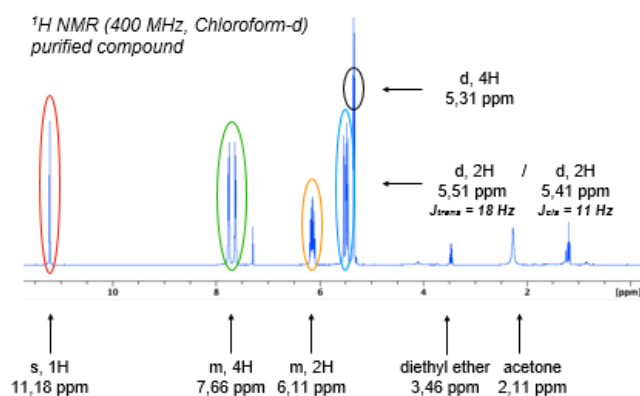


IR data

733 cm^{-1} : =C-H deformation
1264 cm^{-1} : C-N, stretching, amine aliphatic
1377 cm^{-1} : C-N, stretching, amine aromatic
1732 cm^{-1} : C=C aromatic stretching



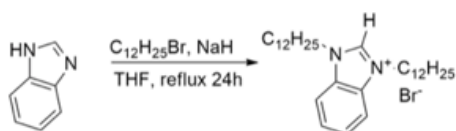
^1H NMR (400 MHz, Chloroform- d) purified compound



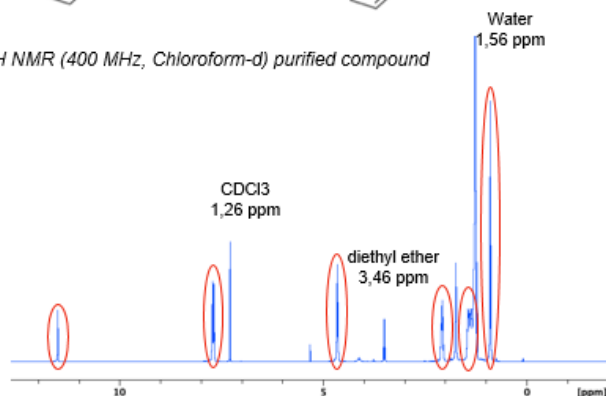
IR data

733 cm^{-1} : =C-H deformation
1264 cm^{-1} : C-N, stretching, amine aliphatic
1377 cm^{-1} : C-N, stretching, amine aromatic
1742 cm^{-1} : C=C aromatic stretching

Appendix

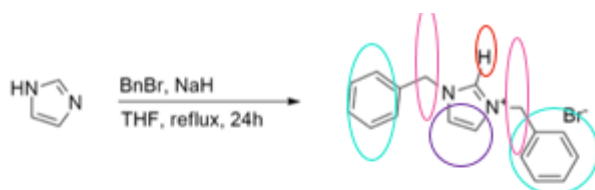


^1H NMR (400 MHz, Chloroform-d) purified compound

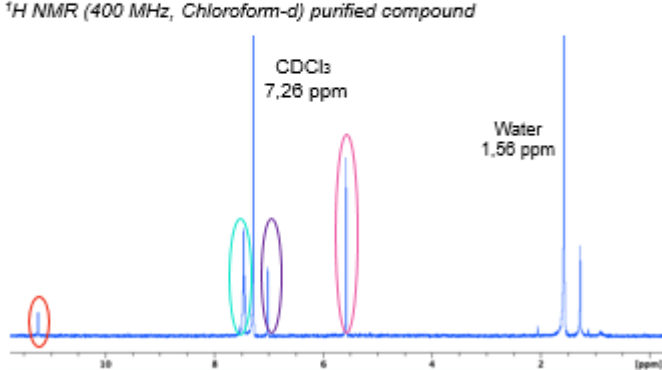


IR data

733 cm^{-1} : =C-H deformation
 1264 cm^{-1} : C-N, stretching, amine aliphatic
 1377 cm^{-1} : C-N, stretching, amine aromatic
 1742 cm^{-1} : C=C aromatic stretching



^1H NMR (400 MHz, Chloroform-d) purified compound

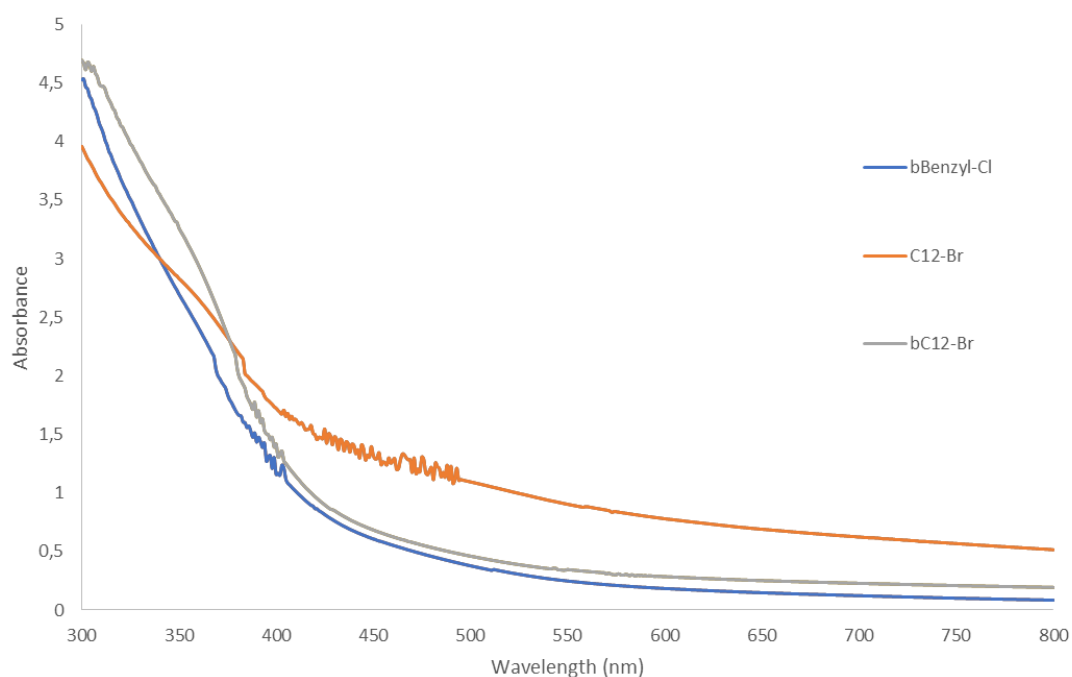


IR data

733 cm^{-1} : =C-H deformation
 1222 cm^{-1} : C-N, stretching, amine aliphatic
 1377 cm^{-1} : C-N, stretching, amine aromatic
 1742 cm^{-1} : C=C aromatic stretching

Appendix

UV-Visible spectra for AuNCs samples synthesized in EtOH from $\text{HAuCl}_4 \cdot 3\text{H}_2\text{O}$ and NHC precursors C12-Br, bC12-Br, bBenzyl-Cl

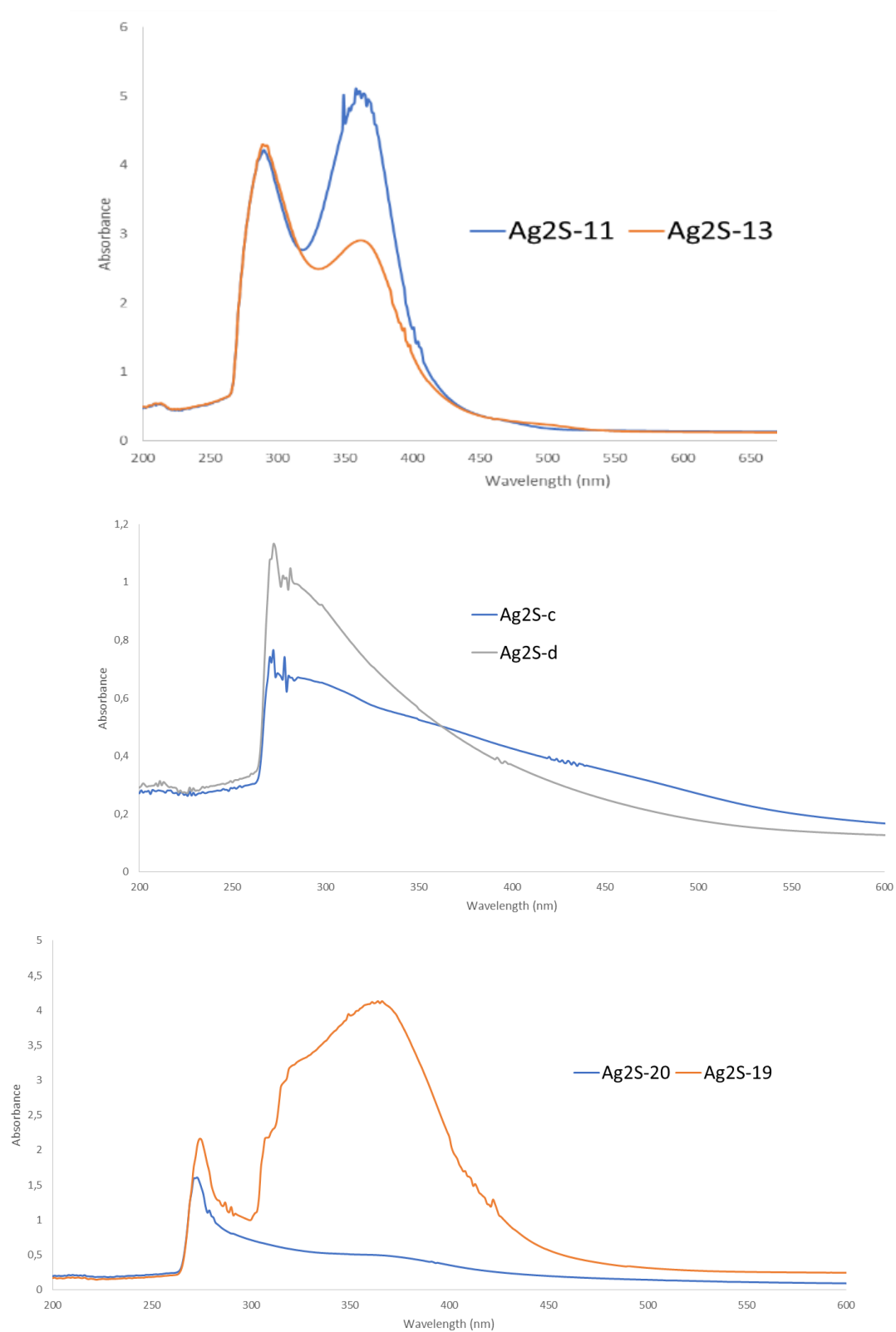


A. Chapter V

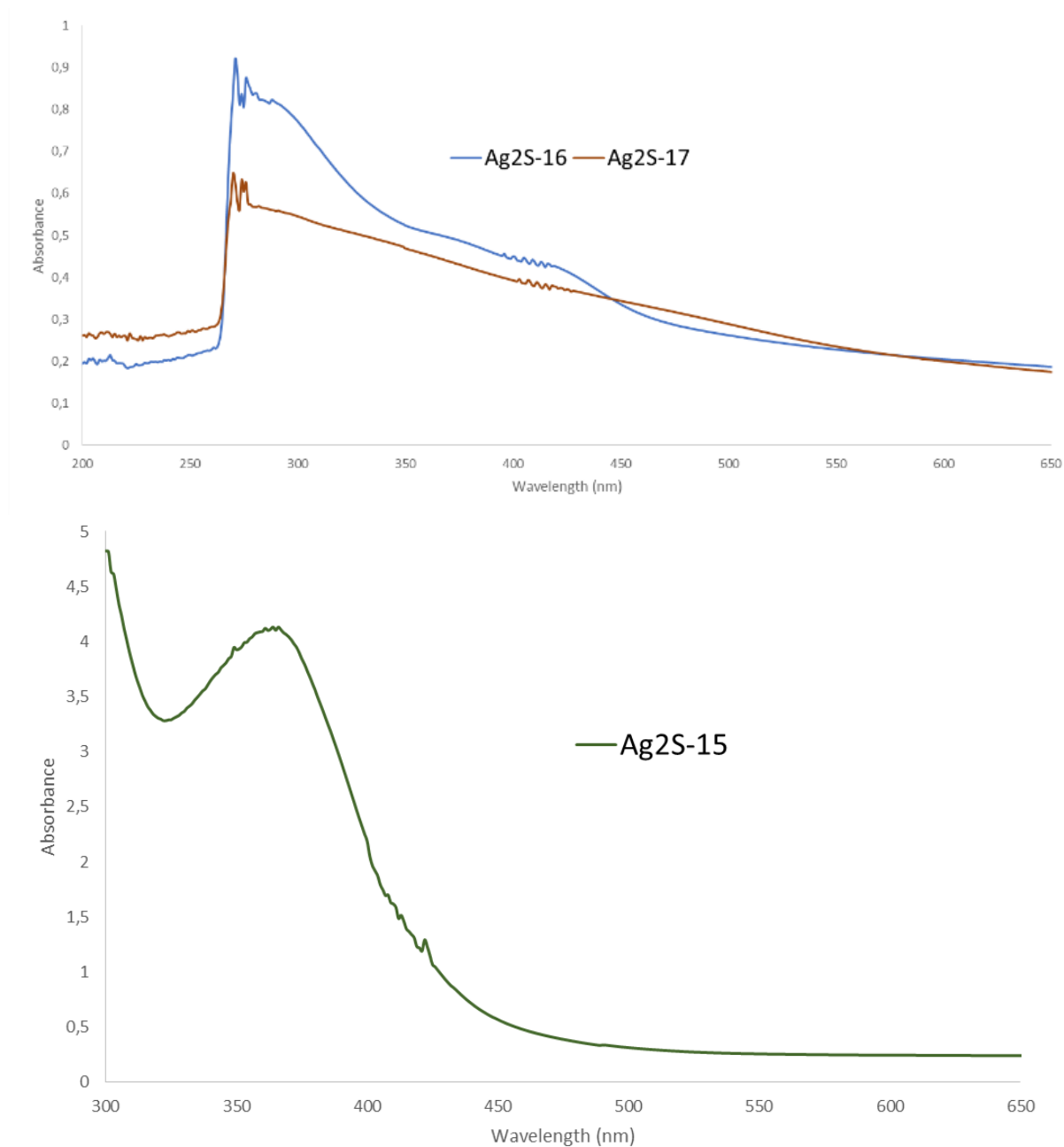
UV-Visible spectra for samples listed in the following table

| sample | solvent | [Ag] mM | Ag/S | Ligand/Ag | T (°C) | t (min) | Sulfur source |
|----------------------|---------|------------|-------|-----------|--------|---------|-------------------------------------|
| Ag ₂ S-11 | DMSO | 5 | 1 | 25 | 100°C | 5 | Na ₂ S·9H ₂ O |
| Ag ₂ S-13 | DMSO | 5 | 2 | 25 | 100°C | 5 | Na ₂ S·9H ₂ O |
| Ag ₂ S-15 | DMSO | 5 | S = 0 | 5 | 100°C | 5 | none |
| Ag ₂ S-16 | DCM | 5 | 1 | 5 | 100°C | 5 | Na ₂ S·9H ₂ O |
| Ag ₂ S-17 | DCM | 5 | 2 | 5 | 100°C | 5 | Na ₂ S·9H ₂ O |
| Ag ₂ S-19 | DMSO | 5 | 1 | 5 | 100°C | 5 | S ⁰ |
| Ag ₂ S-20 | DCM | 5 | 1 | 5 | 100°C | 5 | S ⁰ |
| Ag ₂ S-c | DCM | 5 | 1 | 1 | 100°C | 5 | Na ₂ S·9H ₂ O |
| Ag ₂ S-d | DCM | 5 | 2 | 1 | 100°C | 5 | Na ₂ S·9H ₂ O |

Appendix



Appendix



B. INSTRUMENTATION

Electrospray ionization mass spectrometry, ESI-MS analysis settings

The samples were prepared for analysis in various solvents: toluene/MeOH, EtOH with 100 µg/ µl concentration and addition of CsOAc as a calibrant. The silica capillaries were washed with MeOH and acetone to prevent contamination.

All samples were analyzed with the same mass spectrometer conditions in positive ion mode (capillary temperature, 250 °C; spray voltage, 5 kV). Resolution $m/\Delta m = 40,000$ for our Q-TOF, acquisition speed 20Hz. For our FT-ICR, resolution $m/\Delta m = 120,000$ for m/z 200 and 20,000 for m/z 2000 for a 7 Tesla magnet and 1 Hz detection. Instrument tune parameters were carefully optimized on the prominent peaks for the total mass spectrum obtained from 250–10000 m/z and 250-7000 m/z (these settings were used for all experiments).



Figure B-1 FT-ICR mass spectrometer

Transmission electronic microscopy, TEM

The samples are prepared by depositing a drop of suspension of the compound in the solvent to be characterized on a copper grid covered with a thin layer of carbon. The analysis of the morphology of the nanoparticles is then carried out by observation of the sample in transmission electron microscopy (TEM) (Tecnai G2 Spirit Twin) with an accelerating voltage of 120 kV. The processing of the TEM images is done with the open source software Image J.

Appendix

UV-Vis-NIR spectrometer

Absorption spectra are recorded with a UV-Vis-NIR spectrometer CARY 5000 from Agilent Technologies, operating between 200 nm and 900 nm. The solutions were prepared by appropriate dilution of stock solutions then transferred in a closed quartz cuvette for analysis.

Nuclear Magnetic Resonance Spectroscopy, NMR

^1H NMR and ^{13}C NMR spectra were recorded at room temperature on Bruker Avance 300 or Avance 400 spectrometers. Shifts (δ) are given in parts per million (ppm).

Spectra were recorded with a Thermo ESCALAB 250 X-ray photoelectron spectrometer with a monochromatic Al-K α X-Ray source ($h\nu = 1486.6$ eV) operating at 10^{-10} Torr. The analyzer pass energy was 50 eV. All spectra were calibrated versus the binding energy (BE) of hydrocarbons (C1s at 285.0 eV). Spectra were recorded and analyzed using Thermo Advantage software

High Resolution Transmission Electronic Microscopy, HRTEM/ Energy Dispersive X-Ray Analysis, EDX

The samples are prepared by depositing a drop of suspension of the compound in the solvent to be characterized on a copper grid covered with a thin layer of carbon. The analysis of the morphology of the nanoparticles is then carried out by observation of the sample in high resolution transmission electron microscopy (MET 2100 PLUS). Other characteristics: - Acceleration voltage: 200 kV - Resolution: 1.9 angstrom - Camera CCD Gatan (Orius) - Software Gatan - Beam scanning system (STEM = scanning transmission electron microscope).

The analysis of the chemical composition of the nanoparticles is performed with a dissipative energy spectroscopy probe EDS analyzer (SDD 80 mm²-Oxford, AZtec software)

Monomode Microwave

A single mode microwave is used in this thesis (Monowave 300, Anton Paar, Figure B-2 a.). A temperature of 100°C is reached within the reactor in less than one minute. To reach such a performance, the power delivered by the furnace is 300 W. The pressure inside the reactor when the temperature plateau is at 100°C is 10 bars (the safety threshold set by the manufacturer is 30 bars). At the end of the temperature plateau, the reactor is cooled by a compressed air flow. This allows a rapid decrease in temperature (50°C in 4 min) of the reaction medium. The samples are put in a reactor with external (infrared sensor) and internal (ruby immersion temperature probe) temperature controls (Figure B-2 b.).

Appendix

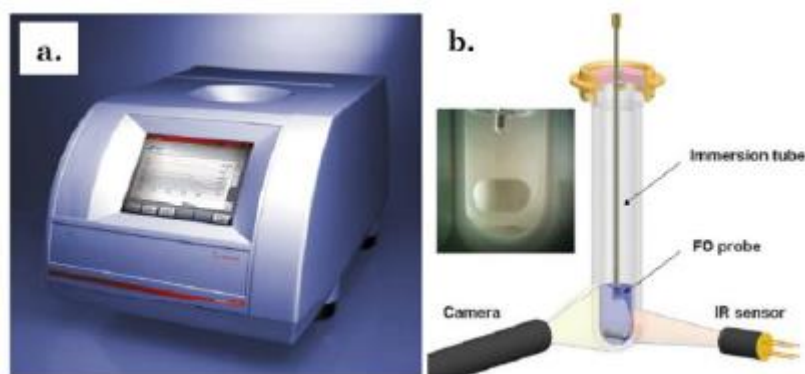


Figure B-2 a. Monowave 300, Anton Paar. b. reactor with external (infrared sensor) and internal (ruby immersion temperature probe) temperature controls.

Photoluminescence measuring device

The photons emitted by the silver sulfide are collected by an optical fiber equipped with a 1000 nm high-pass filter (to avoid detecting of parasite signals). The photons are then sent to a monochromator (Figure B-3 b.). The output slit of the monochromator is connected to the hyperspectral camera (PyLoN-IR, Princeton). The hyperspectral camera used is (PyLoN-IR, Princeton) to detect the photoluminescence signal of Ag_2S . It is equipped with an Indium and Gallium Arsenide (InGaAs) sensor (Figure B-3 a.). It is the most sensitive material for detecting photons in the second transparency window of biological tissues. Thus, it can detect the signal of photoluminescent probes emitting between 1000 nm and 1400 nm. The InGaAs detector is a photodiode, allowing to convert a light signal into current. The measurement of the current induced by the absorption of photons allows to get the number of photons detected for a given wavelength range. The monochromator coupled to the InGaAs photodetector allows to obtain the photoluminescence emission spectrum of silver sulfide with a spectral resolution of 0.43 nm. All photoluminescence spectra are acquired at 25°C for an aqueous suspension volume of 0.7 mL (sample concentration 0,5 mg.mL^{-1}). The temperature of the sample is controlled using a heated sample holder (Quantum Northwest). A 730 nm LED (ThorLabs, 0.1 W.cm^{-2}) is used as the excitation source.

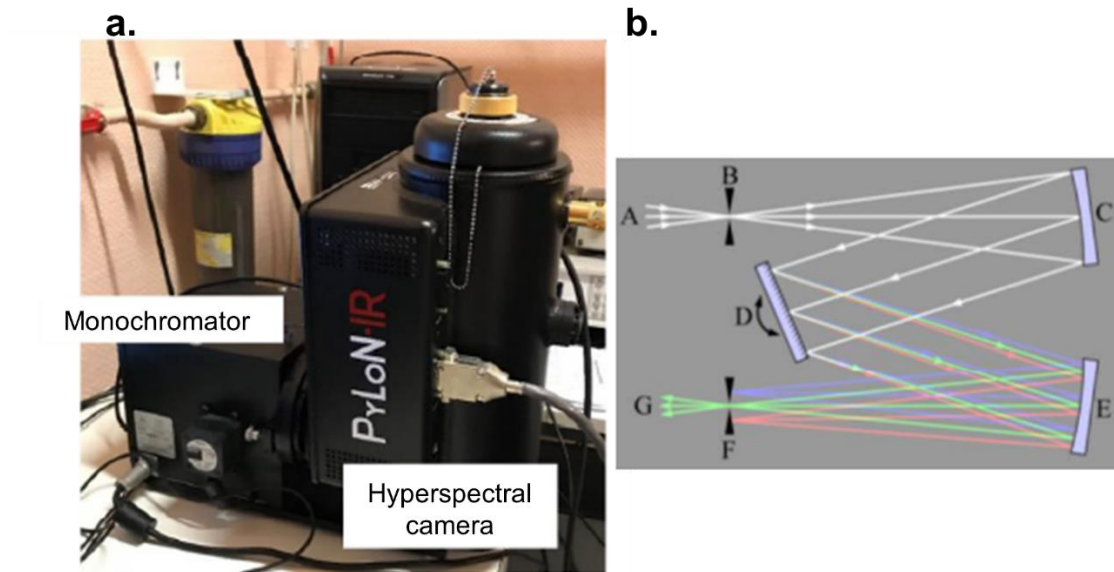


Figure B-3 a. Hyperspectral camera connected on a monochromator. b. Path of the polychromatic light beam from the source to the outlet of the monochromator.

Abstract

In the present work, we developed a novel synthesis of gold nanoclusters stabilized by N-heterocyclic carbenes (NHCs). The syntheses of gold nanoclusters (AuNCs) were confirmed by characterizations techniques, especially electrospray ionization mass spectrometry (ESI-MS). We were able to analyze very complex gold nanoclusters mixtures of PPh₃ and NHC capped nanoclusters. First, a AuNC synthesis was carried out in ethanol and resulted from AuClPPh₃ reduction by NaBH₄ in presence of imidazolium salts as NHC precursors. We were able to prove that mostly PPh₃ capped nanoclusters are synthesized even though Au-NHC bond are generally stronger than Au-PPh₃ bond. However, it was highlighted that a highly stable Au₁₁(PPh₃)₇(NHC)Br²⁺ is synthesized. Following of samples aging by ESI-MS showed evolution of the suspensions over time. Unstable nanoclusters primary formed decompose to form more stable nanoclusters structure. Then, the second synthesis was also carried out in ethanol and resulted from HAuCl₄.3H₂O reduction by NaBH₄ in presence of imidazolium salts as NHC precursors and NaH as a base. NHC capped gold nanoclusters were obtained with various gold nuclearities. A strong NHC ligand effect was highlighted since the nanoclusters suspensions stabilities varied depending on the imidazolium salt used for the synthesis. Also, the composition of the suspensions (nanoclusters formula) varied depending on the NHC ligand. Synthesis with imidazolium salt 1,3-didodecylimidazoliumbromide allowed formation of highly stable [Au₁₃(C12)₉Br₃]²⁺ nanocluster. Various reaction parameter were tested to assess their effect on the nanoclusters formation (solvents, base, ligand/Au ratio ...). It was also shown that synthesis with a water soluble imidazolium salt 1-methyl, 3-tetraethyleneglycolimidazolium bromide, in similar reaction conditions as previously, led to the formation of gold nanoparticles. It showed that the border between gold nanoclusters and gold nanoparticles synthesis is thin. Finally, synthesis of Ag₂S nanoparticles stabilized by water soluble NHC was reported. Silver-NHC complex was synthesized then put in presence of a S²⁻ source. Synthesis through microwave heating showed promising results as Ag₂S nanoparticles emitting in the second window of the infrared was demonstrated. Indeed, it is the window of biological tissues transparency which is of interest for biological applications.

Résumé

Dans ce travail, nous avons développé une nouvelle synthèse de nanoclusters d'or stabilisés par des carbènes N-hétérocycliques (NHCs). Les synthèses de nanoclusters d'or (AuNCs) ont été confirmées par des techniques de caractérisation, notamment la spectrométrie de masse par ionisation électrospray (ESI-MS). Nous avons pu analyser des mélanges de nanoclusters d'or très complexes stabilisées par des ligands PPh₃ et NHC. Tout d'abord, une synthèse de AuNC a été réalisée dans l'éthanol. Elle résulte de la réduction de AuClPPh₃ par NaBH₄ en présence de sels d'imidazolium comme précurseurs de NHC. Nous avons pu prouver que la plupart des nanoclusters synthétisés sont stabilisés par des PPh₃ même si la liaison Au-NHC est généralement plus forte que la liaison Au-PPh₃. Cependant, il a été mis en évidence qu'un nanocluster Au₁₁(PPh₃)₇(NHC)Br²⁺ très stable est synthétisé. Le suivi du vieillissement des échantillons par ESI-MS a montré l'évolution des suspensions au cours du temps. Les

nanoclusters instables détectés au départ dans les échantillons se décomposent pour former des structures de nanoclusters plus stable. Ensuite, la deuxième synthèse a également été réalisée dans l'éthanol et résulte de la réduction de $\text{HAuCl}_4 \cdot 3\text{H}_2\text{O}$ par NaBH_4 en présence de sels d'imidazolium comme précurseurs de NHC et de NaH comme base. Des nanoclusters d'or coiffés de NHC ont été obtenus avec différentes nucléités d'or. Un fort effet du ligand NHC a été mis en évidence puisque les stabilités des suspensions de nanoclusters varient en fonction du sel d'imidazolium utilisé pour la synthèse. De même, la composition des suspensions (formule des nanoclusters) varie en fonction du ligand NHC. La synthèse avec le sel d'imidazolium 1,3-didodécylimidazoliumbromide a permis la formation de nanoclusters $[\text{Au}_{13}(\text{C}_{12})_9\text{Br}_3]^{2+}$ très stables. Différents paramètres réactionnels ont été testés afin d'évaluer leur effet sur la formation des nanoclusters (solvants, base, rapport ligand/Au...). Il a également été montré que la synthèse avec un sel d'imidazolium soluble dans l'eau, le bromure de 1-méthyl, 3-tétraéthylèneglycolimidazolium, dans des conditions réactionnelles similaires aux précédentes, conduisait à la formation de nanoparticules d'or. Cela a montré que la frontière entre la synthèse de nanoclusters d'or et de nanoparticules d'or est mince. Enfin, la synthèse de nanoparticules d' Ag_2S stabilisées par des NHC solubles dans l'eau a été rapportée. Le complexe argent-NHC a été synthétisé puis mis en présence d'une source de S^{2-} . La synthèse par chauffage micro-ondes a donné des résultats prometteurs puisque des nanoparticules d' Ag_2S émettant dans la deuxième fenêtre de l'infrarouge a été démontrée. En effet, il s'agit de la fenêtre de transparence des tissus biologiques qui présente un intérêt pour les applications biologiques.